THE DETERMINATION OF COPPER IN SEAWATER USING FLOW INJECTION WITH CHEMILUMINESCENCE DETECTION

by

Richard Charles Sandford

A thesis submitted to the University of Plymouth in partial fulfillment for the degree of:

DOCTOR OF PHILOSOPHY

Department of Environmental Sciences

Faculty of Science

In collaboration with

Plymouth Marine Laboratory

August 2002

Abstract

The Determination of Copper in Seawater Using Flow Injection with Chemiluminescence Detection

Richard Charles Sandford

This thesis describes the design, optimisation and shipboard deployment of a flow injection - chemiluminescence (FI-CL) technique for the determination of labile Cu(II) and total copper (by UV irradiation) in seawater. The operational parameters of the FI manifold in a UHP water sample matrix and the 1,10-phenanthroline CL reaction were rigorously optimised. Interferences to the CL reaction were investigated and the good analytical figures of merit obtained presented. The FI-CL method was modified for the determination of ultra trace levels of Cu(II) in seawater by the incorporation of a new design of micro-column containing 8-hydroxyquinoline (8HQ) resin for in-line matrix separation and preconcentration. Reagent clean-up techniques, blank procedures and a standard addition protocol are detailed. The optimised method is selective for Cu(II) in the linear range 0.1 - 50 nM, with precision of <4% (n=4) for a typical seawater analysis, and a limit of detection (3s) of 25 pM for a loading time of 90 s.

The FI-CL analyser was fully automated and then validated by field deployment on the Tamar Estuary, during which its robustness, reliability and stand alone capability were demonstrated. Good accuracy was achieved for a seawater CRM analysed onboard. The near real time Cu data obtained was in good agreement with a comparative voltammetric method.

The FI-CL method was further validated by field deployment on the Atlantic Meridional Transect (AMT 9) during which Cu(II) (filtered, acidified (pH 2) HNO_3) in the surface waters (<250 m) of the North and South Atlantic (50 ^{o}N to 50 ^{o}S) was mapped. Spatial variation in Cu(II) concentrations was observed (<0.7 to 6.1 nM) through the contrasting biogeochemical provinces encountered that representated coastal, upwelling and oligotrophic regions. Copper (II) enrichments were imposed on a trend of decreasing Cu(II) concentrations away fom European coastal waters (>2.5 nM) to open ocean gyres (< 1 nM). Away from strong input mechanisms, upper water column Cu(II) concentrations were ca. 1.5 nM, being dominated by long range aerosol input mechanisms. Input sources are fingerprinted via correlation with nutrients and hydrographic data, whilst the dominant sinks are active biological uptake and particle reactivity. Cu(II) vertical distributions through the upper mixed layer display strong relationships with chlorophyll *a*, particularly in remote oceanic regimes.

An in-line UV photo-oxidation system was constructed and optimised for the digestion of organically complexed Cu to enable near real time determination of total Cu in seawater by FI-CL. It achieved very efficient digestion of DOM (96.3 %) using a short irradiation time (600 s), with good recovery of Cu. Robustness, reproducibilty of irradiation, effective operational life and safety were considerably improved compared to existing systems. DOM rich Tamar Estuary and Celtic Sea samples were in good agreement with Cu(II) results from conventional batch UV digestion and voltammetric detection.

Acknowledgements

I would like to express my sincere thanks to my supervisors for their constructive advice throughout my Ph.D. research and for their critical comments on this manuscript. Firstly to Paul Worsfold, who has provided a wealth of valid guidance and knowledge, who has been a good friend and was very supportive throughout some personally challenging times during this PhD. To Eric Achterberg, who has provided succinct advice and guidance during my studies (even if I returned the same on the squash court) and who has been a good friend – right on sailor. Thanks also to Fauzi Mantoura, to whom I am grateful, for his depth of knowledge and for provision of the excellent opportunity to participate on the Atlantic Meridional Transect 9 (AMT 9) and inspiring me to explore oceanic trace element biogeochemistry. Thanks also to Ian Doidge, the two Andys, Sally, Rob and Adrian for their help in all the background logistics that is required for such a project.

I am also very grateful to those who have helped me in a many ways during the field studies and oceanographic cruises. I would like to acknowledge the Atlantic Meridional Transect steering group for providing a platform to deploy the FI-CL monitor. Thanks to Nigel Rees for his support as principle scientist, Malcolm Woodward for logistics, Hester Wilson, Vassilis Kitidis and all other participants of the AMT project who have helped make it an unforgettable experience. A special thanks to Kathryn Lamble and Martin Barham ("de family") for their timely and much appreciated bottle washing/ cruise preparation efforts – sterling work guys, you will be rewarded somewhere in life. A special thanks also to Joanna Hughes for her sampling efforts during the cruise. Many thanks also to the captain, officers and crew of the magnificent R.R.S James Clark Ross for their provision of an excellent research platform and their kindness and adaptability in the face of difficult news.

Thanks also to members of the old "106" research group (now 102) and other companions who have provided friendship and support in (and out of) the lab. Cheers to Simon 'the dude' Coles, Andy (who wisely decided that chemistry works better in a hot country), 'Dazza' Darren, Rob, Matt, Phil 'I will never write a thesis', Paulo 'the party and topical discussion man', Vinni 'personal crisis' Cannizaro, Grady the 'antithesis of George W', Kate, Simon (the surfer), Thierry, Ana, all the visiting researchers and to all the new lads and lassies, best wishes to all for the future. Thanks also to fellow researchers in other groups, who are to numerous to mention for the good times during this research.

A very special thanks also to Sheila without whom I would not be the the person I am. It is a great personal sorrow for me that you cannot be here to celebrate this. Finally, and most importantly for me, a big thank you to Kathryn for her support, guiding influences and her patience with someone who takes a large bite out of life and occasionally get indigestion as a result. Out time together has been very special and it is my dearest wish that our dreams come true.

I shall not cease from mental fight,

Nor shall my sword sleep in my hand.

William Blake (1757 – 1827)

Authors Declaration

At no time during the registration for the degree of Doctor of Philosophy has the author been registered for any other University award. This study was financed with the aid of a studentship from the University of Plymouth and carried out in collaboration with Plymouth Marine Laboratory. The field work performed during the Atlantic Meridional Transect forms part of larger, multi-disciplinary project and the assistance of all those involved is duly and gratefully acknowledged. This study has also contributed to the Marine Science and Technology MAST project sponsored by the European Community (grant number MAS3 - CT97 - 0143, MEMOSEA).

A programme of advanced study was undertaken, which included guided reading in topics related to environmental analytical chemistry and chemical oceanography, and training in the analysis of trace metals using a variety of ultra-clean analytical techniques. Relevant scientific seminars and conferences were regularly attended at which work was often presented, external institutions were visited for consultation purposes, material prepared for publication and data prepared for dissemination *via* password-protected sites on the World Wide Web.

All data presented in this thesis (unless otherwise stated in the text) was prepared by the author, whom the ownership rests with. Before using this data in any presentation or printed publication, please contact the author and include full acknowledgements. All enquiries regarding the sampling, analysis and data preparation can be directed to:

Richard Charles Sandford
Dept. of Environmental Sciences
University of Plymouth
Drake Circus
Plymouth PL4 8AA
United Kingdom
Tel +44 1752 233128
Fax +44 1752 233035
E-mail rsandford@plymouth.ac.uk

Signed:

Date: 1/11/02.

Publications

Spectroscopic Techniques for In Situ Mapping of the Aquatic Environment, P.Worsfold, E.Achterberg, K.Andrew, S.Auflitsch, M.Bloxham, A.Bowie, S.Coles, T.David, R.Howland, F.Mantoura, T.McCormack, I.McKelvie, A.Morris, D.Peat, D.Price, R.Sandford and A.Sax in S.McLeod (Ed.), Proceedings of the 14th Australian Symposium on Analytical Chemistry, RACI, Melbourne 1997, pp 24-27.

Flow injection techniques for in situ and shipboard monitoring. P.J.Worsfold, E.P.Achterberg, A.R.Bowie, A.R.J. David, , R.F.C.Mantoura, D.Price, and R.C.Sandford, in *Proceedings of Marc'h Mor Workshop, IUEM Brest, France*, 27-31 (1997).

Flow injection with chemiluminescence detection for the shipboard monitoring of trace metals, P.J.Worsfold, E.P.Achterberg, A.R.Bowie, R.C.Sandford and R.F.C.Mantoura in M.S.Varney (Ed.), Chemical Sensors in Oceanography, Gordon and Breech, Amsterdam, 2000, 71-94.

Long Term Response of Loch Ness, Scotland, to changes in inputs from its catchment. Patrick O'Sullivan, Mick Cooper, Adriane Shine, Elizabeth Huckerby, Nina Mathews, Neil Salter, Derek Henon, Viviene Jones, Tamsin Williams, Martin Nicholson, Richard Sandford and Anthony Morris. Verh. Internat. Verein. Limnol. 27, 2307-2311 (2000).

UV digestion of seawater samples prior to the determination of copper using flow injection with chemiluminescence detection, E.P.Achterberg, C.B.Braungardt, R.C.Sandford and P.J.Worsfold, Analytica Chimica Acta, 440, 27-36 (2001).

Flow injection techniques for the in situ monitoring of marine processes, P.J.Worsfold, E.P.Achterberg, A.R.Bowie, R.Sandford, V.Cannizzaro, P.Gardolinski in A.Gianguzza, E.Pelizzetti and S.Sammartano (Eds.), Chemistry of Marine Water and Sediments, 2002, pp. 385-402, ISBN 3-540-42055-X.

Presentations and Conferences Attended

Atlantic Meridional Transect Workshop II, Plymouth Marine Laboratory (UK). February 1997.

Young Researchers Meeting and National Congress, Royal Society of Chemistry, Newcastle (UK). "Shipboard Determinations of Cu(II) in Seawater using a Novel FI-CL Manifold", poster presentation, April 1997.

MARC'H MOR International Workshop, Brest (France). "*Determination of Copper in Marine Waters*", poster presentations, paper in conference proceedings, November 1997.

Iron in the Marine Environment, Challenger Society Meeting, London (UK). December 1997.

In situ determination of copper in seawater using flow injection with chemiluminescence detection. R.C. Sandford, R.F.C.Mantoura, E.P.Achterberg and P.J. Worsfold, in *Proceedings of Marc'h Mor Workshop, IUEM Brest, France*, 227-320. (1997).

Progress in Chemical Oceanography II, Southampton Oceanography Centre (UK). "Determination of Cu(II) using Flow Injection with Chemiluminescence Detection", poster presentation, September 1998.

Young Researchers Meeting and National Congress, Royal Society of Chemistry, Durham (UK). "Shipboard Determinations of Cu(II) in Seawater using a Novel FI-CL Manifold", poster presentation, April 1998

Young Researchers Meeting and National Congress, Royal Society of Chemistry, Greenwich, London. "Shipboard Determinations of Cu(II) in Seawater using a Novel FI-CL Manifold", poster presentation, April 1999.

Contents

List of Figures

List of Tables

Glossary of Commonly Used Terms

8HQ	8-hydroxyquinoline
A/D	analogue to digital
AAS	atomic absorption spectrometry
AC	Azores current
AdCSV	adsorbitive cathodic stripping voltammetry
AMT	Atlantic Meridional Transect
ASV	anodic stripping voltammetry
AW	Amazon water
BC	Brazil current
BFCC	Brazilian and Falkland currents convergence
BraC	Brazil current
CanC	Canary current
CASS	coastal surface seawater
CC	Canary current
CCUp	Canary current upwelling
CEDAB	cetylethyldimethylammoniumbromide
CL	chemiluminescence
CRM	certified reference material
CSV	cathodic stripping voltammetry
CTAB	hexadecyltrimethylammonium bromide
CTD	conductivity, temperature and depth
CZS	colour zone coastal scanner
DOC	dissolved organic carbon
DOM	dissolved organic matter
EC	external conversion
ECSW	European continental shelf waters
EDTA	ethylenediaminetetraacetate
EF	enrichment factor
Eq	equator
ENAW	Eastern North Atlantic water
ENAWt	Eastern North Atlantic water mixed with Azores current
ENACW	East North Atlantic Central Water
ESW	Equatorial surface waters
ETAAS	electro-thermal atomic absorption spectrometry
FAAS	flame atomic absorption spectrometry
FC	Falklands current
FEP	fluorinated ethylene propylene
FI	flow injection
FMN	flavin-mononucleotide
Gdom	Guinea dome
HDPE	high density polyethylene
H-Hg	high pressure mercury
HNLC	high nutrient low chlorophyll
IC	internal crossing
ICPAES	inductively coupled plasma-atomic emission spectrometry
ICP-MS	inductively coupled plasma-mass spectrometry
IOC	Intergovernmental Oceanographic Commission
ISC	intersystem crossing
ITCZ	inter-tropical convergence zone
LOD	limit of detection

L-Hg	low pressure mercury
M-Hg	medium pressure mercury
NAA	neutron activation analysis
NAC	North Atlantic current
NAG	North Atlantic gyre
NASE	North Atlantic subtropical gyre east
NASS	North Atlantic surface seawater
NatD	North Atlantic drift
NEAOG	North-east Atlantic oligotrophic gyre
NEC	North equatorial curent
NECC	North equatorial counter current
NeqC	North equatorial current
NWAUp	North-west African upwelling
PAR	photosynthetically available radiation
PEEK	polyetheretherketone
PMT	photomultiplier tube
PTFE	polytetrafluoroethylene (Teflon®)
PVC	poly(vinyl) chloride
Q-HNO_3	sub-boiled, quartz distilled nitric acid
Q-HCl	sub-boiled, quartz distilled hydrochloric acid
SPM	suspended particulate matter
RMC	reagent mixing coil
RSD	relative standard deviation
S	salinity
SACW	South Atlantic central water
SACZ	sub Antarctic convergence zone
SAG	South Atlantic gyre
SAOG	South Atlantic oligotrophic gyre
SASh	South Atlantic shelf
SASW	Sub Antarctic surface water
SATG	South Atlantic Tropical Gyre
SeaWifs	sea-viewing wide field-of-view sensor
SeqC	South equatorial current
SST	sea surface temperature
STF	Subtropical front
Sup/Neq	south of upwelling/north of equator
SWApp	South-West approaches
T	temperature
TEPA	tetraethylenepentamine
TER	tropics and equatorial region
TSM	total suspended material
TTL	transistor-transistor logic
UHP	ultra high purity
UPM	urban particulate material
WNAW	Western North Atlanic Water

THE DETERMINATION OF COPPER IN SEAWATER USING FLOW INJECTION WITH CHEMILUMINESCENCE DETECTION

by

Richard Charles Sandford

Chapter One

Introduction

Introduction

1.1 Chemical Properties of Copper

Copper (Cu) has been utilised by humankind since the Bronze Age (5000 BC) when it was first alloyed with tin to produce bronze. The word copper originated from *Kypros*, Greek for the island of Cyprus later incorporated into Roman as *aes cyprium* (the metal from Cyprus) and the Latin *cuprum* which was later simplified to *cyprium*.

Copper is the twenty-fifth most abundant crustal element (~0.01 %) and occurs in the lithosphere mixed with other metals e.g. Ag, Pb, as copper pyrites (chalcopyrite, $CuFeS_2$), chalcocite (Cu_2S) and bornite (Cu_5FeS_4), from which the metal is refined by flotation, the sulphur then being oxidised in converters. Copper also occurs naturally as the oxide of cuprite (Cu_2O), and the carbonates of malachite (bright green, $Cu_2(CO_3)(OH)_2$) and azurite (bright blue, $Cu_3(CO_3)_2(OH)_2$) which are used as pigments. Trace impurities significantly reduce the metals conductivity and it is purified electrolytically or by heating in an air current. Owing to its softness, Cu forms more than a thousand alloys, especially brasses and bronzes (Townshend, 1995). Uses include electrical wiring (~55 %), plumbing (15 %), catalysts (CuCl, $CuCl_2$, CuO), fungicides ($CuCl_2$, CuO), printing, dyeing, pigments and paints. Copper also plays a central role in important enzymatic actions (e.g. ascorbic acid, cytochrome oxidases and tyrosinases) and is the oxygen carrier in snails, crabs and some crustaceans.

In its native form Cu crystallises in a face centred cube with close packing, the closest distance being $2.56*10^{-8}$ cm with each atom being surrounded by 12 identical atoms. Copper has two natural isotopes, ^{63}Cu (68.94 %) and ^{64}Cu (31.06 %) with eleven known isotopes. Of these ^{64}Cu has been used as a radioactive tracer. With an electronic configuration of $3d^{10}\ 4s^1$, copper is a typical transition element. In the electrochemical series Cu is below hydrogen, is attacked by halogens, oxidising acids, ammonia and KCN solutions (the latter two in the presence of oxygen), does not react with non-oxidising acids and at ambient temperatures is not easily oxidised by oxygen (Dictionary of Chemistry, 1993).

Exposure limits in the USA have been legislated for at 1 mg m^{-3} for Cu dusts and mists, and at 0.1 mg m^{-3} for Cu fumes. The maximum level for treated, potable waters is currently 3 mg L^{-1} at the tap, with the EC guide level being 100 µg L^{-1} at the treatment plant.

Table 1.1 Physiochemical Properties of Copper

Electronic configuration	$1s^2 2s^2 2p^6 3s^2 3p^6 3d^{10} 4s^1$
Relative atomic mass	63.54
Relative density	8.95
Mohs density	3.0
Melting point	1083^{O} C
Boiling point	2595^{O} C
Heat of fusion	205 kJ kg^{-1}
Heat of vaporisation	4810 kJ kg^{-1}
Standard electrode potentials	
$Cu^{2+} + 2e^- = Cu$	$E^{O} = 0.337$ V
$Cu^{2+} + e^- = Cu^+$	$E^{O} = 0.153$ V
$Cu^+ + e^- = Cu$	$E^{O} = 0.52$ V

Encyclopedia of Analytical Science, Townshend, 1995.

and 0.003 mg ml^{-1} after 12 hours in piping. The mean global sea concentration has been reported as 0.12 μg L^{-1} and for total Cu in Pacific water as 0.3-0.8 μg L^{-1} (Townshend, 1995).

1.2 Sources and Sinks of Copper in Seawater

The continental and oceanic crusts are the principle natural sources of oceanic Cu. The average crustal concentration of copper is 32 μg g^{-1} and for soils 30 μg g^{-1}. Continental crustal elements are mobilised by low temperature weathering and transported to the oceans via fluvial and atmospheric processes. Along the oceanic crust, high temperature volcanic activity mobilises materials (Chester, 2000). Glacial transport mechanisms are less significant due to the restricted nature of the polar regions. Sources of Cu to the worlds oceans have been studied for some time and although a consensus has been reached regarding the fluxes and speciation in a typical enviroment, continuing investigations e.g. in hydrothermal vents, illustrate the uncertainities that still exist.

The three primary sources of Cu to seawater are riverine, atmospheric and hydrothermal with anthropogenic Cu contributing to the first two. Figure 1.1 provides a schematic summary of the global biogeochemical Cu cycle. Anthropogenic sources are dominated by the discharge of domestic and industrial wastes and sludges into the rivers and oceans, with atmospheric inputs e.g. smelting also contributing. In localised ecosystems the influence of anthropogenic inputs can dominate natural inputs. The interpretation of the biogeochemical cycling of Cu in seawater requires knowledge of its sources and sinks, its individual species, especially the bio-available fraction, and their concentrations and oceanographic processes.

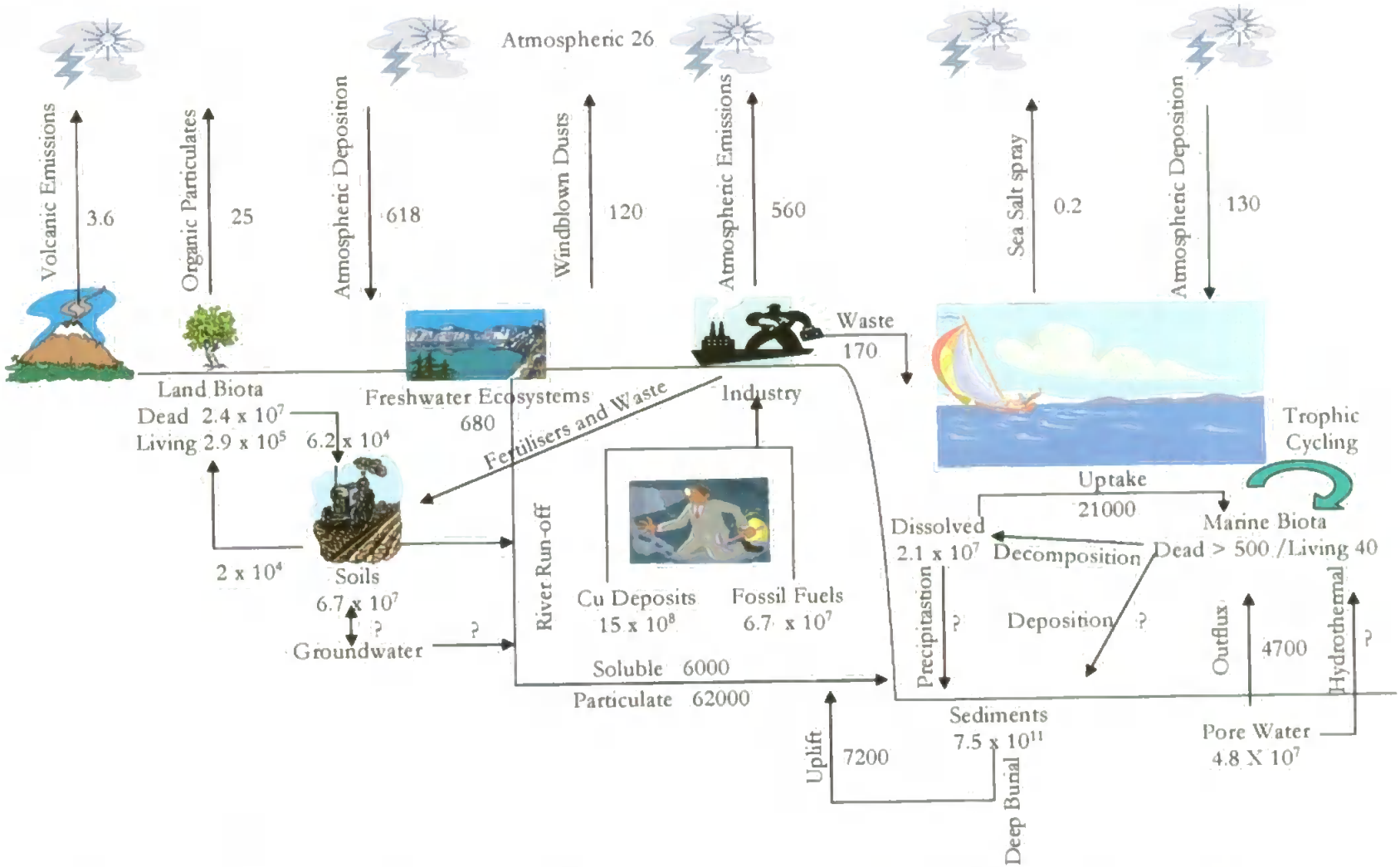

Figure 1.1 Global Biogeochemical Cycle of Cu: (g x 10^8 y^{-1}) Cu from industrial and fossil fuels has a global atmospheric flux of 2,630 x 10^8 g y^{-1} compared to 193 x 10^8 g y^{-1} from continental dust and volcanic dust (Benjamin and Honeyman, 1992).

1.2.1 Riverine Sources

The terrestrial flux of Cu to oceanic reservoirs is dominated by riverine inputs (Figure 1.1), which historically were thought to be several hundred times greater than either atmospheric or anthropogenic sources (Chester, 2000). The concentration of Cu in river waters is influenced by the geology of the river catchment and chemical constraints within the water system, especially particulate-dissolved equilibria involving inorganic and biotic suspended particulates. These processes are influenced by physico-chemical parameters such as pH, concentrations of the complexing ligands, anthropogenic inputs and the riverine particulate fraction. The dissolved phase of Cu consists of the free Cu(II) ion, inorganic and organically complexed Cu, and Cu associated with the colloidal phase. Dissolved Cu in river waters ranges from 0.3 to 6.3 $\mu g\ L^{-1}$ (Chester, 2000) although the latter represents the river Rhine, an anthropogenically influenced source. The crystalline, metal oxide and organic host fractions are the principal particulate trace-metal carriers in rivers that receive their trace metals from natural sources, with Cu in the particulate phase ranging from 30 – 266 $\mu g\ kg^{-1}$ although the majority of rivers have </=100 $\mu g\ kg^{-1}$. Estimates of the net global riverine flux of Cu to the world's oceans vary by an order of magnitude for the dissolved phase from $0.06 \times 10^{12}\ g\ y^{-1}$ (Chester, 2000) to $0.6 \times 10^{12}\ g\ y^{-1}$ (Benjamin and Honeyman, 1992). In the particulate phase the net global riverine flux of Cu varies from $0.155 \times 10^{12}\ g\ y^{-1}$ (Chester, 2000) to $6.2\ g\ y^{-1}$ (Benjamin and Honeyman, 1992).

Before reaching coastal or open ocean regions, fluvial material must pass through the estuarine environment which can act, mainly due to dissolved-particulate reactions, as a filter modifying the fluvial Cu signals. The modifications can vary widely from estuary to estuary. Cu can display both conservative and non-conservative behaviour (Chester, 2000), depending on the particular estuary under investigation. Approximately 90 % of the particulate phase is trapped in the estuarine environment which, in association with other processes e.g. flocculation, is reflected in the reduced levels of Cu in seawater (Chester, 2000).

1.2.2 Atmospheric Sources

Seawater receives atmospheric inputs from the mineral dust veil over the oceans, which originates from aeolian transported anthropogenic and crustal material. Atmospheric input of Cu is dominated by particulate matter, 90 % of which originates from smelting, fossil fuel burning and other human activities. Urban and crustal aerosol end-members can be distinguished by different partitioning signatures for Cu. Approximately 15% of Cu in

aerosol urban particulate material (UPM) is refractory compared to 80 % in a crustal sample. In addition, a much greater proportion of UPM Cu is loosely bound, reflecting the often high temperature origin of Cu in aerosols and its subsequent association with particles < 1μm (Chester, 2000) that consequently can travel further than larger diameter crustal particles. Anthropogenic Cu forms ~ 90 % of atmospheric Cu in the Northern Hemisphere, reflecting its urban and industrial origins, in comparison with ~ 10 % from this source in the Southern Hemisphere. Waters close to urban areas are thus likely to be significantly influenced by anthropogenic sources. The loosely bound fraction of Cu was reported as decreasing on a N/S transect from the European coast due to aeolian dispersion e.g. in the North East Trade winds (Chester, 2000). Ambient levels for Cu in rain in clean areas have been reported as 0.4 - 2.3 μg l^{-1} and in urban snow 15 - 70 μg l^{-1}, in comparison with remote pristine locations of 2 ng l^{-1}, e.g. Hawaii in 1972 (Chester, 2000).

Chester (2000) concluded that in coastal regions, solubilisation from atmospheric particulates can play a significant role in governing the trace metal burden of the surface water, especially in the North Atlantic. Unlike riverine fluxes, which can undergo transformation and be retained in estuarine and coastal waters, atmospheric Cu fingerprints imposed on dissolved trace metal distributions are often more apparent away from the immediate coast. Therefore, they can be a significant contributor to surface seawater Cu levels, especially in remote oceanic regions. These aspects are discussed further in relation to field deployment in Chapter 5.

1.2.3 Hydrothermal Sources

Hydrothermal plumes have only more recently been recognised as potentially significant sources of trace metals to the global oceans. Tectonic plate activity at spreading seabed ridges results in black smokers that are characterised by the release of high temperature (> 350 ^{o}C) acidic, metal and sulphide rich hydrothermal solutions that have enhanced Cu levels and can be a significant contributor to oceanic Cu. At intermediate temperatures, the entrainment of Cu in seawater causes a fraction of Cu to precipitate out as insoluble fine-grained sulphides (the black smoke) and oxides of Cu, although the acid plume also retains some Cu in solution. Values of Cu in such plumes vary from < 0.02 μmol kg^{-1} up to 35 μmol kg^{-1}, in comparison to a mean of ~ 0.007 μmol kg^{-1} for seawater, with the average high temperature system reported as contributing 3.0 – 13 x10^{8} mol $year^{-1}$ (Chester, 2000).

1.2.4 Sinks

A major sink for Cu in seawater is its association with suspended particulate material (SPM), both biogenic and lithogenic in origin. The vertical distribution of SPM through the water column comprises a surface layer, where SPM concentrations are highest and more variable in nature, followed by a clear water minimum layer where SPM undergoes vertical movement by advective processes or becomes degraded. At the base of the water column a deep water layer exists in which resuspension of bottom sediments can take place.

The oceanic concentrations of copper associated with the SPM have been determined at 145 mg g^{-1} in surface waters and 200 mg g^{-1} in deep water (Buat-Menard and Chesselet, 1979). The down column flux of copper associated with the total suspended material (TSM) in the sea varies from 56 to 7000 ng cm^{-2} $year^{-1}$, depending on the ocean and the depth (Chester, 1990). Two further major sinks for Cu are biological uptake and organic complexation (Section 1.2.3). In the surface ocean, biogenic material interacts with dissolved and particulate Cu from fluvial and atmospheric inputs. Cu in seawater is both an essential micronutrient with nano- to pico-molar optimums for organisms, but can also act as a toxicant at levels above this, as discussed below.

1.3 Marine Biogeochemistry of Copper

Riverine waters reflect the composition of the end-member rocks over which the water has flowed and consequently have a higher dissolved Cu concentration than seawater (Chester, 2000). River water and seawater also differ in their ionic composition and concentration of inorganic complexing ligands, with Ca^{2+} and HCO_3^- dominating in the former, and Na^+ and Cl^- in the latter (Chester, 2000). When river waters mix with higher salinity seawater, the Ca^{2+} and Mg^{2+} in the latter can displace trace metals from the organic material, reducing the fraction of Cu complexed. This is less significant for Cu than for other metals, reflecting the Irving-Williams series with regard to the strength of metal binding to humic materials (Mg < Ca = Cd < Mn < Co < Zn < Ni < Cu < Hg). Up to 40 % of the dissolved Cu in river waters can undergo flocculation when mixing with seawater.

1.3.1 Redox Speciation and Bioavailability

In oxygenated seawater, total dissolved copper comprises the free Cu(II) ion with its associated hydration sphere, $Cu(H_2O)_6^{2+}$ dissolved organic, inorganic and colloidal fractions (Apte and Batley, 1995). The naturally occurring valencies of Cu are +1 and +2,

with +3 only being found in synthetic compounds. In seawater Cu(II) is the bio-available form and therefore more influential on marine life than other forms, although it comprises < 0.5 % of total Cu (Sunda and Huntsman, 1991), with organically complexed Cu making up 96 – 99.5 % of total Cu (Section 1.3.3). Figure 1.2 is a schematic of the speciation of Cu in seawater.

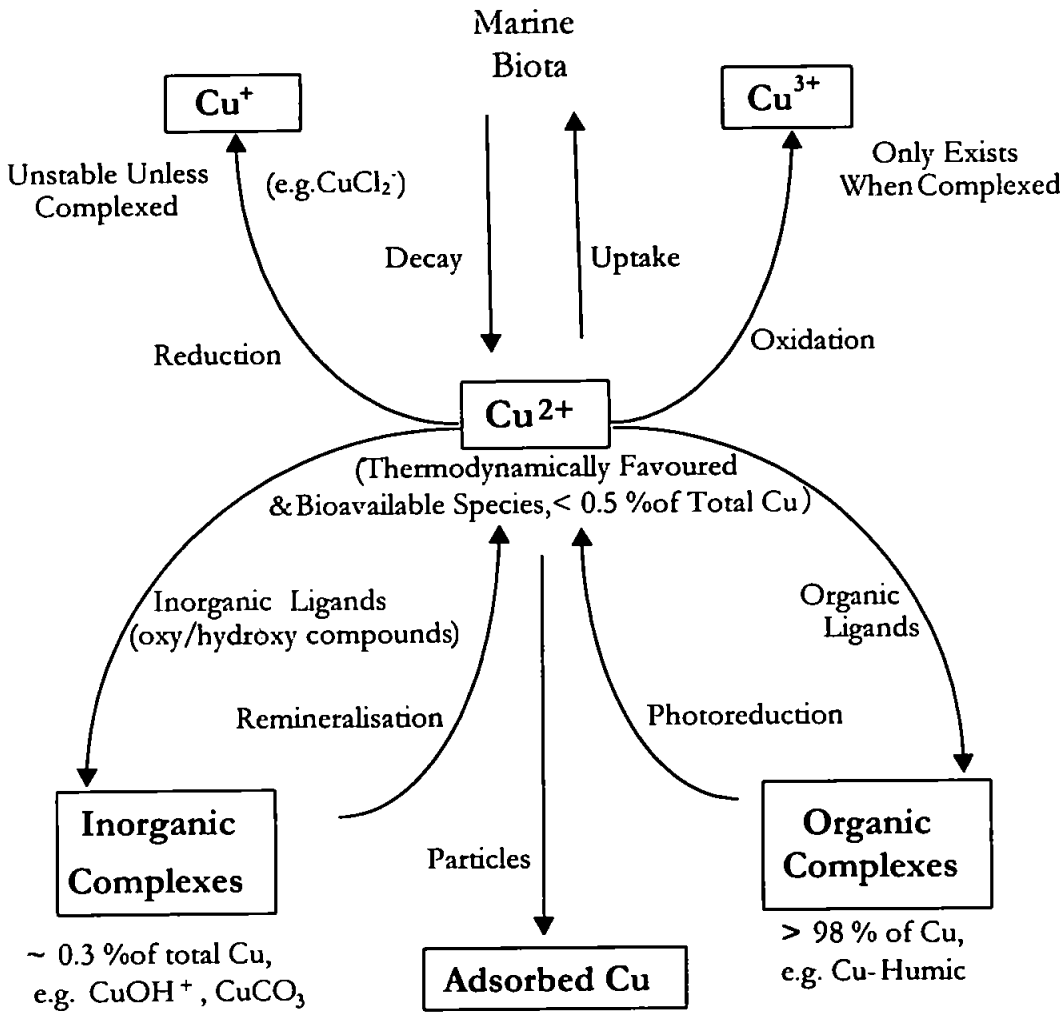

Figure 1.2 Schematic of Cu Speciation in Seawater.

Cu(I) is unstable, forming Cu(0) and Cu(II) in seawater due to the disproportionation reaction (equilibrium constant (K) of $1.1*10^6$ l mol^{-1}).

$$Cu(I) \longrightarrow Cu(O) + Cu(II)$$

Stabilisation of Cu(I) can occur by complex formation e.g. with cyanide or by the formation of insoluble chlorides (CuCl) and iodides (CuI) which are colourless or pale yellow. Moffett and Zika, (1985) reported the photo-oxidative induced formation of Cu(I) and the reduction of Cu(II) by hydrogen peroxide in seawater.

Copper(II) salts have a Jahn-Teller distorted co-ordination, with 4 near, plus 2 far neighbours and forms many complexes, especially with nitrogenous ligands. Cluster compounds, e.g. $Cu_4I_4(PMe_3)_4$, and Cu-Cu bonding can be found in many Cu(II) derivatives. Cu(III) is a strong oxidant, which does not exist in aqueous solution unless stabilised through complexation. Copper(III) is also found in complex oxides and fluorides and amino compounds.

The amount of Cu(II) in seawater is determined largely by the formation of stable inorganic and organic complexes which influence its bioavailability, toxicity and mobility (Stumm and Morgan, 1996; Buffle, 1988; Mantoura, 1981). Complexation of Cu(II) minimises its reduction and accelerates the oxidation of the Cu(I) species. Ambient concentrations of Cu(II) of 0.1 - 6 nM have been reported in seawater (Coale & Bruland 1988), with reported optimal biotic concentrations of $10^{-12.4}$ - $10^{-13.4}$ M (Coale and Bruland, 1990; Moffett and Zika, 1987). These values have been shown to hold true even for estuarine environments, where increased levels of copper correlate with reduced salinity and raised ligand concentration (Nelson, 1985; van den Berg and Nimmo, 1986). Concentrations of Cu(II) in surface waters of coastal and shelf regions have been observed at 1.4 nM in the Pacific, 4 nM in the Atlantic, 1.6 nM in the Arctic and 2.5 nM in the Antarctic (Capodaglio *et al.*, 1994). Anthropogenic Cu inputs from mine waste, sewage and antifouling paints can often exceed natural fluvial and aeolian inputs. Such sources contribute to the raised Cu levels in coastal and estuarine waters (10-20 nM) and make a significant contribution to the µM levels found in some perturbed estuarine systems e.g. the River Fal in Cornwall, UK.

Reported vertical profiles of Cu in seawater have described primary surface water input, nutrient type surface water depletion, removal in the upper water column due to biological uptake and scavenging onto SPM (both biogenic and lithogenic in origin). Regeneration of Cu from intracellular and particulate processes occurs at different points through the upper water column (0 – 250 m) e.g. at the thermocline. Intermediate and deep-water scavenging and benthic regeneration of Cu also occurs (Chester, 2000). Typical upper water column (0 - ~300 m) depth profiles for Cu at three stations in the North East Atlantic are shown in Figure 1.3. The sites are presented to demonstrate the oceanographic consistency of the Cu data obtained by FI-CL during this study (Atlantic Meridional 9 (AMT 9)) research cruise (Chapter 5) with comparable surface water data from geographically similar waters during the same season i.e. late summer/early autumn. The

equivalent AMT 9 stations were for profile a) – AMT 902; profile b) mid way between AMT 904 – AMT 905 and profile c) - AMT 906.

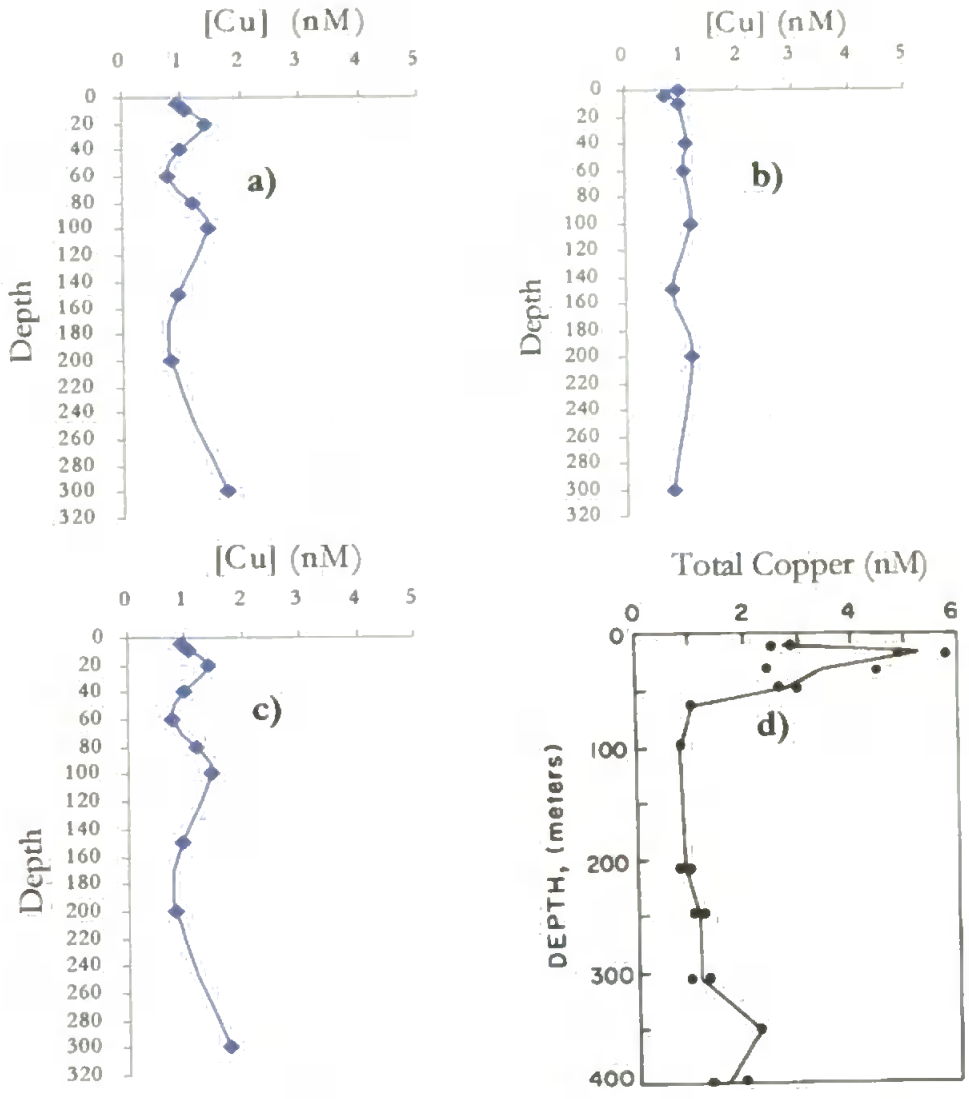

Figure 1.3 Typical Cu Depth Profiles through the Upper Water Column of the Atlantic. Profiles a), b) and c) derived from raw data from Saager *et al.*, 1997 - Joint Global Oceanographic Flux Study (JGOFS) research cruise of late summer 1989 in the North East Atlantic. **a)** Site 4, JGOFS 1, station 21/22 at 46° 59′ N, 20° 00′ W; **b)** Site 5, JGOFS 1, station BM3 at 40° 30′N, 20° 03′ W; **c)** Site 6, JGOFS 2, station BM4 at 32° 58′ N, 19° 58′ W. **d)** from Zuehlke and Kester, 1985) - Western Northern Atlantic.

These profiles illustrate the relative consistency of Cu data through the Atlantic, although it can be seen that there is considerable fluctuation in concentration through the upper water column. Historical Cu data and the oceanographic processes that influence the surface water concentrations and depth profile of Cu are discussed in Chapter 5.

1.3.2 Inorganic Complexation

In oxygenated seawater the major inorganic ligands e.g. Cl^-, SO_4^{2-}, CO_3^{2-}, OH^-, organic ligands e.g. humic and fulvic acids and suspended particulate matter (SPM) compete for complexation of Cu. The inorganically complexed fraction of Cu in seawater, which accounts for 0.05-0.27 % of total Cu, (Buckley and van den Berg, 1986) is made up of dissolved chloro-, carbonato-, sulfato-, oxo-, and hydroxo complexes. Figure 1.4 illustrates the interactions of Cu(II) in seawater.

These interactions are governed by three physico-chemical variables, namely ionic strength, pH and the character of the complexing ligands. Seawater has an ionic strength of ~ 0.7 M, a mean pH of 8.2 compared with a lower although variable ionic strength, and a pH of 5 - 8 in riverine and estuarine waters. Table 1.2 illustrates the various inorganic forms of Cu in seawater expressed as a percentage of the total inorganic Cu.

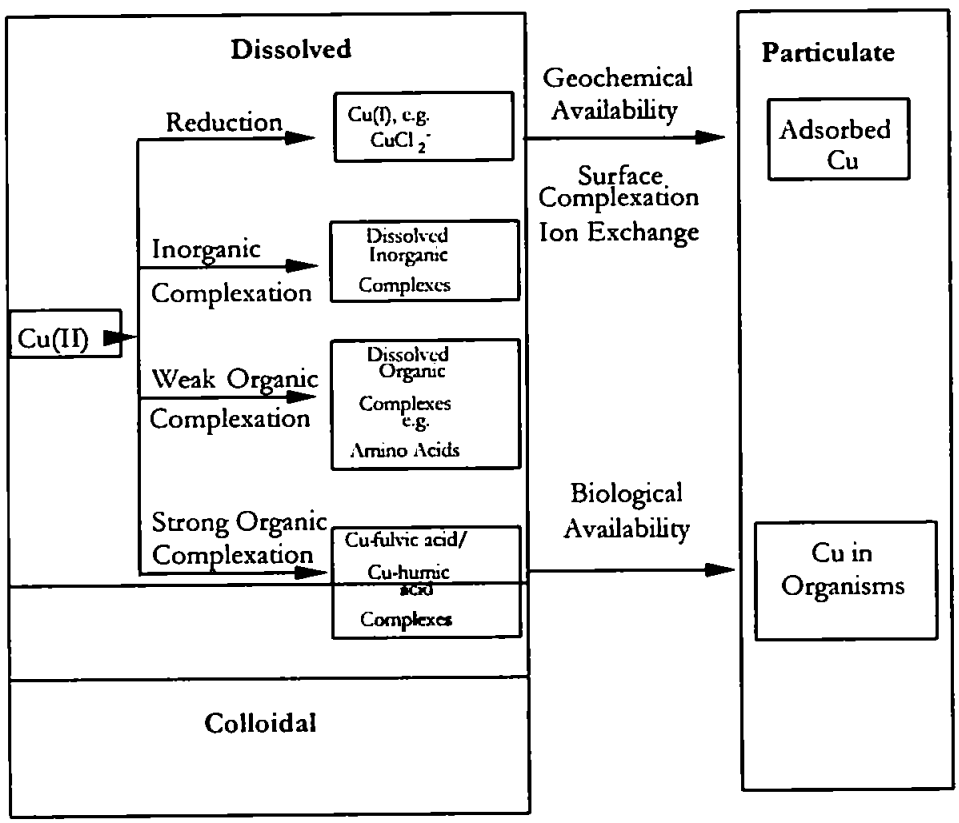

Figure 1.4 Interactions of Cu(II) in Natural Waters

Butcher *et al.*, (1992) also reported that the inorganic speciation of Cu in seawater is dominated by $CuCO_3$ and $CuOH^+$, with total dissolved Cu having a mean seawater

Table 1.2 Inorganic Speciation of Cu(II) in Seawater as % of Total Inorganic Fraction	
Cu^{2+}	3.9
$Cu(OH)^{+}$	4.9
$Cu(OH)_2$	2.2
$CuSO_4$	1.0
$CuCO_3$	73.8
$Cu(CO_3)_2^{2-}$	14.2
$CuHCO_3^{+}$	0.1

Source Turner *et al*, 1995

concentration of 120 ng kg^{-1}. At the surface (pH 8.2, 25° C) the free Cu(II) ion can be 4-5 % of the total inorganic Cu. At increased depth, where the pH and temperature decrease (pH 7.5, 5 °C), the free Cu(II) contribution to the total inorganic Cu fraction may be greater than 30% (Byrne *et al.*, 1988). Sulphide complexation may also contribute significantly to the total inorganic Cu fraction (Cutter and Oatts, 1987; Elliott, 1988; Dyrssen, 1988) but data on this is limited.

1.3.3 Organic Complexation

The largest fraction of dissolved Cu in seawater is organically complexed (90-99 % of total Cu, van den Berg *et al.* 1986; 99.7-99.95 %, Sunda and Huntsman, 1991) although this fraction has only been partially characterised, especially in reference to operational parameters such as pH, conductivity and salinity. In riverine, estuarine and coastal waters, terrestrial fulvic and humic compounds make up a large proportion of the organic complexes, with in-situ supplementation of organic ligands in the oceans by intra-cellular exudation.

The organic ligands which complex Cu and other trace metals in seawater have been classified as weak ligands (conditional stability constant $K_{CuL} = 10^{7-11}$) usually restricted to the upper or mixed layers of the oceans, together with strong ligands (conditional stability constant $K_{CuL} = 10^{12-15}$) found throughout the water column (Moffett *et al.* 1990; Robinson and Brown, 1991). Coale and Bruland, (1988, 1990) reported a concentration of 2 nM for the stronger ligand L_1 (log $K_{CuL} = 11.6$), which coincided with a maximum in primary production and chlorophyll in surface waters, with a concentration of 5 – 10 nM for a weaker ligand L2 (Log $K_{CuL} = 8.6$) that was distributed throughout the water column. The variation in Cu speciation at different depths in the Pacific was due to the weaker ligands that predominate at depths of ~ 1000 m. These authors found a seasonal correlation between the distribution of the strong Cu complexing ligands and the

depth of the mixed layer, suggesting a ligand source in the lower mixed layer. Ligand concentrations were reported as varying only by a factor of two between all stations and to result in a reasonably constant Cu(II) concentration of ~ 10^{-14} M in surface waters and to ~ 10^{-11} M at depth, effectively buffering the Cu(II) activity in seawater and suggesting a regulated ligand production mechanism. Moffet and Zika, (1987) reported similar results.

Apte *et al.*, (1990) also reported the complexation of Cu in seawater by ligands of varying affinity for Cu, with ligand concentrations ranging from 20 nmol L^{-1} (log K_{CuL} > 14) to 70 nmol L^{-1} (log K_{CuL} > 8). These authors also found ligands with a strong affinity for Cu in estuarine waters (complexing capacity of > 200 nmol L^{-1}), with freshwaters exhibiting a mixture of weak and strong ligands, although a complexation capacity of > 200 nmol L^{-1} was also found. Where very low aquatic metal concentrations exist (< 1 nmol L^{-1}), complexation was found to occur at sites exhibiting the strongest binding for the metal e.g. log K_{CuL}>11 for Cu (Mota and Correia Dos Santos, 1995).

The inorganic/organic speciation of Cu affects the extent of particle interactions and therefore the conservative/non-conservative behaviour of Cu. In seawater, organic complexing of metals such as Cu is constrained by competition for the ligand from Ca(II) and Mg(II) and inorganic complexation of the metals. Organic complexation of Cu reduces its adsorption onto particulate surfaces and therefore the extent of its particle scavenging, which itself induces non-conservative behaviour. This is important in controlling the transport of dissolved Cu out of the estuarine environment. In support of this Huizenga and Kester, (1983) found that for total and labile Cu, during a North West Atlantic shelf transect (unfiltered samples), a linear relationship (i.e. conservative behaviour) existed between total Cu and salinity, with < 5% of total Cu being in a labile form. This conservative behaviour may reflect the fact that the non-labile Cu (e.g. organically complexed species) is less affected by particle scavenging and biological uptake than the free Cu(II) ion.

The copper complexing capacity of marine waters was found to alter in the order of inner shelf > outer shelf > open ocean, a trend that correlates with decreasing dissolved organic carbon (DOC) and a reduction in suspended particulate matter concentrations (Mantoura, 1978). The same author also reported that Cu in seawater was found to be associated with dispersed colloids and with the surface of suspended particulate matter.

1.3.4 Micronutrient and Toxicological Aspects

Copper is a metabolically essential metal for virtually all organisms, being essential to growth at low, but variable concentrations but also toxic at higher concentrations that also vary. Copper is included in several proteins in which it is co-ordinated to N, S or O containing ligands. The toxicity of Cu has been utilised to reduce marine growth of unwanted algae and fungi in natural waters. Gledhill *et al.*, (1997) reviewed the speciation and toxicological aspects of Cu in seawater. It can act as an electron donor/acceptor in enzyme reactions and is involved in electron transport mechanisms in photosynthesis. Copper has also been shown to inhibit photosynthesis (Rijstenbil *et al.* 1994), disrupt electron transport in the photosystem II (Shio *et al.*, 1978), reduce nitrate uptake and the production of nitrate reductase (Harrison *et al.*, 1977), disrupt gametophyte development (Garman *et al.*, 1994), restrict growth (Florence and Stauber, 1986; Lage *et al.*, 1994), decrease pigment concentrations (Lage *et al.*, 1994; Stauber and Florence, 1987), affect the permeability of the plasma membrane (De Filippis, 1979), and alter the isotopic distribution of lipids, sterols, sterol esters, and free fatty acids (Lage *et al.*, 1994; Stauber and Florence, 1987).

Gerringa, *et al.*, (1995) and Grashoff, *et al.*, (1999) found an optimal Cu(II) concentration of 10^{-11} to 10^{-14} M for diatoms, with a 40 % reduction in diatom growth reported at a 10^{-14} and growth ceasing between $10^{-8.6}$ M (Sunda and Guillard, 1976) and 10^{-7} M (Rueter and Morel, 1981). Copper can cause inhibition of growth of dinoflagellates at $< 10^{-13}$ M, with a decrease in fecundity and even death at higher levels. The toxicological aspects of Cu(II) have been attributed to its competition for metals at active sites in enzyme systems or forming complexes with proteins and nucleic acids rendering them non-functional. The toxicological effects of Cu result from concentrations that are several orders of magnitude less than ambient seawater levels. Sunda *et al.*, (1981) also found the addition of Cu to a natural water resulted in a shift from diatoms to green flagellates. This illustrates the variable micronutrient and toxicological responses of marine biota to trace levels of Cu. This may help to explain why certain areas of the worlds oceans e.g. Equatorial Pacific and Southern Ocean have high macro-nutrient levels (e.g. N or P) but are low chlorophyll (HNLC) areas.

The bioavailability and toxicity of Cu is thus directly related to its speciation, primarily the activity of the dissolved free Cu(II) ion (Sander *et al.*, 1983; Andrew *et al.*, 1977). Phytoplankton in seawater discriminate against the strongly complexed forms of Cu, especially the organically complexed (non-labile) species, preferring the free Cu(II) ion and

weakly complexed labile forms (Bernhard and George, 1986). Thermodynamic modeling has suggested the Cu complexation by inorganic ligands is not strong enough to detoxify Cu(II) ions. However, the addition of acetate, proline, cysteine or EDTA results in a much reduced toxicological effect of Cu (Cabral, 1994), suggesting that the presence of DOM and the intracellular exudation of organic ligands in natural waters can also reduce the toxicity of Cu(II). Sunda and Hunstman, (1995), reported strong evidence of regulation of Cu concentrations in remote oceanic nutriclines by phytoplankton uptake and regeneration processes. These aspects are discussed in more detail in relation to field deployment in the Atlantic (Chapter 5).

1.4 Sampling and Analytical Methods for the Determination of Copper

It is clear that in order to more fully understand the biogeochemistry of Cu(II) in marine processes accurate, systematic determination of Cu(II) at subnanomolar levels is required, ideally with a wide temporal and spatial spread. A number of analytical methods for Cu in natural waters have been developed although not all are suitable for seawater analysis. However, homogenous and representative sample collection utilising trace metal clean protocols is a vital first step on which the validity of the data for all methods is dependent.

1.4.1 Contemporary Sampling Protocols

Reported Cu levels have varied for the same waters, a factor that has limited reliable inter-comparisons and reduced the ability to distinguish between environmental variability and analytical data quality. Sampling and storage is a critical component of any trace metal determination due to the potential for contamination, species alteration, and/or systematic errors degrading analytical accuracy and precision. Ideally, a sampling protocol will be frequent enough to avoid biases from dynamic marine biological processes. The choice of the sampling equipment can also dictate sample validity and different sampling techniques can introduce biases. The series of workshops on the Intercalibration of Sampling Devices, organised by the Intergovermental Oceanographic Commission (IOC) (Crompton, 1989), helped minimise these biases. The workshop identified that the major contribution to variation in trace metal values was due to analytical artifacts between various laboratories, with a smaller fraction of the variation due to the choice and use of sampling devices. The workshop also concluded that an ideal sampler for vertical profiling of the water column should be based on large volume plastic samplers with metal

components replaced by silcone, suspended on a non-metallic coated rosette frame utilising Kevlar® hydroline. A typical conductivity-temperature-depth (CTD) carousel used for sample collection is shown in Figure 1.5.

Figure 1.5 Sea Bird SBE 32 Carousel Water Sampler with a high quality, epoxy coated stainless steel carousel frame, fitted with 12 grey poly(vinyl) chloride (PVC), Teflon® lined, free flushing water sampler bottles (Ocean Test Equipment Inc., model 110, 12 L capacity) fitted with latex tubing spring closures, with silicone 'O' rings and seals and HDPE plastic drain valves to minimise metal contamination.

During storage, sample integrity can be affected by a number of factors including the adsorption of surface active Cu onto container walls, photolysis through exposure to sunlight, the production of highly reactive species e.g. enzymes derived from biologically mediated reactions, and changes in pH through the addition of mineral acids. Biological activity and hence Cu uptake/regulation of concentration can be enhanced through the 'bottle effect' whereby the increased surface area promotes multiplication of the previously free floating and relatively slow growing bacteria (Jannasch and Pritchard, 1972). Also affecting sample integrity are the presence of dissolved material (e.g. salinity, hardness), complexing agents, dissolved gases, especially oxygen (redox alterations) and suspended matter (sorption processes). Physical factors e.g. temperature, light and agitation also affect

sorption losses. Biological activity and sorption losses can be effectively minimised by sample acidification.

Capodaglio *et al.*, (1994) reported an international intercomparison of sampling devices (Go-Flo, Niskin, van Dorn and Ruttner) of varying capacity (2-30 L) and different sample collection procedures in Mediterranean waters. Results showed that samplers became progressively cleaner with continued use, especially for sampling protocols that incorporated a washing cycle. Results also improved when using high-capacity samplers due to the reduced contact surface/volume ratio, which can affect sample integrity during storage.

Cu in seawater can be associated with SPM, colloidal matter and organic and inorganic complexes and thus an operational definition of the size fraction by filtration will affect the subsequent analysis. Scarponi *et al.*, (1982) reported that acid cleaning of filters used for sample filtration during field deployment minimised leaching in comparison with uncleaned filters. The ability to perform shipboard analysis minimises storage, subsequent preservation, transport and processing artifacts and reduces anomalies due to the use of different analytical methods and personnel. Field based measurements can also provide near real time high resolution data with the opportunity to modify onboard research strategy according to the results obtained and to identify and eradicate sampling problems. These are considerable advantages over sample collection and subsequent shore based determinations using one of the laboratory analytical methods available for Cu in seawater.

1.4.2 Overview of Analytical Methods for Copper in Seawater

The advent of ultra-clean techniques has promoted the development of reliable Cu methodologies for the determination of dissolved and particulate Cu in seawater. A variety of analytical techniques e.g. ICP-MS, ET-AAS have been used based on shipboard sampling, filtration and acid preservation of 0.5 - 1 L volumes of seawater followed by shore based analysis. These require a dedicated shore based laboratory, with stable power supplies, air extraction and cooling systems. The seawater matrix can inhibit selectivity and even damage instrumentation. Therefore, Cu is often isolated from the complex seawater matrix using an extraction stage that may also preconcentrate it to enable trace level (sub nM) determination. High instrumental sensitivity and selectivity for Cu are priorities for analytical methods. Classical methods based on gravimetry and titrimetry for Cu do not have sufficient sensitivity for use in seawater, with LOD's significantly above ambient Cu levels in seawater. Furthermore, the seawater matrix can often cause selectivity problems, with such methods not being ideally suited to incorporation into FI systems or amenable to

automation for continuous monitoring. Shore based instrumental methods with increased sensitivity compared to classical methods are discussed below.

1.4.3 Electro-thermal Atomic Absorption Spectrometry (ETAAS)

Atomic Absorption Spectrometry (AAS) has a wide application for the determination of total metals (Imdadullah 1994; Nakamura *et al.* 1994; Groschner and Appriou, 1994), especially transition metals in seawater (Grashoff *et al.*, 1999), being relatively free from spectral interferences. However, Flame AAS (FAAS) has insufficient sensitivity for many trace metals including Cu and it often requires preconcentration and matrix elimination. ETAAS utilises a graphite furnace and has two or three orders of magnitude greater sensitivity than FAAS and requires only a small sample volume (e.g. 10 – 50 µl). However, it is limited by the volatilisation of the high salt seawater matrix, which causes spectral and chemical interferences and results in poor precision and degrades LODs. Chemical and physical interferences can be reduced by the use of high quality graphite materials and accurate background correction techniques (Slavin *et al.*, 1984). Matrix separation and preconcentration steps are also required.

ETAAS with preconcentration has sub-nanomolar LODs for Cu, e.g. 0.016 nM (Zhuang and Hong, 1992); Nakamura *et al.*, 1994), 0.27 nM (Sperling *et al.*, 1992), 0.038 nM (Liu and Huang, 1992), 0.34 nM (Garcia *et al.*, 1993). Without preconcentration, ETAAS for a single injection has a typical LOD of 5.5 nM and for multiple injections an LOD between 1.1 nM (Huang and Shih, 1993) and 17.0 nM (Garcia *et al.*, 1993). Instrument size, stability of electrical power, movement, transport and safety of use issues that preclude its shipboard deployment for the determination of Cu.

1.4.4 Inductively Coupled Plasma-Atomic Emission Spectrometry (ICP-AES) and Inductively Coupled Plasma-Mass Spectrometry (ICP-MS)

Although ICP-AES is a multi-element technique, it is not sensitive enough for the determination of Cu in seawater (Grasshoff *et al.*, 1999). ICP-MS is a fast, highly sensitive technique, with a linear calibration range often over five orders of magnitude and a multi-element and multi-isotope capability. It is a total metal method, requiring solubilisation of the metal. Major disadvantages are high costs of the instrument and interference from the seawater matrix that commonly necessitates matrix separation to eliminate seawater matrix deposition on the sampling interface (the sampler and skimmer cones and the ion lenses). This reduces instrument sensitivity and long term stability. Bloxham *et al.*, (1994) using ICP-MS with Metpac CC-1 separation reported an LOD of 1.4 nM for Cu whilst Lan and

Yang, (1994), deploying ICP-AES with preconcentration, achieved an LOD of 1.1 nM for Cu. However, ICP-MS has high running costs due to argon consumption which, coupled to the instrument size, the requirement for stable high-power supply, dedicated laboratory facilities and instrument transportation and safety issues preclude its use shipboard for determination of Cu in seawater. Both ETAAS and ICP techniques also require specialised engineers to make effective repairs when at sea, further limiting their field deployment.

1.4.5 Voltammetry

Voltammetric techniques have been used for the determination of Cu in seawater, and their relative merits and deficiences are discussed in more detail in Section 1.6.1. They have the advantage, over the methods discussed up to this point, of being field deployable and therefore capable of near real time data acquisition. This eliminates the generation of analytical inaccuracies through species preservation protocols and storage effects. In voltammetry the voltage to the working electrode potential is controlled or scanned whilst the current generated from oxidation and reduction reactions is measured at a working electrode.

In anodic stripping voltammetry (ASV) species preconcentrated on the mercury drop and then oxidised and the oxidation current measured, whilst in cathodic stripping voltammetry (CSV) the elements are reduced during the potential scan and the reduction current measured. An important step in any voltammetric technique is the prconcentration step. CSV is more commonly used for the determination of Cu, during which, the Cu (after the addition of a ligand and appropriate buffering) is preconcentrated by adsorption onto a Hg electrode as a surface active complex that is produced by the ligand/species interaction. Salicylaldoxime is a commonly used ligand for copper with a borate buffer (pH 8.5), resulting in an LOD of 0.1 nM (Campos and van den Berg, 1994).

1.4.6 Spectrophotometric Techniques

Spectrophotometric methods are generally fast and precise and can be applied directly to seawater samples although only at elevated trace metal concentrations, typically in the μM to nM range, the former occurring in anoxic waters of the deep ocean close to active hydrothermal regions. Islidak *et al.*, (1999) reported the spectrophotometric determination of Cu(II) in seawater with an LOD of 15.7 nM. This lack of sensitivity makes it an unsuitable technique for Cu at sub-nanomolar concentrations in seawater.

1.4.7 Other Techniques

There are other methods that have been used to determine Cu at the low nanomolar level although they each have their disadvantages. Neutron Activation Analysis (NAA) is an absolute method that is matrix independent. Rao and Chatt, (1993) reported an LOD for Cu of 3.9 nM for NAA, with successfully determination of Cu in the certified reference material (CRM) CASS-2. However, to map the subnanomolar Cu concentrations in seawater this method is not sufficiently sensitive and has significantly more field deployment problems than AAS, ICP-MS and other shore based methodologies due to the requirement for a nuclear reactor.

Ion chromatography combines matrix isolation and preconcentration and depending on the detector, has a reported LOD of 80 nM (Caprioli and Torcini, 1993), although Paull *et al.*, (1994) reported the accurate determination of Cu in the CRM CASS-2 (low nM Cu). Thus, it also is not sensitive enough for the subnanomolar concentrations of Cu in seawater. Gas chromatography is of limited use for the determination of Cu in seawater due to the volatile organic metal chelates or derivatives being unstable at the temperatures required for sufficient volatilisation. However, it is does have high sensitivity, requires only small sample volumes, has relatively low instrument costs and the capability of providing near real time analysis.

1.5 In-line Solid Phase Matrix Separation

Matrix separation and preconcentration by solid phase extraction offers the advantages of a fast separation/preconcentration step, incorporation as an on-line stage into FI, simple operation and mild experimental conditions. Chelating resins have been used for matrix separation of which MetPac® (iminodoacetate group) and Cellex P (cellulose phosphate ester group) are examples. Micro-columns have also been used to isolate analytes and often consist of a solid inert backbone onto which active groups are immobilised. Although micro-columns are of smaller size than those commonly used for MetPac® and Cellex P and therefore of lower total capacity, this aspect is unlikely to be exceeded at the sub-nanomolar levels of Cu found in seawater. Micro-columns utilise mild eluents unlike the harsh eluting conditions required by many alternative resins, provide an eluent that is matrix matched with the reagents in use and require minimal use of new reagents, thus reducing the risk of introducing contamination. In addition, the analyte ions are often eluted in a free, uncomplexed form from micro-columns. In comparison to batch or continuous flow systems, micro-columns offer higher enrichment factors (5-50 greater), a high sampling frequency coupled with short operational times (10-200 s per

determination) than MetPac or similar columns. In comparison to batch or continuous flow systems, micro-columns, although often of much smaller capacity than batch procedures, offer a low consumptive index for samples and reagents, often 1-2 orders of magnitude less than batch procedures. This is important during field deployment where either can be limited. Micro-columns also have good reproducibility (RSD's of 1-5 %), are relatively simple to automate and incorporate in on-line procedures (e.g. FI), in-situ continuous monitoring and process control systems.

The principle of a micro-column is shown schematically in Figure 1.6. The micro-column is loaded by pumping the sample through it, during which the analyte of interest is retained by the active sites. The micro-column is then washed to remove residual matrix ions that can be weakly retained or lodged in the interstitial pore spaces of the resin and which would be co-eluted, possible acting as interferents. The analyte of interest is then eluted off the micro-column by a suitable solvent. Equilibration of the micro-column can then follow, although this step is not always required.

The design and operation of the micro-column has a significant impact on its performance. In order to achieve high efficiency coupled with a low sample and reagent consumption, the factors that must be considered include (Fang, 1993);

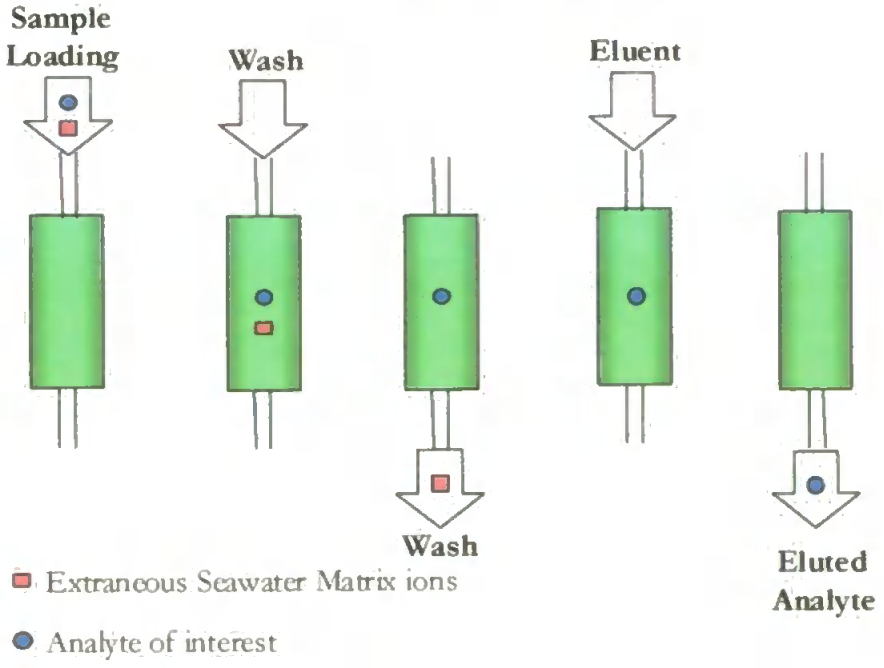

Figure 1.6 Schematic of Operation of Micro-column

- the sample flow rate and loading time,
- the breakthrough capacity of the sorbent resin used for the analyte in question

- the particle size and specificity of the packing material
- the extent of the interference experienced.

An evaluation of the efficiency of a micro-column used for SPE is the enrichment factor (EF) which is theoretically

$$EF = C_e/C_s$$

where C_e = analyte concentration in the concentrate and C_s = analyte concentration in the original.

However, since the concentration in the concentrate C_e is unknown, EF is more usually defined for practical purposes as the ratio of the slopes of the calibration curve prior to and after preconcentration, based on the response achieved from C_s. Other indices that help define micro-columns are the consumptive index (CI) or efficiency of sample use, and the phase transfer factor (P) or the completeness of the transfer of the analyte from the sample phase into the concentrated phase.

For micro-columns of the same capacity and provided the breakthrough capacity of the column is not exceeded, a high aspect ratio (column length/column internal diameter i.e. L/i.d.) will usually result in a high enrichment factor (EF). The upper limit of the aspect ratio is often limited by high back pressures within the FI manifold e.g. as encountered when high flow rates through the micro-column are used (Fang, 1993). For micro-columns with similar aspect ratios, a larger column capacity will result in a column with a higher tolerance to interferents but a lower EF.

The height of the elution peak correlates to the concentration of the eluted analyte and therefore the dispersion characteristics of the eluted Cu(II) and peak shape are of primary importance and should be optimised to give sharp elution peaks. The use of 3D mixing coils that increases radial mixing can dramatically influence peak shape, producing a tall thin peak. Column resin materials that are of a fine particle size will generally increase the EF by producing sharper elution peaks (Fang, 1993). However, this has to be balanced against an increase in back pressure that can result from a resin of fine particle size, which can lower the column loading flow rate and thus reduce the maximum EF achievable. For matrix separation by sorption onto a suitable resin, the EF value has a direct relationship to the amount of sample loaded onto the column, which in turn is related to the sample loading time and sample flow rate. An optimal sample flow rate is a compromise between sensitivity and selectivity.

The kinetic aspects in a micro-column are of much more importance than in a batch system due to the sample flow through it. The kinetics of the resin should promote high

selectivity and strong retention of the analyte, whilst enabling a rapid, efficient elution. High EF values are best achieved through high sample loading rates although the maximum flow rate is more often limited by the kinetic aspects of the column resin than by the limitations of contemporary fluid delivery systems.

Dispersion of the analyte during sorption onto the column resin and elution of the micro-column is influenced by;

- the column geometry
- the characteristics of the sorbtive material in relation to the analyte
- the eluent properties
- the eluent flow rate
- the overall system design in relation to the micro-column.

The sorbent material used in the micro-column can affect the dispersion characteristics of the analyte (Fang, 1993). The sorbed analyte band is acted upon by the eluent prior to its release, with the degree of dispersion being related to the distribution coefficient of the analyte between the stationary column packing phase and the mobile eluent phase. The dispersion can be reduced by the use of the shortest, thinnest lines possible together with 3D knitted mixing coils (Chapter 2). This is of particular importance when micro-columns with focused eluate zones are used.

The micro-column can be equilibrated prior to loading by rinsing with a buffered carrier solution, followed by washing with distilled water after loading to remove the residual sample matrix. Fang (1993) concluded that washing and/or equilibration did not enhance the sensitivity or precision when using Flame AAS. When column equilibration was not used, the buffered sample acted as an equilibrant for the column within a few seconds of loading, minimising sample loss and resulting in a simpler and more efficient micro-column system.

The kinetic factors of elution from a micro-column are of much greater importance than with a batch system. A strong eluent requiring a short equilibrium time is required in order not to degrade the EF of a micro-column. It is also important that the eluent should not attack the column packing during its potentially long life. Although the optimum eluent flow rate is dependent on how strongly the analyte is retained on the column resin and on the strength of the eluent, the use of a low eluent flow rate often maximises EF, although a higher flow rate would increase the sampling frequency.

Due to the concentration of the analyte in a band on the column, the use of a reversed flow for elution helps minimise the dispersion, an important consideration, and also

reduces the progressive compaction of the column particles that can occur with uni-directional flow through the column. Reverse elution also improves the EF of a micro-column. The degree of swelling or shrinkage of the resin when the conditions of the column are altered e.g. pH, should be negligible and the resin should also be physically robust to withstand the flow rates used to ensure a long column lifetime.

1.6 Field Analytical Methods

The continuing investigation of the marine biogeochemical cycling mechanisms in the world's oceans has stimulated the need to map oceanic trace levels of both labile (Cu(II)) and total Cu. This is best achieved by shipboard, highly sensitive, accurate, precise and rapid analytical methodologies, which should also be robust, reliable, portable and capable of incorporation into relatively simple instrumentation. As reviewed by de Jong *et al.*, (2000), shipboard deployment enables the collection of (near) real time data, which enables the modification of research programmes to accommodate the observed data and highlights the occurrence of contamination in sample collection protocols. The transfer of laboratory techniques to the field creates a major challenge in terms of considerable extra demands on the instrumentation including its robustness, reliability and maintaining analytical performance with the increased risk of contamination. The ability to perform underway monitoring through shipboard field deployment during research cruises enables a higher degree of spatial resolution than was previously achievable, which if repeated in different seasons can add a substantial degree of temporal resolution.

The adoption of trace metal clean protocols during sampling and sample manipulation is an important feature upon which the sample analysis is dependent for accuracy. The operational differentiation of the dissolved from the particulate fraction by sample filtration has become a commonly adopted protocol using a 0.4 μm pore size filter, although there is a current trend towards 0.2 μm pore size or cross flow ultrafiltration techniques. Sample treatment protocols have become standardised to include sample acidification to pH 2 to preserve the metal species in solution, with UV digestion also used to break down the dissolved organic material, releasing the organically complexed metals.

During sample manipulation and analysis, it is important to utilise the purest reagents obtainable and even to utilise secondary purification techniques to further purify the regents. Often matrix separation techniques are used to prevent interference from seawater matrix ions and it is important to ensure that the recovery is very close to 100 % to ensure accurate determination of the metal content. Whichever methodology is used, its

response should be independent of the seawater matrix analysed, maintaining good analytical performance throughout.

The standardisation and certification of methods can be achieved by the use of certified reference materials, supported by independent quality assurance, to demonstrate the reliability of trace level metal determination in the field. Further verification of the accuracy of the data can be obtained through oceanographic consistency, whereby the observed trace metal trends should correlate to other onboard hydrographic data e.g. trace metals to nutrient data. Further independent support can be obtained by comparison with previously obtained trace metal data for the same region, although the dynamic nature of the ocean and the seasonal and spatial effects must be noted.

Of the many different analytical techniques for Cu, most are not suitable for field deployment due to the requirement for dedicated laboratory facilities and associated disadvantages as described above (Sections 1.4.2 to 1.4.6). However, shipboard analysis also imposes additional challenges to scientific personnel in a demanding environment (e.g. seasickness), and also one that is potentially contaminating, constantly moving and subject to vibration, experiences power spikes and requires the adequate provision of spares, coupled to the ability to effect repairs onboard by scientific personnel. Shipboard deployment also necessitates the development of shipboard trace metal clean protocols (Section 2.2.5). Such aspects have driven the development of shipboard methods for trace metals. Suitable shipboard techniques for Cu are few in number, with flow injection-chemiluminescence (FI-CL) and voltammetry being at the forefront of current field deployable techniques. Although voltammetry will be considered in brief, this research focused on the development of Cu catalysed chemiluminescence (CL) chemistries, which are discussed in detail later in this chapter (Section 1.6.2).

1.6.1 Voltammetry

Voltammetric methods have high sensitivity for a limited number of elements including Cu, fast analysis, minimal sample volume requirements (e.g. 5 – 50 ml), the capability of determining chemical speciation (Donat and Bruland, 1990) and are suitable for shipboard analysis at a relatively low capital cost. For certain elements (Co (II), Cu(II), Fe(III) and Zn(II), sample pretreatment with HCl and UV radiation is required to break down strong organic complexes (Nimmo *et al.*, 1989). Anodic stripping voltammetry (ASV) has been used for the determination of Cu (Daih and Huang, 1992; Scarano *et al.*, 1990) with an LOD of 0.5 nM. Cathodic stripping voltammetry (CSV) (Quentel *et al.*, 1994) has an LOD of 0.1 nM for a 60 s adsorption time (van den Berg *et al.*, 1994).

However, reduced sensitivity can result from competitive adsorption by surface-active organic compounds, which may also affect the kinetics of the stripping step in anodic stripping voltammetry. In addition, adsorption of organically bound Cu on the hanging drop mercury electrode could negate complexing capacity values. Furthermore, voltammetry can often only be used over a narrow pH range, sampling frequency can be low and the technique is less robust than automated wet chemistry manifolds such as FI. CSV electrodes can also be sensitive to vibration, electrostatic changes and power surges that are characteristic of shipboard deployment.

1.6.2 Chemiluminescence

Luminescence can be defined as the emission of electromagnetic radiation arising from the decay of an atomic or molecular species from an excited to a lower energy state. CL is the chemically stimulated emission of electromagnetic radiation (UV, visible or IR) that results from the change of enthalpy (ΔH) of the chemical reaction, and which is emitted via a radiative pathway as light instead of being dispersed via a non-radiative pathway. Synthetic chemiluminescent compounds have been known since the late 1800`s with analytical applications of CL steadily increasing since the 1970's, many of which utilise an ultraweak CL emission that is only detectable by photosensitive detectors e.g. photomultiplier tubes (PMT). A Jablonski diagram (Figure 1.7) schematically describes the photophysical pathways to the primary and secondary excited states and the subsequent decay pathways.

The photophysical pathways can be radiationless transitions, intersystem crossing, singlet-triplet conversion, collisional deactivation and internal conversion and includes the competition between phosphorescence (relatively slow) and fluorescence (relatively fast) that can occur within an atom or molecule. Organic compounds generally have, in the ground state (G) known as the singlet ground state (S_0), a pair of electrons with opposing spins (Pauli exclusion principle) as shown in Figure. 1.8. The absorption of UV or visible radiation can raise an electron to an excited singlet state (S), which then can then follow either a non-radiative (internal/external conversion or intersystem crossing) or radiative (fluorescence or phosphorescence) pathway to relax back to the ground state.

Non-radiative processes

Non-radiative processes are collisional deactivation, internal conversion, external conversion and intersystem crossing. Collisional deactivation is the vibrational relaxation of

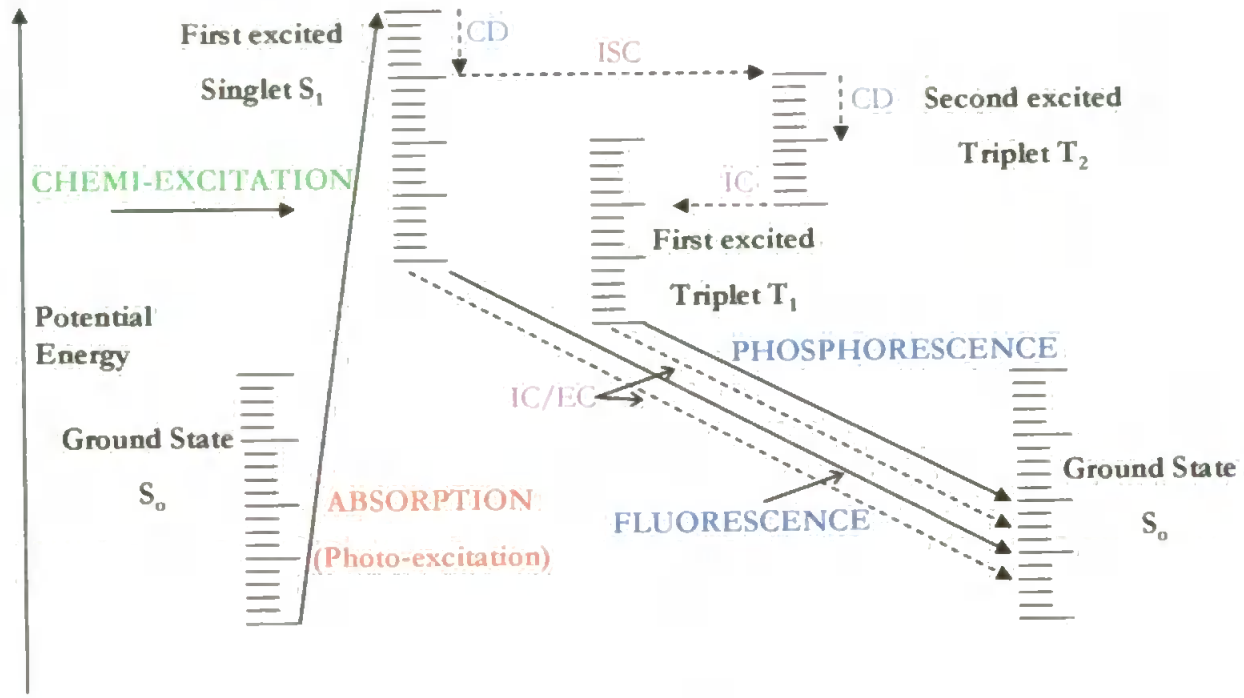

Figure 1.7 Jablonski Diagram illustrating the molecular excitement due to the absorption of a photon and the various pathways for returning to ground state. CD – collisional deactivation, ISC – intersystem crossing, IC – internal conversion, EC - external conversion, ----▶ non radiative transitions, ⟶ radiative transitions (derived from The Effects of UV Irradiation in the Marine Environment, (2000) Edited by De Mora, Demers and Vernet).

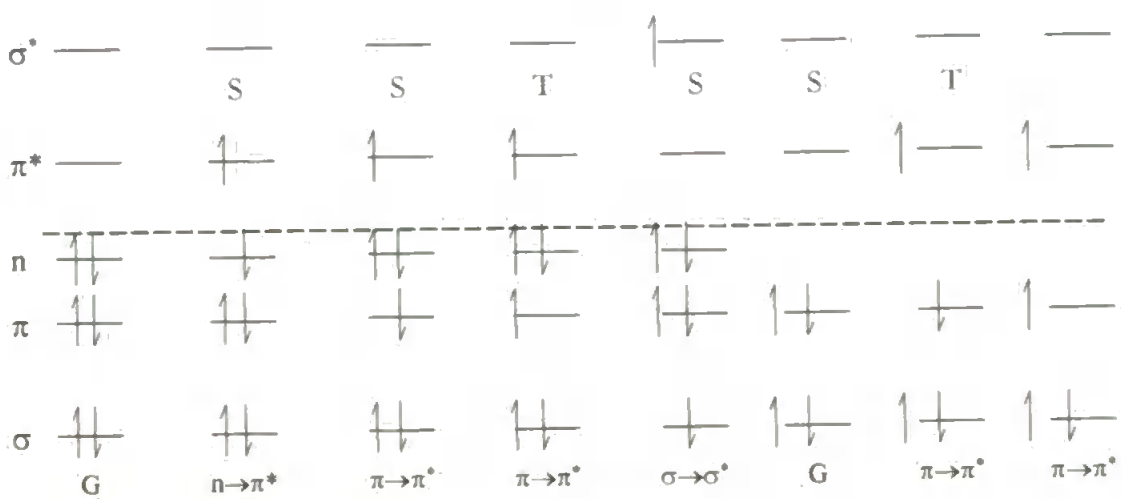

Figure 1.8 Schematic of Electronic Transitions from Ground state (G) to Singlet States (S), and Triplet States (T) (σ - sigma bonding orbital, π - pi bonding orbital and n - non-bonding orbital).

energy levels within a given electronic state. Internal conversion (IC) is a radiationless transition between states with the same spin quantum numbers (*e.g.* S_1 to S_0) as occurs when the two energy levels are close enough for the vibrational energy levels to overlap, allowing vibrational relaxation. External conversion (EC) is the transfer of electronic energy from one molecule to another. Intersystem crossing (ISC) is a radiationless transition between states with different spin quantum numbers (*e.g.* T_1 to S_0).

Fluorescence

Fluorescence is characterised by the relaxation of an excited molecule to a lower vibrational energy level within the excited singlet state. The molecule can then relax to any of the vibrational energy levels in the ground singlet state by the emission of a photon with the corresponding amount of energy. The transition is very rapid (10^{-9}– 10^{-7} s) due to no change of spin being required for fluorescence to occur, such transitions being known as 'allowed' transitions.

Phosphorescence

Transitions involving a change of spin multiplicity prior to emission result in phosphorescence, which is a much slower process (10^{-4}- 10 s) than fluorescence. Such transitions are known as 'forbidden', the change of spin usually being from an excited singlet state to a triplet state. Phosphorescence is rarely observed due to non-radiative processes being comparatively very fast and therefore favoured.

The quantum yield (efficiency) of a process can be defined as

$$\Phi = \frac{\text{number of events}}{\text{number of photons absorbed}}$$

In the absence of any photochemical reactions, the sum of the quantum efficiencies for fluorescence (Φ_F), phosphorescence (Φ_P) and non-radiative processes (Φ_I) is 1;

$$\Phi_F + \Phi_P + \Phi_I = 1$$

In very effectively catalysed biological systems the CL quantum yield (Φ_{CL}) can reach 0.88, although typical experimental CL quantum yields are 0.01 - 0.1 Quenching of the CL signal is analogous to diminishing the number of molecules in the first excited state or singlet state.

A generic CL reaction can be characterized by the reaction

$$A + B \xrightarrow{k_1} C^* \xrightarrow{k_2} C + light \quad (1)$$

the electronically excited species C^* relaxing to the ground state with the emission of a photon. If A and B are in excess the radiative decay is very fast (1 to 10 ns), $k_2 >> k_1$, the equilibrium is to the right (a requirement for CL) and thus k_1 is the rate limiting step. A direct measurement of k_1, represented by the gradient of the graph, is possible when using a logarithmic time scale.

CL reactions can be characterised by their colour, rate of production of CL and its subsequent decay. CL measurements are direct measurements of the reaction rate which is proportional to light intensity. A high intensity emission requires the most efficient production of the excited state C^*. The CL intensity can be described by the reaction (Campbell, 1988);

$$I_{CL} = \Phi_{CL} \frac{dP}{dt} = \Phi_{Ex} \Phi_{Em} \frac{dP}{dt} \quad (2)$$

where

I_{CL} = the CL emission intensity (photons emitted per second)

Φ_{CL} = the CL quantum yield (photons emitted per molecule)

dP/dt = the rate of chemical reaction (number of molecules reacting per second)

ΦEx = the excitation quantum yield (number of excited states produced per molecule)

ΦEm = the emission quantum yield (the number of photons emitted per excited state)

When using a CL reaction in an analytical system it is desirable to raise the CL quantum yield (Φ_{CL}) to a value >/= 0.20 by maintaining the appropriate reaction medium (Campbell, 1988). CL can last over several hours i.e. glowing continuously or for less than a second. The overall efficiency of a CL reaction can be described by the equation (Campbell, 1988);

$$\Phi_{CL} = \Phi_c * \Phi_f * \Phi_e \quad (3)$$

where

Φ_{CL} = the CL quantum yield, a measure of the overall efficiency of the CL reaction.

Φ_c = the chemical yield, or the fraction of molecules that follow the radiative pathway

Φ_f = the fluorescence yield or the fraction the excited molecules that undergo fluorescence decay

Φ_e = the yield of the excited molecules (the number of molecules that are produced in an excited state).

In order for CL to occur the following four conditions have to be satisfied (Campbell, 1988);

i) the reaction product (C in equation 1) has to be able to be raised to an electronically excited state;

ii) the reaction enthalpy has to reach a high enough value, with typical free-energy changes of 170 – 300 kJ mol^{-1};

iii) the reaction rate has to be high enough for detection;

iv) the production of the excited state has to be favoured.

For i) to occur, according to quantum theory the energy of a light quanta (E) is given by equation 4;

$$E = h * \nu = \frac{h * c}{\lambda} \quad (4)$$

where h = Planck's constant (6.63*10-34Js^{-1}), ν = the frequency, c = the velocity of light (2.998*108 m s^{-1}), λ = the wavelength [m].

The energy required to reach an electronically excited state is derived from bond cleavage or electron transfer. For luminescence to occur the enthalpy (ΔH) has to be 167 to 292 kJ mol^{-1}, as is often achieved in redox-reactions. An energy source of at least 187 kJ/mol is required for an emission red light (640 nm), and >/= 300 kJ mol^{-1} for blue light (400 nm).

For (ii) to occur, the luminescence from organic molecules can be described as folows

a) the emission of UV or visible radiation can originate from the easily achieved transition of π electrons in an organic molecule from a bonding π orbital into an antibonding π orbital (π→π*) and also from a non-bonding n-orbital into an anti-bonding π* orbital (n→ π*). Subsequent decay to the ground state results in radiative emission.

b) CL derived from oxygen due to the decay of excited singlet oxygen $^1O_2$ ($^1\Delta_g$) to the triplet $^3O_2$ ($^3\Sigma^-_g$) ground state.

1.6.3 Chemiluminescence Detection Systems

Due to the weak emission of many CL reactions, highly sensitive photoemissive detectors are required. Photomultiplier tubes (PMT, Figure 1.9), are the preferred detectors for quantifying weak or short-lived light emissions. A PMT comprises a quartz side or end window, a photocathode, a secondary emission multiplier and an anode, all housed in a vacuum tube.

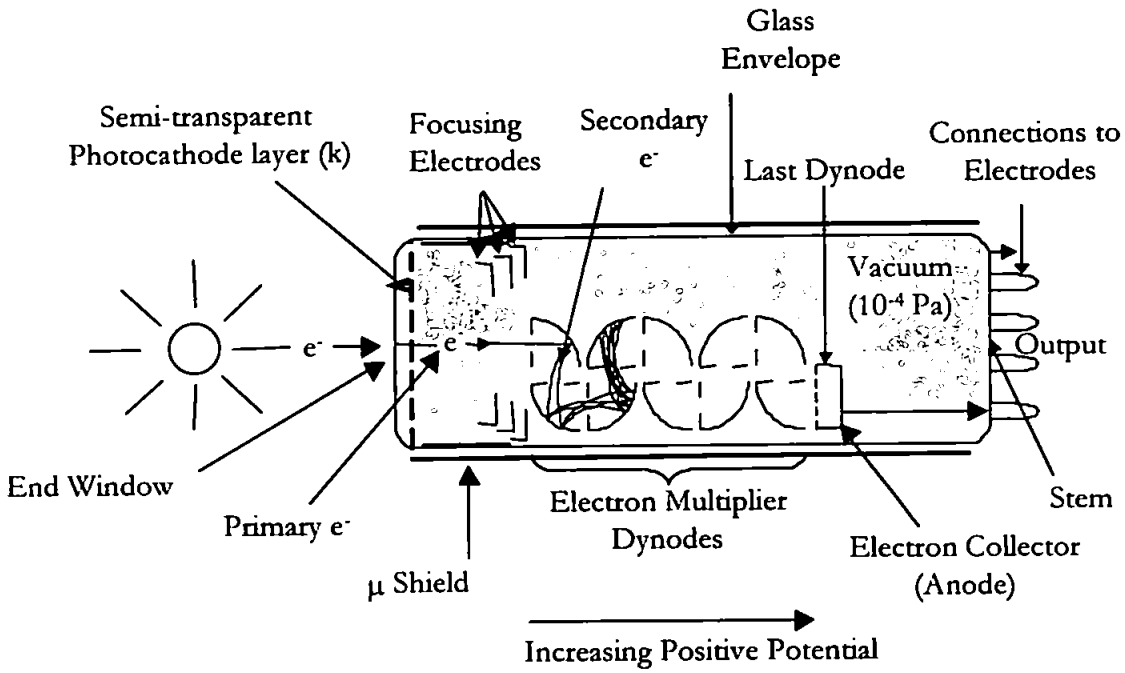

Figure 1.9 Photomultiplier Tube (derived from Electron Tubes Ltd., 1998). The schematic shows the electron cascade only part way along the multiplier dynodes.

Photons impinge on the photosensitive photocathode, stimulating the ejection of an electron that is accelerated and focused by a high voltage as it moves towards a secondary electrode, the dynode. Dynode systems (typically 9-12 in number) provide signal amplification through the ejection of a secondary electron shower, one cathodic electron stimulating as many as 10^8 electrons at the anode (Electron Tubes Ltd., 1998).

The quality of signal recovery has an upper limit imposed by the statistical nature of light detection. The photon counting method provides superior performance to the current measuring method, which can be degraded by noise in the multiplier gain process and by the nature of the dark current. The variation in detector performance due to changes in temperature, shock, vibration and magnetic field effects are also significantly reduced when using the photon counting method. The effects of dead-time can be also be corrected for when using a photon counting method which enables a superior dynamic range to be used.

Commercially available PMTs have a fast rise time (1-2 ns for side window and 10-15 ns for end window), a wide linear dynamic range (typically 10^7 or better) and low dark current (typically 0.1-30 nA). PMTs also generate a dark current, which is a background signal originating from;

a) thermionic emission from the photocathode

b) a current at the anode due to electromagnetic radiation e.g. cosmic rays which can be minimised by Mu shielding of cathode tube, ionisation of residual gases, fluorescence of the envelope material and leakage currents.

However, they can suffer from three types of instability;

a) time drift consisting of a slow irreversible change of the spectral response,
b) fatigue consisting of reversible drift over time periods of minutes or hours,
c) hysteresis, a temporary current instability after a change in the overall applied voltage.

A PMT must not be exposed to ambient light with the high voltage applied since as little as 10^{-5} lm causes the anode current to exceed its permissible limit (Electron Tubes Ltd., 1998)

1.6.4 Chemiluminescence Reactions

In solution phase, CL has found many analytical applications for the determination of metal ions, inorganic anions, biomolecules, carcinogens and drugs in a variety of environmental and clinical matrices, often incorporating flow injection for sample delivery. These have been reviewed extensively (Robards and Worsfold, 1992; Lewis *et al.*, 1993; Bowie *et al.*, 1996; Fletcher *et al.*, 2001) and it is evident that during the 1990's novel CL techniques, often focused on the classical luminol CL reaction, were developed for metal ions in environmental matrices. A trend was also noted towards the use of novel CL reactions utilising the oxidation of specific organic compounds, which are inherently more selective despite often having reduced CL yields. The alteration of the reaction media by the use of surfactant assemblies and the use of non-radiative transfer to sensitisers has also been used to enhance the weak CL emissions (Saitoh *et al.*, 1998; Segawa *et al.*, 1994).

CL was selected for this study due to its inherent sensitivity, typically fast reactions with a wide linear/dynamic range (3 to 4 decades in solutions, 6 to 7 in gas phase reactions). CL is also easily incorporated into FI, enabling on-line sample analysis that facilitates field deployment. A variety of CL chemistries are catalysed by Cu, and are therefore potentially of use in an FI manifold for the determination of Cu.

Luminol-Hydrogen Peroxide

The Cu catalysed luminol CL reaction does not require oxygen or hydrogen peroxide, although their use greatly increases the CL yield. The reaction is pH dependent, buffered solutions (to pH 10) increasing the signal, with the type of buffer being very influential. The Cu-luminol system suffers from low selectivity for Cu and thus requires a

matrix separation technique e.g. a micro-column containing a chelating ligand. Kamidate *et al.*, (1992) used a luminol based chemiluminescence-delay method for the determination of copper, and reported an LOD of 3 μM with the method being linear up to 20 μM. The high LOD makes this CL reaction unsuitable for the determination of ambient levels of Cu in seawater.

Lophine-Hydogen Peroxide

Macdonald *et al.*, (1979) deployed the lophine-H_2O_2 CL reaction in a basic reaction medium. This CL reaction is unselective for Cu, with MnO_4^-, Cr(III), Ag(I), Co(II), and Pb(II) also catalysing the CL reaction. The oxidation of the hydrogen peroxide or the lophine has been proposed as the rate determining step. With a 5 μM LOD, this CL reaction is not sensitive enough for the determination of ambient seawater levels of Cu.

β-Nitrostyrene

Yamada and Suzuki, (1987) utilised the Cu catalysed aerobic oxidation of nitrostyrene in an alkaline medium, the reagent solution consisting of nitrostyrene, NaOH, hexadecyltrimethylammonium bromide (CTAB) with fluorescein, (a sensitiser), being added to enhance the weak CL. CTAB was required to solubilise the nitrostyrene in water via micellar incorporation. A basic solution increased reagent stability but reduced the CL signal. The sample was injected into the reagent stream in a cyclic flow injection manifold. The manifold was found to be selective for Cu(II) with (Fe(II), Cr(II), Ni(II), Fe(III) and Mn(II) generating a signal of 4, 1, 0.4, 0.4, 0.1, and 0.1 % respectively of Cu. However, the LOD of the β-Nitrostyrene CL reaction at 79 nM (20 μl aliquot) was too high for use at ambient Cu levels in seawater.

Flavin-Mononucleotide-Hydrogen Peroxide

As reported by Yamada and Suzuki, (1985), the Cu(II) oxidation of flavin-mononucleotide (FMN) by hydrogen peroxide at pH 6 and 60 ^{o}C exhibited a linear range over 3 orders of magnitude. It had a high degree of selectivity for Cu, with the main interferents being Cr(II), Cr(IV) and Fe(II), which generated a low CL response. However, again the LOD of 47 nM (10 μl aliquot) was too high for the determination of Cu at trace concentrations in seawater.

Cyanide-Uranine

As reported by Wu *et al.*, (1989), the reduction of dissolved oxygen by cyanide and the subsequent oxidation of the superoxide ion by Cu(II) formed singlet oxygen and thus

generated CL. Uranine, the sodium salt of fluorescein, acted as a sensitiser to enhance the CL yield as did 2-propanol (up to 100 % enhancement), although the addition of surfactants reduced the signal. The system was selective for Cu(II), although the presence of Fe(II), Fe(III), Ni(II), Co(II) and Zn(II) also resulted in low CL emission. A log calibration graph was linear over three decades although, with an LOD of 10 nM (20 µl aliquot), the reaction was not sufficiently sensitive for trace level Cu determination in seawater.

1,10-Phenanthroline

Coale *et al.*, (1992) reported the use of the Cu(II) catalysed, H_2O_2 oxidisation of 1,10-phenanthroline in an alkaline medium to produce CL in an FI manifold utilising a Milli-Q carrier stream. Matrix separation was achieved by an 8 hydroxyquinoline (8HQ) micro-column. The PMT detector was cooled to – 20 °C and the sample was injected into the MQ carrier stream. An LOD of 0.4 nM was reported with an 8 min sample processing time. Ca and Mg were found to be the main interferents.

Yamada and Suzuki, (1984) also reported the use of the Cu catalysed 1,10-phenanthroline CL reaction in an FI manifold, but with the addition of tetraethylenepentamine (TEPA) in a micellar environment provided by cetylethyldimethylammoniumbromide (CEDAB), although the latter increased the reagent background noise. Interferents were Pb(II) Zn(II) and Fe(II), which resulted in CL signals of 25 %, 6 % and 2 % respectively compared with a CL signal from Cu at 10^{-8} M (100 %). Cr, Mn, Al, Ni, and Co resulted in no emission, thus indicating a high degree of selectivity for Cu(II). A λ max of 445-450 nm was recorded with a log/log calibration graph linear over three decades (slope of 1). The reported LOD for Cu(II), utilising blank subtraction, was 0.2 nM.

Sunda and Huntsman (1991), also incorporated the 1,10-phenanthroline CL chemistry with tetraethylenepentamine (TEPA) into a batch ligand competition technique (EDTA) to determine Cu with a speciation capability. Peak height and later integration of peak area was used. Blank corrected LODs (200 µl aliquot) of 0.1 nM for Cu(II) in artificial seawater and 0.3 nM for seawater were reported.

The 1,10-phenanthroline CL reaction was chosen for this study due to its sub-nanomolar sensitivity, good selectivity for Cu and a rapid reaction. The reaction mechanism of the 1,10-phenanthroline CL reaction is fully discussed in Section 2.3.1. CL chemistries have received increased attention since the advent of FI due to the ability to combine them

to enable shipboard, near real time determination. Automation and the ability to incorporate further on-line processes, e.g. a photoxidative stage for the determination of labile and total metals, are other advantages of combining CL with FI.

1.7 Flow Injection Analysis

The transient but rapid nature of solution phase CL requires a rapid and reproducible method of mixing sample and reagents. Developed from air-segmented analysis systems in the early 1960s, Ruzicka and Hansen (1988), pioneered flow injection (FI) techniques. Several texts discuss FI theory, instrumentation and practice (Ruzicka and Hansen, 1988; Valcarcel and Luque de Castro, 1987; Karlberg and Pacey, 1989). Flow injection is a powerful tool enabling contamination free manipulation of solutions. It is characterised by its simplicity, utilisation of inexpensive equipment with ease of operation and easily varied experimental parameters. It can be configured as a robust, compact and reliable system that enables reproducible mixing in close proximity to the detector. Reproducibility (typical RSD's of 1-5 %), high throughput and accuracy are the other hallmarks of FI. A schematic diagram of a basic single channel manifold is shown in Figure 1.10 (a) with a typical recorder output illustrated in Figure 1.10 (b).

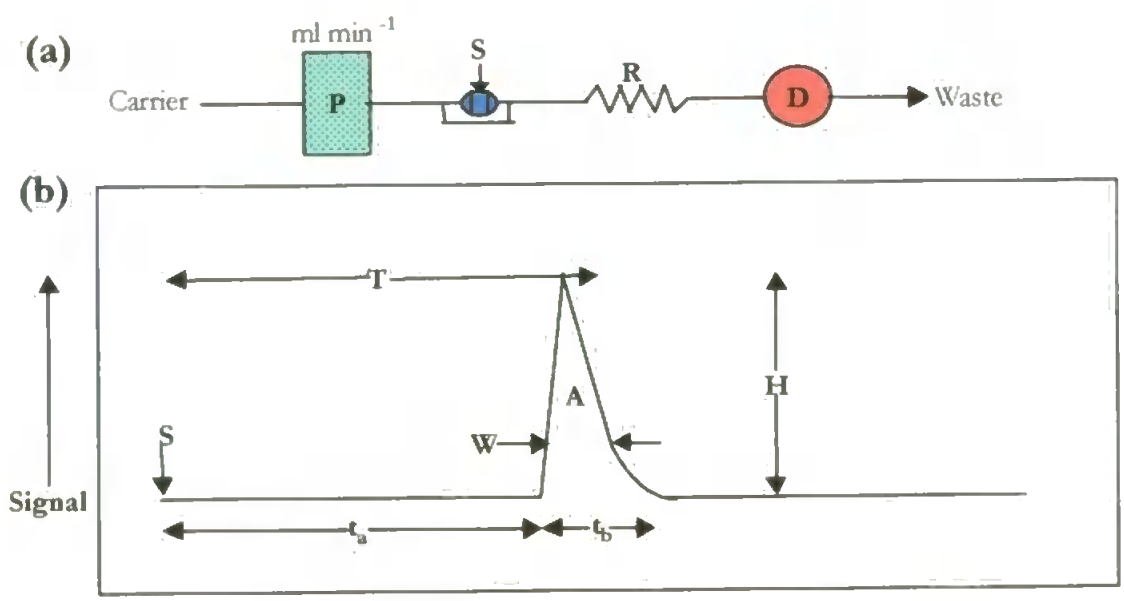

Figure 1.10 a) Schematic of Single Channel FI manifold; P=pump, S=sample injection valve; R=reagent mixing coil D=detector incorporating flow cell; (b) Single Peak Chart Recorder Output, S=sample injection; H=peak height, W=peak width, A=peak area, T=residence time, ta=travel time, tb=baseline to baseline time.

FI manifolds commonly consist of narrow bore (0.5 – 0.8 mm) PTFE tubing and fittings, peristaltic delivery pumps, rotary injection valves, a flow cell and an appropriate detector. More sophisticated systems include 3D mixing coils, automated switching valves to direct flow and matrix separation stages. The response curve forms a peak, which reflects the concentration gradient at time t, the peak height (H), width (W) and area (A) being related to analyte concentration. The residence time T, is defined as the time between sample injection (S) and the signal maximum, with the travel time (t) representing the time between the start of the signal and the return to baseline.

Injection of a highly reproducible sample volume into a moving carrier or reagent stream without the addition of air results in minimal dispersion. The injected sample forms a zone (Figure 1.11) that resembles a cone or annulus and which undergoes dispersion as it moves downstream to the detector.

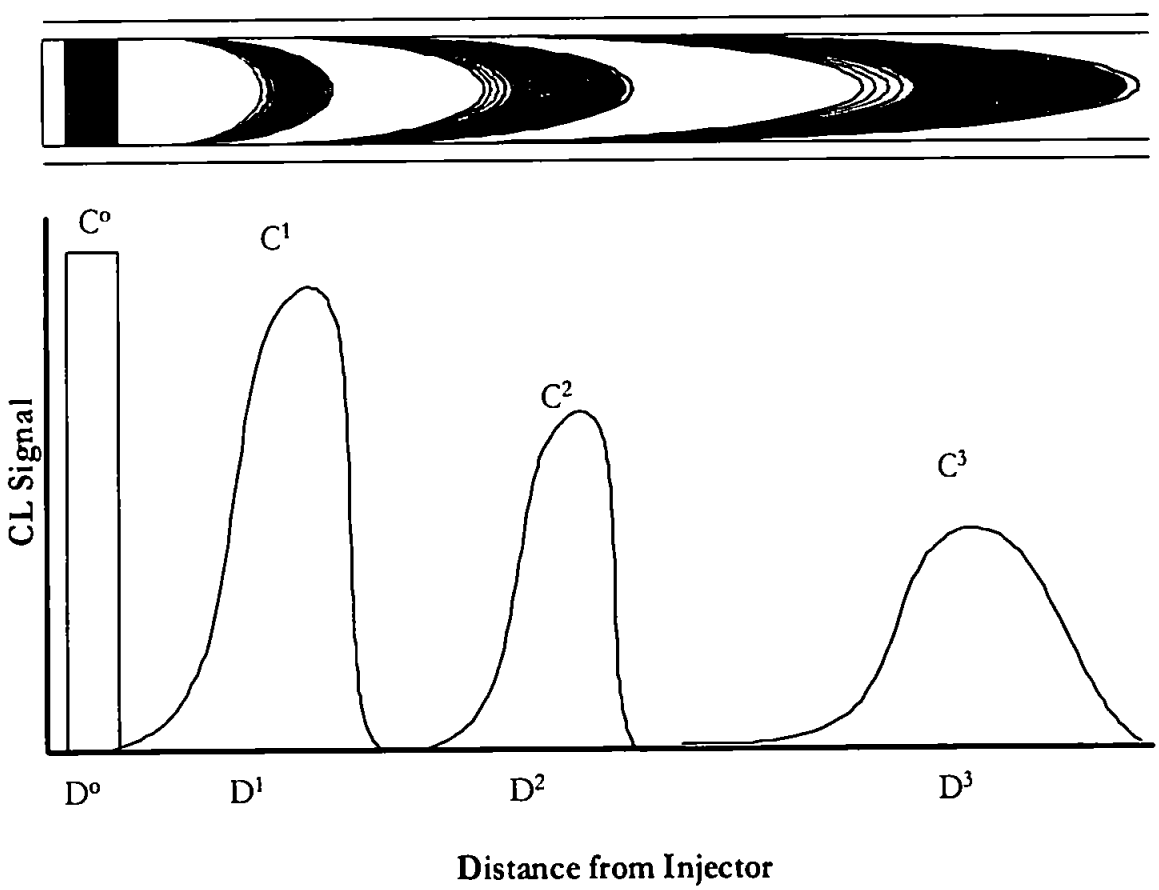

Figure 1.11 Dispersion within an FI Manifold The injected sample zone undergoes progressive dispersion as it moves along the FI line. This is reflected in a reduced height but broader peak. (Fang, 1995), where C^n = the concentration at distance D^n from the injector. The peak shape is a schematic representation only to illustrate dispersion.

Dispersion is primarily caused by convection, although molecular diffusion is also important. The dispersion coefficient can be critically dependent on the volume injected, with small volume changes potentially producing large alterations in signal. The detector continuously records the change in physicochemical parameters that occurs as the reaction zone passes through a flow cell.

Control of the degree of dispersion is a central tenet of FI and results in the excellent reproducibility coupled with short residence times that (due to the non-equilibration conditions at the detector) are characteristic of FI. The extent of the dispersion can be characterised by the dispersion coefficient (D), which is related to peak height (often at the detector) where the dispersion coefficient (D) is at a minimum (Flow Injection Analysis, 1991). At maximum peak height

$$D = Co/Cg$$

where Co = analyte concentration prior to dispersion and Cg = concentration in the dispersed sample zone on the dispersed concentration gradient at time t (commonly at detection).

When utilising FI, sample and reagent consumption is low, an important aspect where samples are limited or reagents are expensive or in short supply.

1.8 Dissolved Organic Matter and Photo-oxidation

The ambient range of dissolved organic matter (DOM) in seawater is 0.5 – 2 mg l^{-1} (Mopper and Kieber, 2000) forming one of the largest planetary stores of organic carbon. However, only 25-50 % of DOM has been characterised, a fraction that has been found to comprise amino acids, peptides, proteins, lipids and polysaccharides, humic and fulvic acids and glycollic acid (Benner *et al.*, 1992; Zika, 1981), although the individual components e.g. humics still remain to be fully characterised. Anthropogenic influences in coastal zones can contribute other compounds e.g. surfactants, tartaric acid, citric acid, and ETA and NTA (Buffle, 1988). In surface waters, the characterised fraction undergoes rapid biotic transformation. The uncharacterised fraction is thought to consist of biologically refractory heterpoly-condensates of terrestrial and in-situ origin (Heisssenberger and Herndl, 1994; Tranvik, 1993) although this terrestrial based definition does not describe fully these photoreactive chromophores (Zafiriou *et al.*, 1984).

DOM is the most efficient light absorbing component of seawater, especially in coastal waters (Hojerslev, 1982) and it therefore has a major role in marine photochemical and photophysical reactions (Moran and Zepp, 1997) that influence the marine biogeochemical cycling of Cu (Miller and Moran, 1997). Organic complexation is much

slower to reach equilibrium than inorganic complexation (Duinker and Kramer, 1977), due to interaction with the major cations (Raspor *et al.*, 1980), the variable structure of the organic ligands and their existence at lower concentration than inorganic ligands in seawater. On suspended particulate matter the trace metals can be organically complexed by surface organics.

1.8.1 UV Irradiation of Dissolved Organic Matter

The UV fraction (10 to 400 nm (Campbell, 1988)) of the electromagnetic spectrum can be subdivided into UV-C (180 – 290 nm), UV-B (290-320 nm) and UV-A (320-400 nm). Chromophores in DOM and some inorganic substances e.g. NO_3 & NO_2 absorb the ultra-violet (UV, 1 - 400 nm) and blue-violet wavelengths (400 – 470 nm) (Kieber and Blough 1990 and 1996; Cooper *et al.*, 1989; Miller, 1994). These wavelengths are photochemically active, containing sufficient energy to either cleave chemical bonds directly or promote the electronic excitation of molecules and so induce chemical degradation by primary or secondary processes (Section 1.8.2). Coastal waters, especially near marsh outflows and organically rich surface microlayer films may absorb longer wavelengths (~ 600 nm) of the visible spectrum.

Natural UV radiation affects marine biogeochemical cycles through breakdown of DOM, producing CO, CO_2 and other low molecular weight organic compounds (Miller and Zepp, 1995). Photoxidation of organic material by UV radiation with the addition of oxidants such as H_2O_2, O_3, HNO_3 and $K_2Cr_2O_7$ to facilitate the mineralisation, has been used experimentally to liberate organically complexed trace metals to enable determination of total metal concentration. The breakdown of DOM by natural and artificial UV irradiation (Hg vapour lamps) has been reviewed (Golimowski and Golimowska, 1996) and the mechanisms and products of UV phototochemistry have been recorded for many compounds e.g. DDT, PCP, TNT and atrazine.

Natural UV irradiation transforms DOM into more labile, low molecular weight compounds which may increase the available food stock for bacterioplankton, a major constituent of the marine microbial food web. However, this has to be balanced against the detrimental effect of increased natural UV-B radiation reaching the earth's surface due to the thinning of the ozone layer. UV-B may also penetrate deeper into the water column due to photobleaching of DOM. Direct detrimental effects at the molecular and cellular level have been demonstrated for some marine organisms although the overall effect on ecosystems has still to be defined.

The environmental mobility, bioavailability and toxicity of trace metals in seawater are directly influenced by their oxidation states which can be altered by both the direct photoreduction of the colloidal metal oxide-hydroxides into more labile and bioavailable dissolved species and the production of reactive species. Photo-reduction of copper (Moffett and Zika, 1987 and 1988) may therefore modify its toxicity towards micro-organisms, especially in perturbed waters e.g. industrialised and coastal environments (Sunda and Gillespie, 1979), which therefore affects phytoplankton productivity (de Mora, Demers and Vernet, 2000).

1.8.2 Photochemistry of Dissolved Organic Matter

The photochemical sites and reactions in marine DOM are only partly known, although they can affect the biogeochemical cycling of trace metals (Palenik *et al.*, 1991). The light absorbency of DOM regulates the photochemical radical production rate and thus coastal waters with inherently higher DOM levels can exhibit a flux of photochemically produced radicals up to two orders of magnitude greater than oligotrophic seawater.

The absorption of UV light by DOM results in the formation of singlet excited species (DOM^*) that subsequently decay by a series of photophysical and photochemical pathways (Figure 1.12). The photochemical degradation of organic matter can be divided into primary and secondary reactions (Achterberg and van den Berg, 1994). DOM directly absorbs UV and blue wavelength radiation by chromophores in DOM e.g. -C=C-, -C=O-, or -N=N-, initiating the formation of highly reactive, transient excited species that decay to form new ground state products. If reactive, these products can undergo further secondary intramolecular or intermolecular reactions, which may involve electronic deactivation (Zika, 1981). Most of the absorbed energy of the excited state DOM dissipates via various photophysical and photochemical pathways (Figure 1.12) e.g. vibrational and rotational relaxation, internal conversion, collisional deactivation and radiative decay e.g. fluorescence (Blough and Zepp, 1990).

The singlet excited DOM can, via intersystem crossing (ISC), reach the longer lived triplet excited state ($^3DOM^*$) which then undergoes photophysical deactivation, producing heat and light (phosphorescence). A small fraction of the singlet and triplet excited DOM decays through energy transfer to acceptor molecules e.g. oxygen. Oxygen is the dominant solute in oxygenated water (Acheterberg and van den Berg, 1994; Zepp *et al.*, 1985) due to its excited singlet state ($^1O_2$) being only 92.5 kJ above its triplet ground state ($^3O_2$), the dominant acceptor molecule in water. Therefore, another important electronic decay

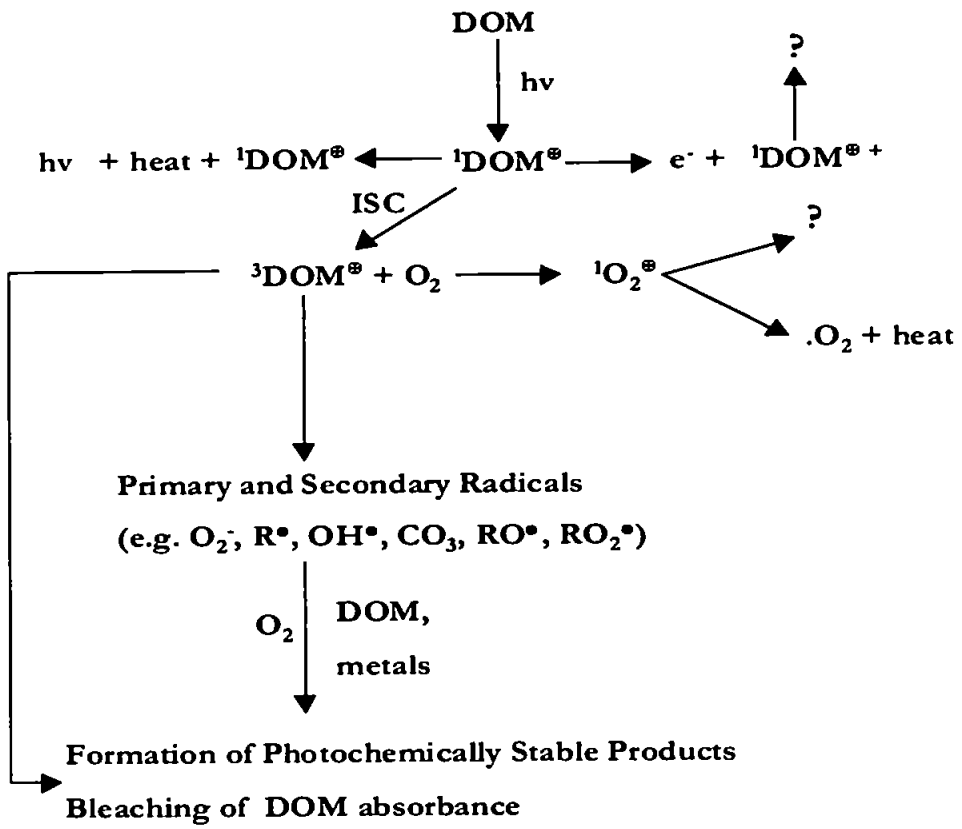

Figure 1.12 General Pathways for the Photochemical Oxidation of Excited Dissolved Organic Matter (DOM) in Natural Waters. (Mopper and Kieber, 2000), from The Effects of UV Irradiation in the Marine Environment, 2000 Edited by De Mora, Demers, and Vernet).

pathway in natural waters is the energy transfer from $^3DOM^*$ to oxygen in its triplet ground state ($^3O_2$), producing singlet oxygen ($^1O_2$). However, in natural waters singlet oxygen is rapidly quenched through collisional deactivation with water molecules. Thus, under 1 % of the singlet oxygen may attack phenols, electron rich centres such as reduced sulphur compounds, e.g. dimethylsulphide (Kieber *et al.*, 1996) and those compounds containing easily oxidisable functional groups.

The excited DOM can also decay by molecular re-arrangements, fragmentation and/or reaction with metal ions and oxygen, forming a variety of radicals and non- radical species (Table 1.3). The primary radicals form within pico-seconds to nano-seconds, but react with the high concentration of oxygen found in surface waters at diffusion controlled rates, on a time scale of microseconds, yielding a suite of secondary oxygenated radicals as well as forming singlet oxygen. Many of the secondary processes result in partly oxidised products

Table 1.3 Photochemically Transient Species in Natural Waters Exposed to Sunlight

Species	Symbol	Estimated Conc. (M)	Probable Sources
Singlet oxygen	$^1O_2$	$10^{-14} - 10^{-13}$	DOM energy transfer to triplet oxygen
Hydrated electron	e^-_{aq}	$10^{-17} - 10^{-15}$	DOM photolysis
Superoxide anion	$O_2^{-\bullet}$	$10^{-9} - 10^{-8}$	e^- transfer to & e^-_{aq} reaction with triplet oxygen
Hydrogen peroxide	H_2O_2	$10^{-8} - 10^{-7}$	Dismutaion of O_2^-
Humic cation	$Humic^{+\cdot}$	$\sim 10^{-10}$	DOM photolysis
Humic triplet excited state	$Humic^{*\cdot}$	$\sim 10^{-10}$	DOM photolysis
Organoperoxides	$RO_2^\bullet$	10^{-14}–10^{-10}	DOM photolysis
Hydroxyl radicals	$OH^\bullet$	10^{-19}–10^{-17}	NO_3^-, DOM photolysis
Dibromide anion	Br_2^-	n/a	$^\bullet OH$/Br reactions
Carbon centred radicals	RH_2C	10^{-13}–10^{-11}	DOM photolysis
Carbonate radical	CO_3	$\sim 10^{-14}$	$^\bullet OH/HCO_3^-$ and Br_2^-/ HCO_3^- reactions
Cu^+, Mn^{2+}, Fe^{2+}, Cr^{3+}		$< 10^{-12}$	Ligand to metal charge transfer reactions

Photochemically formed transient species in sunlit natural waters (Mopper and Kieber, 2000). n/a – data not available.

that can be oxidised (Achterberg and van den Berg, 1994). This transition from primary to secondary states is oxygen dependent. The transient species produced include hydroxy radicals ($OH^\bullet$), singlet oxygen ($^1O_2$), superoxide radicals, ozone (O_3), carbon centred radicals, organoperoxy and alkylperoxy radicals ($RO_2^\bullet$), hydrated electrons, the relatively stable oxidant hydrogen peroxide (H_2O_2), halogen radicals, NO and CO_2 and DOM in various excited states (Table 1.3). The formation of other reactive species such as the humic acid radical cation, the carbonate radical (CO_3^-), and bromine containing radicals, particularly $Br_2^{-\bullet}$, have been postulated but not studied.

Superoxide radicals can form from the reduction of dissolved oxygen by excited DOM via direct electron transfer or reaction of hydrated electrons with O_2.

$$(e^-{}_{(aq)}) + O_2 \longleftrightarrow O_2^{-\bullet}$$

Electrons trapped by CO_2 also form superoxide radicals.

$$CO_2^{-\bullet} + O_2 \longleftrightarrow CO_2 + O_2^{-\bullet}$$

The superoxide radicals both oxidise and reduce DOM, although all the radicals produced eventually form non-radical (diamagnetic) species through radical to radical reactions or disproportion.

$$2O_2^{-\bullet} + 2H^+ \longleftrightarrow H_2O_2 + O_2$$

The concentration of H_2O_2 in seawater supports this theory. Free radicals are also generated by direct photolytic cleavage and by photo-induced charge transfer reactions involving the organic and inorganic molecules present in seawater. The free radicals degrade DOM by auto-oxidation reactions. The hydroxyl radical is the most reactive of these radicals (Zhou and Mopper, 1990). Typical hydroxyl radical reactions are

$$OH^{\bullet} + RH \longrightarrow R^{\bullet} + HOH$$

$$R^{\bullet} + O_2 \longrightarrow ROO^{\bullet}$$

$$Ar^{\bullet} + O_2 \longrightarrow Ar\,OO^{\bullet}$$

$$ROO^{\bullet} + RH \longrightarrow ROOH + R^{\bullet}$$

(from Achterberg and van den Berg, 1994).

The addition of a radical to an aromatic ring promotes its complete oxidation, often producing more radicals in the process. The decay of excited DOM also results in the direct formation of non-radical species e.g. CO.

In summary, photochemical induced reactions result in the oxidation of DOM, cleavage of humic compounds, oxidation of reduced sulphur, photobleaching, absorbance and fluorescence, loss of dissolved oxygen, photo-reduction of trace metals, release of complexed or bound species e.g. phosphate, and the formation of a variety of relatively stable low molecular weight species e.g. hydrogen peroxide, NO and NO_2, hydrocarbons, organic acids, CO_2 and CO, and NH_4.

1.8.3 Artificial Breakdown of Dissolved Organic Matter

Historically the artificial digestion of dissolved organic matter (DOM) prior to metal analysis has used wet oxidative methods (Gorsuch, 1970) involving H_2O_2 or concentrated acids e.g., HNO_3, H_2SO_4 or perchloric acid or sodium persulphate to degrade the organic matter. However, these methods are time consuming, often involve high temperatures with the addition of large volumes of hazardous reagents and are difficult to accomplish in closed systems due to evaporative losses. The use of additional reagents in an open system can introduce contaminants that can degrade the accuracy of trace metal determinations.

A clean and efficient alternative to wet oxidative digestion of DOM is UV photo-oxidation using mercury lamps which minimises the use of hazardous hot reagents e.g. percholric acid, with added oxidants e.g. hydrogen peroxide. Analytical UV applications include the breakdown the DOM prior to sample analysis to overcome the distortive effects during electro-analytical techniques (Golimowski and Golimowska, 1996) for trace

metals and the oxidation of nitrogenous and ammoniacal organic compounds to nitrates and nitrites with detection by molecular spectrophotometry. When using electro-analytical techniques, DOM can form deposits on the electrode limiting its active area, a particular problem with adsorptive voltammetry. The DOM may also form complexes with metals, preventing their reduction at the electrodes and/or shifting the electrochemical reduction and oxidation potentials. DOM can also shift the peak potential, distort the signal and undergo electrochemical oxidation or reduction resulting in increased background currents.

During metal preconcentration used with flame atomisation techniques such as AAS, DOM can reduce nebuliser performance (Golimowski and Golimowska, 1996). Sample acidification can breakdown the weaker organic complexes, the Cu being replaced by hydrogen ions, although the more refractory organic complexes are resistant to acid digestion. UV irradiation is also commonly used for disinfection of water and air, food sterilisation, production of DOM free water for trace analysis, cosmetic and electronic industries, swimming pools, for remediation of toxic compounds in urban and industrial wastes and as a final treatment in some more advanced sewage treatment works.

1.8.4 UV Instrumentation

Mercury vapour lamps in low (L-Hg), medium (M-Hg) and high pressure (H-Hg) forms can be used for UV breakdown of DOM. The emission spectrum of mercury is characterised by a maximum emission at 254 nm, corresponding to the relaxation of the lowest excited state (6 $^3P_0$) to the ground state (6 $^1S_0$). A weaker emission at 184 nm corresponds to the transition from 6 $^1P_1$ to the 6 $^1S_0$ ground state. These wavelengths are the most efficient for UV degradation of DOM (Golimowski and Golimowska, 1996; Kolb *et al.*, 1992; Yokoi, *et al.*, 1995). A small number of atoms can also reach excited states higher than 6 $^1P_1$, although their emission lines are weak. The spectral output of the medium pressure Hg vapour lamp used for this study is shown in Figure 1.13.

Mercury lamps, especially H-Hg, can cause the sample to boil unless cooled. This can be accomplished by immersive techniques, although they are potentially contaminating. High pressure Hg lamps also remove the dissolved oxygen, inhibiting the oxidation of DOM by side reactions e.g. the oxidation of chloride to hypochlorite (Yokoi *et al.*, 1995). Low pressure Hg lamps have a larger fraction of their output at 254 and 184 nm compared with M-Hg and L-Hg lamps.

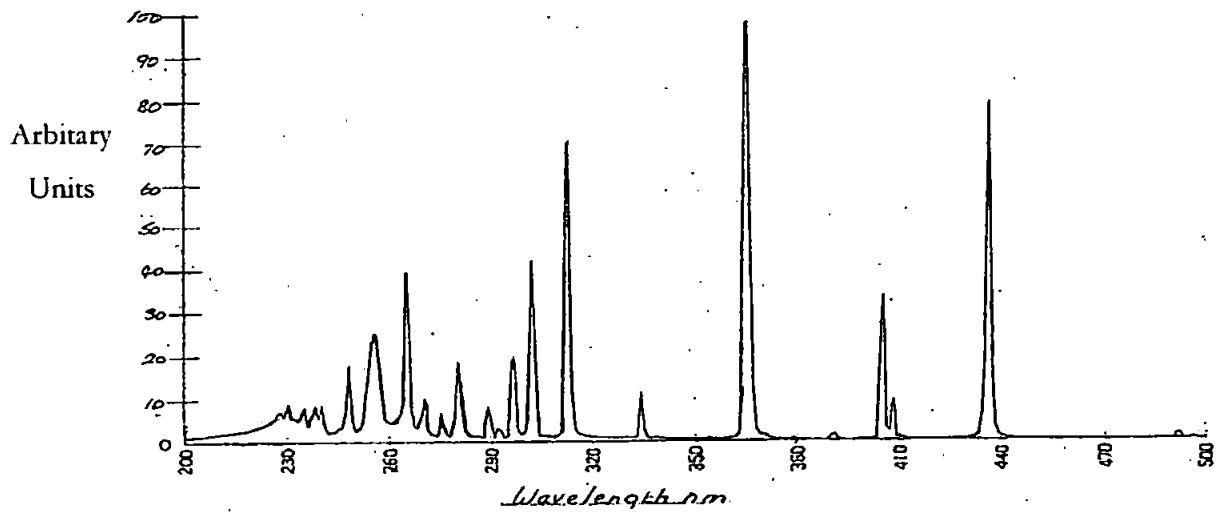

Figure 1.13 Spectral Output from a Medium Pressure Hg-vapour lamp (Photochemical Reactors Ltd.)

1.9 Research Objectives

The specific research objectives for this study were;

- To review CL reaction chemistries and select a reaction with appropriate sensitivity and selectivity for the determination of labile Cu(II) in seawater (Chapter 1).
- To design, construct and optimise a flow injection manifold incorporating the selected CL chemistry. for the determination of dissolved Cu(II) at ambient seawater concentrations in UHP water (Chapter 2).
- To evaluate potential seawater interferences on the selected CL chemistry (Chapters 2 and 3).
- To adapt the FI manifold to determine Cu(II) in a seawater matrix. This will entail the selection, characterisation and optimisation of the geometry and of the elution and regeneration phases of a chelating micro-column. This would enable selectivity for

Cu(II) by isolation of Cu(II) from the seawater matrix and enhance the sensitivity of the system. Ideally, this phase should not contaminate or alter the sample, be robust enough to enable continuous use, and be capable of regeneration without degradation of analytical performance (Chapter 3).

- To automate the FI-CL manifold to enable near real time, in situ mapping of Cu(II) without operator error or fatigue and to improve reproducibility and free analytical time for other procedures. This will promote the mapping of Cu(II) and continuous monitoring during future field deployment (Chapter 4).
- To validate the FI-CL system with the certified reference material NASS-5, in local field trials and by comparison with other laboratory analytical techniques e.g. voltammetry (Chapter 4).
- To deploy the system on-board an oceanographic cruise of opportunity to investigate the distribution of Cu in coastal and remote regions of the Atlantic Ocean and to map Cu(II) levels through the upper water column (Chapter 5).
- To determine total dissolved Cu by the development of an on-line UV photo-oxidation stage to breakdown the organically complexed fraction of Cu(II) and therefore to operationally distinguish between labile Cu(II) and total Cu (Chapter 6).

The development of a highly sensitive, robust, shipboard FI-CL system with a high sampling frequency could potentially fulfil these research objectives. A shipboard detection method for dissolved Cu would ideally be able to determine open ocean trace levels of Cu as well as the elevated levels found in coastal and estuarine waters. It would also enable spatial and temporal variations in Cu to be investigated. Shipboard deployment would minimise the species alteration and contamination issues that can be a feature of sampling, storage, transport and subsequent processing during shore based analysis.

Chapter Two

Development of an FI-CL Analyser For the Determination of Cu(II) in UHP Water

Chapter Two

2.1 Introduction

This chapter describes the design and construction of an FI-CL manifold for the determination of Cu(II) at sub-nanomolar concentrations in UHP water. The Cu(II) catalysed oxidation of 1,10-phenanthroline by hydrogen peroxide was chosen as the CL reaction for this study due to its sensitivity and selectivity for Cu(II). In order to develop a robust, portable instrument, the CL reaction was incorporated in an FI manifold and the key analytical variables for both were rigorously optimised. The FI-CL manifold minimised sample manipulation and the potential for contamination whilst providing reproducible experimental conditions, high sensitivity and rapid, near real-time analysis using inexpensive instrumentation. Such characteristics are important factors for in-situ mapping of Cu(II) and continuous monitoring during field deployment.

2.2 Experimental

2.2.1 Reagents and Standards

All reagents were Aristar® grade or equivalent unless otherwise stated and were used as received, with the exception of the Aristar® HNO_3 (15.5M) and Aristar® HCl (11.3M) acids, which were further purified by secondary distillation in a custom designed, quartz sub-boiling still (Figure 2.1). The stock acids were introduced into the still until their surface reached the level of the outlet tube. The purification relies upon vaporisation by radiative heating of the acid surface, a process which prevents the violent boiling action typical of a conventional distillation apparatus that often leads to a significant carry-over of raw solvent with the distillate. The surface evaporation process does not generate such a spray or droplets and the condensate is therefore of higher purity.

Heating of the acid was achieved using a high power, infrared lamp (250 W), directed onto the acid surface with care taken to prevent it boiling. An upright, water-cooled cold finger condensed the acid vapour and led the condensate into a pre-cleaned collecting bottle. A constant head device was used to feed the still reservoir, which was periodically flushed with fresh acid to prevent the build-up of contaminants. The distillation still was in continual operation and the typical rate for purification of hydrochloric acid was 250 ml per day. Titration of the purified acids resulted in concentrations of Q-HCl (9.2 M), Q-HNO_3 (12.1 M). These acids have been designated by a Q-prefix, e.g. Q-HNO_3, throughout the thesis.

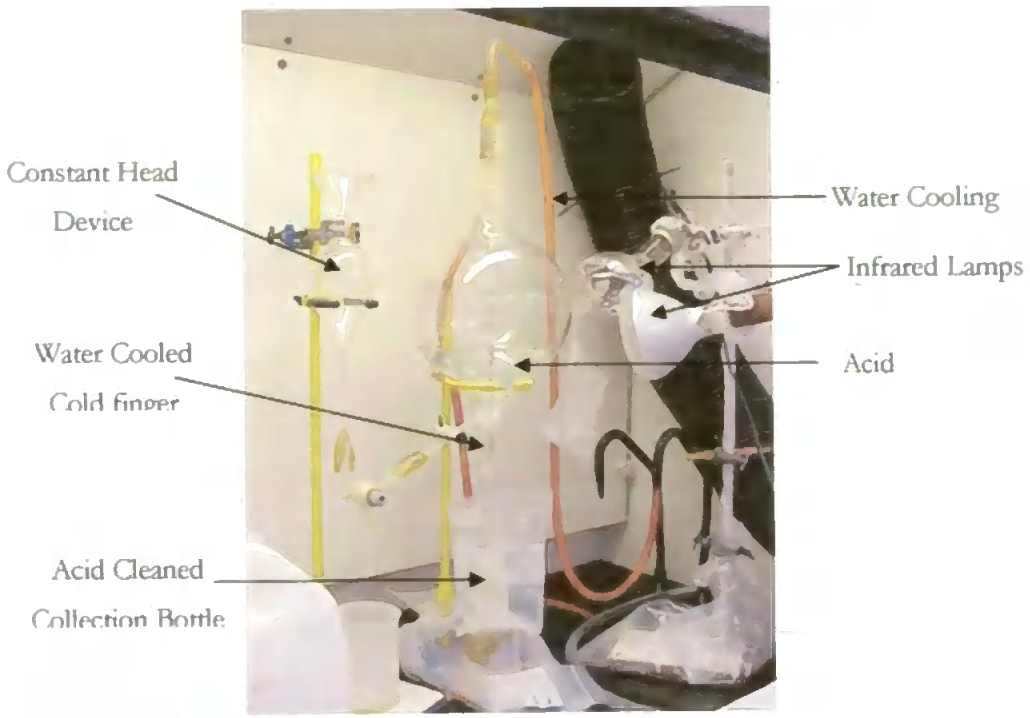

Figure 2.1 Sub Boiling Reflux Still in Fume Hood

Stock solutions of the reagents were prepared as described below, with working solutions for immediate use prepared by serial dilution as required. Ultra high purity (UHP) de-ionised water (18.2 Mohm cm^{-1}, Elgastat Maxima), which was low in trace metals and fitted with UV treatment (and thus also low in dissolved organic carbon (DOC)) was used for solution preparation and labware rinsing throughout this work. High density polyethylene (HDPE, Nalgene® and Gradplex®, BDH) labware was used for all reagent and standard solutions. A list of reagents for the 1,10-phenanthroline CL reaction is given in Table 2.1.

Table 2.1 Reagents

Reagent	Supplier	Grade	Purity (%, w/w)	[Cu] (mg l^{-1})
Hydrochloric acid	BDH	Aristar®	37	0.02
Nitric acid	BDH	Aristar®	69	0.02
1,10-Phenanthroline monhydrate	Aldrich	Puriss	99.5	
1,10-Phenanthroline (anhydrous)	Fluka	Puriss		
Sodium hydroxide	BDH	Aristar®	98	0.5
Cetylethyldimethylammoniumbromide (CEDAB)	Aldrich	Reagent	85	
Tetraethylenepentamine (TEPA)	Aldrich	Technical		
Spectrosol Cu ICP standard	BDH	AnalaR		
Hydrogen peroxide	Aldrich	Aristar®	30 (v/v)	0.001

Cu(II) Standards: A 1 mM Cu(II) stock standard was prepared from an ICP standard (1,000 mg l^{-1} in 2.0 % (v/v) HNO_3, Spectrosol, BDH) by making up 157.3 µl of

the ICP standard to 100 ml with UHP water. A fresh stock solution (1 mM) was prepared monthly, a 10 µM intermediate stock solution prepared weekly, and serial dilutions to working standards were prepared daily. All Cu(II) standards in UHP water and UHP water blanks were acidified to pH 2.0 by inclusion of 50 µl of Q-HNO_3 in 100 ml of standard.

Hydrogen Peroxide solutions: Working H_2O_2 solutions were prepared for laboratory use by serial dilution of the reagent with UHP water. A titrimetric method was used to establish the concentration of the hydrogen peroxide as supplied. Potassium permanganate (0.02 M) in acid solution (H_2SO_4, 2 M) was titrated against H_2O_2 (0.05 M), the end point of the titration being when a permanent faint pink coloration occurred. The potassium permanganate solution was prepared as a primary standard in UHP water from Aristar® grade reagent. The permanganate was warmed to hasten the oxidation of any organic matter present, followed by crucible filtration to remove any manganese dioxide formed by the reaction. The solution was stored in the dark to prevent decomposition. These procedures enhanced the stability of the permanganate solution.

$$2KMnO_4 + 5H_2O_2 + 3H_2SO_4 \longrightarrow 2MnSO_4 + 5O_2 + 8H_2O + K_2SO_4$$

At the outset of this study a 12 mM 1,10-phenanthroline monohydrate stock solution was prepared by dissolving 1.189 g in 100 ml of UHP water. 1,10-phenanthroline monohydrate has low solubility in cold water (CRC Physical Constants 1977/8, 58th Edition) and therefore the solution was warmed to 55° C in a water bath and sonicated for 10 min. The primary reagent containing the 1,10-phenanthroline was prepared by dissolving 1.5 g of sodium hydroxide in 400 ml of UHP water, adding 2.5 ml of the 12 mM 1,10-phenanthroline monohydrate stock solution and making up to 500 ml with UHP water. This produced a primary reagent containing 75 mM NaOH and 60 µM 1,10-phenanthroline. The surfactant cetyldimethylammonium bromide (CEDAB) and tetraethylenepentaamine (TEPA) were not added to the primary reagent during the initial stages of the research.

The initial response from the manifold was erratic due to the difficulty of dissolving and stabilising the 1,10-phenathroline monohydrate stock solution. An anhydrous 1,10-phenanthroline, with improved solubility (CRC Physical Constants 1977/8, 58th Edition), was therefore prepared at a 3 mM stock concentration (0.0541 g in 100 ml of UHP water). CEDAB was incorporated into the primary reagent to improve the solubility of the 1,10-phenanthroline. Its addition altered the preparation of the primary reagent in that the CEDAB (3.3396 g in 500 ml) was first added to 400 ml of UHP water with sonication (10

min) to promote dissolution. To this, 10 ml of 3 mM anhydrous 1,10-phenanthroline stock solution, 6.65 ml of 6 M stock NaOH (24 g in 100 ml of UHP water) and 50 µl of 4 mM stock TEPA (94.5 µl of 4.23 M solution (as supplied) in 100 ml of UHP water) were added. The 1,10-phenanthroline/NaOH/CEDAB/TEPA solution was made up to 500 ml with UHP water and left to equilibrate overnight prior to use. These volumes represent the final reagent concentrations as determined by a rigorous optimisation. This solution is hereafter called the 1,10-primary reagent.

2.2.2 Instrumentation

The FI-CL manifold (Figure 2.2) was constructed using chemically inert, 0.75 mm i.d. poly(tetrafluoroethylene) (PTFE) tubing (Anachem), flanged to produce fluid tight junctions with standard FI connectors. For the FI manifold development described in this chapter, a volume based sample delivery system utilising an inert carrier stream to displace a fixed volume of sample from a sample loop was used. Sample injection was accomplished using a six port rotary valve (Rheodyne Type 5020, HPLC Chromatography, Figure 2.3), that had chemically inert, polyetheretherketone (PEEK) wetted parts to minimise metal contamination and resist acid degradation.

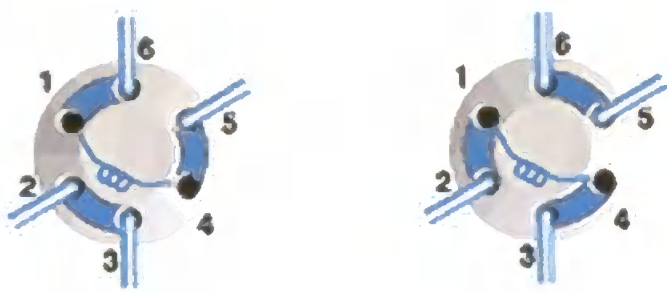

(a) Position A – Load (b) Position B - Inject

Figure 2.2 Operation of a Rheodyne 5020 Rotary Injection Valve - coil represents sample loop or micro-column a) load position (b) injection/elution position)

A multi-channel, variable speed peristaltic pump (Watson Marlow 503S, 6 channel, 8 roller head) and a single speed peristaltic pump (Ismatec Mini-S 820, 4 channel, 8 roller head) were used at the outset as reagent and sample pumps respectively. All pumps where regularly calibrated to ensure accurate and reproducible flow rates. High precision, chemical resistant pump tubing (Acu rated poly(vinyl) chloride, (PVC) Elkay), of varying i.d.s signified by different bridge colours, was used throughout. The CL emission was

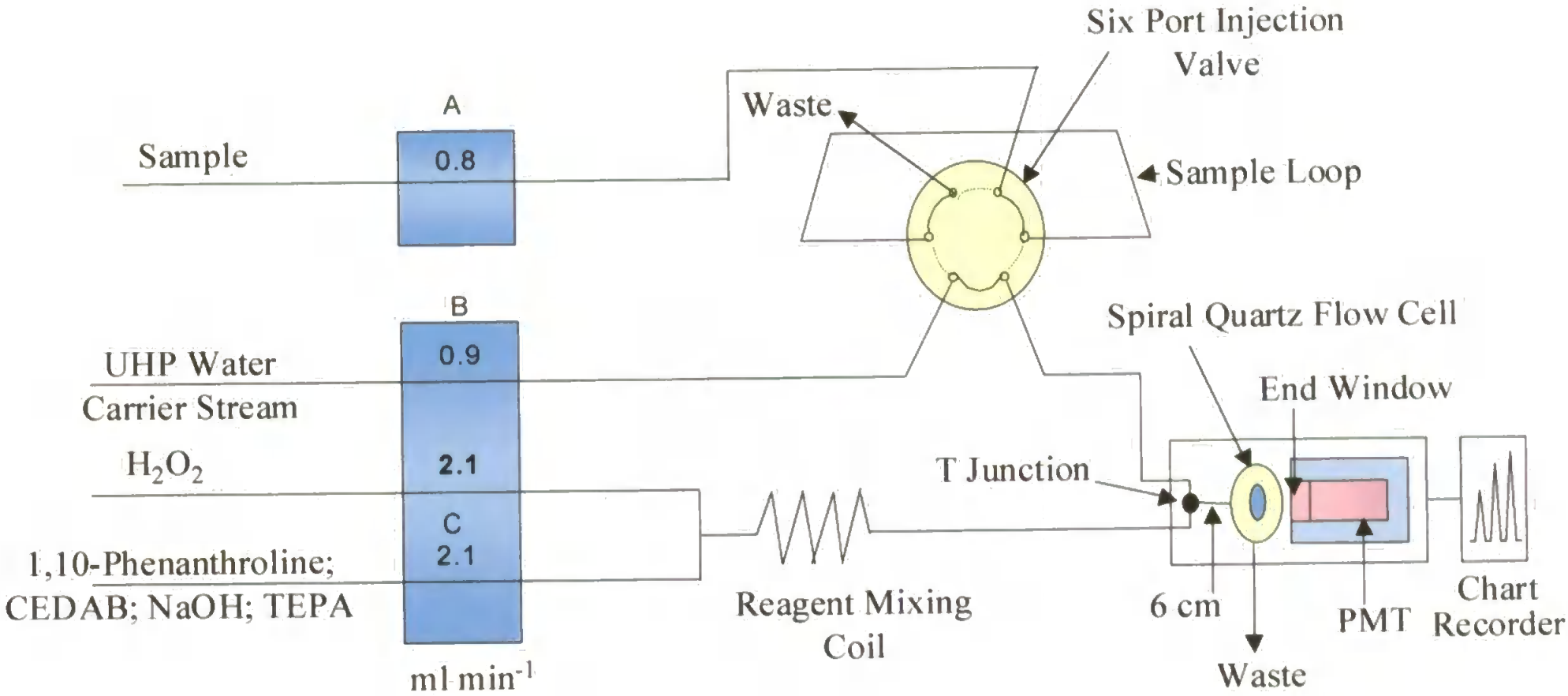

Figure 2.3 FI-CL Manifold for Cu(II) in UHP Water. Incorporating Rheodyne 6 port injection valve and sample loop. A - Sample pump, B – UHP water carrier stream pump, C – Reagents pump

detected by an end-window photomultiplier tube (PMT, model 9789QB, Thorn EMI) contained in a μ-metal shield to insulate against electromagnetic fields (MS52D), an ambient temperature rf shielded housing (B2F/RFI) and a 1.1 kV power supply (Thorn EMI, PM28B). The PMT gave low dark current (0.3 nA, quoted by Thorn EMI) and dark voltage signals. Background electronic noise was minimised by using high quality leads and a low noise PMT (Section 2.3.2). Injection of a Cu(II) standard or sample into the FI-CL manifold resulted in a sharp, reproducible CL peak superimposed on the background CL emission. The transient CL emission was recorded on a flat bed chart recorder (Chessel BD 40 04), with the peaks measured manually with a ruler. The PMT was left switched on since it required a minimum of 2 h after powering up for the dark current to stabilise.

2.2.3 Flow Cell Design

In order to monitor the CL emission, a purpose designed flow cell (Figure 2.4) was mounted immediately in front of the end window of the PMT detector. The flow cell was constructed from inert quartz tubing (140 mm length, 160 μl internal volume) tightly coiled into a flat spiral which promoted effective mixing of the sample and reagents. A light tight aluminium housing enclosed the flow cell, which was connected through an internal screw flange to the reagent/sample FI 'T' junction, also enclosed in a light proof housing. A mirror was mounted on the flow cell side of the internal flange to maximise, by reflection, the detection of the CL emission.

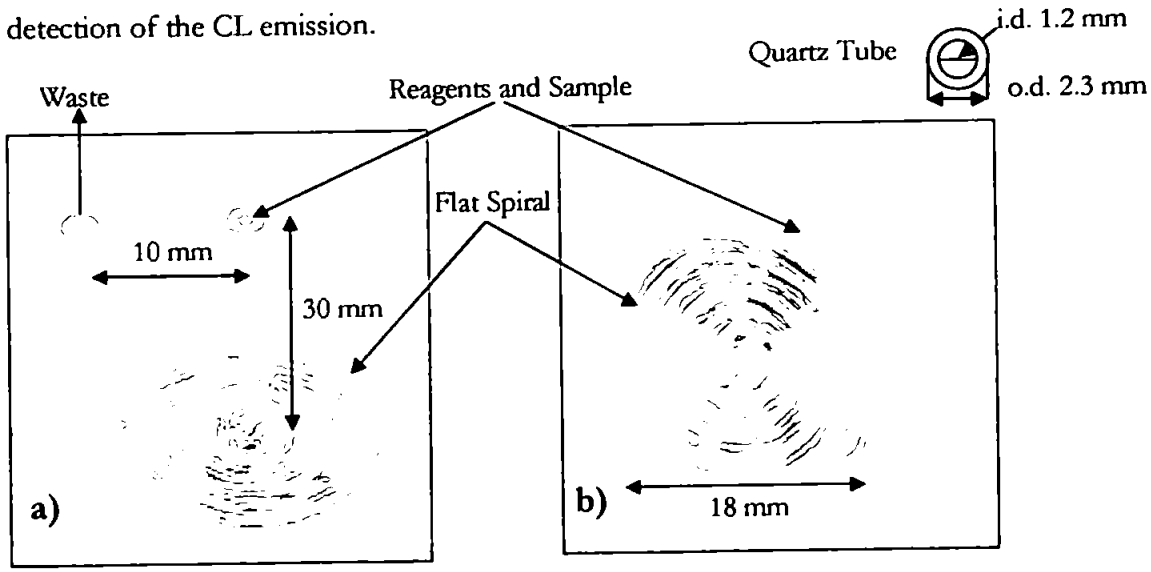

Figure 2.4 Purpose Designed Quartz Flow Cell a) single entry flow cell b) flat spiral

Finn® pipettes were used for all solution delivery in the laminar flow hood and Eppendorf pipettes (ceramic piston) used for fieldwork. All pipettes were used exclusively for trace metal analysis, regularly calibrated to ensure the accurate delivery of successive

volumes and stored in the laminar flow hood to minimise contamination. A calibrated four-figure balance (A 200 S, Sartorius) was used for reagent preparation and to verify the accuracy of pipette delivery. All pH measurements in the laboratory were performed with a pH meter (Hanna Instruments, HI 9021), calibrated daily using standard pH 4, 7 and 10 buffers (Colourkey, BDH). A sonic bath (Branson 2210) was used as required to promote reagent dissolution and homogeneity of solutions. Laboratory film (Parafilm, BDH) was used where necessary to prevent airborne contamination.

2.2.4 Procedures

For the manual FI-CL system (Figure 2.5), a UHP water carrier stream displaced a sample from a fixed volume PTFE loop. The 1,10-primary reagent and hydrogen peroxide were mixed in the reagent mixing coil, prior to merging with the sample at an FI 'T' junction immediately before the flow cell. A CL reaction was catalysed in the quartz flow cell by the Cu(II) in the sample, the CL emission detected by the PMT and recorded as a transient peak, the height of which was directly related to the Cu(II) concentration. All peak measurements were done by hand. Valves were switched manually with stopwatch timing used throughout the work described in this chapter. The FI-CL manifold was regularly acid cleaned (0.2 M Q-HNO_3) and rinsed with UHP water to minimise sample carry over and contamination. Due to the nature of the analytical method, it is imperative to ensure high accuracy and precision in the preparation and delivery of reagent, standard and sample solutions. High precision, variable volume micropipettes (Eppendorf Research 3110, 10-100 µl, 100-1000 µl and 500-5000 µl) with ceramic pistons were used throughout the work reported in this chapter. They were regularly re-calibrated using a five-figure analytical balance (Sartorius, A 200 S). Fresh pipette tips were used for each analysis, each tip being kept exclusively for each solution, stored in designated 25 ml sterilin vial and changed if memory effects were noted.

2.2.5 Clean Protocols

Due to the ubiquitous presence of Cu(II) in reagents, the atmosphere and on new labware, rigorous labware cleaning and clean working protocols were employed to enable accurate determination of Cu(II) at trace levels. All labware was thoroughly cleaned by first soaking in hot 5 % v/v micro detergent (Decon, BDH) for 24 h to remove organic contamination, followed by five days in HCl (50 % v/v, Aristar®) and three days in HNO_3 (50 % v/v, Aristar®). After each stage the labware was triple rinsed with UHP water.

Sample bottles were stored full of 0.1 M Q-HCl. All labware was immediately closed and double bagged in zip lock plastic bags to prevent contamination.

In order to minimise aerosol contamination, a potentially serious problem with metal determination at trace levels, solution preparation and manipulation were conducted in a class 100 laminar flow hood (Bassaire, model A3VB) with experimental work conducted in a class 1000 clean room whenever possible. Rigorous clean protocols were followed. A full body suit (Tyvek®), poly-latex boots and polythene gloves were worn at all times in the clean room. In the laboratory, a free-standing laminar flow hood and polythene gloves were used for sample, standard and reagent preparation. A sealable Perspex cube (350 x 350 x 400 mm) containing the reagents and sample was incorporated into the FI-CL instrumentation to provide a clean working area when not in the clean room e.g. during field deployment, with solutions transferred to the FI-CL analyser via PTFE tubes. All solution containers were closed and doubly sealed in plastic bags, except during solution manipulation.

2.3 Results and Discussion

All results presented in this chapter were obtained with the manifold shown in Figure 2.3, unless stated otherwise. Initial experimental conditions were 50 μM 1,10-phenanthroline, 50 mM NaOH, CEDAB at 12 mM, TEPA at 0.2 μM and H_2O_2 at 5 % (v/v). Reagent flow rates of 1.5 ml min^{-1} and a UHP carrier flow rate of 1 ml min^{-1} were used at the outset. A 100 nM Cu(II) standard was used initially with a 10 nM Cu(II) standard used for further refinement once optimisation had raised the sensitivity. Blanks consited of acidified UHP water (50 μl Q-HNO_3 100 ml^{-1}). Error bars on all graphs utilise a criterion of three times the standard deviation (3 s) of the signal (mV) for five replicate injections (n=5). Dixons Q-test was used to evaluate possible outliers.

2.3.1 1,10-Phenanthroline CL Reaction

The 1,10-phenanthroline CL reaction was selected for this study due primarily to its inherent sensitivity and selectivity for Cu(II). As reported by Federova *et al.*, (1982), the Cu(II) ion was chelated by one or two 1,10-phenanthroline molecules, each of which had a pair of nitrogen atoms with unpaired electrons that formed covalent bonds with the Cu(II) $[Cu\ phen_n]^{2+}$ (where n=1 or 2) (Figure 2.5 and I in Figure 2.6).

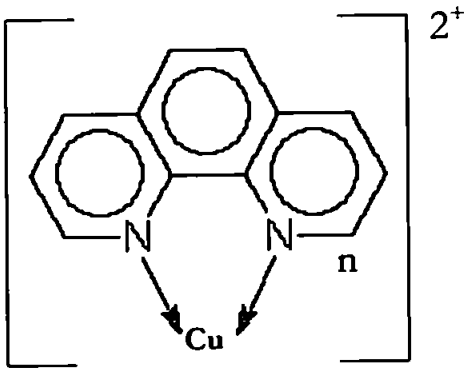

Figure 2.5 Chelation of Cu(II) by 1,10-phenanthroline

The chelated copper catalysed the decomposition of the hydrogen peroxide to produce superoxide radicals, although only a small fraction of them acted as oxidants, the majority propagating the catalytic decomposition of the hydrogen peroxide. The superoxide radicals oxidised the 1,10-phenanthroline to the excited CL emitter 3,3'-diformyl-2,2 dipyridyl (designated IV in Figure 2.6) and finally to 2'-dipyridyl-3,3'-dicarboxylic acid (V in Figure 2.6).

(Metal catalyst + 1,10-phenanthroline) + Oxidant in alkaline medium $\longrightarrow$ CL

The 1,10-phenanthroline underwent oxidative ring cleavage between the fifth and sixth carbon (C_5=C_6) by the superoxide radical ($O_2^{\cdot\bullet}$), which was reversibly added, resulting in the formation of a peroxide radical (I in Figure 2.6). The subsequent addition of an H^+ ion produced an uncharged radical (II in Figure 2.6), which then formed a dioxetane (III in Figure 2.6). This in turn decomposed to an electronically excited 3.3'-diformyl-2,2'-dipyridyl (IV in Figure 2.6), which decayed back to the ground state resulting in chemiluminescence (CL). Both compounds IV and V in Figure 2.6 have photoluminescent spectra similar to the CL spectra previously recorded by (Federova *et al.*, 1982) and are therefore possible CL emitters in the 1,10-phenanthroline CL reaction.

Several aspects of the 1,10-phenathroline reaction were investigated by Federova *et al.*, (1982). The intensity of the CL emission and the time to maximum CL emission were reported as dependent on the experimental conditions. The kinetics of the reaction follow;

$$\frac{dI}{dt} = -\alpha I^{3/2}$$ where I = Intensity of CL, α = coefficient of CL intensity

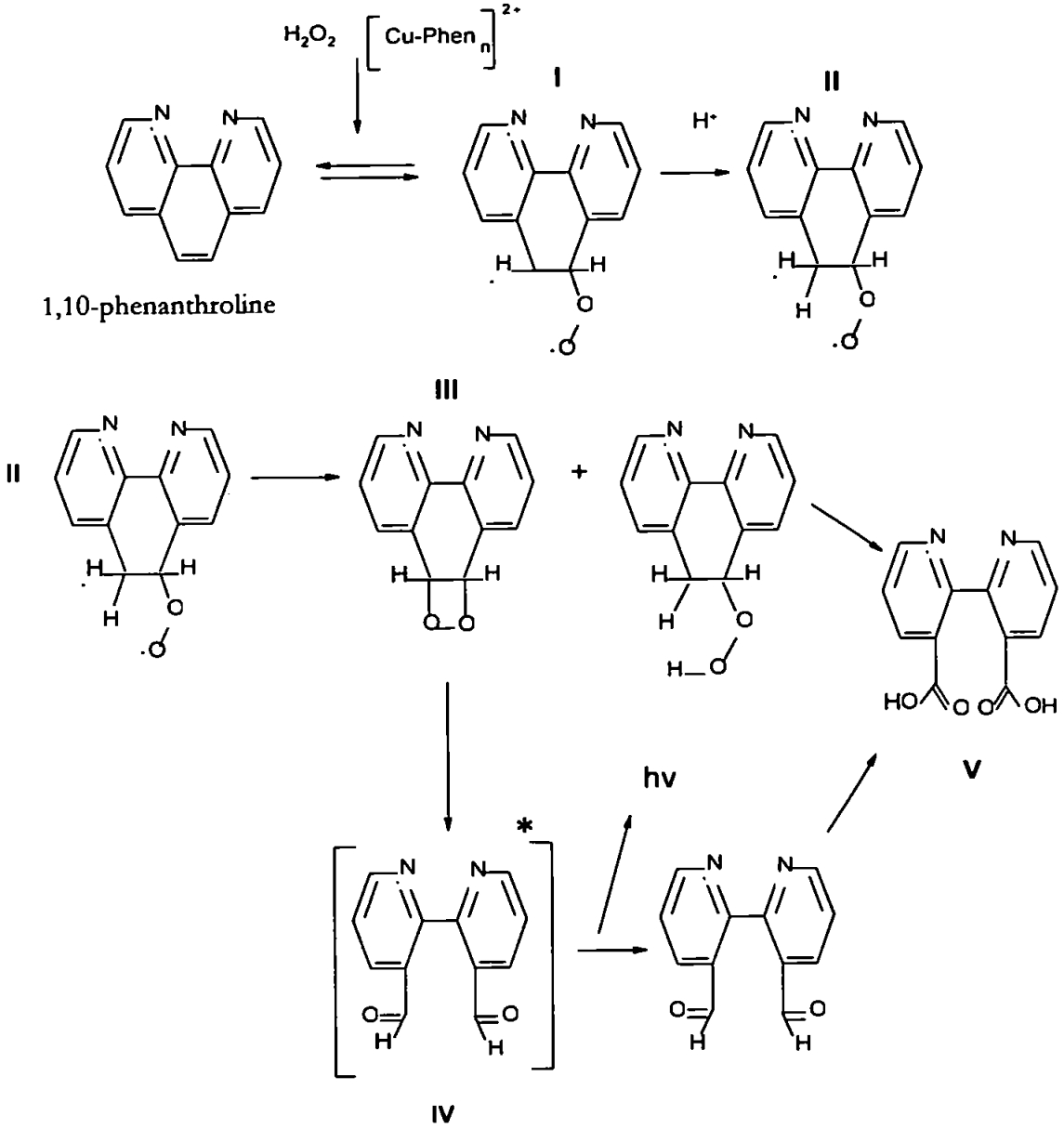

Figure 2.6 Mechanism of 1,10-phenanthroline CL Reaction

These authors also observed that when an alcohol was added, the CL quantum yield increased to a maximum 10^{-4} photons per molecule of 1,10-phenanthroline oxidised, compared to a mean of 10^{-6} photons per molecule in an alcohol free system. They postulated that the hydroxyl radicals formed from the alcohol did not participate in the formation of the excited state compounds. Sunda and Huntsman, (1991), utilising the 1,10-phenathroline CL reaction in a batch system, reported that the CL peak occurred 0.6-0.7 s after the mixing of the reagents and sample, enabling it to be used for near real time determination of Cu(II) in an FI manifold.

2.3.2 Optimisation of PMT Voltage

The sensitivity of the PMT detector was determined in part by the applied high voltage, which was optimised using a 10 nM Cu(II) standard in UHP water. The CL signal and PMT noise (measured as peak-to-peak noise on the baseline) are reported in Figure 2.7 over the applied voltage range of 950 – 1100 V, which was the maximum PMT operating voltage.

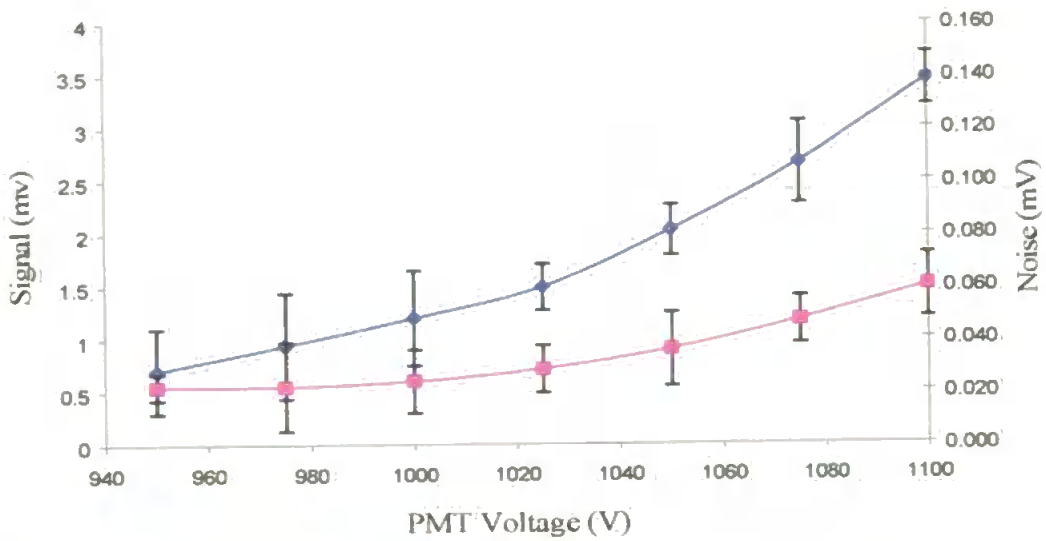

Figure 2.7 Optimisation of PMT Voltage. Sensitivity (mV) ——, Noise (mV) —— Cu(II) 10 nM in UHP water.

PMT sensitivity increased with voltage, although a corresponding increase in PMT dark current i.e. noise originating primarily from the thermionic emission of the cathode tube, also occurred. An optimal signal to noise ratio was found at 1075 V which was selected for all future work. This voltage also represented a balance between sensitivity and PMT lifetime, which would have been substantially reduced at higher applied voltages.

2.3.3 FI-CL Manifold Optimisation

Preliminary work: This focused on familiarisation with the Cu(II) catalysed 1,10-phenanthroline CL reaction and optimisation of the FI-CL manifold to enhance its sensitivity. In order to simplify the system, and its subsequent optimisation, the tetraethylenepentamine (TEPA) and the surfactant cetylethyldimethylammoniumbromide (CEDAB) were not included in the 1,10-primary reagent in the initial research. A 10 cm reagent mixing coil was used. Typical initial CL signal peaks for a 100 nM Cu(II) standard in UHP water were small, broad and ragged in profile. Increasing the flow rates of reagent and carrier streams from 1.22 to 1.91 ml min^{-1} resulted in a 100 % increase in signal.

Reducing the distance between the sample/reagent mixing "T" junction and the flow cell from 19 to 6 cm, the minimum distance achievable, also increased the CL signal.

After an initial good response from the FI-CL manifold, a 75 % reduction in sensitivity occurred with a concomitant decrease in reproducibility. The experimental parameters in use were therefore investigated. Fresh reagent solutions and standards were prepared, and the reagent/carrier flow rates varied. A full manifold decontamination protocol was put in place (0.2 M HCl soak, 1M HCl wash with a UHP water rinse), together with a full manifold rebuild. Heating of the reagent stream was introduced over the temperature range of 10 – 40° C without any effect. The addition of the surfactant cetylethyldimethylammoniumbromide (CEDAB) to the primary reagent (Section 2.2.1) restored the sensitivity and reproducibility of the CL reaction. All subsequent work used the 1,10-primary reagent incorporating CEDAB.

The experimental variables were optimised using a univariate approach and subsequently a simplex algorithm (Section 2.3.5). For the univariate method the physical operational parameters of reagent mixing coil length (both knitted and coiled), sample loop volume (µl) and reagent flow rate (ml min^{-1}) were optimised. This was followed by univariate optimisation of the concentration of the components of the 1,10 primary reagent, namely 1,10-phenanthroline (µM), CEDAB (mM), NaOH (mM) and TEPA (µM), and also the H_2O_2 (% v/v).

2.3.3.1 Reagent Mixing Coil Length

Sunda and Huntsman, (1991) reported the use of a water bath to preheat the reagents to 40° C to accelerate the production of the superoxide radical from the H_2O_2 and increase the activity of the mixed reagents. Although a necessity for the generation of a CL signal in the early part of this research, the practicalities of using a water bath made it unsuitable for field deployment and therefore it was removed, simplifying the system. Increasing the reagent mixing coil length from 10 to 450 cm substantially improved mixing and compensated for the loss of sensitivity due to the absence of a water bath. Optimisation of the geometry, i.e. both knitted and coiled designs, and of the length of the reagent mixing coil (Table 2.2), were therefore important in order to maximise manifold sensitivity.

Table 2.2 Reagent Mixing Coil Length

Knitted Length (cm)	Signal (mV)	RSD (%)		Coiled Length (cm)	Signal (mV)	RSD (%)
0	14.6	7.7		0	13.9	1.9
100	16.6	2.1		100	16.7	2.9
200	17.2	2.9		150	17.0	3.5
300	15.7	1.4		200	16.6	1.2
400	16.0	1.8		250	16.2	2.2
500	15.8	0.0		300	15.9	0.0
600	16.0	1.8		400	16.2	2.6
650	15.5	1.3				

Acidified Cu(II) (pH 2, 100 nM) in UHP water

A CL signal maximum was reached at 200 and 150 cm for the knitted coil and coiled reagent mixing coils respectively with good reproducibility (< 4 %, n =5) seen for both types of coil. The 200 cm knitted coil was selected for future use to maximise manifold sensitivity, although the incorporation of both types of coil significantly improved manifold sensitivity compared with their absence. The improved mixing of the two reagent streams enhanced the migration of the superoxide radicals, produced from the catalytic decomposition of the H_2O_2, to the micellar environment of the 1,10-primary reagent. However, provided there was a minimum mixing time for the CL reagents, extending the coil length had no significant effect on the signal. The use of a reagent mixing coil, particularly the knitted coil, increased the three dimensional disorientated flow due to the development of secondary flows which promoted very effective radial dispersion and reduced axial dispersion (Section 2.3.4). This occurred without the drawbacks of bead reactors such as the possible entrapment of small bubbles and solid particles. More efficient reagent mixing occurred with the reagent mixing coil, the dispersion coefficient (D) was decreased and the CL signal was enhanced.

2.3.3.2 Sample Volume

An efficient FI manifold minimises dispersion of the sample in the reagent stream, an important factor that impacts significantly on sensitivity. Dispersion was strongly influenced by the sample injection volume, which was thus optimised over a 10 to 400 µl range (Figure 2.8).

The CL signal rose to a signal plateau (230 – 400 µl) as the sample injection volume increased, due to a reduction in the dispersion coefficient (D) of the sample into the reagent stream, which improved the stoichiometric ratio between Cu(II) and the CL

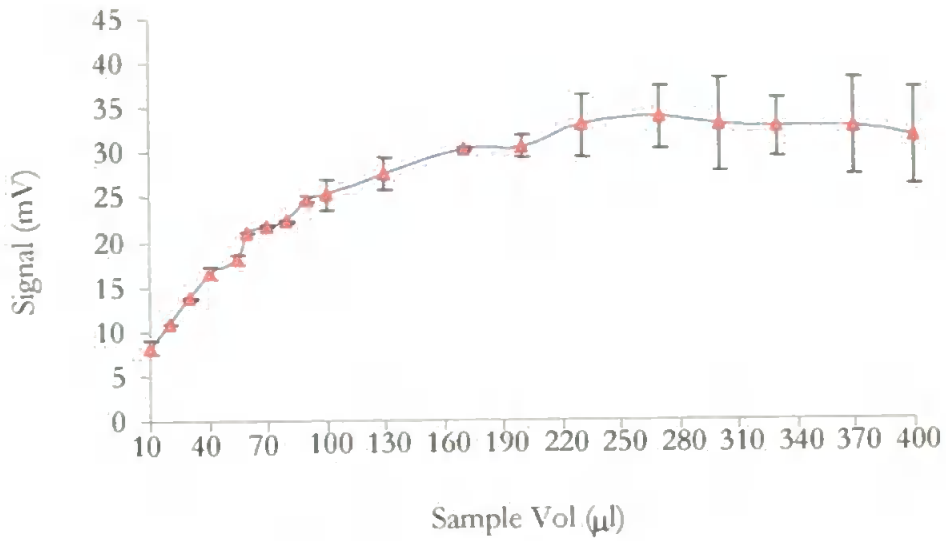

Figure 2.8 Sample Loop Volume Optimisation (µl). Cu(II) 100 nM in UHP water.

reagents. Minimisation of the length of FI lines after reagent/sample mixing also reduced the dispersion. At the larger sample volumes used, a stoichiometric limitation of the CL reaction occurred due to the binding of the Cu(II) by the 1,10-phenanthroline becoming rate limiting. A deterioration in reproducibility was observed at larger sample volumes, which was attributed to the stoichiometric limitation of the 1,10-phenanthroline, the production of secondary CL emitters (Federova *et al*, 1982) and the variability in mixing at the confluence zone due to the different sample and reagent flow rates causing channelling of the streams. A sample volume of 270 µl was chosen as an optimum balance between sensitivity (the priority) and maintaining good reproducibility.

2.3.3.3 1,10-Phenanthroline Solubility and Concentration

The 1,10-phenanthroline was central to the selected CL reaction (Section 2.3.1) and therefore its role was investigated. At the outset of this study two different forms of 1,10-phenanthroline were used, initially a monohydrate and then, due to difficulty in ensuring complete dissolution of the monohydrate, an anhydrous form that CRC data reported had improved solubility in both cold and hot water.

Solubility of 1,10-phenanthroline: In order to investigate their sensitivity at different stock concentrations, three monohydrate and anhydrous 1,10-phenanthroline concentrations were prepared from which appropriate aliquots were included in the 1,10-primary reagent to produce a 50 µM final concentration. The CL responses are shown on Figure 2.9.

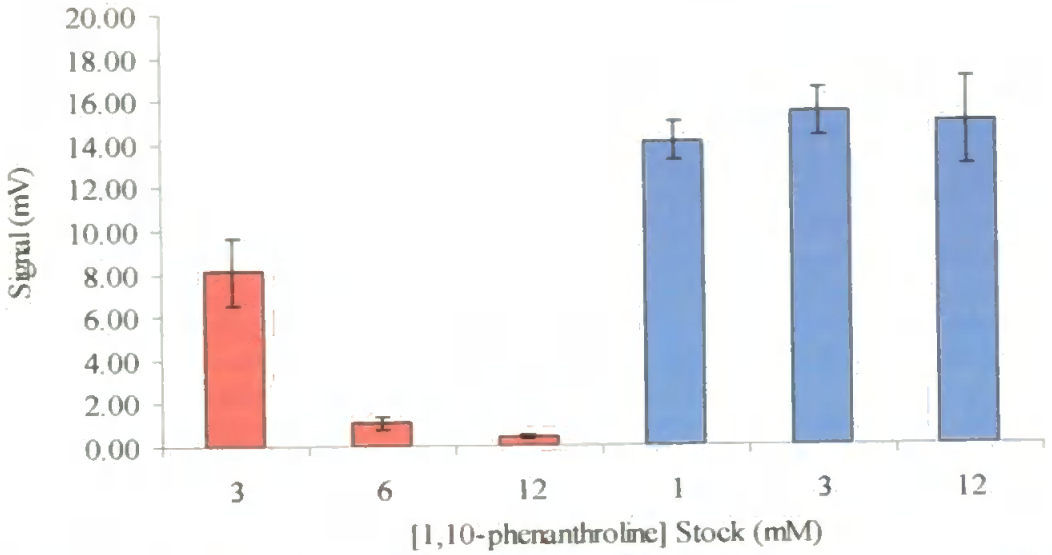

Figure 2.9 Solubility of 1,10-phenanthroline. Monohydrate 1,10-phenanthroline , Anhydrous 1,10-phenanthroline . Cu(II) 100 nM in UHP water.

For the monohydrate 1,10-phenanthroline, the CL signal was substantially improved at a 3mM stock concentration, which required a 10 min sonication to achieve complete dissolution. The difficulty in dissolving the monohydrate form was very evident when preparing the 12 mM 1,10-phenanthroline stock. Heating in a water bath (55 ^{o}C) with prolonged sonication (30 min) was required for its complete dissolution. This was an observation supported by CRC data, which specified low solubility for the monohydrate in either cold or warm water.

The anhydrous 1,10-phenanthroline, in comparison with the monohydrate, gave a much improved CL signal over the whole concentration range. It was considerably easier to prepare, requiring only a little warming, with a 5 min sonication used to ensure homogeneity of solution. The anhydrous 3 mM solution (0.0541g in 100 ml of UHP water) had good reproducibility with a marginally better response, and was thus selected for subsequent use. It is clearly important to use the anhydrous 1,10-phenanthroline to simplify preparation, ensure CL occurs and maximise the sensitivity of the FI-CL manifold. This is not reported in the literature and the anhydrous reagent is only available from a limited number of suppliers.

Equilibrium Time for the 1,10-Phenanthroline Primary Reagent: The CL emission is a direct function of the optimum interaction of the CL active components in the 1,10-primary reagent. The optimum time for equilibration between components of the 1,10-primary reagent was therefore investigated (Figure 2.10).

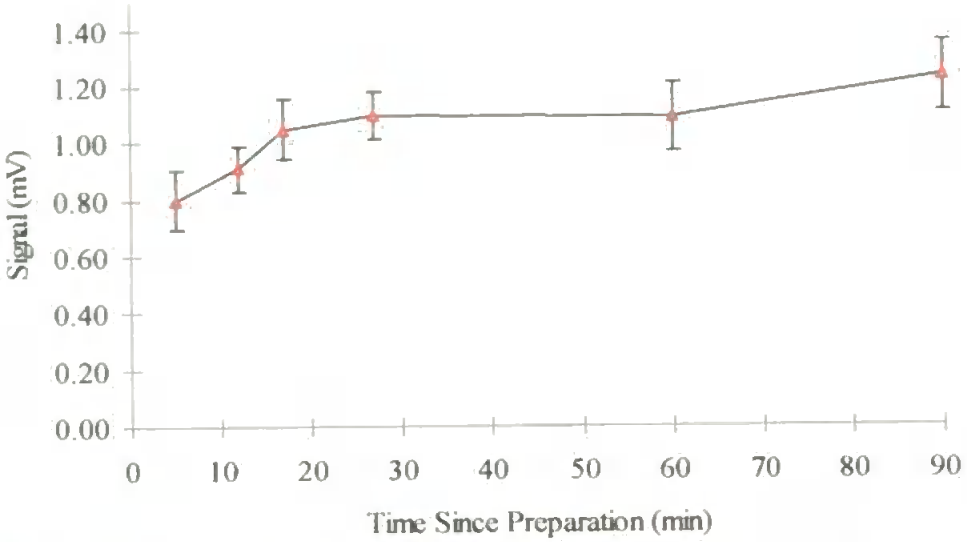

Figure 2.10 Equilibration Time for 1,10-phenanthroline/CEDAB. 100 nM Cu(II) in UHP water.

A rise in CL was observed as the time after preparation of the 1,10-primary reagent rose. When left to age overnight (12 h, not shown), the CL increased a further 56 % above that observed at 90 min. The overnight equilibration established a stable micellar microenvironment (Section 2.3.3.5), with the uncharged 1,10-phenanthroline positioned at the micellar interface where the polarity was less pronounced. This stabilised the active CL excited state species e.g. 3.3'-diformyl-2,2'-dipyridyl, promoting the formation of the excited species and aiding the resonance energy transfer between them and their decay back to ground state with CL emission. For subsequent experiments the 1,10-phenanthroline primary reagent was allowed to equilibrate overnight prior to use. Subsequent observation showed that this reagent, when stored in the dark at 4 ^{o}C, was stable for 3 weeks without any significant reduction in signal. The optimum concentrations of the 1,10-phenanthroline, NaOH and CEDAB in the 1,10-primary reagent were then determined by a univariate method.

1,10-Phenanthroline Concentration in the Primary Reagent: The 1,10-phenanthroline has a critical role in the CL reaction, binding with Cu(II) to form a complex which catalyses the decomposition of the hydrogen peroxide and is also oxidised to the electronically active dioxetane species from which CL is emitted. The concentration of the 1,10-phenanthroline was therefore investigated over the ranges 20 - 200 µM and 10 - 90 µM (Figure 2.11).

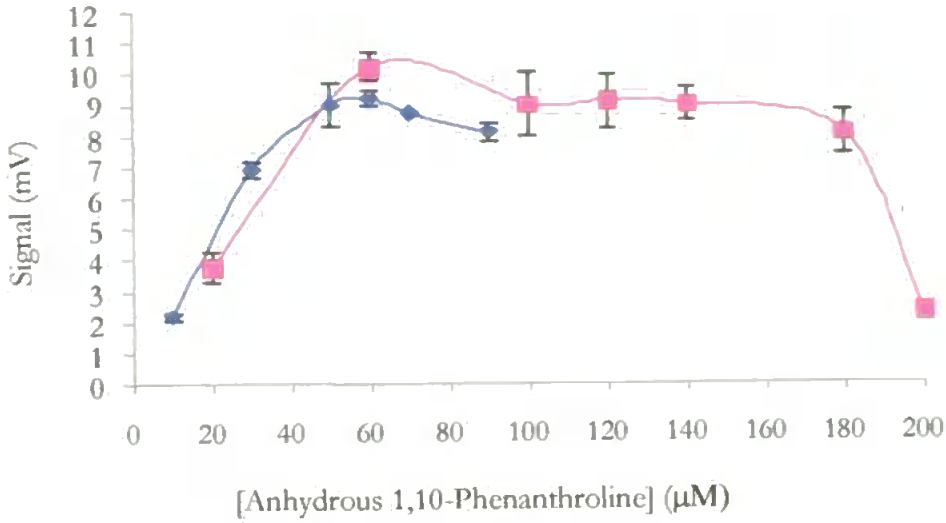

Figure 2.11 Optimisation of 1,10-phenanthroline Concentration (20 μM to 200 μM) in 1,10-primary reagent. Cu(II) 100 nM in UHP water. Two experiments, first over the full range 1,10-phenanthroline and the second focused on the experimental maximum observed from the first experiment.

The optimum 1,10-phenanthroline concentration was found to be 60 μM in both experiments. Below 30 μM the formation of the 1,10-phenanthroline-Cu(II) complex, an essential first step in the CL reaction, was limited. At the lower concentrations of 1,10-phenanthroline used it was more dispersed at the micelle interface, restricting the CL quantum yield. A rapid quenching of the signal was seen above 180 μM due to molecular aggregation which bound up the Cu(II) or a reduction of micelle stability. The quenching occurred by dissipation of the CL emission via a non-radiative pathway such as molecular collisions, intersystem crossing or internal conversion, rather than CL.

Federova *et al.*, (1982) reported that the concentration of the 2,2'-dipyridyl-3,3'-dicarboxylic acid at the cessation of the CL reaction was the same as the concentration of the 1,10-phenanthroline at the outset, showing that it was all converted. The same authors also found that the CL emission did not remain constant until the oxidisation of the 1,10-phenanthroline was almost complete and that the overall number of photons emitted was always proportional to the concentration of the 1,10-phenanthroline. Furthermore, the CL intensity was also reported to correlate with the rate of disappearance of the 1,10-phenanthroline and not with the initial reaction rate. The concentration of the 1,10-phenanthroline therefore determines the intensity of the CL emission with respect to time (Federova *et al.*, 1982), demonstrating its central role in the CL reaction and highlighting the importance of its solubility. A concentration of 60 μM was used for all subsequent studies.

2.3.3.4 Sodium Hydroxide Concentration

The 1,10-phenanthroline CL reaction has been reported to be sensitive to pH (Coale *et al.*, 1992), a factor principally influenced by the NaOH concentration in the 1,10-primary reagent. This was therefore investigated over the range of 10 to 100 mM NaOH (Figure 2.12 and Table 2.3).

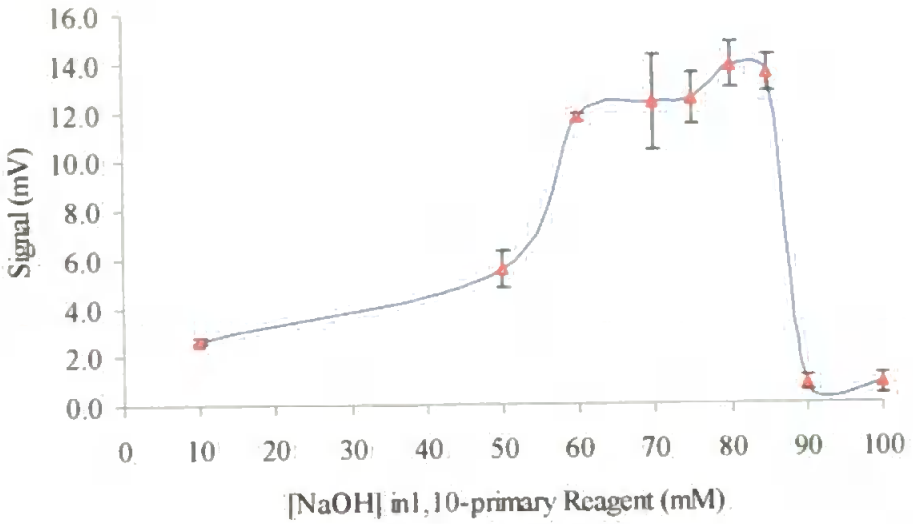

Figure 2.12 Optimum NaOH Concentration (mM) in 1,10-primary Reagent. Cu(II) 100 nM in UHP water.

Table 2.3 Optimal pH Provided by [NaOH] (mM)

[NaOH] (mM)	pH of Waste	Signal (mV)	RSD (%)
10	9.4	2.7	2.5
50	10.3	5.5	5.9
60	10.4	11.8	4.8
70	10.5	12.3	2.8
80	10.5	13.9	2.7
85	10.5	13.5	4.2
90	10.6	0.9	6.4
100	10.7	0.8	6.9

Cu(II) 100 nM in UHP water

The optimum NaOH concentration in the 1,10-primary reagent was 80 mM, with a significant reduction in signal at 90 mM due to a non-radiative decay pathway occurring at NaOH concentrations in excess of 85 mM. The alkaline pH of the 1,10-primary reagent was thus important, the basic CL reaction medium it produced also promoting the catalytic decomposition of hydrogen peroxide to produce superoxide radicals. The latter were also stabilised in a basic medium (Federova *et al.*, 1982), which also promoted the formation of the CEDAB micelles.

2.3.3.5 CEDAB Concentration

The significantly reduced signal reported earlier (Section 2.3.3) and observed again in the simplex optimisation (Section 2.3.5) was due to the omission of the surfactant cetylethyldimethylammoniumbromide (CEDAB) from the 1,10-primary reagent. This demonstrated the central role of CEDAB in the 1,10-phenanthroline CL reaction, and the need to the optimise its concentration in the 1,10-primary reagent (Figure 2.13).

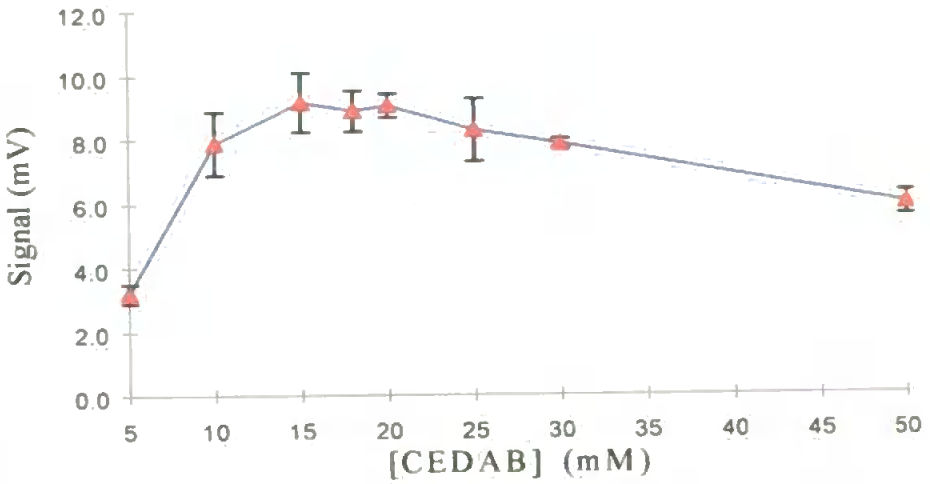

Figure 2.13 Optimum CEDAB (mM) Concentration in 1,10-primary Reagent. Cu(II) 100 nM in UHP water.

The optimal CEDAB concentration was 15 mM at which stable micelles are formed. Previously reported work (Coale *et al.*, 1992) indicated that the CEDAB enhanced the CL signal but was not a primary requirement for a reproducible CL reaction. The erratic CL emission observed early in this study until the inclusion of CEDAB in the 1,10-primary reagent suggested it was an absolute requirement.

As an organised assembly, CEDAB promoted the solubilisation, compartmentalisation and concentration of the three other components of the 1,10-primary reagent, i.e. 1,10-phenanthroline, NaOH and TEPA. In the stable micellar microenvironment the energy transfer and deactivation processes that resulted in CL emission were enhanced. The uncharged non-ionic species of 1,10-phenanthroline that is thought to be formed in an alkaline medium (Federova *et al.*, 1982), migrated to the apolar Stern region at the micelle surface rather than the polar water molecules. The anionic superoxide radical was also attracted to the positively charged micelle surface.

The active CL species were thus brought into close proximity, reducing the distances between the energy donor and acceptor molecules (Bowie *et al*,. 1995), enhancing

the resonance energy transfer that occurs when the excited donor and acceptor are a maximum of 10 nm apart. The formation of dioxetane, the electronically excited CL emitter was therefore promoted, enhancing the quantum efficiency of the CL reaction. It is unlikely that the CL emitter entered the micelle itself, which is a more hydrophobic environment than the Stern region, since this enclosed environment would restrict non-emissive energy transfer (Yamada and Suzuki, 1984).

The wavelength (λ max) for the CL emission was reported as 445- 450 nm by Federova *et al.* (1982). However, when the surfactant (CEDAB) was added, λ max was reduced to 380 nm due to alteration of the polarity of the microenvironment of the emitting species.

2.3.3.6 Hydrogen Peroxide Concentration

The central role of the hydrogen peroxide to the CL reaction was highlighted by the absence of a CL signal when a new batch of Aldrich H_2O_2 was used. The Aldrich hydrogen peroxide was then compared to batches from BDH and Fluka. A CL signal was not observed using the same bottle of Aldrich hydrogen peroxide, indicating that it was faulty, since both Fluka and BDH brands resulted in CL. The Fluka brand was used for the subsequent optimisation of its concentration (Figure 2.14) and all subsequent studies.

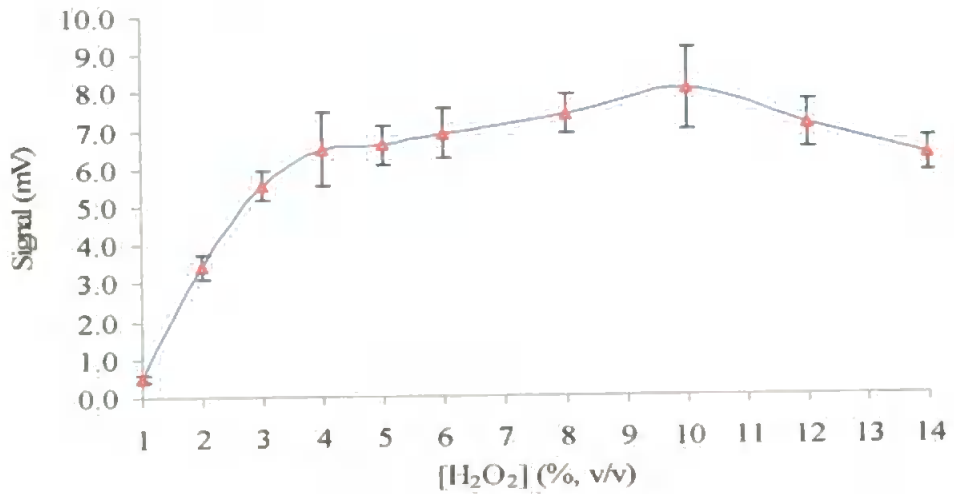

Figure 2.14 Optimisation of H_2O_2 Concentration

A signal maximum was seen at 10 % (v/v) H_2O_2, with a reduction in CL at higher concentrations due to the formation of an alternative, non-emissive reaction pathway. The sequential oxidation of the 1,10-phenanthroline to produce the electronically excited dioxetane species occurred when the 1,10-phenanthroline reacted either with the H_2O_2

flow cell. The former required cooling to –20 °C to reduce its magnitude. TEPA was added to the 1,10-primary reagent as a final component, in order to reduce the baseline CL 'noise' catalysed by the trace Cu(II) impurities. Investigation of the TEPA concentration resulted in an optimum of 0.4 μM. The effect on the noise of the addition of TEPA (0.4 μM) to the 1,10-primary reagent was evaluated 5 and 60 min after its addition (Figure 2.15).

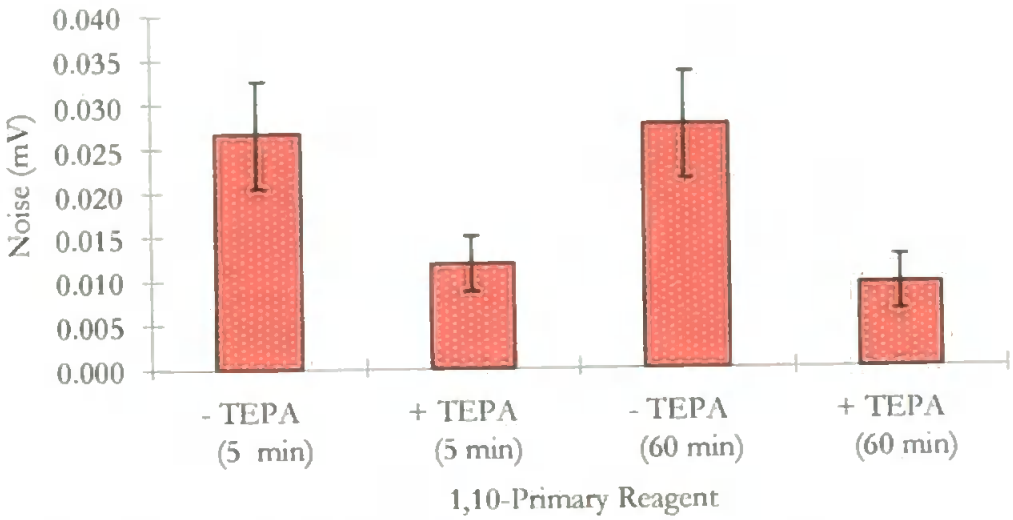

Figure 2.15 Incorporation of TEPA into 1,10-primary Reagent. With (+) and without (-) TEPA (0.4 μM), with time (min) after addition of the TEPA to the 1,10-primary reagent.

The baseline noise level was substantially reduced after the addition of the TEPA (55 % at 5 min, and 64 % at 60 min), a complexing agent for Cu(II), due to it chelating the Cu(II) impurities in the 1,10-primary reagent. The further decrease in the noise at 60 min suggested that the kinetics of the TEPA chelation were relatively slow. The TEPA also affected the position of the baseline trace on the chart recorder. The noise originating solely from the PMT, without the reagent streams flowing, was recorded as a baseline trace (0.0 mV) on the chart paper. With the reagents flowing, but without TEPA, the chart pen moved up the chart due to the noise catalysed by Cu(II) impurities in the primary reagents, stabilising at + 0.75 mV (5 mV full scale). After the addition of TEPA to the 1.10-primary reagent and with the reagents flowing, the baseline moved down off the chart to the 'stop', requiring a manual adjustment to return the pen to the chart. This confirmed the scavenging action of the TEPA. The stabilisation of the CL reactive species by the CEDAB microenvironment may have also enhanced the TEPA action.

2.3.4 Flow Rates in the FI-CL Manifold

2.3.4.1 Pump Tubing Calibration

An important criterion in FI is reproducible dispersion, which requires constant flow rates within the FI manifold. A range of pump tubing (Acu Rated, Elkay) of varying internal diameters was therefore calibrated (Figure 2.16) using a multi-channel, variable speed peristaltic pump (Watson Marlow 503S, 6 channel, 8 roller head).

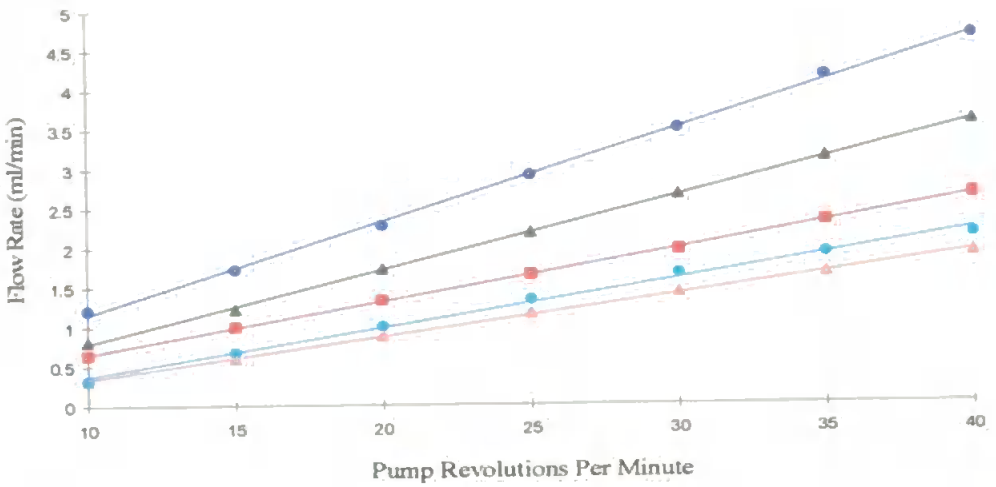

Figure 2.16 Calibration of Pump Tubing and Watson Variable Speed (503 S) Pump. Elkay Acu Rated Auto Analysis Pump Tubing used, i.d. signified by the different bridge colours. Bridge Colour - Blue/Yellow ▬, Grey ▬ ,Red ▬, White ▬, Orange ▬.

The flow rates for the pump tubing were linear over the range of pump speeds used. The pump tubing was routinely replaced after 30 h usage to ensure accurate flow rates. All pump tubing was conditioned by acid cleaning (0.2 M HCl) for 1 h followed by a 1 h UHP water rinse prior to use.

2.3.4.2 Reagent Flow Rates

CL reactions are typically very fast (0.1-10 s) compared with spectrophotometric derivatisation reactions and the response is transient. It was therefore important to ensure the time for the in-line CL reaction to develop was at its optimum, i.e. that the maximum CL emission took place in the spiral flow cell in front of the detector window. This required optimisation of the flow rates of the 1,10-primary reagent and the H_2O_2 (Figure 2.17), to ensure efficient mixing.

A linear increase in the CL emission ($R^2 = 0.9826$) was seen over the flow rate 1.0 – 3.5 ml min^{-1}. The improvement in CL was attributed to increased turbulence that improved the mixing of the reagents and their mixing with the sample. In addition, the time for the

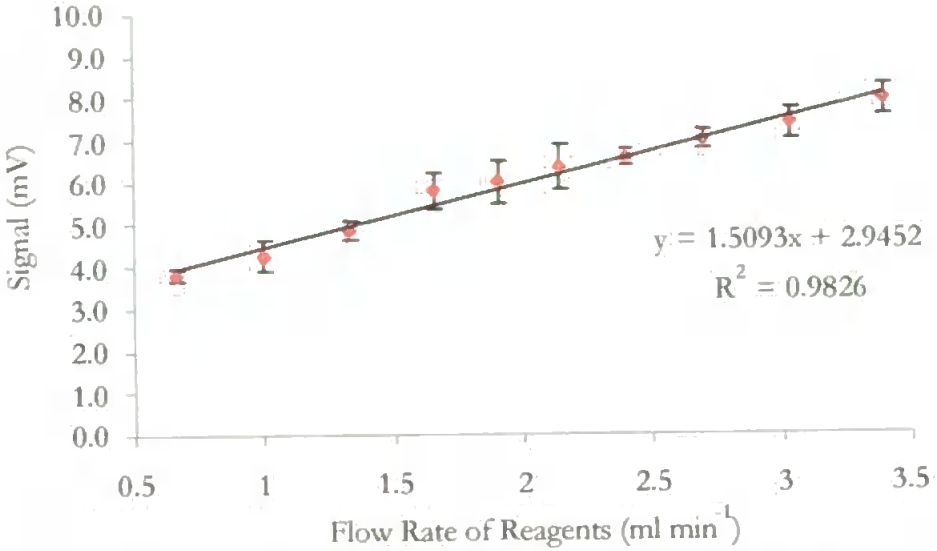

Figure 2.17 Flow Rate of CL Reagents – 1,10-primary Reagent and H_2O_2. Cu(II) 100 nM in UHP water.

CL reaction to reach the flow cell was reduced at higher flow rates, with a greater number of molecules reacting in front of the detector window. An increased flow rate could be used to enhance the sensitivity of the FI-CL analyser if environmental Cu(II) concentrations were close to the LOD. At lower flow rates, the maximum reaction rate (and therefore the CL emission) occurred before the sample/reagent zone reached the detector window.

A flow rate of 2.6 ml min^{-1} was selected for subsequent work, which represented a balance between high sensitivity and low reagent consumption. These were important factors for shipboard deployment.

2.3.5 Simplex Optimisation

A Simplex algorithm is a mathematically based experimental design that can be utilised for investigating and optimising a surface response, which is a graphical representation of a response as a function of one or more factors. A simplex program is a geometrical figure with f + 1 sides for f factors, e.g. a simplex for two factors is a triangle (Figure 2.18). The points or vertices of the simplex are used as the co-ordinates, the worst response being rejected each time as it searches the solution space (Miller and Miller, 2000). The method works best when the response or the factors vary in a continuous manner within a specific range, and this study was so designed i.e. a set range with specifically sized steps.

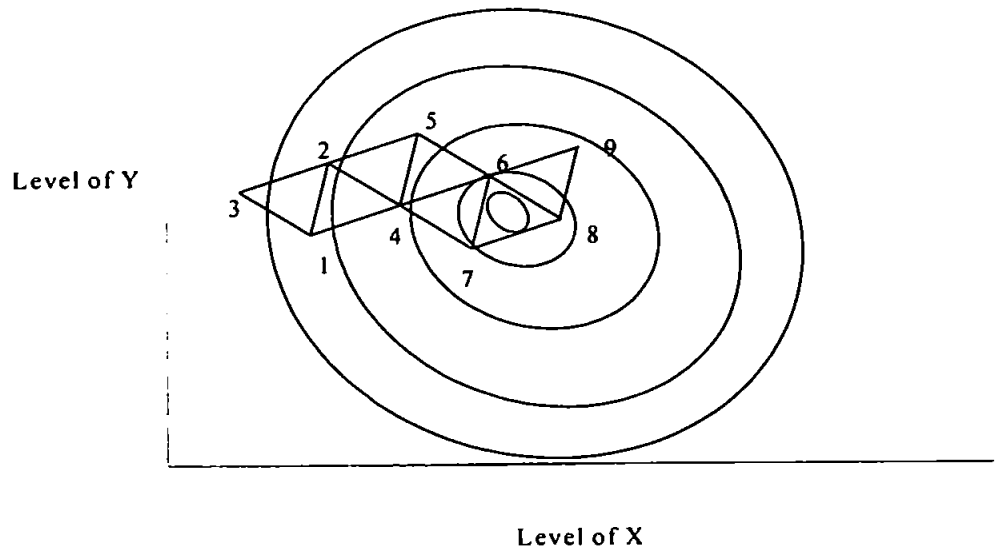

Figure 2.18 Pictorial Depiction of Simplex (Miller and Miller, 2000)

The aim of the simplex optimisation was to improve the sensitivity of the FI-CL manifold for the determination of Cu(II). The large number of analytical variables (eight), could have resulted in an unacceptably large number of iterations in a one stage simplex and therefore a two stage simplex was utilised for this study. The first stage optimised the physical operational variables of knitted reagent mixing coil length, reagent flow rates, and sample injection volume. The second stage optimised the concentrations of the 1,10-phenanthroline, the CEDAB, the NaOH and the TEPA in the 1,10-primary reagent, together with the concentration of the H_2O_2.

2.3.5.1 Simplex for Physical Variables Using 100 nM Cu(II)

The range of values used for the simplex optimisation of the key analytical variables for the Cu(II)-FI-CL manifold was centred on the univariate optimised conditions for the FI-CL manifold, shown in Table 2.4. The values used at the outset of the simplex optimisation of the physical variables are shown in Table 2.5. The simplex size (starting values), were selected as one third of the total range under investigation. Precision regulated the size of the simplex steps, for which values were chosen which enabled the full range to be investigated in an acceptable number of iterations. e.g. for sample volume the simplex searched the range 10 – 400 µl, beginning at 120 µl using a possible thirteen 30 µl steps.

Table 2.4 Summary of Univariate Optimised Parameters

Experimental Parameter	Optimised Value
Reagent flow rates	3.6 ml min^{-1}
Knitted reagent mixing coil	200 cm
Sample injection volume	270 µl
[1,10-phenanthroline]	60 µM
[NaOH]	80 mM
[CEDAB]	15 mM
[TEPA]	0.4 µM
$[H_2O_2]$	8 % (v/v)

Cu(II) 100 nM in UHP water

Table 2.5 Simplex Variables and Iteration Parameters for Optimisation of Physical Variables

Variable	No	Precision	Max.	Min	Simplex Size	Units
Sample volume.	1	30	400	10	120	µl
RMC length	2	100	600	0	200	cm
Flow rate	3	0.33	3.63	0.5	1.3	ml min^{-1}

Reagent concentrations of 1,10-phenanthroline (60 µM), CEDAB (15 mM), NaOH (80 mM), TEPA (0.4 µM) and hydrogen peroxide (8 %) were used. RMC – reagent mixing coil

The simplex was concluded after eighteen iterations (Table 2.6).

Table 2.6 Results of Simplex Algorithm for Physical Parameters

Iteration Number	Sample Volume (µl)	Reagent Mixing Coil length (cm)	Flow Rate (ml min^{-1})	Signal (mV)	RSD (%)
1	120	0	1.33	7.2	2.2
2	240	200	1.33	8.8	1.6
3	180	400	1.33	8.4	1.8
4	180	300	2.64	9.2	4.6
5	270	400	2.31	9.2	2.3
6	270	200	2.97	10.8	1.1
7	330	100	3.63	11.4	4.3
8	300	300	3.63	12.2	2.3
9	270	100	3.63	11.9	1.2
10	300	0	3.63	11.0	3.3
11	300	200	3.63	12.5	1.3
12	390	200	3.63	13.1	2.6
13	270	500	3.63	12.0	1.7
14	330	300	3.63	13.0	2.4
15	390	0	3.63	11.7	2.1
16	360	100	3.63	13.6	1.5
17	360	600	3.63	13.1	0.8
18	300	600	3.63	11.8	0.7

Cu(II) 100nM in UHP water

After 18 iterations, a sufficient number that ensured the algorithm was not trapped in a local maximum, the simplex reached a plateau in response. The optimum physical variables as derived by simplex (100 nM Cu(II)) were a sample injection volume of 360 µl, a 100 cm knitted reagent mixing coil and a primary reagent flow rate of 3.6 ml min^{-1} (iteration 16). The simplex fitted the CL reagent flow rates to the upper boundary value indicating that, if environmental Cu(II) concentrations were very low, higher reagent flow rates could be used to increase manifold sensitivity.

2.3.5.2 Simplex for Physical Variables Using 10 nM Cu(II)

Ambient oceanic Cu(II) concentrations are 0.5 – 6 nM (Coale *et al.*, 1992) and therefore to simulate seawater concentrations of copper a further simplex optimisation of the physical parameters was performed (Table 2.7) using a 10 nM Cu(II) standard prepared in UHP water. The simplex starting variables and reagent concentrations were those used for 100 nM Cu(II) (Table 2.5).

The physical operational variables derived by simplex for 10 nM Cu(II) were in good agreement with those derived by simplex for 100 nM (Table 2.8). Comparison of CL

Table 2.7 Results of Simplex for Physical Variables

Sample Volume (µl)	Knitted RMC Length (cm)	Reagent Flow Rate (ml min^{-1})	Signal (mV)	RSD (%)
120	200	1.33	1.1	5.6
240	200	1.33	1.5	3.8
180	400	1.33	1.4	4.5
180	300	2.64	1.5	2.5
180	300	2.31	1.8	4.7
360	500	2.64	2.2	3.1
270	600	3.30	1.8	3.3
390	600	3.63	2.0	4.2

10 nM Cu(II) in UHP water. Reagent concentrations of 1,10-phenanthroline (60 µM), CEDAB (15 mM), NaOH (80 mM), TEPA (0.4 µM) and hydrogen peroxide (8 %) were used. RMC – Reagent Mixing Coil.

peaks at the outset and upon conclusion of the simplex (10 nM Cu(II)) showed a 48 % improvement in the sensitivity of the FI-CL manifold. As with the 100 nM Cu(II), the sample volume and reagent flow rates were more influential than the reagent mixing coil length. The reduction in optimum flow rate for the reagents to 2.6 ml min^{-1}, reduced the dispersion of the Cu(II) and so enhanced the stoichiometric ratio of sample to reagent. The optimum length for the knitted reagent mixing coil rose to 500 cm for 10 nM Cu(II), which

enhanced the mixing of the reagents and resulted in a more efficient migration of the superoxide radicals to the CEDAB microenvironment.

Table 2.8 Summary of Simplex Derived Physical Variables

[Cu(II)] (nM)	Sample Injection Volume (µl)	Knitted RMC Length (cm)	Reagent/Carrier Flow Rate (ml min^{-1})
100	360	100	3.6
10	360	500	2.6

Cu(II) 10 nM and 100 nM in UHP water

2.3.5.3 Simplex for Reagent Concentrations Using 10 nM Cu(II)

A simplex optimisation of the reagent concentrations was conducted utilising the simplex derived optimum physical parameters for 10 nM Cu(II) (Table 2.8). The starting values shown in Table 2.9 and results in Figure2.19 and Table 2.10.

Table 2.9 Simplex Variables and Iteration Parameters

Variable	No	Precision	Max	Min	Simplex Size	Units
[1,10 Phenan]	1	20	100	20	40	µM
[CEDAB]	2	10	25	5	15	mM
[TEPA]	3	0.2	1	0	0.4	µM
[NaOH]	4	20	120	40	80	mM
[H_2O_2]	5	2	11	1	5	% (v/v)

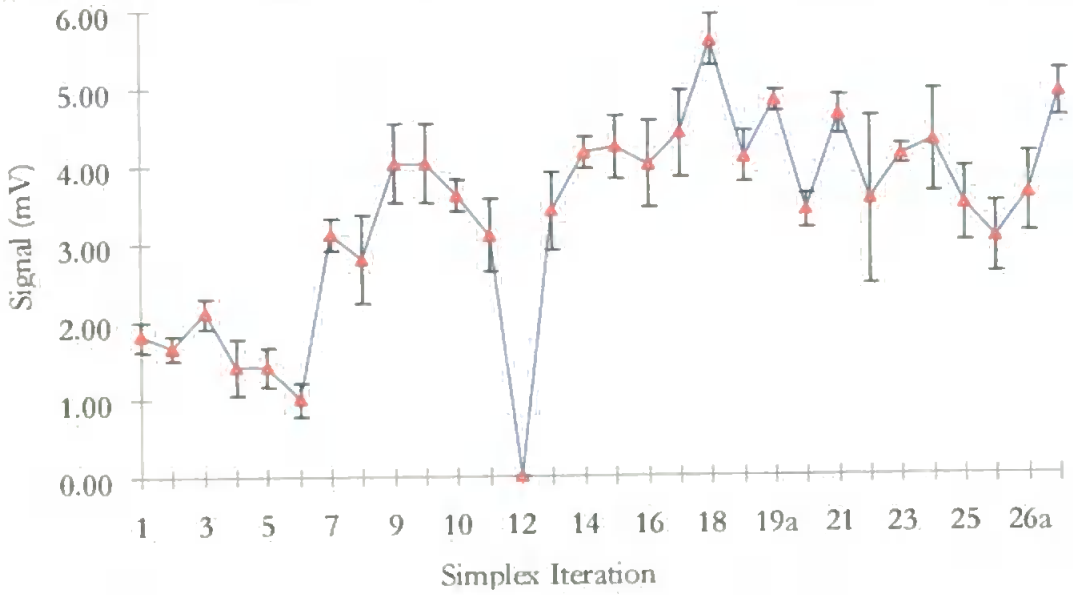

Figure 2.19 Simplex Optimisation of Reagent Concentrations. Cu(II) 10 nM in UHP water. The simplex derived variables of a sample volume of 360 µl, a knitted reagent mixing coil of 500 cm and a reagent and carrier flow rate of 2.6 ml min^{-1} were used.

Table 2.10 Significant Responses of Simplex Optimisation of Concentration of Reagents

Iteration No	1.10 (μM)	CEDAB (mM)	TEPA (μM)	H_2O_2 (%)	NaOH (mM)	Signal (mV)	RSD (%)
5	60	15	0.8	4	80	1.4	6.8
6	60	15	0.4	4	120	1.0	6.7
9	60	5	0.6	8	60	4.0	1.6
12	60	0	0.6	10	60	0.0	0.0
15	80	15	0.4	10	60	4.2	3.7
16	40	15	0.4	10	60	4.0	5.2
18	60	15	0.2	8	80	5.6	2.2
19a	80	5	0.2	6	60	4.8	1.0
21	80	15	0.4	8	60	4.6	4.5
24	60	5	0.2	8	60	4.3	5.9
27	60	15	0.4	10	80	4.9	2.9

Due to the time required for CEDAB to dissolve, concentrations of 0, 5, 10, 15, 20 and 25 mM were first prepared, to which appropriate aliquots of NaOH, 1,10-phenanthroline and TEPA were added. Each batch of 1,10-primary reagent was allowed to stand for 2 h before use to reach equilibration. The simplex algorithm required 3 days to reach conclusion, with day to day correlation of results achieved by repetition of the last optimisation upon continuation of the simplex the next day.As can be seen from Figure 2.19, a clear CL signal maximum was obtained for iteration 18, which utilised a 1,10-phenanthroline concentration of 60 μM, CEDAB at 15 mM, NaOH at 80 mM, TEPA at 0.2 μM and hydrogen peroxide at 8 (% v/v). These were the reagent concentrations used for all subsequent experiments. A good correlation was seen between the optimisations repeated on successive days. The omission of CEDAB from the 1,10-primary reagent (iteration 12), resulted in no measurable response being observed due to the absence of a micellar microenvironment, confirming a conclusion arrived at earlier in this study (Section 2.3.3). At lower concentrations of hydrogen peroxide (4 % v/v, iteration 5), a significantly reduced signal was seen, showing the essential role of superoxide radicals in the CL reaction. At higher NaOH concentrations (120 μM, iteration 6), the CL signal was also reduced in comparison to iteration 5, highlighting the importance of NaOH and pH in the CL reaction.

The univariate and simplex optimisation of the operational variables of the FI-CL manifold were compared (Table 2.11).The optimum reagent concentrations derived by

Table 2.11 Comparison of Univariate and Simplex Optimisations

Reagent	Simplex	Univ.	Physical Parameter	Simplex	Univ.
[1,10-Phenan.] (μM)	60	60	Flow Rate (ml min^{-1})	2.6	3.6
[CEDAB] (mM)	15	15	Knitted Reagent Mixing Coil Length (cm)	500	200
[NaOH] (mM)	80	80	Sample Volume (μl)	360	270
[H_2O_2] (%)	8	8			
[TEPA] (μM)	0.2	None			

Univ – Univariate optimisation. Cu(II) 10 nM in UHP water.

simplex were identical to those determined by the univariate optimisation. The optimum physical operational variables were in good agreement, with the simplex derived mixing coil length and the sample volume within the signal plateau seen in the univariate optimisation, namely 200 - 650 cm and 230 – 370 μl respectively (Sections 2.3.2.1 and 2.3.2.2).

Federova *et al.*, (1982) postulated that at 10^{-4} mol l^{-1} Cu(II) the rate determining step was the reversible addition of the superoxide radical to the 1,10-phenanthroline, which could also be rate limiting at 100 nM Cu(II). At 10 nM Cu(II) an alternative rate limiting step may be chelation of the Cu(II) by the 1,10-phenanthroline, the first step in the CL reaction.

2.3.6 Interference Studies

Many CL reactions are unselective with respect to the metal ions that catalyse them. The enhancement or quenching effect of the seawater matrix ions on the 1,10-phenanthroline CL reaction was therefore investigated. The experimental parameters used (Table 2.12) were those derived by the 10 nM Cu(II) simplex optimisation, with the exception of the flow rate of the primary reagents for which 3.6 ml min^{-1} was used to increase the sensitivity, as discussed in Section 2.3.4.2.

Table 2.12 Parameters for Seawater Matrix Interference Study

Experimental Parameter		Experimental Parameter	
1,10-Phenanthroline (μM)	60	Sample injection volume (μl)	360
CEDAB (mM)	15	Reagent mixing coil length (cm)	500
NaOH (mM)	80	Reagent Flow rate (ml min^{-1})	3.63
TEPA (μM)	0.2		

A total of 24 ions were investigated. These were injected at their typical seawater concentration (Practical Handbook of Marine Science, 1994) and then at 1 μM (200 times the upper ambient seawater [Cu(II)] of 5 nM), both in UHP water, to evaluate their effect on the CL signal. This was followed by injection of a 10 nM Cu(II) UHP water standard, the CL signal was designated as 100 % and to which all other responses were normalised. Finally, in order to investigate their effect on a Cu(II) catalysed CL signal, 10 nM and 1 μM Cu(II) additions were made to each ion at their typical seawater concentration in UHP water. All lines were acid washed (0.2 M HNO_3, BDH, Aristar) and UHP water rinsed between each series of injections. The ions, at their typical seawater concentration with the 10 nM Cu(II) addition, for which a significant difference was observed are shown in Table 2.13.

Table 2.13 CL Signal Catalysed by Seawater Matrix Ions

Quenching Species & [M]	Normalised CL Signal (%)	CL Enhancing Species & [M]	Normalised CL Signal (%)
Cu^{2+} ($5*10^{-9}$)	100	Cu^{2+} ($5*10^{-9}$)	100
Sn^{2+} ($6.7*10^{-9}$)	97	Sr^{2+} ($9.1*10^{-5}$)	100
As^{3+} ($5.3*10^{-8}$)	90	B ($4.4*10^{-4}$)	122
Pb^{2+} ($2.4*10^{-10}$)	97	K^{+} (0.01)	271
Ag^{+} ($2.7*10^{-9}$)	93	Ca^{2+} (0.01)	110
Ni^{2+} ($9.2*10^{-8}$)	86	SO_4^{2-} (0.03)	117
Al^{3+} ($7.4*10^{-8}$)	96	Mg^{2+} (0.06)	143
Zn^{2+} ($1.9*10^{-7}$)	89	Cl^{-} (0.56)	131
Mn^{2+} ($2.7*10^{-8}$)	83	Cr^{3+} ($5.8*10^{-9}$)	127
Fe^{3+} ($1.2*10^{-7}$)	76	Co^{2+} ($4.6*10^{-9}$)	105
BO_3^{3-} ($4.3*10^{-4}$)	82	Cd^{2+} ($1*10^{-9}$)	108
HCO_3^{-}	19		
F^{-} ($7*10^{-5}$)	80		
Na^{+} (0.48) (Acetate)	51	Typical Blank	4.6

Seawter matrix ions at their seawater concentration in UHP water with a 10 nM Cu(II) addition. All data normalised to 10 nM Cu(II) in UHP water (100 %). All elements added as metal ion in nitric acid (4 %, ICP standard Spectrosol solutions) except where indicated.

The ions at their typical seawater concentrations, in the absence of Cu(II) did not generate any CL signal. The need to isolate the Cu(II) from the seawater matrix was clearly demonstrated by the quenching seen with some major seawater matrix ions e.g. Na(I), and enhancement by others e.g. K(I), Mg(II). This is discussed further in Section 3.3.5.3 in relation to the chelating characteristics of the 8 hydroxyquinoline (8HQ) micro-column used to separate Cu(II) from the seawater matrix.

2.3.7 Analytical Figures of Merit

In order to determine the linear range of the Cu(II)-FI-CL manifold, calibrations using Cu(II) standards in UHP water were performed. Three calibration ranges were studied using the experimental parameters shown in Table 2.14, with typical graphs for each calibration range shown in Figures 2.20, 2.21 and 2.22.

Table 2.14 Parameters for Calibration in UHP Water

Experimental Parameter		Experimental Parameter	
1,10-Phenanthroline (μM)	60	TEPA (μM)	0.4
CEDAB (mM)	15	Sample injection volume (μl)	360
NaOH (mM)	80	Reagent mixing coil (cm)	500
H_2O_2 (%, v/v)	8	Flow rate (ml min^{-1})	3.6

At Cu(II) concentrations greater than 60 nM, the CL signal reached a plateau (Figure 2.20), due to broadening of the FI peaks. This loss of linearity was attributed to a reagent based stochiometric limitation of the CL reaction. Doublet peaks were observed at 500 nM Cu(II) and above due to reagent limitation within the sample zone. The doublets were eliminated for Cu(II) concentrations of 500 nM or greater by reduction of the sample injection volume from 270 μl to 120 μl.

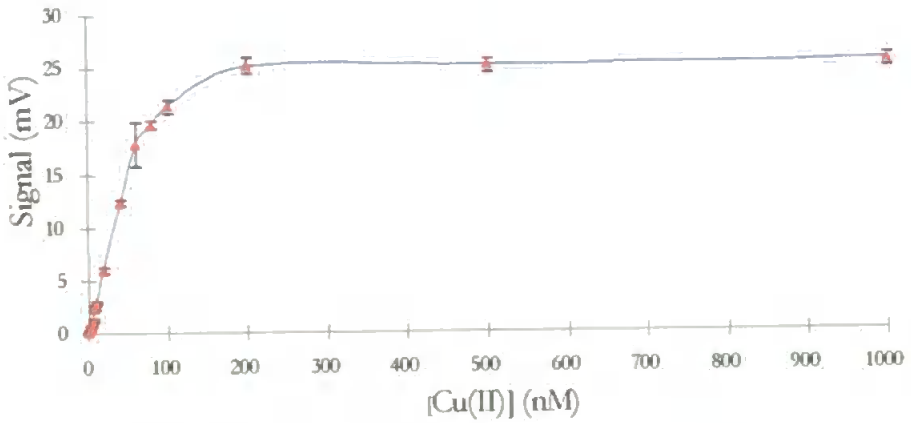

Figure 2.20 Calibration Graph for 0.1 nM - 1 μM Cu(II) in UHP Water

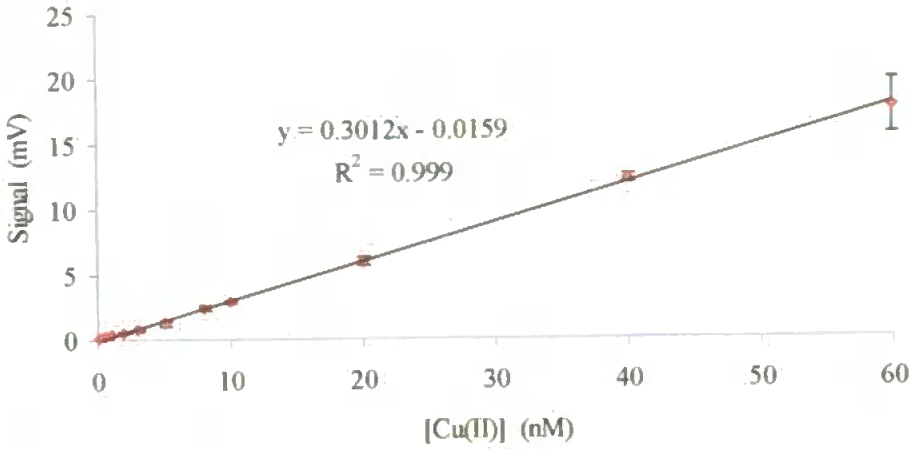

Figure 2.21 Calibration Graph for 0.1- 60 nM Cu(II) in UHP Water

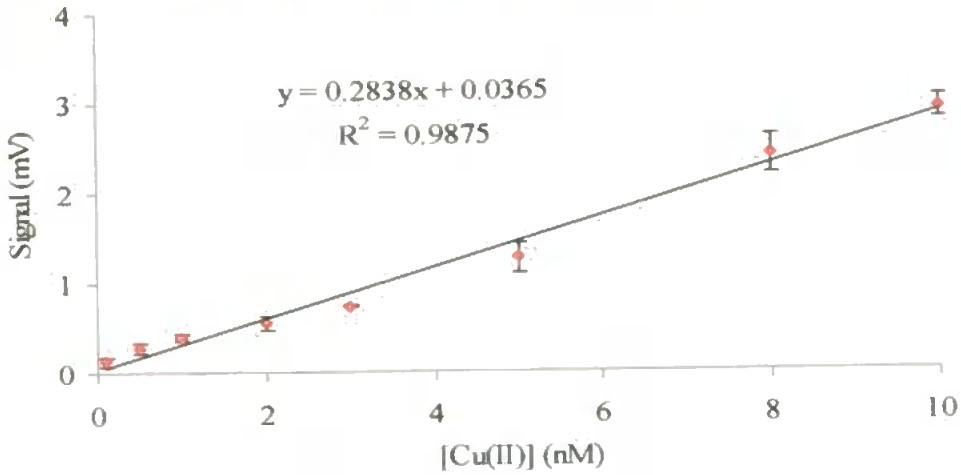

Figure 2.22 Calibration Graph for 0.1-10 nM Cu(II) in UHP Water

Analytical figures of merit are shown in Table 2.15. The Cu(II) FI-CL manifold had a wide analytical range in UHP water, with good linearity seen for all the calibration ranges studied. Excellent sensitivity was observed with a 0.1nM LOD and a linear range ten times the ambient range of Cu(II) found in seawater (0.5 – 6 nM). Typical RSD's were 2-5 %, illustrating the very good reproducibility of the FI-CL manifold for replicate injections (n = 5) at environmentally relevant levels of Cu(II). However, using the IUPAC LOD criterion of the blank plus three times its standard deviation, the LOD calculated using the equation of a straight line from the 0.1-60 nM Cu(II) calibration graph (R^2 0.999) was 0.1 nM.

Table 2.15 Analytical Figures of Merit	
Sample Throughput	**30 h^{-1} (n=5)**
Linear Range	**0.1 - 10 nM (R^2 = 0.988)**
	0.1 - 60 nM (R^2 = 0.999)
	0.1 - 100 nM (R^2 = 0.969)
LOD (Blank + 3s)	**0.1 nM**
Limit of Determination	**0.55 nM**
RSD (0.1 nM)	**5.8 % (n=5)**
RSD (1 nM)	**3.4 % (n=5)**
RSD (10 nM)	**1.4 % (n=5)**

Blank – acidified (Q-HNO_3) in UHP water.

2.4 Conclusions

This chapter reported the successful design and construction of an FI manifold and the selection and incorporation of the 1,10-phenanthroline CL reaction. The stabilisation of the 1,10-primary reagent, by the use of anhydrous 1,10-phenanthroline and the surfactant CEDAB, was an important factor enabling reproducible use of the 1,10-phenanthroline CL reaction, with its inherent sensitivity and selectivity for Cu(II). The key analytical variables for both the physical characteristics e.g. sample volume and flow rates, and the concentration of the reagents have been extensively investigated and rigorously optimised to produce a highly reproducible CL reaction.

The FI-CL analyser had a low LOD (0.1 nM), and a highly linear analytical range of 0.1 – 60 nM (R^2 0.999), suitable for the determination of Cu(II) in UHP water. The FI-CL manifold utilised robust, inexpensive instrumentation, had a high sampling frequency and minimised sample contamination though controlled sample handling and solution manipulation. For higher Cu(II) concentrations e.g. as found in some estuarine systems, or polluted waters, reduction of the sample injection volume or sample dilution would be required. The use of FI will facilitate full automation of the system, thus reducing operator error and freeing up time for other analytical tasks as well as enabling continuous, in-situ monitoring to map Cu(II) levels in natural waters.

The analytical figures of merit reported in this chapter demonstrated the suitability of the FI-CL analyser for the determination of Cu(II) at typical open ocean concentrations and in coastal or estuarine waters where higher levels of Cu(II) can be found. The investigation of possible interferents in a seawater matrix to the 1,10-phenanthroline CL reaction highlighted the need to separate the Cu(II) from the seawater matrix. Ideally, this

reaction highlighted the need to separate the Cu(II) from the seawater matrix. Ideally, this stage should also preconcentrate Cu(II) to enable determination of the ultra trace (sub nM) levels of Cu(II) present in open ocean waters. The further development of the FI-CL analyser for the determination of Cu(II) at trace levels in seawater is described in Chapter 3.

Chapter Three

Development of the FI-CL Analyser For the Determination of Cu in Seawater

Chapter Three

3.1 Introduction

This chapter reports the substantial modification of the FI-CL manifold developed for the determination of Cu(II) in UHP water (Chapter Two) for use with the complex matrix of seawater. The experimental parameters for the Cu(II) catalysed oxidation of the 1,10-phenanthroline CL reaction were rigorously optimised in Chapter Two and the focus of this chapter is on the selection, optimisation and use of a micro-column for matrix separation and analyte preconcentration. This enabled the preferential chelation of Cu(II), isolating it from potential interferents to the CL reaction in the seawater matrix. It also preconcentrated the Cu(II), enabling detection of sub-nanomolar levels of Cu(II) as found in the open ocean.

3.2 Experimental

3.2.1 Reagents

The reagents used were as detailed in Chapter Two unless otherwise stated. All Cu(II) standards were acidified to pH 2 by the addition of 50 µl of Q nitric acid per 100 ml of UHP water. For seawater samples 80 µl per 100 ml was required due to the buffering capacity of the seawater matrix. UHP water blanks were acidified as for the seawater samples. The immobilisation of the 8-Hydroxyquinoline (8HQ) on Fractogel® required the reagents listed in Table 3.1.

Table 3.1 Reagents for Immobilisation of 8HQ

Reagent	Formula	Supplier	Grade
Fractogel TSK-Gel Toyopearl		Anachem	HW 75-F
Sodium hydroxide	$NaOH$	BDH	Aristar®
Hydrochloric acid	HCl	BDH	Aristar®
Acetic acid	CH_3COOH	BDH	Aristar®
Acetone	$(CH_3)_2O$	Rathburn	Glass distilled
Dichloromethane	Cl_2CH_2	BDH	AnalaR
Triethylamine	$(C_2H_5)_3N$	Aldrich	
Ethanol	C_2H_5OH	BDH	AnalaR
p-Nitrobenzoyl chloride	$C_7H_4ClNO_3$	Fluka	Puriss
Sodium nitrite	$NaNO_2$	BDH	AnalaR
Sodium dithionite	NaS_2O_4	BDH	GPR
8-Hydroxyquinoline (8HQ)	C_9H_7NO	BDH	AnalaR
Whatman glassfibre filters		BDH	GF/F
Ultra high purity water (18 MΩ)	H_2O	Elgastat	18.2 MΩ

Two buffers were selected with appropriate pK_a values to buffer the acidified sample (initially pH 2) to the optimum pH for loading onto the 8HQ micro-column. The tri-protonated citrate buffer had a pK_a1 of 3.13, a pK_a2 of 4.76, and a pK_a3 of 6.4 (Perrin 1972), and was therefore suitable for loading from pH 2 to 7.5. It was prepared by combining appropriate volumes of citric acid (2 M, BDH AnalaR) and sodium hydroxide (2 M, BDH, Aristar®) (Table 3.2). An ammonium acetate buffer (2 M, pK_a ammonia of 9.25) was used to investigate column loading at pH 7.5 to 10.5. It was prepared by combining NH_4OH (25 % m/m, Fluka, Puriss) with acetic acid (BDH, Aristar®) in appropriate volumes, (Table 3.2). A working buffer (0.4 M, pH 9.15) was prepared by serial dilution. All buffers were made up to 100 ml with UHP water.

Three buffers (Table 3.2) were used to investigate the buffering of the alkaline reaction medium created by the 1,10-primary reagent (pH 12.8) against the effects of the acid eluent used to elute the complexed Cu(II) from the 8HQ micro-column. An ammonium acetate buffer (pK_a 9.25) was prepared as described above. A carbonate buffer (pK_a2 10.33) at pH 10.3 was prepared by combining Na_2CO_3 (BDH, AnalaR) and $NaHCO_3$ (BDH AnalaR) solutions. A phosphate buffer (pK_a1 of 2.15, pK_a2 of 7.2, pK_a3 of 12.33) was prepared by combining Na_2HPO_4 (BDH, AnalaR) and NaOH (BDH, Aristar®) solutions, which was adjusted to pH 12.8 with aliquots of NaOH solution. For all buffers, fine adjustment of the pH was achieved by the addition of aliquots of the appropriate solution. The buffers were mixed in-line with the sample and 1,10-primary reagent solutions using three dimensional disorientated reactor coils or 'knitted' coils.

Table 3.2 Buffer Preparation

Citrate Buffer				**Acetate Buffer (M) (ml)**		**pH**
Citric Acid (ml)	NaOH (ml)	**pH**		NH_4OH (7M) (90ml)	Acetic Acid(17M) (22.5 ml)	9.15
10	6	3.0		**Carbonate Buffer (M) (ml)**		
10	13	4.0		Na_2CO_3 (0.1 M) 75	$NaHCO_3$ (0.1 M) 25	10.3
10	21	5.0		**Phosphate Buffer (M) (ml)**		
10	28	6.0		Na_2HPO_4 (0.05 M) 50	NaOH (0.1 M) 26.9	12.3

Buffers prepared from Perrin, 1974 and Beynon, 1996

3.2.2 Preparation of 8HQ Chelating Resin

The resin for the 8HQ column was prepared by modification of Fractogel TSK HW 75 (F), followed by covalent attachment of the 8HQ after Landing *et al.*, (1986) as shown in Figure 3.1. A three necked round bottom flask, a cooler with a calcium chloride drying tube, a magnetic stirrer and a heating plate were used for preparing the 8HQ resin.

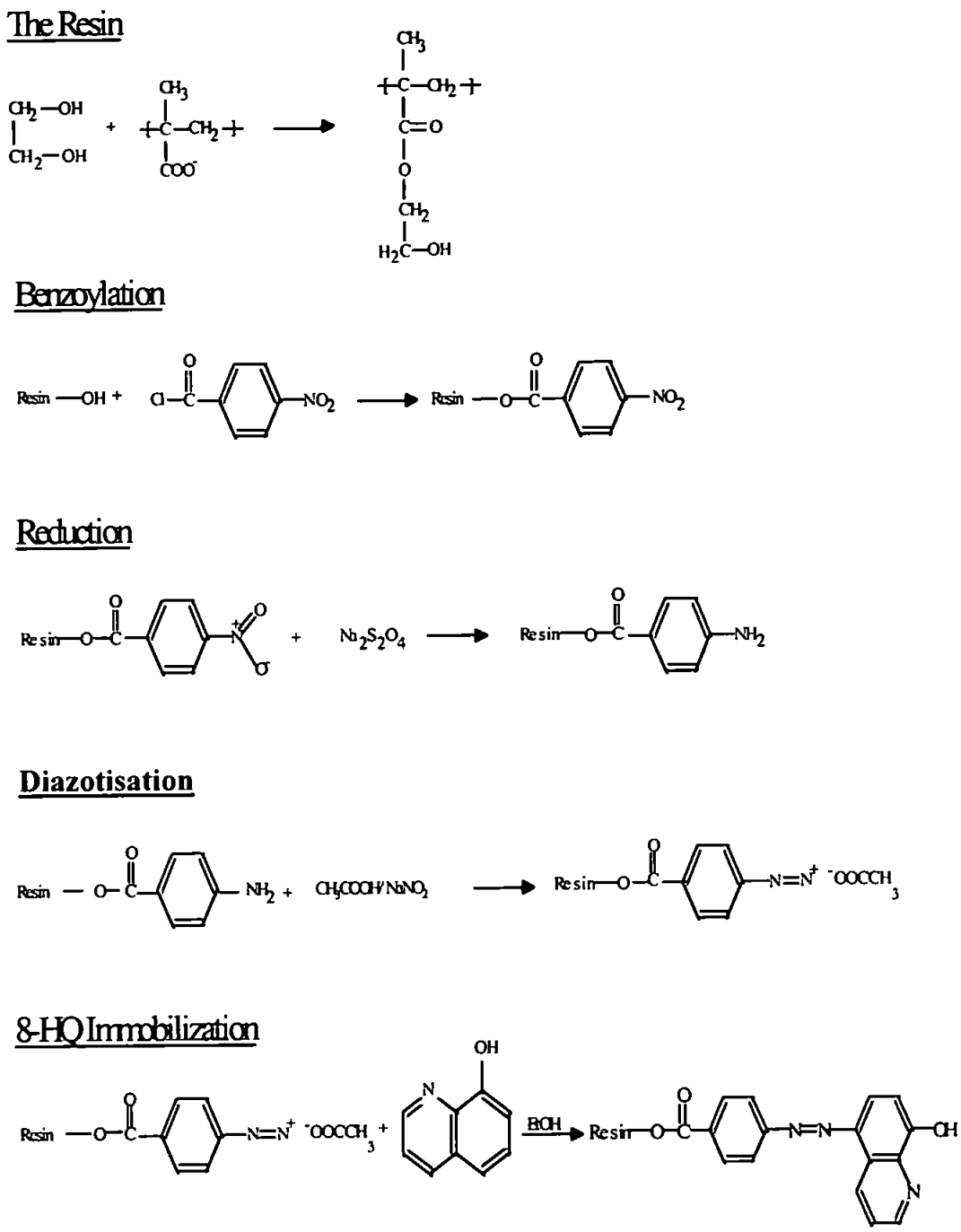

Figure 3.1 Reaction Scheme for the Immobilisation of 8HQ

Firstly, a 50 ml slurry of Fractogel was suspended in 100 ml of UHP water, the beads allowed to resettle and the supernatant decanted. The slurry was then vacuum filtered onto a Whatman glass fibre filter, removing the filter cake with caution so as not to include particles of the filter. The beads were washed twice with UHP water. Resin cleaning was accomplished by a series of rinses – 2 x 50 ml of NaOH (1.0 M), 3 x 50 ml of UHP water, 2 x 50 ml of HCl (0.5 M), 3 x 50 ml of UHP water, 2 x 50 ml of ethanol, 2 x of 50

ml of acetone and finally 2 x of 50 ml of dichloromethane (CH_2Cl_2). The resin was thoroughly dried in a desiccator overnight followed by oven drying at 105 ^{o}C (3 h).

After drying, the Fractogel resin was benzoylated in an esterification reaction by the attachment of p-nitrobenzoyl chloride to the resin. Five grams of the resin were combined with 2 g of the p-nitrobenzoylchloride (0.011 M), 5 ml of triethylamine (0.036 M) and 95 ml of dichloromethane in a three necked round bottom flask. The sub-boiling (40 ^{o}C) reflux reaction was gently stirred for 12 h using a magnetic stirrer. The benzoylated product was filtered through a GF/F Whatman filter, rinsed with 3 x 50 ml of dichloromethane and filtered to dryness. The resin was then rehydrated by rinsing thoroughly with UHP water.

The benzyl-nitro group on the resin was then reduced to an amine. Five grams of sodium dithionite (0.03 M) dissolved in 100 ml of UHP water was added to the resin in a HDPE bottle and shaken periodically for 3 h. A pH rise from 5.0 to 6.5 occurred after 2.5 h, with a maximum pH of 7.2 observed. To remove any sulphur, the resin was rinsed 3 x with 50 ml of acetone and 3 x with 50 ml of UHP water to remove the acetone.

The wet resin was ice-cooled and then diazotizated by adding 5 g of sodium nitrite (0.073 M) in 100 ml of ice-cooled acetic acid (0.2 M). The reaction continued for 45 min with agitation every 10 min, after which the resin was vacuum filtered and rinsed 3 x with ice-cooled water.

The final stage was the attachment of the 8HQ group to the Fractogel resin backbone. An ice-cooled solution of 2 g of 8HQ in 100 ml of ethanol (0.014 M) was quickly added to the resin. The slurry was shaken periodically and kept for 45 min in a cooler. The immobilised 8HQ resin was rinsed 2 x with 0.5 M NaOH during which the resin darkened in colour, 3 x with UHP water and 2 x with 1.0 M HCl (when the resin lightened in colour) and finally 3 x with UHP water. The resin slurry was allowed to settle and the supernatant discarded. The immobilised 8HQ was stored as a slurry, suspended in UHP water in a HDPE bottle at room temperature. The overall time for the immobilisation was 25 h.

3.2.3 FI-CL Manifold

3.2.3.1 FI-CL Instrumentation

The FI-CL manifold used for the determination of Cu(II) in UHP water (Chapter 2) required extensive modification to incorporate the 8HQ micro-column. All results reported for this chapter were obtained using the modified FI-CL manifold (Figure 3.2). The instrumentation used was as described in Chapter 2, with the following alterations

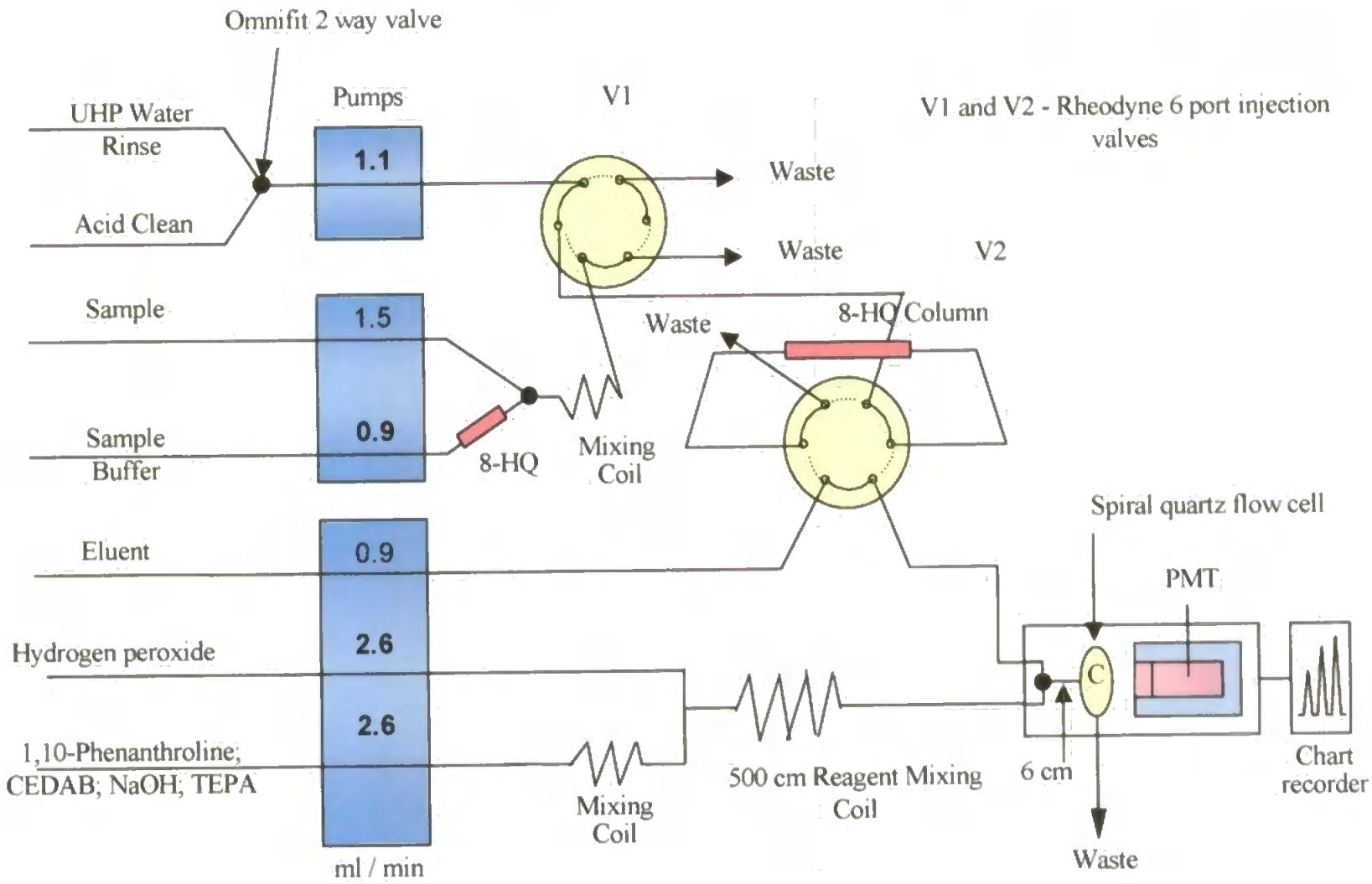

Figure 3.2 FI-CL Manifold for the Determination of Cu(II) in Seawater Incorporating an 8HQ Micro-column

The single speed sample (Watson Marlow, 503S) and reagent (Ismatec, S 820) pumps were replaced by two variable speed peristaltic pumps (Gilson, Minipuls 3), which facilitated alteration of flow rates and automation via TTL inputs. A single speed pump (Ismatec, S 820) was used to acid clean and UHP water rinse the 8HQ micro-column. A second 6 port PTFE rotary valve (Rheodyne 5020, HPLC Technology, V2 in Figure 2.2, and Figure 3.3), was used to incorporate the 8HQ column as shown in Figure 3.2. A three port valve (Omnifit, Figure 3.4, and V1 in Figure 3.2) was also incorporated to switch between the column acid clean and UHP water rinse solutions.

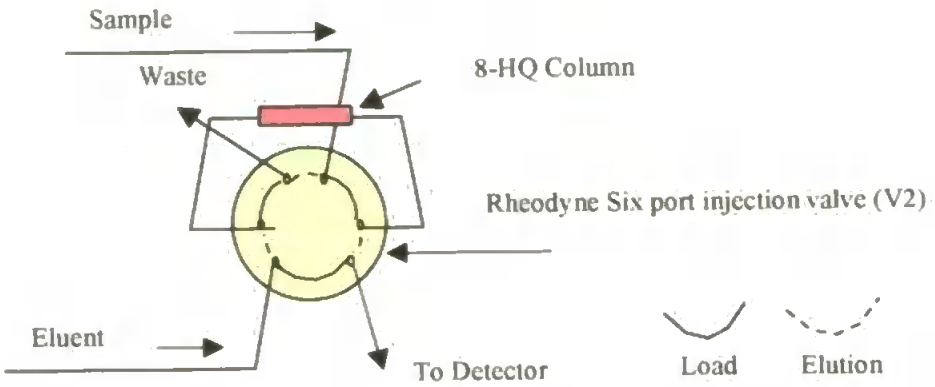

Figure 3.3 Six Port Rotary Valve with 8HQ Column (load position) (see also Figure 2.2)

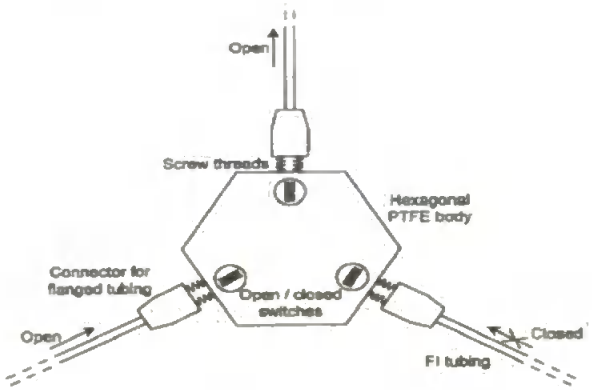

Figure 3.4 Omnifit Three Port Valve

3.2.3.2 8HQ Micro-columns

When using the high aspect ratio (column length/column id), push fit 8HQ micro-columns described below, especially at higher flow rates, increased pressure in the manifold caused by restricted flow through the column resulted in leakage at the junctions with the pump tubing. ABS plastic (Butylstyrene) micro-tubes were sourced, flanged and fitted through enlarged FI screw connectors and glued (Loctite 406 cyanoacrylate) into the pump tubing. The ABS plastic was pre-conditioned by acid cleaning and UHP water rinsing.

Push fit 8HQ micro-columns (Figure 3.5) were first used in this study. These were prepared by plugging one end of an acid washed HDPE tube (1.4 mm id) with an acid washed (0.2 M HCl) quartz wool plug. The micro-columns were packed by pumping (0.5 ml min^{-1}) a slurry of the 8HQ resin into the column followed by the insertion of a second quartz wool plug. The column was sleeved down to the FI line size by inserting PVC pump tubing and pushing into place. The junctions of the 'push fit' 8HQ micro-column and also the primary reagent pump tubing to the FI line were shrink wrapped using two overlapping sizes of wrapping to ensure fluid tight fittings.

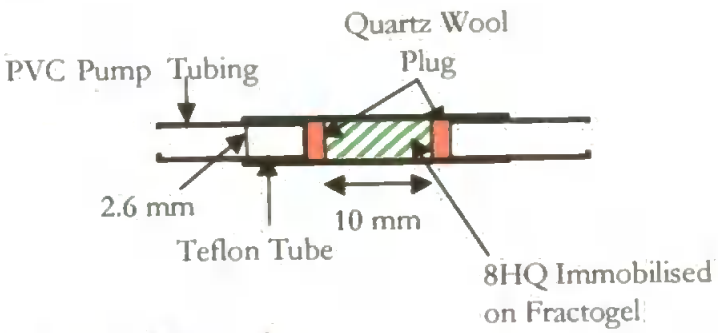

Figure 3.5 Push Fit 8HQ Micro-column

Columns (1.4 mm id) with resin beds of 15 and 20 mm length and aspect ratios of 10.7 and 14.3 respectively were prepared, as was a wider column (2.6 mm id) with a shorter resin bed length of 10 mm and a reduced aspect ratio of 3.9. In order to overcome the restriction in flow observed with the push fit columns and to improve reproducibility, a new column (Section 3.3.1) was designed and machined from a solid acrylic rod (Figure 3.6), using 2 polycarbonate fibre pads layered between 3 nylon mesh frits to retain the 8HQ resin.

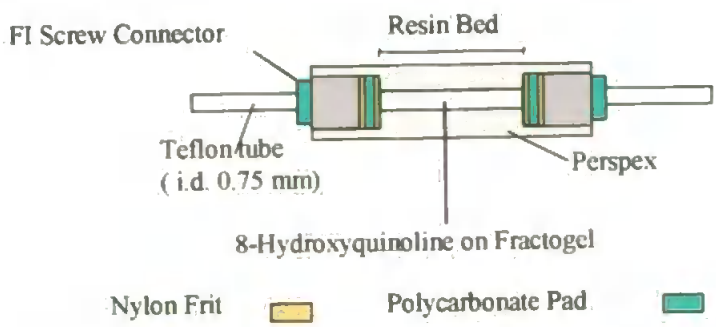

Figure 3.6 Machined 8HQ Micro-column

Standard FI screw unions were used to retain the flanged FI tubing. All columns were conditioned by an 8 h acid wash and UHP water rinsing protocol prior to use.

3.2.4 Procedures

The experimental procedures used for this chapter were as described in Section 2.2.3 with the following alterations.

3.2.4.1 Trace Metal Clean Up of Sample Buffer

Copper(II) impurities in the CL reagents degrade the analytical accuracy of the FI-CL method for Cu(II), especially at the trace levels of Cu(II) found in open ocean waters. In addition, Cu(II) impurities in the citrate buffer and Q-HCl eluent generated a background CL emission when the two reagent streams were mixed in front of the PMT end-window. An elevated background would seriously degrade the detection limit of the FI-CL method. Trace metal clean-up procedures were therefore employed. The clean up of the 1,10-phenanthroline primary reagent was accomplished by the addition of tetraethylenepentamine (TEPA, Section 2.3.3.7).

The sample buffer was cleaned by first pumping (0.5 ml min^{-1}) through an off-line Chelex 100 chelating column, prior to passing through an in-line 8HQ micro-column incorporated in the FI manifold. The Chelex columns were prepared by first washing 5 ml pipette tips in micro-detergent (hot 5 % Decon, BDH), followed by an acid clean (0.5 M Q HCl) and a UHP water rinse. The tips were then plugged with acid washed (0.2 M Q HCl) quartz wool, packed with Chelex 100 and the wide end sleeved with silcone tubing down to the size of the FI line. The Chelex 100 columns were used to clean 200 ml of buffer before being regenerated, the first 50 ml of the cleaned buffer being discarded. Columns were pre-conditioned and regenerated by washing first with 100 ml of UHP water, regenerating with 50 ml of 1 M HCl, further washing with 100 ml of UHP water and then with 100 ml of 1 M ammonia solution to convert the resin into the NH_4^+ form. Finally, the columns were rinsed with UHP water until a neutral eluent was obtained.

3.2.4.2 Analytical Protocols

The analytical sequence (Figure 3.7) consisted of firstly a short acid clean and UHP water rinse of the manifold, followed by mixing of the sample and buffer in a 3D dis-orientated flow mixing coil, prior to loading onto the 8HQ column. The 1,10-primary reagent and hydrogen peroxide were then mixed in a mixing coil, prior to merging with the eluted Cu(II) ions in the eluent stream at the ' T ' junction immediately before the flow cell where the CL emission occurred. This was detected by the PMT and recorded as a

transient peak on the chart recorder. Early in this study the 8HQ micro-column was regenerated by acid clean and UHP water equlibration cycles.

The design and later use in this study of the machined acrylic column substantially improved the flow through the column, enabling regeneration of the column's complexing sites to be accomplished by the acid eluent that continued to flow after elution of the Cu(II). This enabled the separate acid clean and UHP water equilibration cycles to be removed from the analytical cycle. At first valves were switched manually using stop watch timing, although later the manifold was fully automated. In order to overcome possible effects on the CL emission due to the seawater sample matrix the method of standard additions was used.

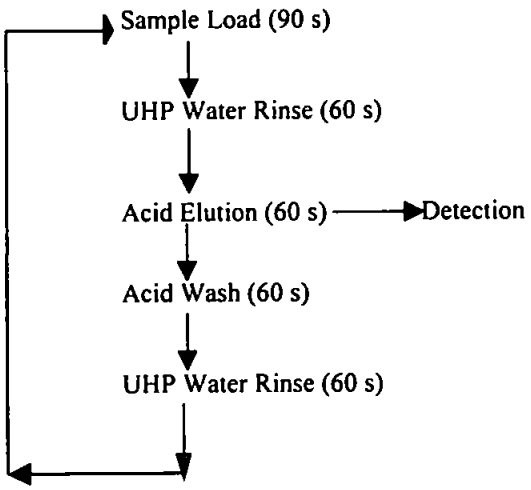

Figure 3.7 Initial Analytical Sequence for FI-CL Manifold with 8HQ Column

3.3 Results and Discussion

Unless otherwise stated all results presented here were obtained using optimal reagent concentrations and flow rates as determined in Chapter Two, with all Cu(II) standards and seawater samples acidified to pH 2 with Q HNO_3. The experimental variables used at the outset of the research in this chapter were an acidified 10 nM Cu(II) standard in UHP water, which was mixed with a citrate sample buffer (0.2 M, 0.5 ml min^{-1}, pH 6), and then loaded onto the 8HQ column at 2.0 ml min^{-1}, with column elution by an aqua regia eluent (0.6 M Q HCl and 0.2 M Q HNO_3). Replicate injections (n=4) were used, with all error bars in figures expressing +/- 3s. Any changes in signal size were due to changes in the sensitivity of the PMT due to it nearing the end of its operational life. When a new PMT was obtained before instrument deployment on the AMT cruise, the sensitivity of the analyser increased considerably and also stabilised. This illustrated that changes in the size of the mV signal can be caused by changes in PMT sensitivity.

3.3.1 FI-CL Manifold Modifications

In order to raise the enrichment factor of the 8HQ column, higher flow rates were used for column loading during optimisation of the 8HQ micro-column manifold. However, this increased the pressure in the FI manifold causing leaks e.g. at the shrink wrapped, push fit junctions of the sample and buffer pump tubing to FI lines, especially when using the higher aspect ratio, push fit columns. This restricted in practical terms the upper limit of the enrichment factor. Therefore, flanged ABS (butylstyrene) plastic micro-tubes with modified FI screw connectors were used as described in Section 3.2.3. It was also important to limit the dispersion of the eluted Cu(II) during transport to the detector from the 8HQ micro-column. The use of the minimum length of narrow bore (0.5 mm) tubing from the column to the detector achieved this objective.

8HQ Micro-column Modifications Due to its selectivity and enhancement of sensitivity roles, the 8HQ column was central to determination of trace level Cu(II) in seawater. Continuous shipboard monitoring also required long-term column stability and reproducible column performance. Variable packing density, due to the non-reproducible tamping into place of the quartz wool plugs, made it difficult to maintain an even flow through the high aspect ratio (10.7 and 14.3), push fit columns originally used (Section 3.2.3.2). Reproducibility became erratic and manifold sensitivity was reduced due to the occurrence of preferential flow channels through the column and increased manifold pressure. With continued use the quartz wool packing of an 8HQ column could also become loose, resulting in the resin being washed away. In order to overcome these deficiencies a wider HDPE column (2.6 x 10 mm) was then used, which promoted a more even flow and reduced the pressure, so reducing leakage, although the column aspect ratio was also reduced to 3.9.

However, it was still difficult to obtain a reproducible flow through the column, especially during column bedding in. Therefore, a new column was designed and machined from a solid acrylic rod (Section 3.2.3.2 Figure 3.6). The flow rate of the new column was monitored over a 4 h period and varied by less than 5 %, representing a very reproducible and much improved flow through the 8HQ column.

3.3.2 Selection of Chelating Resin and Support

The separation and preconcentration stage should promote the preferential retention of Cu(II) from the seawater matrix. The chelating properties of 8-hydroxyquinoline (8HQ) and its preference for transition metal cations (e.g. Fe, Co, Mn, Cu, Al, Zn, Cd, Ni, Pb) relative to alkali and alkaline earth metals has been previously

reported (Landing, *et al.*, 1986; Nickson, *et al.*, 1995). Solvent extraction, coprecipitation and evaporation techniques can also be used for separation and preconcentration (Gueguen *et al* 1999), but are time consuming and not easily automated. A solid phase extraction stage in the form of a micro-column was selected due to several advantages over alternative extraction methods e.g. reduced contamination from trace level metal residues in the extra reagents used in the alternative methods, reduced solvent use, lower detection limits (due to the whole sample being analysed) and rapid analysis. Micro-columns are also easier to incorporate into the FI-CL manifold, facilitate system automation and in-situ deployment.

In order to achieve an efficient mass transfer coupled with low reagent consumption, the column design and the use of fully optimised operational variables e.g. loading flow rate, are critical. The selectivity of the chelating ligand for Cu(II), the breakthrough capacity of the 8HQ resin for Cu(II), the 8HQ particle size and the extent of the matrix interference are also important factors that were investigated.

For the in-line solid phase extraction, the chelating resin 8-hydroxyquinoline (8HQ, Figure 3.8) was immobilised on Fractogel TSK, a commercial hydrophilic vinyl co-polymer (Fractogel TSK gel, Toyopearl HW 75F, 32-63 micron fine, Toso Hass Co.). The 8HQ was selective and strongly retained the Cu(II), having a high stability constant for Cu(II) (log K_1 of 12.1, Sillen, 1964). It also promoted efficient elution, achievable by a weak acid eluent that, upon mixing with the primary reagents, would not adversely affect the pH of the selected CL reaction, an important consideration due to many CL reactions being pH sensitive. The 8HQ resin was also robust and therefore should not degrade during long term use.

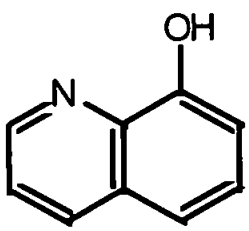

Figure 3.8 Structure of 8-hydroxyquinoline (Oxine) C_9H_7ON

A strong, inert backbone on which to immobilise the 8HQ was an important criterion. Fractogel TSK HW 75F is a hydrophilic, semi-rigid spherical gel constructed of intertwined vinyl polymers that form inert vinyl polymer agglomerates. These are characterised by high mechanical and chemical stability, good porosity and high hydrophilicity. The presence of ether linkages and hydroxyl groups enabled chemical modification to immobilise the 8HQ via phenyl-azo linkages. The Fractogel immobilised

8HQ resin was resistant to physical degradation, which ensured a long operational lifetime for the column, even at higher flow rates. The 8HQ Fractogel resin was also stable in acid solutions, the resin preserving 88 % of its capacity after 240 h of acid treatment (2.0 M HCl/0.1 M HNO_3) when used to extract Cu(II) (Landing *et al.*, 1986). The same author also demonstrated that the 8HQ Fractogel resin showed a 32% reduction of breakthrough capacity after 48 h of base treatment (0.5 M NaOH), due to base catalysed hydrolysis of the benzoylester linkages of the resin. In comparison, 8HQ immobilised on silica suffered a reduction of 38 % of its total exchange capacity after 24 h at pH 12 (0.5 M NaOH) due to extensive hydrolysis of the silica support (Landing *et al.*, 1986).

The resin beads were small and uniform spheres (32-63 μm diameter), promoting even flow around them, which enhanced the enrichment factor (EF, see section 3.3.5.5) through the production of sharp elution peaks (Fang, 1993). Smaller diameter beads could have restricted the maximum flow rates and increased the pressure in the manifold, factors that would have lowered the maximum EF achievable. It was also important that the column resin did not undergo a volume change when the column conditions were altered. Fractogel does not either swell or shrink in strongly alkaline or acidic conditions. The polymer backbone itself shows no cation exchange capacity and does not concentrate dissolved organic species present in seawater. Chelex 100® was considered as an alternative solid phase chelating resin. It has the iminodiacetic functional group (IDA, Figure 3.10), was selective for transition metals and had a log K of 9.01 for Cu(II) (Pesavento and Baldini, 1999). However, it has a polymer substrate that would shrink during the acid elution stage and was therefore unsuitable as for use as the micro-column resin due the development of preferential flow through the column and thus inefficient retention and elution of Cu(II). It also requires a lengthy regeneration process between each analysis, which would severly limit sample throughput. However, Chelex 100® was used for the off-line buffer clean up (Section 3.2.4.1 and 3.3.4.2).

3.3.3 8HQ Chelating Resin Preparation

The preparation of the 8HQ resin, as described in Section 3.2.2 (Figure 3.1), entailed commercial Fractogel TSK HW 75 (F) first undergoing a benzoylation reaction to attach the p-nitrobenzoyl chloride to the resin. The nitro group was then reduced to an amino group, which was then diazotised, with the 8HQ subsequently attached to the two nitrogen atoms of the modified resin.

Firstly, an initial suspension in UHP water removed the preservative sodium nitrite (NaN_3) and the fine particles. To prevent the p-nitrobenzoyl chloride reacting with water

or ammonia, which could reverse the esterification reaction, after rinsing the resin was thoroughly oven dried (105 ^{o}C). The triethylamine used in the esterification reaction scavenged the chloride, so minimising the reduction in the reaction that its presence would promote. The dichloromethane stabilised the reaction temperature due to its low boiling point (42 ^{o}C). The reduction of the nitro group consumed protons and if the pH was allowed to become too high the reaction would have stopped (Landing, 1996). Although a pH rise was recorded this was limited and it was not necessary to adjust the pH with HCl or NH_4OH. Ice cooling at the diazotization stage and during the attachment of the 8HQ was necessary due to the diazonium salt being unstable at room temperature. The colour of the slurry turned from orange to brick red after two hours, indicating an efficient preparation of the immobilised 8HQ resin (Landing, 1986).

3.3.4 Buffers for Sample and CL Reaction

The loading of Cu(II) onto the 8HQ column was pH sensitive and therefore the acidified Cu(II) sample (pH 2) required buffering to the optimum loading pH (see Section 3.3.5.3). Citrate and ammonium acetate buffers have a range of appropriate pK_a values, e.g. citrate has three pK_a values, to buffer the acidified sample (pH 2) over the pH range 3 to 10.5. The effect of the individual sample buffers on the optimal pH for column loading was investigated by buffering the pH of the acidified (pH 2) Cu(II) standard (10 nM) over pH 3 to 10 (Table 3.3,) measured at the column, immediately prior to loading.

Table 3.3 Effect of Citric and Ammonium Acetate Buffers

Buffer	Cu(II) (10nM)	pH	Signal (mV)	RSD (%) (n=4)
Citrate	Yes	3.0	0.4	34
Citrate	Yes	5.0	3.1	4.0
Acetate	Yes	7.0	1.7	3.8
Acetate	Yes	10.0	1.2	7.0
Citrate	No	6.0	1.3	2.3
Acetate	No	7.0	1.5	1.4

Cu(II) 10 nM, acidified to pH 2. Blank – Acidified UHP (Q HNO_3)

As shown above and also later (Section 3.3.5.3), the optimal pH of the citrate buffer (0.2 M) for loading Cu(II) in UHP water onto the 8HQ resin was pH 5. This pH was used in all future studies for loading all Cu(II) in UHP water. The action of a buffer is described by the Henderson-Hasselbach equation;

$$pH = pK_a + \log_{10} \frac{[A^-]}{[HA]}$$

where pK_a is the negative log of the dissociation constant (K_a) of the weak acid HA and A^- represents the corresponding conjugate weak base. This equation enables the pH of a particular buffer to be predicted if the dissociation constant and the concentration of the acid and base are known. When the concentration of the acid and base are equal, pH = pK_a. Furthermore, as the maximum buffering capacity (β) occurs at its pK_a value, the buffer should ideally be used within +/- 1 pH unit of it's pK_a value and the pH change of the buffered solution should ideally be towards the pK_a of the buffer (Beynon, 1996; Perrin 1974).

The 1,10-phenanthroline CL reaction has been reported as being pH sensitive, with an optimum pH of 10.1 at the waste side of the flow cell (Coale *et al.*, 1992). The 1,10-phenanthroline primary reagent (pH 12.8) controlled the pH of the reaction medium, which became more acidic upon mixing with the acid eluent. Phosphate, carbonate and acetate buffers were therefore prepared to maintain the pH of the reaction medium. The phosphate buffer, when run with a UHP water blank, enhanced the CL signal due to direct interference with the CL reaction. This factor, together with the possible formation of insoluble Cu(II) complexes e.g. orthophosphate ($Cu_3PO_4)_2.3H_2O$), precluded its use. A significant suppression of the CL signal was seen when using the carbonate buffer, possibly due to the formation of insoluble $CuCO_3$. The acetate buffer significantly enhanced the CL signal when used to buffer a UHP water blank. None of the buffers used maintained the pH of the reaction medium as measured at the waste, with a strong CL signal still observed over a pH range of 1.8 (aqua regia eluent, no buffer) to 10.4 (0.2 M HCL eluent, with buffer) as measured at the waste. This clearly indicated that buffering of the 1,10-phenanthroline primary reagent was unnecessary for this study and use of a buffer for the primary reagent was discontinued.

3.3.4.1 Buffering Capacity of Citrate Buffer

The pH buffering capacity of the citrate buffer was investigated by measuring the pH of the buffered sample after in-line mixing. Both 0.2 M and 0.4 M citrate buffer at pH 5 and 6 were used to load an acidified UHP water standard (pH 2) and an Irish Sea sample (pH 2, Table 3.4).

The 0.2 M citrate buffer at pH 5.0 buffered an acidified 10 nM Cu(II) standard in UHP water (pH 2) to the optimal pH of 5.0. However, when used with an Irish Sea sample

Table 3.4 pH of Sample/Buffer Stream at Column

Citrate buffer		Sample with 10 nM Cu(II)	pH at Column
Molarity	pH		
0.2	5.0	UHP std	5.0
0.2	5.0	Irish Sea	4.0
0.2	6.0	UHP std	6.0
0.2	6.0	Irish Sea	5.1
0.4	6.0	UHP std	6.0
0.4	6.0	Irish Sea	5.5

the same citrate buffer resulted in a pH of 6.5. The difference was caused by the increased ionic strength of the seawater matrix, which altered the pK_a of the buffer, which changed the pH and reduced its buffering capacity (β). The extra matrix ions (counter ions of opposite charge) caused a differential shielding of the conjugate acid and base ions, which reduced the activity coefficient of the buffer. This changed the acid/base equilibrium and the pH of the buffered solution was thus altered.

These factors resulted in the citrate buffer being less efficient in seawater at buffering the acidified sample to optimum pH. Whereas an increased buffer concentration e.g. 0.4 M (pH 5) would have increased the buffering capacity, this was not used due to increased trace Cu(II) impurities in the buffer solution. Subsequent work with acidified seawater samples (pH 2) therefore used a 0.2 M citrate buffer at pH 6 to counteract these factors and resulted in a pH of 5.1 for column loading.

3.3.4.2 Blank Reduction

An important factor in the LOD of the FI manifold was the size of the blank signal, which originated in part from Cu(II) impurities in the citrate buffer. In order to reduce the blank signal the trace metal content of the buffer was reduced by off-line clean up through a Chelex 100® column (0.5 ml min^{-1}) and then through an in-line 8HQ column incorporated in the buffer stream (Figure. 3.2), prior to mixing with the sample. The efficiency of the buffer clean up was investigated by loading uncleaned (experiment 1) and cleaned (experiment 2) citrate buffer (02 M, pH 5) only. The effect of the buffer clean up on the UHP water blank was then evaluated by loading UHP water plus uncleaned (experiment 3) and cleaned (experiment 4) citrate buffer. All were loaded at the optimum pH for column loading (Section 3.3.5.3) and the results shown in Figure 3.9 and Table 3.5.

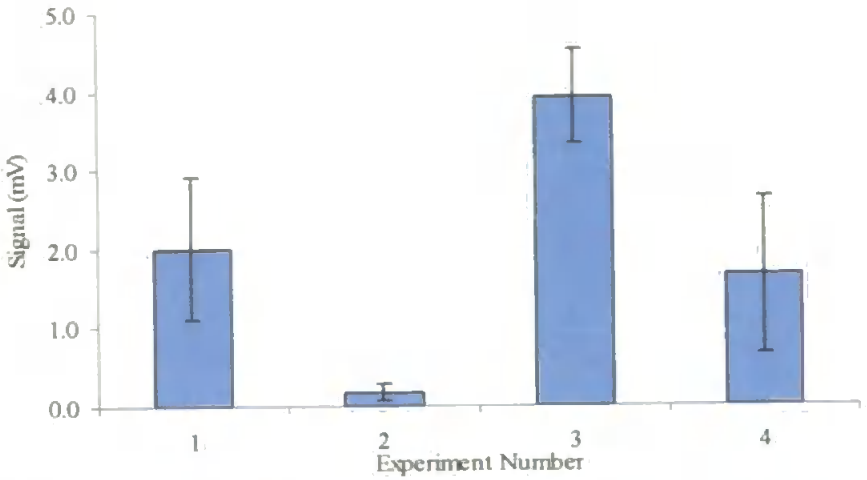

Figure 3.9 Citrate Buffer Cleaned of Trace Metals by Off-line Chelex 100® Column and in-line 8HQ Micro-column

Table 3.5 Citrate Buffer Cleaned of Trace Metals by Off-line Chelex 100® Column and in-line 8HQ Micro-column

Exp. No	Buffer Status	Signal (mV)	RSD (%)
1	Citrate buffer only (uncleaned)	2.0	15
2	Citrate buffer only (cleaned)	0.17	30
3	Blank + Citrate buffer (uncleaned)	3.9	4.9
4	Blank + Citrate buffer (cleaned)	1.7	21

Cu(II) impurities in the citrate buffer alone and with the UHP water blank catalysed a CL signal as is shown in Figure 3.9 and Table 3.5 (experiment 1 and 3). This CL signal was significantly reduced after it was cleaned off-line with Chelex® 100 and on-line with 8HQ column (experiments 2 and 4). Chelex 100® is widely used in applications that involve removing or concentrating trace metals in natural waters. It is a macroporous polystyrene divinylbenzene polymer on which polyvalent metal ions such as Cu(II) are preferentially chelated over commonly occurring monovalent cations such as Na^+, by the paired iminodiacetic acid (IDA) functional groups (Figure 3.10). The quantity of metal cations

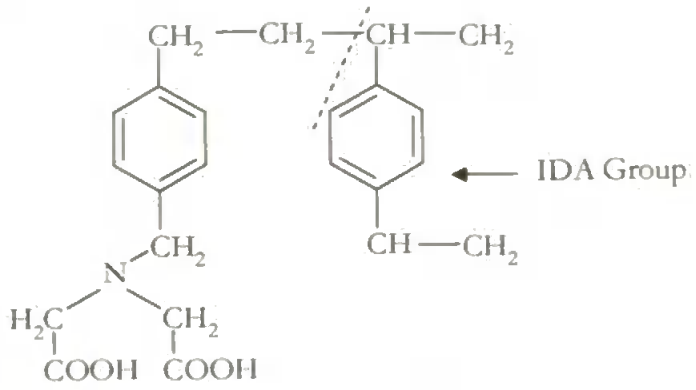

Figure 3.10 Structure of Chelex 100® Showing the Iminodiacetic Acid Group

retained is a function of pH. Below pH 2, the resin acts as an ion exchanger and no metal cations are chelated; conversely, effective adsorption occurs in the pH range 4 - 14, when the metal cations replace an equivalent amount of resin cations (NH_4^+). The citrate buffer was cleaned using these two protocols for all subsequent studies.

3.3.5 8HQ Column Parameters

Within the 8HQ column, the dispersion of the sample zone during loading and elution was influenced by the column geometry, the pH of column loading, the kinetic characteristics of the 8HQ resin in relation to Cu(II), chelation from seawater ions, the flow rate of the sample and the eluent/elution efficiency. These factors were investigated and optimised. In addition, the column enrichment factor (EF), breakthrough capacity, the efficiency of the UHP water rinse after column loading, the column regeneration phases and the flow rates for column loading and elution and of the 1,10-primary reagent were also optimised.

3.3.5.1 Column Geometry

The geometry of the column, principally the aspect ratio (length/i.d.), affected column performance, especially its flow characteristics, and therefore the enrichment factor. Four different geometries of the machined acrylic column were compared to ascertain the optimum design, the results being shown in Figure 3.11.

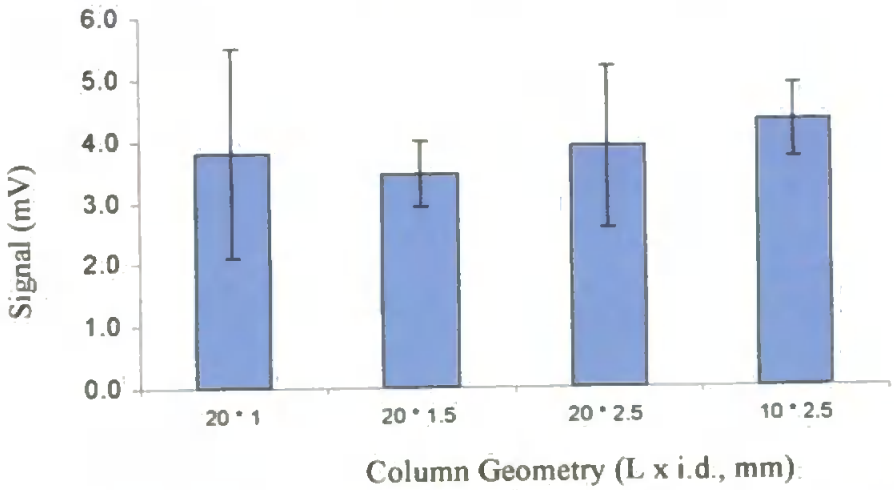

Figure 3.11 Comparison of Different Column Geometries. Length (L) = the length of the 8HQ resin bed (mm), i.d. = internal diameter of the machined acrylic column. A 5 nM Cu(II) standard in UHP water (acidified, Q HNO_3) was used with simplex determined optimal reagent concentrations with a 0.2 M HCl eluent. Loading was at 1.5 ml min^{-1} for 90 s, using a citrate buffer (0.2 M, pH 5).

The 10 x 2.5 mm 8HQ resin bed gave the maximum signal (although the differences between the columns were small), with good reproducibility (RSD 4.9 %, n=4) and was therefore used for all subsequent studies.

3.3.5.2 Column Loading Time

The enrichment factor (EF) (Section 3.3.5.5) of the 8HQ micro-column was related to the volume of sample loaded, a factor governed by the loading time and flow rate. Due to its increased flexibility for field work, time based loading was selected for use with the 8HQ micro-column manifold, instead of sample displacement from a loop by a UHP water carrier stream as used for the manifold without a column. An investigation of the time for column loading (10 nM Cu(II)) over the range 30 to 180 s (not shown) found that it was a linear process (R^2 0.9986). Ninety seconds was selected as the optimum column loading time, this being a balance between sensitivity at sub-nano molar Cu(II) concentrations and minimisation of the analytical cycle time and sample consumption.

3.3.5.3 Optimal pH for Column Loading

The loading of Cu(II) in UHP water onto the 8HQ column is a pH sensitive process (Section 3.3.4). Therefore, to ensure selective and quantitative separation of Cu(II) from a seawater matrix, the optimum pH for retention of Cu(II) by the immobilised 8HQ from an acidified seawater sample spiked with Cu(II) (10 nM) was investigated (Figure 3.12 and Table 3.6). The seawater sample was buffered by citrate and acetate buffers, prepared as described in Section 3.2.1, and used as previously described (Section 3.3.4). The pH was measured at the column, after the sample and buffer had mixed, in order to account for the alteration in pH due to the effect of the seawater matrix ions (Section 3.3.4.1) and to compare with the optimum loading pH observed for Cu(II) in UHP water (Section 3.3.4).

A CL maximum with the best reproducibility for the acidified (pH 2) seawater sample spiked with 10 nM Cu(II) was observed at pH 5.0, as measured at the column, after using a citrate buffer (0.2 M, pH 6). These conditions were therefore utilised for all future seawater analysis. At pH 3 Cu(II) retention was substantially reduced due to competitive binding from H^+ ions in the mobile phase. At pH 7 and above the retention was much lower due to the competitive loading of alkali and alkaline earth metal ions from the seawater matrix (Esser *et al.*, 1994).

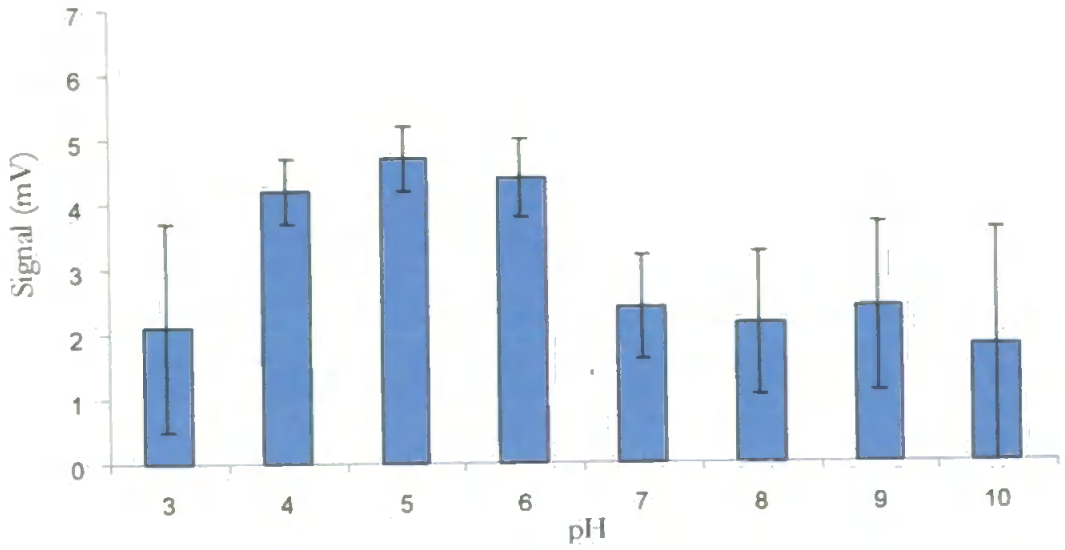

Figure 3.12 Optimal pH for Loading on 8HQ Column. 10 nM Cu(II) addition to an open ocean, South Atlantic seawater sample. Citrate and acetate buffers (0.2 M) used. Error bars represent 3s.

Table 3.6 Optimal pH for Loading on 8HQ Column

Buffer (0.2 M)	pH at Column	Signal (mV)	RSD (%) (n=4)
Citrate	3.0	2.1	26
Citrate	4.0	4.2	3.8
Citrate	5.0	4.7	2.1
Citrate	6.0	4.4	4.7
Acetate	7.0	2.4	3.7
Acetate	8.0	2.2	4.5
Acetate	9.0	2.4	4.9
Acetate	10.0	1.8	8.6

Cu 10 nM in UHP water with citrate and acetate buffers.

These results are in good agreement with the literature data. Lan and Yang (1994) reported optimum retention of Cu(II) at pH 5-6 for 8HQ immobilised on silica, in close agreement with these results. Daih and Huang (1992), also using 8HQ immobilised on silica, found a maximum retention at pH 4 with efficient retention over the pH range of 2-8. Beinrohr *et al.* (1990) reported greater than 90 % retention of Cu(II) over a pH range 2-12 using a spherical cellulose sorbent with chemically bound 8HQ.

3.3.5.4 Chelating Characteristics of 8HQ Column

It was important that the 8HQ micro-column was selective for Cu(II) for efficient extraction from the seawater matrix. The kinetics of an in-line FI micro-column with its high flow rates, are much more important than in batch systems. Daih and Huang (1992) reported that the kinetics of 8HQ chelation were rapid, which, coupled to its high stability

constant for Cu(II) (log K_1 of 12.29, Sillen, 1964) promoted highly selective separation and very strong retention of Cu(II) from seawater. The seawater matrix elements that enhance or quench the 1,10-phenanthroline CL reaction were identified earlier in this study (Section 2.3.6, Table 2.13), and these are included in the study of column loading at pH 5 to demonstrate column selectivity for Cu(II) (Table 3.7).

Table 3.7 8HQ Column in Seawater Matrix

CL Quenching Species	% Quenching	Group	8HQ Log K_1	CL Enhancing Species	% Enhancement	Group	8HQ Log K_1
Na(I)	51	Ia		K(I)	335	Ia	
Ni(II)	86	VIII	9.9				
Al(III)	96	IIIb		Ca(II)	110	IIa	3.27
B(III)	122	IIIb		Sr(II)	100	IIa	
Sn(III)	97	IVb		Mg(II)	143	IIa	4.5
Pb(I)	97	IVb		Cr(II)	127	VIII	
As(I)	90	Vb		Co(II)	105	VIII	9.1
Ag(I)	93	1b		Cd(II)	108	VIII	8.2
Zn(II)	89	VIII	8.5	Cl^-	131	VIIb	
Mn(III)	83	VIII	7.3	HCO_3^-	19		
Fe(III)	76	VIII	11.3	SO_4^-	117		
F^-	80	VIIb					
$H_3BO_3^{3-}$	82						

All data (%) normalised to 10 Cu nM in UHP water (100 %). Log K_1 for Cu is 12.29 (Sillen, 1964)

The 8HQ resin was selective for transition metals e.g. Cu(II), in preference to the alkali metals of Na(I) and K(I) and alkaline earth elements of Ca(II) and Mg(II), which have negligible retention at pH 5 (Beinrohr *et al.*, 1990). The same authors reported the optimum retention of Ca(II) and Mg(II), the principal seawater matrix ions, at pH 9 to 10.

The selectivity of 8HQ for Cu(II) as a transition metal led to its preferential loading relative to Ni(II), Al(III), Sn(III), Pb(I), As(I), and Ag(I). In support of this hypothesis As has been shown to exhibit reduced recovery at pH 5 for 8HQ on cellulose (Beinrohr *et al.*, 1990). With respect to the transition metals Cd(II), Co(II), Fe(III) and Zn(II) present in seawater, 8HQ has a higher stability constant for Cu(II) than for these metals and was therefore preferentially retained by the 8HQ. Beinrohr *et al.*, (1990), also reported recoveries of less than 50 % at pH 5 for Cd(II) and Mn(III) with Zn(II) also exhibiting reduced recovery, when using 8HQ immobilised on cellulose. Chloride and the HCO_3^- are anionic

and therefore are not chelated by 8HQ. In conclusion at the optimal pH of 5, the 8HQ column was selective for Cu(II) which was strongly retained in preference to the potential interferents in the seawater matrix.

3.3.5.5 Column Efficiency – Enrichment Factor

One indicator of column performance is the enrichment factor (EF, see also Section 3.3.5.2) which can be defined as;

$$EF = C_e/C_s$$

were C_e = [analyte] in the eluent and C_s = [analyte] in the original sample.

For practical purposes the enrichment factor is not usually defined as a concentration increase, but as a response enhancement by comparing the ratio of the slopes of the linear section of the calibration graph prior to and after matrix separation. This avoids the possible large errors arising from comparison of peak heights before and after preconcentration. Using a manifold with and without a column for the calibration studies for 0.1 – 10 nM Cu(II), the ratio of the slopes was 1.191/0.2838 = 4.2. This was a relatively low factor that was attributed to the 4.5 fold decrease in volume from sample to eluent and the difference in dispersion between the manifolds with and without an 8HQ micro-column. The micro-column enhanced the sensitivity of the FI-CL manifold, thus promoting the determination of Cu(II) at trace levels in the open ocean.

A further indicator of column performance is the consumptive index (CI) which measures the amount of sample required for seawater analysis. The Cu(II) FI manifold incorporating the 8HQ micro-column had a very efficient use of sample, requiring only 10 ml for a two point standard addition to a seawater sample at ambient Cu(II) concentrations.

3.3.5.6 Column Breakthrough Capacity

The 8HQ column was further characterised by investigating the breakthrough capacity of the 8HQ resin for Cu(II). This can be defined as the amount of metal ion that can be chelated per unit mass of 8HQ resin under existing dynamic operating conditions, before the analyte is detected in the column eluent. A fresh 8HQ column was incorporated directly in line with the detector in a modified FI-CL manifold (Figure 3.13). Acidified seawater (pH 2), with a 10 μM Cu(II) addition was buffered (citrate, 0.2 M) in line and then

pumped continuously through the 8HQ column and the results shown in Figure 3.14. The optimum analytical variables described in this chapter were used.

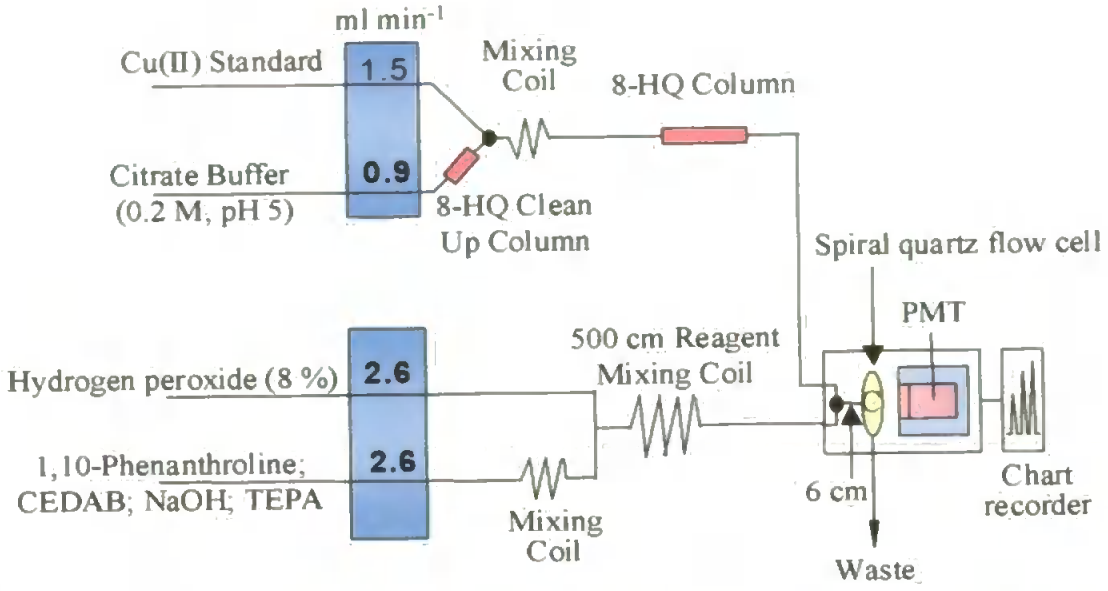

Figure 3.13 FI-CL Manifold for Determination of 8HQ Micro-column Breakthrough Capacity. Sample flow rate 1.5 ml min^{-1}

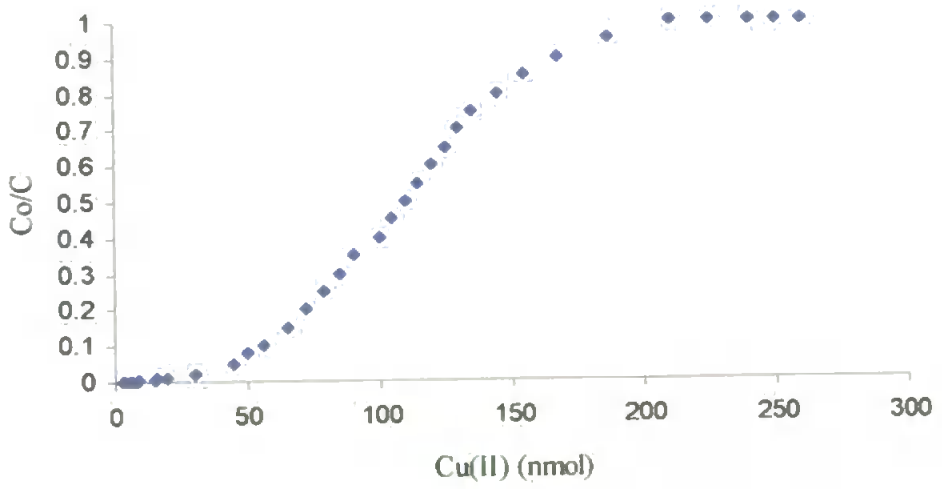

Figure 3.14 Cu(II) Breakthrough Curve for 8HQ Micro-column. Cu(II) 10 µM in acidified seawater (pH 2) buffered (0.2 M, pH 6 citrate buffer). Optimal CL reagent concentrations.

At first a baseline CL signal was observed indicating efficient retention of Cu(II) ions at the 8HQ chelating sites. As column breakthrough occurred, the Cu(II) ions mixed with the continuously pumped CL reagents, generating a CL signal that slowly rose as more Cu(II) ions broke through. The plateau reached indicated saturation of the 8HQ chelating sites. The column breakthrough capacity can be interpolated from the Cu(II) breakthrough

curve (Figure 3.14), using the ratio of the concentration in the eluent (C) over the total concentration in the sample (C_o) at the point were $C/C_o = 0.05$ (Landing *et al.*, 1986) which represented 95 % efficiency of retention of cu(II)..

At 0.05 the column retained 45 nmol of 8HQ resin, much in excess of typical seawater concentrations of Cu(II) (0.1 – 6 nM). Since the dry mass of the resin was 48.4 mg this represented a column total exchange capacity of 945.4 nmol of Cu(II) g^{-1} of resin. Insufficient column capacity would have resulted in a matrix separation system prone to analyte breakthrough and more effected by the seawater matrix.

3.3.5.7 Role of UHP Water Column Rinse and Carrier Stream

After sample loading, any residual seawater matrix ions weakly bound (e.g. van der Waals forces) or retained in the interstitial pores of the 8HQ resin, could be co-eluted with the Cu(II) and act as interferents to the CL reaction. To remove these, a column UHP water rinse (60 s), prior to elution, was incorporated into the analytical protocol for the push fit columns first used in this study (results not shown). Due to a restricted eluent flow through the push fit columns (aspect ratios 10.7 and 14.3), it was also necessary to merge the slow moving eluent stream with a faster flowing UHP water carrier to efficiently transport the eluted Cu(II) to the detector. However, the improved flow characteristics observed with the wider, push fit column (lower aspect ratio of 3.9), led to a further investigation of the requirement for the UHP water column rinse and carrier stream. This was undertaken by loading onto the wider column a Cu(II) (10 nM) standard in UHP water (experiments 1 – 4) and a UHP water blank (experiments 5 – 6, Figure 3.15 and Table 3.8).

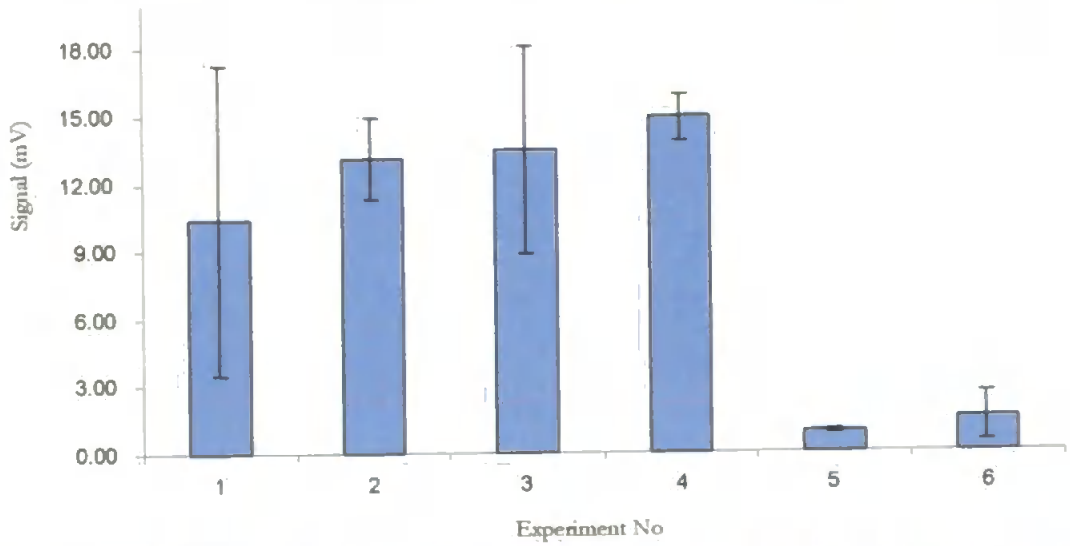

Figure 3.15 UHP Water Rinse After Loading of Column and Prior to Elution and Effect of UHP Water Carrier 10 nM Cu(II) in UHP water, blank – acidified UHP water. Error bars are 3s.

Table 3.8 UHP Water Column Rinse and UHP Water Carrier Stream

Expt. No	Sample	UHP Rinse	UHP Carrier	Signal (mV)	RSD (%)
1	Cu(II)	No	Yes	10.1	4.3
2	Cu(II)	No	No	13.1	4.6
3	Cu(II)	Yes	Yes	13.5	11.4
4	Cu(II)	Yes	No	14.9	2.0
5	Blank (UHP)	No	No	0.9	4.4
6	Blank (UHP)	Yes	No	1.4	7.4

Acidified 10 nM Cu(II) in UHP water, blank – acidified UHP water (Q HNO_3) with wider column. n=5

A signal maximum was observed after rinsing of push fit column after loading, (which removed the seawater matrix ions), but without the UHP water carrier stream. The improved flow through the shorter, wider, push fit column (3.9 aspect ratio) and further substantial improvement through the machined acrylic column enabled the UHP carrier stream to be removed. The manifold without the UHP water carrier stream had improved sensitivity and reproducibility due to the eluted Cu(II) no longer undergoing dispersion in the carrier stream and therefore the carrier was removed for future work. Due to the improved CL signal observed with the column UHP water rinse after loading, it was retained in the analytical protocol for all future studies.

3.3.5.8 Column Regeneration and Equilibration

Push Fit Column; The 8HQ micro-column had a maximum capacity when all the 8HQ chelating sites were free. Early 8HQ column investigations utilised the push fit columns, on which the chelating sites were regenerated after elution by a separate acid clean (0.2 M Q-HCl) followed by column equilibration with a UHP water rinse (pH 5.5) prior to sample loading at pH 5.0. The effect of extending the acid regeneration and UHP water equilibration cycles from 30 s to 60 s for the push fit column were investigated using a 10 nM Cu(II) standard in UHP water and an Irish Sea sample (Table 3.9).

For both the 10 nM Cu(II) in UHP water and the Irish Sea sample, a distinct improvement in CL signal and reproducibility was found for the 60 s acid regeneration and 60 s UHP water equilibration of the push fit column. This was due to a more efficient column regeneration and column equilibration, which minimised sample loss upon commencement of loading. These column extended times were incorporated into the analytical routine for the duration of use of the push fit 8HQ column.

Table 3.9 Extending Acid Regeneration of Column and UHP Rinse Times

Experiment No	Sample	Acid Clean Time (s)	UHP Water Rinse (s)	Signal (mV)	RSD (%)
1	Cu(II) in UHP	30	30	4.7	21
2	Cu(II) in UHP	60	60	16.9	7.4
3	Irish Sea	30	30	7.0	27
4	Irish Sea	60	60	18.2	3.2

10 nM Cu(II) standard in UHP water with citrate buffer (0.2 M, pH 5). Irish Sea sample collected May 94 acidified to pH 2 (HCl) and UV irradiated Sept 97, mean Cu(II) content of 10.6 nM (UoP ASV and CSV measurements). Irish Sea sample analysed with citrate buffer (0.2 M, pH 6). Both samples eluted with an aqua regia eluent (0.6 M HCL/0.2 M HNO_3). Push fit 8HQ columns used.

Incorporation of Machined Acrylic Column; The machined acrylic column exhibited a substantially improved flow through it and therefore the column acid regeneration and UHP water equilibration cycles were further evaluated (Table 3.10). The aim was to reduce the total analytical cycle time by shortening or removing these two stages. A 10 nM Cu(II) addition was made to an English Channel sample (Eddystone Lighthouse), which had been filtered (0.4 μm, Nuclepore) and acidified to pH 2 (Q HCl).

Table 3.10 Column Regeneration and Equilibration Cycles

Expt No	UHP Rinse Post Loading	Acid Clean	UHP Rinse	Signal (mV)	RSD (%) (n=4)
1	60	60	60	4.1	9.8
2	30	60	60	3.9	6.5
3	30	0	60	3.7	1.5
4	30	0	0	3.8	2.6

As Table 3.10 clearly illustrates, when using the machined column no significant difference in signal (*t* test, p = 0.05) was seen between the means of the analytical protocols. This was in contrast to the substantial differences observed for the push fit columns, reported earlier (Section 3.3.5.7 and 3.3.5.8). Reproducibility was also substantially improved (Table 3.10) by removal of the acid clean and UHP water rinse cycles, in contrast to the results for the push fit column. The results demonstrate the significantly improved flow through the newly designed acrylic column, which enabled the modification of the analytical protocols described earlier.

The machined 8HQ micro-column was regenerated by the continuation of eluent flow after elution of the Cu(II). As timed by the entrapment of an air bubble, the eluted

Cu(II) required 12 s to reach the detector. A typical signal peak required 8 s to complete its rise and fall which represented the time required for the acid elution (0.2 M Q HCl) of the Cu(II) from the column. The 30 s acid eluent cycle therefore eluted the Cu(II) off the column for first 8 s, followed by a further 22 s of acid flow which regenerated the column. The buffered sample acted as a column equilibrant very quickly after commencement of loading, minimising sample loss. Fang *et al.*, (1993) also found that column cleaning and/or equilibration did not enhance the sensitivity or precision of a flow injection flame AAS system when compared to a system that excluded these features.

In conclusion, the manifold without a separate equilibration stage resulted in a simpler and more efficient 8HQ solid phase extraction micro-column. The design and incorporation of the machined acrylic column enabled the removal of both the column regeneration and equilibration cycles for all subsequent studies. This reduced the time for processing a single injection from 6 to 2.7 min and therefore a sample analysis (n=4) from 24 to 10.6 min. The time for a full analytical protocol of sample plus a two point standard addition and including sample exchange, column and line rinsing cycles prior to analysis, was significantly reduced from 75 to 35 minutes, more than doubling the sampling frequency. This was a considerable advantage for field deployment with its inherent time constraints. The time saving also halved the amount of eluent required, removed the requirement for the acid clean solution and reduced the amount of UHP water required. These represented real savings in cruise preparation time, reagent usage, storage and transport, all precious commodities prior to and during field deployment.

3.3.6 Flow Rate

An important criterion in an FI manifold is reproducible dispersion, which is determined in part by the ability to provide constant flow rates. A range of pump tubing (Acu Rated, Elkay) with varying internal diameters (signified by the different bridge colours) were calibrated using a multi-channel, variable speed peristaltic pump (Watson Marlow 503 S, 6 channel, 8 roller head) (Figure 3.16).

The pump tubing produced a linear and reproducible flow rate for a wide range of pump speeds. The pump tubing was routinely replaced after 30 h of usage, or if a pulsating flow was observed, to ensure a reproducible flow rate was maintained. All pump tubing was conditioned by an acid wash (0.2 M HCl, 1 h) and a UHP water rinse (1 h) prior to use.

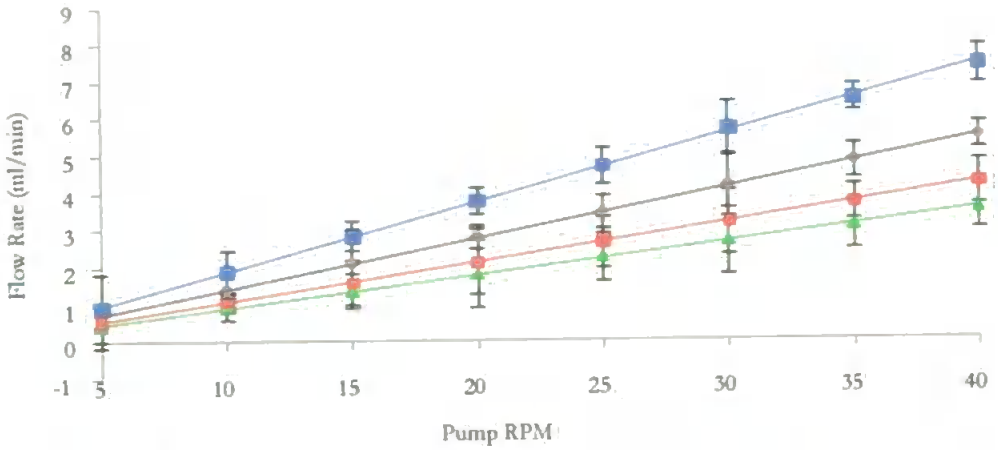

Figure 3.16 Calibration of Pump Tubing. Gilson Mini Pulse 3 Pump, Elkay Acu Rated Auto Analysis Tubing. Bridge Colour - Blue/Yellow, Grey, Red, White

3.3.6.1 Column Loading Flow Rate

During column loading it was important to maximise the phase transfer factor, which determined the efficiency of loading onto, and elution from the 8HQ column of Cu(II). The retention of Cu(II) on the 8HQ column was mass transfer limited and therefore related to the residence time of the sample in the column and its volume through the column. These were functions of the sample loading flow rate, which was investigated using a column loading time of 90 s (Figure 3.17).

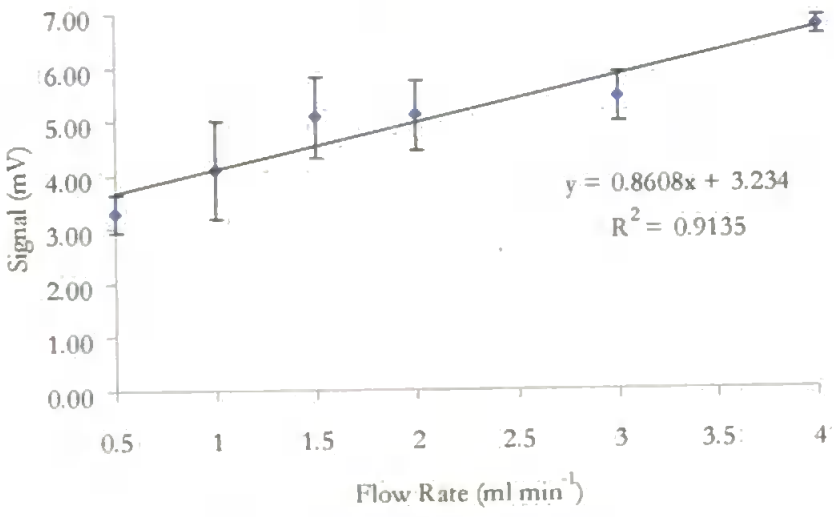

Figure 3.17 Loading Flow Rate (mL min^{-1}) Cu 10nM in UHP water.

A linear relationship (R^2 = 0.9135) was found between loading flow rate and Cu(II) retention. At flow rates of 0.5 ml min^{-1} although a high phase transfer factor occurred, the low volume of sample became limiting, requiring an unacceptably long sample loading time

to maintain the sensitivity of the FI-CL analyser. At flow rates >3 ml min^{-1} sample consumption was high, with the maximum flow rate limited by manifold leaks due to increased pressure at > 4 ml min^{-1}. Furthermore, although the kinetics of the 8HQ resin were reported as rapid (Daih and Huang, 1992), at flow rates > 4 ml min^{-1} an incomplete phase transfer may occur.

Loading for 90 s at 1.5 ml min^{-1} achieved an efficient transfer of Cu(II) from the mobile sample phase to the 8HQ stationery phase, resulting in good sensitivity in a relatively short loading time and was selected for all future work. This was in agreement with Beinrohr *et al*, (1990), who used a loading cycle of 60 s at 2 ml min^{-1} for 8HQ immobilised on a spherical cellulose sorbent. Daih and Huang (1992) selected a flow rate of 2 ml min^{-1} for 8HQ on silica. Using 90 s at 1.5 ml min^{-1} for loading during this study resulted in good sampling frequency with efficient sample consumption. These are all factors important during field deployment. The integrity of the pump tubing was also maintained, as was therefore a reproducible flow rate and thus reproducible mixing.

3.3.6.2 Primary Reagent Flow Rate

The 1,10-phenanthroline CL reaction was fast (0.6-0.7s) with a transient response compared with spectrophotometric derivatisation reactions. It was therefore important to ensure the maximum CL emission took place in the spiral flow cell in front of the detector window. This required optimisation of the flow rates of the 1,10-primary reagent, hydrogen peroxide and eluent in the streams (Figure 3.18). All changes to the flow rates of the two primary reagents were made in parallel to maintain a constant ratio and ensure reproducible mixing at the confluence point.

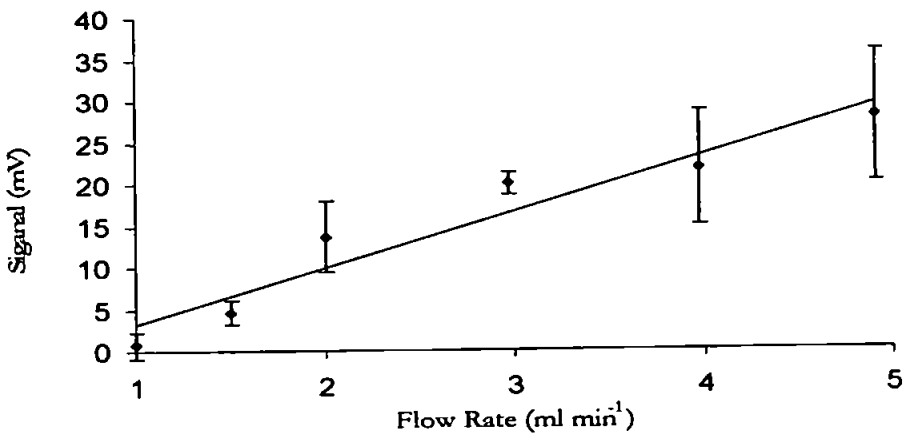

Figure 3.18 Flow Rates of 1,10-primary Reagent and Hydrogen Peroxide

A linear increase in the CL emission (R^2 = 0.9336) was seen over the flow rate range 1 - 5 ml min^{-1}. This response was partly attributed to increased turbulence that

improved the mixing of the reagents together, and their mixing with the sample, producing a more effective microenvironment for the CL emission. In addition, the time for the CL reaction to reach the flow cell was reduced at higher flow rates with a greater number of molecules reacting in front of the detector window. For method development and seawater analysis a flow rate of 3.6 ml min^{-1} was used as a balance between signal intensity, pump tubing integrity and reagent consumption. A flow rate of 4.9 ml min^{-1} maximised manifold sensitivity, although due to the high reagent consumption at this flow rate this option was reserved for analysis at the limit of instrument detection.

3.3.6.3 Direction of Eluent Flow

During column loading the Cu(II) was retained in a zone at the front end of the column. The direction of eluent flow was investigated to optimise the CL signal. An eluent flow in the reverse direction to that used for sample loading resulted in a more efficient and rapid elution that produced a sharp signal peak. This was in contrast to the significantly broader and ragged signal peak observed when the Cu(II) was eluted in the same direction as used for column loading. Reverse elution therefore eluted the Cu(II) in a focused 'plug' that avoided dispersion of the eluted Cu(II) due to it passing through the length of the column. Reverse elution also avoided the progressive compaction of the 8HQ resin due to uni-directional flow through the column, which created resistance to flow, raised the pressure in the FI-CL manifold and resulted in an irreproducible eluent flow rate. Reverse elution of the 8HQ micro-column was therefore incorporated into the analytical protocol for all future studies.

3.3.6.4 Elution Flow Rate

In order to maximise the sensitivity of the manifold and obtain a sharp, well defined signal peak an efficient and rapid column elution that did not degrade the column with continual use was essential. These factors were determined in part by the eluent used (Section 3.3.7) and partly by the elution flow rate. The eluent flow rate was investigated for the push fit and machined acrylic columns, using an aqua regia eluent.

The wider, shorter push fit column (aspect ratio 3.9, results not shown) had an optimal eluent flow rate of 1 ml min^{-1} using reverse elution, with a significant reduction in signal size and reproducibility at flow rates < 0.67 or > 1.33 ml min^{-1}. This was due to a less efficient mass transfer from the 8HQ stationery phase to the mobile eluent phase which increased the dispersion of the eluted Cu(II) in the eluent stream. This indicated the non-linear flow through the push fit columns. The machined acrylic column, utilising reverse

elution, had an optimum flow rate of 1.4 ml min^{-1} (Figure 3.19) at which the mass transfer was most efficient. The small variation in signal strength and reproducibility seen over the range of flow rates used, clearly demonstrated the constant and reproducible flow through the machined acrylic column and supported its choice for future work.

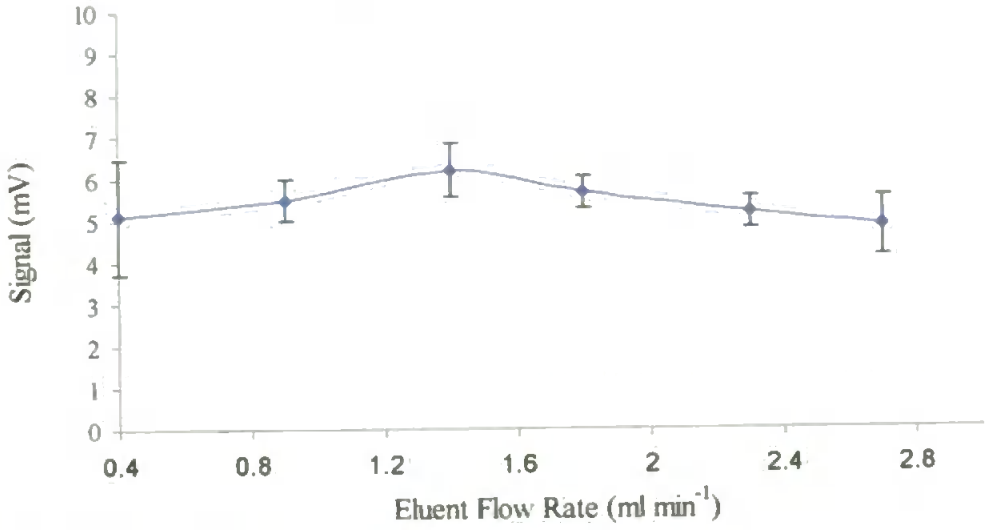

Figure 3.19 Eluent Flow Rate (ml min^{-1}) for Machined Acrylic Column

The eluent flow rate also helped define the position of the CL reaction in the flow cell, although the influence was small compared to the combined flow rate of the reagents. Re-optimisation of the flow rate of the reagents to include the new eluent flow rate for the machined column produced no significant alteration in their flow rate.

CL Peak Shape: Typical peak shapes from the detector for a series of replicate injections (n=4) using a South Atlantic seawater sample are shown in Figure 3.20.

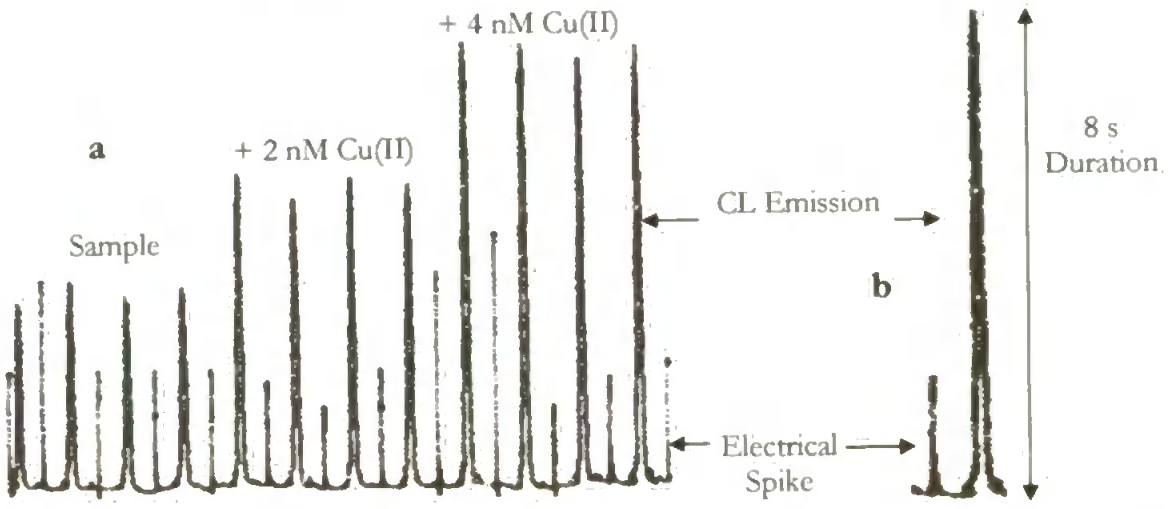

Figure 3.20 Typical Injection Peaks (a) Detector output for a series of four replicate load, rinse and elute cycles using a South Atlantic seawater sample with 2 and 4 nM standard additions of Cu(II); (b) Expanded single CL peak.

Upon commencment of reagent flow, the position of the baseline moved up the chart paper from that originating from the PMT electronic noise, due to an increased background CL signal produced by Cu(II) impurities in the reagents. This reagent noise was stable during the UHP wash and sample load cycles. In order to minimise reagent consumption, the reagent and eluent pumps were switched on for 20 s prior to elution to ensure the baseline was stable. The high impedance of the pumps caused a sharp electrical spike on the chart upon their start up (Figure 3.19). Copper(II) ions were then eluted from the column by switching the acid eluent stream through the column in the reverse direction to sample loading, resulting in a sharp, narrow peak (ca. 8 s for full height, (Figure 3.19 (b). Acid eluent flow continued for a further 22 s to regenerate the chelating sites on the 8HQ column.

Optimisation of the push fit column (not shown) demonstrated how the profile of the elution peak was related to the dispersion of the Cu(II). At 0.17 ml min^{-1} the peak was broad with a slow and eratic rise and fall due to a non-linear and reduced eluent flow through the column. This increased the dispersion of the Cu(II) in the eluent and upon mixing with the primary reagents. At > 0.34 ml min^{-1} a sharp signal peak with a smooth and rapid rise and fall was seen, together with a much reduced background noise level. The sharp elution peaks for the push fit 8HQ column were obtained by selection of an appropriate eluent flow rate (1 ml min^{-1}) and chart speed. The machined acrylic column had a sharp CL signal profile over the whole range of eluent flow rates used, which again demonstrated the constant and reproducible flow through the column.

3.3.7 Selection of Eluent

The kinetic factors of the elution process were of much greater significance for the in-line 8HQ column due to the much shorter residence times, in comparison with batch systems. The in-line column therefore required a strong eluent that promoted an efficient and rapid elution of the Cu(II) to maximise the enrichment factor (EF) and promote sharp elution peaks. Q-HCl and Q-HNO_3 eluents were investigated over the range of 0.2 to 1 M using a 10 nM Cu(II) UHP water standard (Figure 3.20).

Both eluents exhibited a rapid and efficient elution and *t* tests (p=0.05) showed that the differences between the Q-HCl and Q-HNO_3 eluents and between the different concentrations of Q-HCl eluents were not significant. However, the Q-HCl was more efficient and resulted in a larger CL signal over the range of eluent concentrations used (Figure 3.21). Further investigation (not shown) comparing an aqua regia mixture (0.6 M

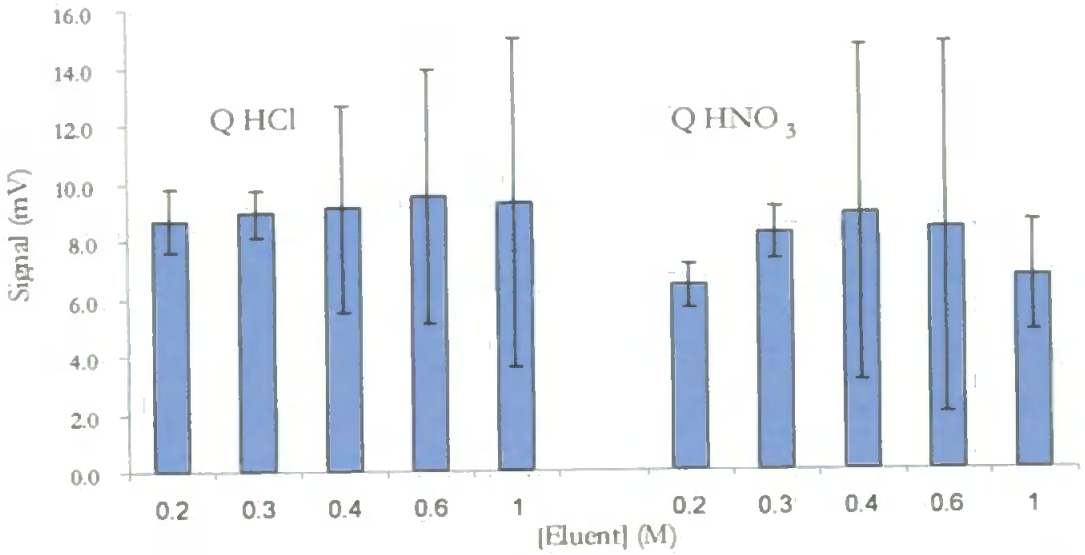

Figure 3.21 Evaluation of Q HCl and Q HNO_3 Eluents 0.2 – 1 M concentration, Cu(II) 10 nM in UHP water

Q-HCl/0.2 M Q-HNO_3) with a 0.2 M Q-HCl eluent demonstrated that the former was marginally more efficient. However, aqua regia was not used due to poorer reproducibility.

Although the CL signal was of similar magnitude for the HCl eluent, the 0.2 M-Q-HCl was selected due to its substantially better reproducibility and the possibility of column degradation when using the stronger eluents, an important factor during long term field deployment. This was not so vital a requirement in batch systems, where the column could be easily changed, or even digested, to release the analyte.

CL Signal from the Eluents: The LOD of the FI-CL analyser was closely related to the blank signal, which was catalysed in part by the Cu(II) impurities in the acid eluent stream. The size of this eluent CL signal was investigated by eluting acidified UHP water blanks with 0.2 M Q-HCl, 0.2 M Q-HNO_3 and 0.6 M Q-HCl / 0.2 M Q-HNO_3 (Figure 3.21).

The results (Figure 3.22) clearly show that the 0.2 M Q-HCl eluent had the lowest blank signal, with optimum reproducibility, and was therefore used for all subsequent studies in order to minimise the blank signal. The higher blank signal from the Q-HNO_3 indicated that it was harder to purify during the sub-boiling distillation process (Section 2.2.1). The size of the blank was an important factor during the determination of sub-nanomolar levels of Cu(II).

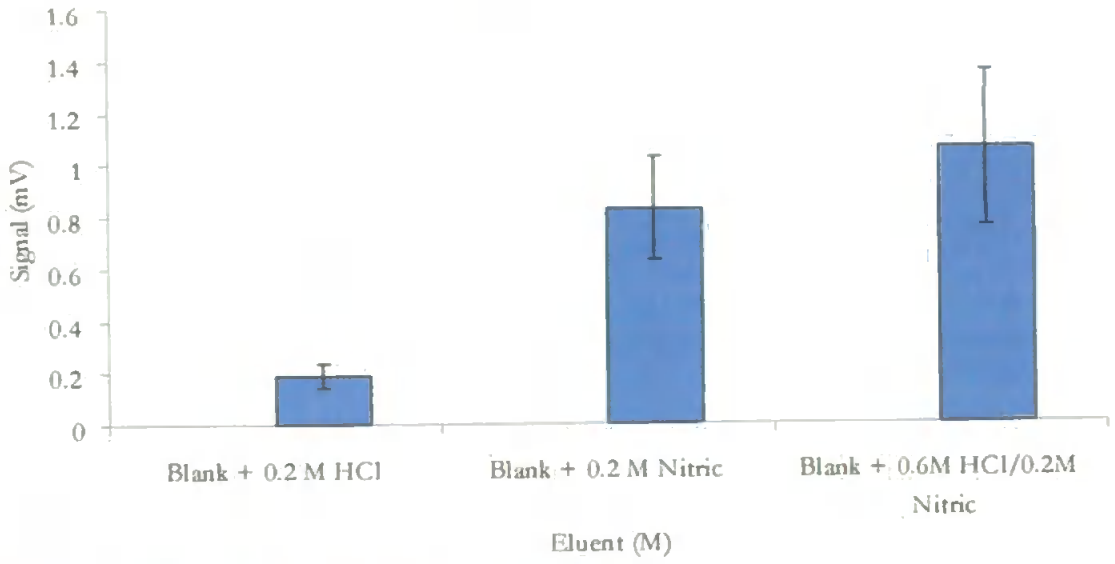

Figure 3.22 Comparison of Blank Signal from Eluents

3.3.8 Blank Subtraction Protocol

An aspect integral to accurate determination of Cu(II) was the blank subtraction protocol. When analysing a seawater sample, a typical blank for seawater analysis had three components, namely the acid used for sample acidification (pH 2, 80µl of Q-HNO_3 for a 100 ml of seawater sample), the UHP water used to prepare the citrate buffer and the citric salt itself. Each of these contained Cu(II) as an impurity.

Prior to Cu(II) determination the citrate buffer was cleaned of trace metals using Chelex 100 and an in-line 8HQ column (Sections 3.2.4.1 and 3.3.4.2, Figure 3.2). The UHP water at pH 5.5 required no buffering to be loaded onto the column. The blank injection protocol (n=4) was run 5 times and the mean values (Table 3.11) used for calculation of the blank signal.

Table 3.11 Blank Determination

Sample	Signal (mV)	RSD (%)
UHP water only (A)	3.15	6.1
UHP + Buffer (B)	3.73	7.8
Acidified UHP + Buffer (C)	4.80	2.3

The optimised reagent concentrations were used at 3.6 ml min^{-1}, with column loading for 90 s at 1.5 ml min^{-1}, and an 0.2 M Q-HCl eluent at 1.4 ml min^{-1}. Due to the FI-CL analyser operating at such low Cu(II) levels, the reproducibility was higher than reported for other determinations. Signal size shown to two decimal places for accuracy of calculations.

It was not appropriate to blank subtract the total blank, which comprised the acidified UHP water sample blank + citrate buffer stream (value C, Table 3.11) since part of this signal originated from the UHP water in the sample stream, which would be replaced by seawater during seawater analysis. The fraction of the total blank to be subtracted was therefore defined first by determining each of the three components of the blank. This was achieved by injecting UHP water only in both the sample and buffer streams, followed by a UHP water blank with citrate buffer (0.2 M, pH 5) and finally an acidified UHP water blank with citrate buffer.

The total volume of UHP water loaded in both sample and buffer streams was calculated, and from this the proportion (%) of the signal from the UHP water in the buffer stream was determined. This was found to be 40 %. This was then converted into a mV value (I in Table 3.12) of the observed UHP water value i.e. 40 % of 3.15 mV (Table 3.11) = 1.26 mV

The mV value originating from the buffer salt itself, and from the acid used for sample acidification was then calculated by subtraction (II & III, Table 3.12) utilising the values in Table 3.11. These were then added to the UHP water only value, resulting in the true value of the blank (mV) value to be subtracted (IV) for this analytical run. Due to the day to day variation in PMT sensitivity due to it nearing the end of its effective life, it was not appropriate to express this as a mV value and therefore this was expressed as a % of the total blank (acid + UHP water + citrate buffer) to be subtracted (V).

Table 3.12 Blank Subtraction Protocol

Component of blank	Derivation using Table 3.11		Value (mV)
UHP water for buffer	40 % of UHP water value (A)	(I)	1.26
Buffer	B – A	(II)	0.58
Sample Acidification (Q HNO_3)	C – B	(III)	1.07
	Total blank subtraction value	(IV)	2.91
Mean acidified UHP blank + citrate buffer with 0.2 M Q HCL eluent			4.80 mV
Percentage of total blank to be subtracted (2.91/4.8) x 100		(V)	60.7 %

A, B and C refer to mV values in Table 3.11

The blank subtraction protocol therefore consisted of calculating 60.7 % of the buffered, acidified UHP water blank signal (mV), expressed as a mV value, which was then subtracted from the CL signal of the sample (mV). This blank correction protocol accounted for the Cu(II) impurities in the acid used for sample acidification and in the citrate buffer stream and was used for all subsequent analysis.

3.3.9 Analytical Figures of Merit

A series of Cu(II) calibrations with the machined acrylic 8HQ column were performed using an open ocean, South Atlantic seawater sample with Cu(II) additions (0.1-50 nM) to investigate the linear range of the FI-CL analyser and its sensitivity at ambient levels of Cu(II) in seawater (typically 0.1 to 6 nM, Coale and Bruland, 1990). Typical calibration graphs over the Cu(II) ranges of 0.1 to 10 nM and 0.1 to 50 nM are shown in Figures 3.23 and 3.24.

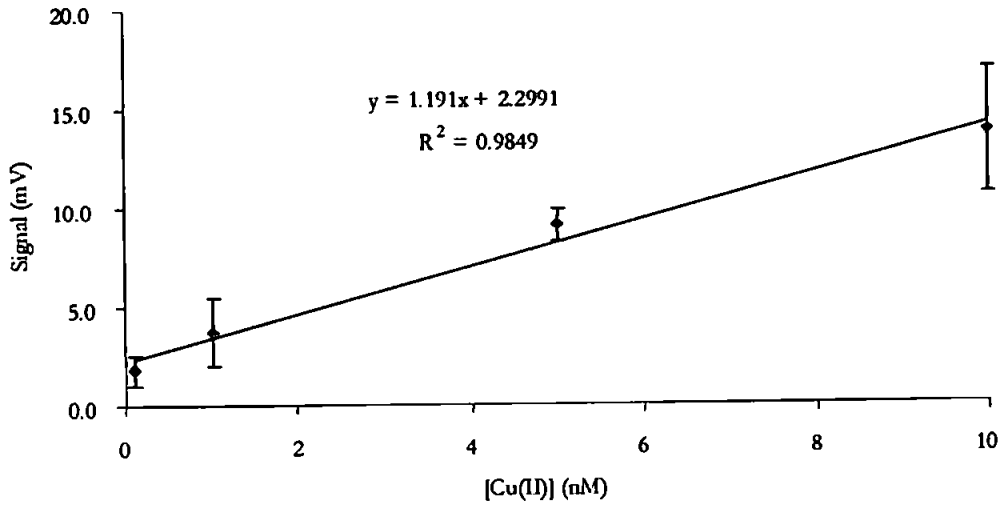

Figure 3.23 Calibration Graph (0.1-10 nM) for Cu(II) in Seawater Using 8HQ Column for Cu(II) additions to South Atlantic Seawater sample. Sample unfiltered, acidified (pH 2, Q-HCl), low in Cu(II) < 2 nM. Optimised FI-CL analyser operational variables used. Error bars are 3s.

The FI-CL analyser with an 8HQ micro-column, over a Cu(II) calibration range of 0.1-10 nM, exhibited a good linearity (R^2 0.9849) and reproducibility, typical RSDs being <5 % (n = 5). The calibration for the FI-CL preconcentration manifold was linear over the range 0.1-50 nM Cu(II) (R^2 = 0.9891), with good reproducibility (RSDs of 3.4 – 10 %, n = 4). Any differences in signal (mV) between the calibrations was due to variation in the sensitivity of the PMT, which was nearing the end of its operational life. When a new PMT was obtained prior to instrument deployment on the AMT cruise, the CL signal stabilised and the sensitivity of the analyser rose considerably. Analytical figures of merit are shown in Table 3.13.

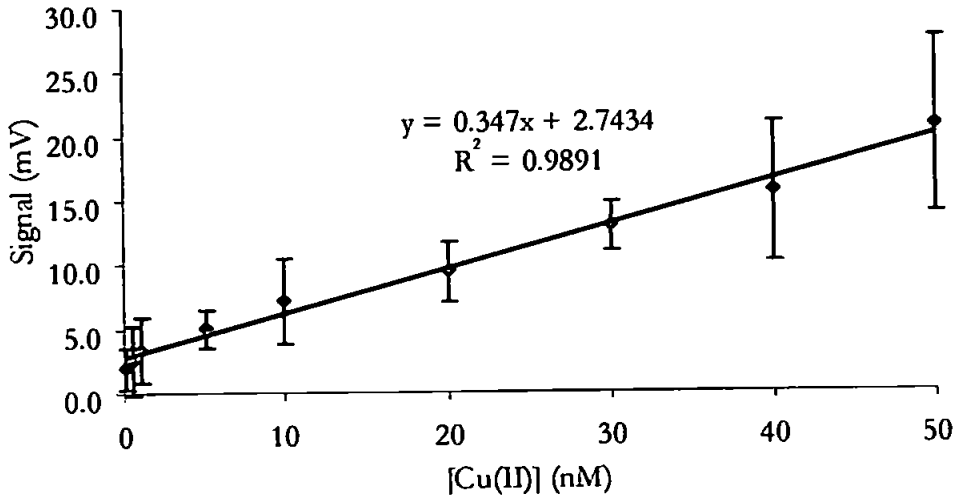

Figure 3.24 Calibration (0.1-50 nM) for Cu(II) additions to South Atlantic Seawater sample with 8HQ Column. Sample unfiltered, acidified (pH 2, Q-HCl), low in Cu(II) < 2 nM. Optimised FI-CL analyser operational variables used. Error bars are 3s (n =4).

Table 3.13 Analytical Figures of Merit

LOD	0.025 nM
RSD (0.1-10nM)	< 5 %
Linear Range	0.1 - 50 nM (R^2 0.9891)
	0.1 - 10 nM (R^2 0.9849)
Analytical Time (n=4)	10.6 min
Full Analytical Cycle (sample + 2 SA, with manifold cleaning)	35 min

LOD defined as a signal that equates to the blank (mV) (acidified UHP water) plus 3s. SA – Standard Additions

The sensitivity and wide linear range of the FI-CL instrument in seawater enabled it to be deployed in a range of environmental conditions e.g. open ocean (0.1 – 6 nM), as well as coastal and estuarine systems (10 - 20 nM, Tappin *et al.*, 1995). Analysis of waters containing Cu(II) concentrations above the linear range can be conducted by sample dilution or by reduction of the column loading time.

3.3.10 Validation of FI-CL Analyser

3.3.10.1 NASS 5 CRM

The role of the 8HQ micro-column was to increase the sensitivity of the FI manifold and to selectively retain the Cu(II), thus removing the possible interference effects of the seawater matrix on the CL reaction. The analytical accuracy and precision of the FI-CL analyser was verified by the determination of Cu(II) in the certified reference material (CRM) NASS 5 (National Research Council of Canada, Marine Analytical

Chemistry Standards Programme), an open ocean CRM. The full data set from a typical analytical run is shown in Table 3.14, whilst Table 3.15 shows the results from three separate experiments.

Table 3.14 Validation of FI-CL Analyser using NASS 5 CRM

Sample	Signal (mV)	Blank subtracted signal (mV)	RSD (%)
NASS 5 only	10.3	5.2	2.7
NASS 5 + 5 nM	15.8	10.7	2.7
NASS 5 + 10 nM	22.0	16.9	3.9
Blank = 8.4 mV, 60.7% of which = 5.1 mV			

Blank – acidified UHP water. All samples where prepared in a Class 1000 clean room, under a class 100 laminar flow hood and analysed using a two point standard addition (Cu(II) 5 and 10 nM) with blank subtraction. The blank signal varied due to changes in PMT sensitivity that occurred as the PMT was reaching the end of its operational life, (Section 3.3.9) with a replacement PMT being required before field deployment on AMT 9.

Table 3.15 Results for Cu(II) Using the FI-CL Analyser

Conditions	Cu(II) (nM)	+/- (nM)	RSD (%)	R^2
Certified CRM	4.68	0.7	n/a	n/a
SB	4.61	na	2.7 – 3.9	0.9988
SB	4.43			0.9952
SB	4.95	0.21		0.9909
CR	4.41	0.21	1.5 – 6.8	0.9896
CR	4.37		*1.7 – 6.2*	0.9984

SB – Shipboard analysis, CR clean room at University. n/a – data not available due to analysis of NASS 5 onboard to verify analytical accuracy and precision of the FI-CL analyser, with inherent time constraints preventing replicate analysis. (n=4) CRM uses 2 s for standard deviation.

A *t* test was used to compare the certified Cu(II) concentration to that obtained by FI-CL in the clean room at the University of Plymouth and onboard during field deployment. The null hypothesis is that the true value (u) of 4.68 nM is not significantly different from the observed FI-CL value and that the observed difference between the sample mean and u arises solely as a result of random errors. A confidence interval of 95 % (p = 0.05) was used. A *t* value of 0.25 was found and therefore the null hypothesis is retained. The absence of systematic errors is not proved, only that no evidence was found to suggest they were present.

The FI-CL determinations of Cu(II) in the NASS 5 CRM all exhibited a high degree of linearity (e.g. r^5 0.9988) with very good reproducibility (</= 5 %), with calculated

Cu(II) concentrations e.g. 4.37 +/- 0.14 nM, being in excellent agreement with the certified value of 4.68 +/- 0.7 nM. This clearly illustrates the good accuracy and precision of the FI-CL analyser.

3.3.10.2 Irish Sea Sample

The FI-CL analyser was further validated by the determination of Cu(II) in an Irish Sea sample (Table 3.16) that had been filtered (0.4 μm, Nuclepore), acidified (pH 2, Q HCl), and batch UV irradiated for an extended period to ensure breakdown of dissolved organic material (DOM).

Table 3.16 Validation of FI-CL Analyser with Irish Sea Sample

Irish Sea sample	Signal (mV)	Blank subtracted (60.7 %) data (mV)	RSD (%)
Irish Sea only	9.2	6.0	1.6
+ 10 nM	12.9	9.7	4.5
+ 20 nM	19.0	15.8	1.3
Blank	5.2	60.7 % of blank = 3.2 mV	2.8

Blank - acidified UHP water.

The same sample had been analysed over a 6 month period by voltammetry (CSV and ASV) and used as an in-house reference material, with an assigned range for total Cu(II) of 10.6 to 11.2 nM, which was in good agreement with the 11.4 nM as determined by the FI-CL analyser (RSDs < 5 %). The good agreement of Cu(II) levels between the two results further validated the accuracy of the FI-CL analyser for Cu(II) in seawater.

3.4 Conclusions

This chapter reported the development of the sensitive, rigorously optimised FI-CL method for the determination of Cu(II) in seawater. The FI-CL manifold used for Cu(II) in UHP water (Chapter Two) was extensively modified to incorporate a solid phase extraction and preconcentration 8HQ micro-column, to selectively retain the Cu(II) in preference to the other seawater matrix ions that were potential interferents to the Cu(II) catalysed 1,10-phenanthroline CL reaction. The 8HQ micro-column was central to the operational success of the FI-CL analyser and was prepared by immobilising the chelating resin 8HQ on an inert Fractogel backbone. This was successfully used as a highly selective, solid phase extraction resin for Cu(II) in seawater. The 8HQ micro-column also increased the sensitivity of the FI-CL manifold by preconcentrating the Cu(II), enabling its determination in seawater at ultra trace levels. The FI-CL analyser was fully automated (Chapter 4).

The final form of the micro-column was a custom designed, machined acrylic column, which, with its linear and reproducible flow, represented a significant improvement in flow characteristics compared to the push fit column originally used. The experimental variables for both columns were rigorously optimised, with the chelating capacity of the column found to be in excess of that required for Cu(II) determination in seawater.

The new machined acrylic design of column also enabled the time for an analytical cycle to be reduced from 24 to 10.6 minutes (n=4) by removal of the column acid regeneration and UHP water rinse cycles, without any significant reduction in instrumental performance. The time saving halved the amount of eluent required, removed the requirement for the acid clean solution and reduced the amount of UHP water required. These were a considerable advantage for in-situ, field deployment with its inherent time constraints and represented real savings in cruise preparation time, reagent usage, transport and storage, all precious commodities prior to and during field deployment.

The analytical figures of merit demonstrated that the FI-CL analyser had a wide linear range for Cu(II) in seawater (0.1 to 50 nM - R^2 0.9891, 0.1 – 10 nM - R^2 0.9849). The analyser had good sensitivity enabling the determination of Cu(II) down to sub-nanomolar concentrations in open ocean waters (0.1 – 6 nM) as well as in coastal and estuarine waters (10 – 20 nM). Increased Cu(II) levels in polluted environments could be accommodated by sample dilution or a reduction in sample loading time. The FI-CL instrument exhibited good precision, RSDs typically being < 5 %.

The analyser was successfully validated by analysis of the open ocean certified reference material (CRM) NASS 5. No significant differences (*t* test, p = 0.05) were found between the NASS 5 certified Cu(II) value of 4.68 +/- 0.7 nM and typical FI-CL determinations (e.g. 4.37, 4.61 and 4.41 nM (RSDs < 5 %)). The Cu(II) concentration in an Irish Sea sample as determined by FI-CL (11.4 nM) was in good agreement with that determined by voltammetric techniques (CSV and ASV, 10.6 – 11.2 nM), further validating the FI-CL analyser. The FI-CL analyser was therefore shown to be accurate, precise, sensitive and robust and therefore suitable for field deployment to map Cu(II) levels in the worlds oceans to further the understanding of the biogeochemical cycling of Cu(II) in seawater.

Chapter Four

Automation of the FI-CL Instrumentation for the Determination of Cu(II) in Seawater

Chapter Four

4.1 Introduction

The deployment of FI-CL instrumentation for shipboard analysis requires full automation to enable reliable shipboard analyses to be performed under all sea conditions. Automation will provide improved precision; reduction in analytical time with increased sample throughput; reduction of operator error, particularly during continuous monitoring and will free up time to complete other analytical tasks. This chapter therefore describes the automation of the manually operated FI-CL instrument described in Chapter 3 and used for the determination of Cu(II) in seawater.

4.2 Experimental

4.2.1 System Requirements

The manual FI-CL instrumentation for Cu(II) in seawater comprised two Gilson Minipuls 3 peristaltic pumps for the CL reagents and sample/buffer streams and an Ismatec S820 peristaltic pump for the eluent stream. Two manual Rheodyne 6 port injection valves were used to incorporate the 8HQ matrix separation column and switch between the 8HQ column loading and regeneration cycles. An Omnifit two-way valve switched between column acid clean and UHP water rinse cycles as required. A PMT detector and a flat bed chart recorder completed the system. Manifold automation required the automation of one of the 6 port valves using an Anachem switching unit and the substitution of the other by solution switching valves. The same valves were also incorporated into the manifold to switch between the sample and standard additions. Each of these components was PC controlled using a Quick Basic software program developed for this study. The hardware consisted of a desktop PC (486 DX 66, Viglen) with an analogue to digital (A/D) converter card. A block diagram illustrating the automation of the components and solution streams of the FI-CL manifold for Cu(II) (Chapters 2 and 3) is shown in Figure 4.1.

4.2.2 PC Interface Card

The FI-CL manifold was controlled by a 12 bit analogue to digital (A/D) interface card (Brainboxes®, model AD 1210). The technical specifications of the AD 1210 card are given in Table 4.1, with the card to the ribbon cable connections shown in Figure 4.2. The card was

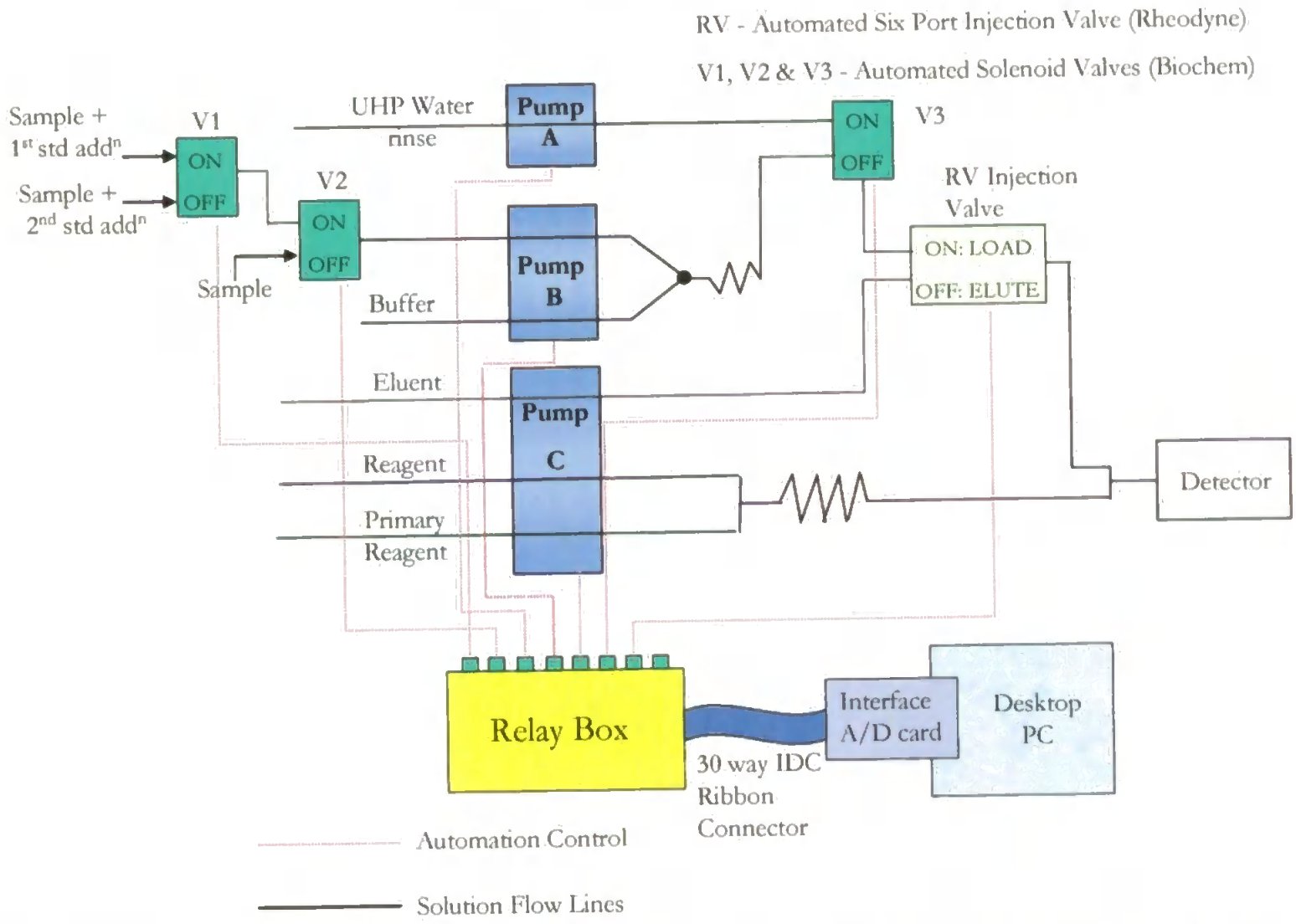

Figure 4.1 Schematic of the Automated FI-CL Manifold for the Determination of Cu(II) in Seawater. Reagent/sample flow lines are shown in black. Control lines for automation of components are shown in red dashed lines.

Table 4.1 A/D AD 1210 Card Technical Specifications Brainboxes®

Component	AD 1210
Analog Input	12 bit
Channels Type (jumper selectable)	16 single ended OR 8 differential of 16 pseudo differential
Channel select	Programmable
Bipolar Input	± 5V, ± 2.5 V
Unipolar Input	0 – 10 V, 0 – 5 V
Programmable Gain (low level)	1 – 10 – 100 - 1000
Throughput (single channel)	100 kHz
Analog Output	Two 12 bit DACs
Bipolar Output	- 10 to + 10 V, - 5 V to + 5 V, - 2.5 V to + 2.5 V
Unipolar Output	0 – 10 V, 0 – 5 V
Throughput	100 kHz per DAC
Digital I/O	
TTL output	8 bit
TTL input	8 bit
Throughput	1 MHz
Timing	
Pacer Clock	0.005 Hz – 600 kHz
External clock	YES (to 1 mHz)
External Trigger	YES (-ve edge)
8254 counter	Yes
Interrupt	A/D done
DMA capabilities	None
FIFO chip	No

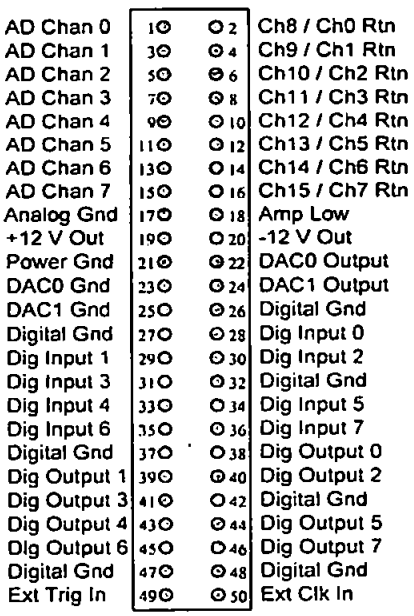

Figure 4.2 Pinout Connections from the AD 1210 Card

installed in a desktop PC (Viglen 486 DX-66). The A/D card received commands from the software program and then supplied TTL (5 V) signals to a converter/relay box, which subsequently supplied TTL, 12 and 240 V signals as required to drive the automated components of the manifold. A standard 30 way IDC ribbon cable was used to directly connect the A/D 1210 interface card in the PC to a terminal output at the rear of the PC with a second 30 way ribbon cable connecting the terminal output to the relay box.

4.2.3 Relay Box

The output from the A/D card provided 8 lines of TTL output (5 V), each of which was used to control a component of the FI-CL system. Due to the power requirements of the automation components, the TTL (5 V) card outputs were fed into a relay box that had the external configuration shown in Figure 4.3 (front panel) and Figure 4.4 (rear panel).

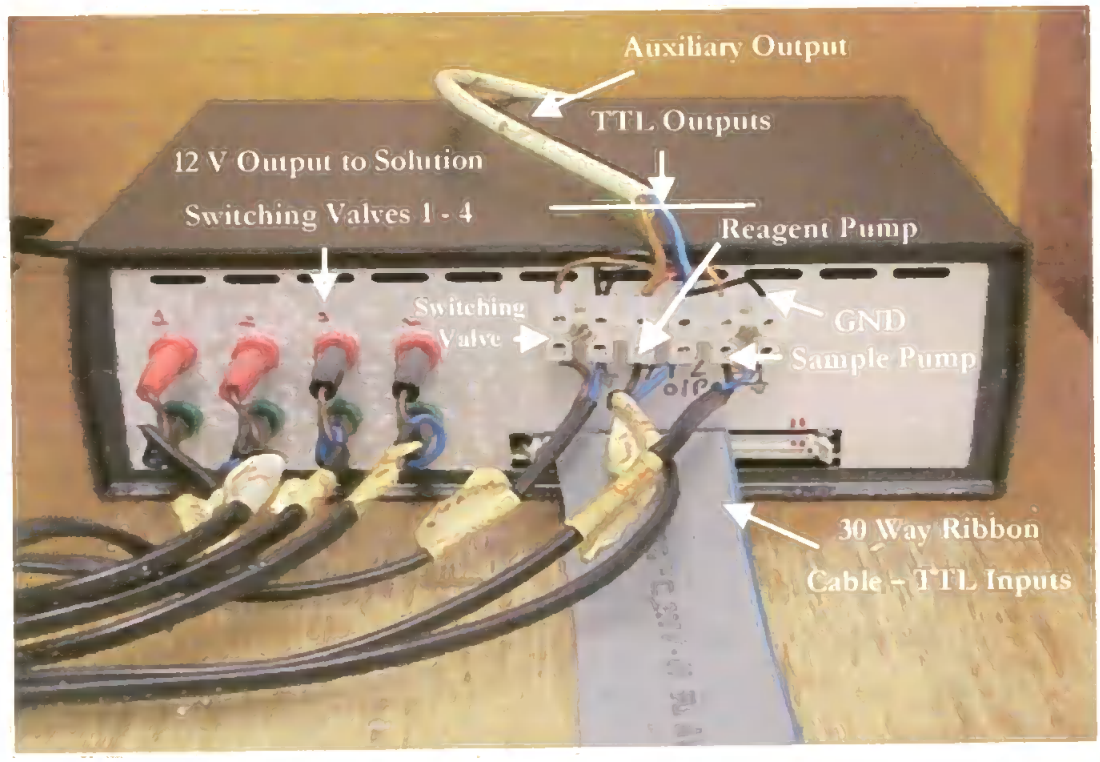

Figure 4.3 Front Panel of Relay Box - Input and Output Connections

The relay box was constructed in-house and included an integrated circuit of four Darlington pair transistors (TIP 141) (Figure 4.5).

Figure 4.4 Rear Panel of Relay Box - Input and Output Connections

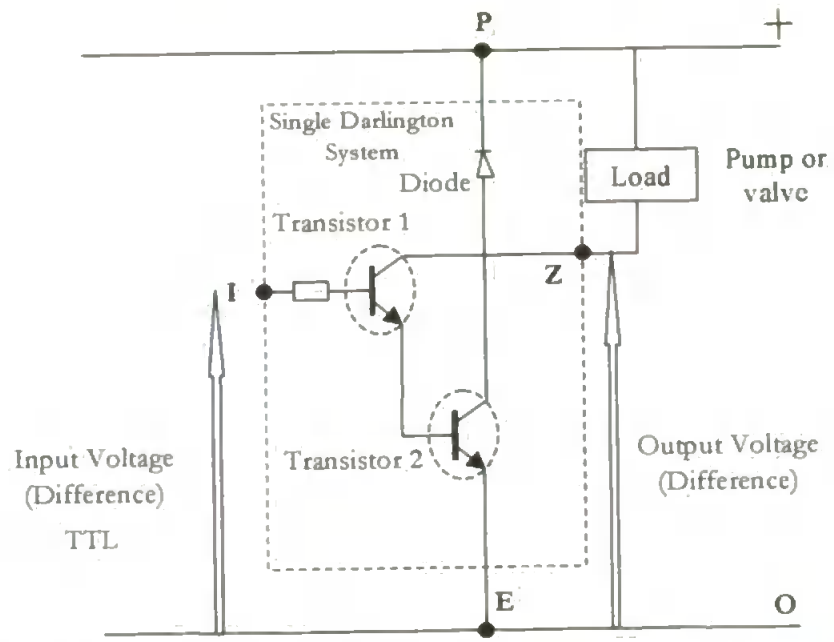

Figure 4.5 A Schematic of a Single Darlinton Pair System - used to regulate the currents utilised during the step up conversion of 5V TTL signals to 12 and 240 V outputs (I = input; Z = output; P = positive; E = earth).

Within the automation design, the TTL lines on the DAQ card were used to control the Gilson Minipuls 3 reagent and sample/buffer pumps and the Anachem auto switching valve. The three 3-way solenoid valves, the Ismatec S820 pump and the flat bed chart recorder were not TTL compatible. Therefore, the TTL lines from the DAQ card were used to switch a

12 V signal to control the three 3-way solution valves, and to switch 240 V to control the Ismatec S820 pump and the flat bed chart recorder. The signals for each automated component, with its individual hexadecimal code notation (0, 2, 4, 8, 16, 32, 64, 128, and 256) are described in Table 4.2.

Table 4.2 Signals Used for Automation of FI-CL Components

PC	Component	Model	Input signal	Hexadecimal code
TTL signals (5 V)	Injection valve	Rheodyne 5020 via Universal Switching Module (Anachem)	TTL direct (0 = Column Elute 1 = Column Load)	2 - Switch valve position
	Peristaltic pumps	a) Gilson Minipuls 3 b) Ismatec Mini S 820	a) TTL direct b) 240 V mains	4 - Sample/Buffer OFF 8 - Reagent OFF
TTL (5V) to relay Box	3 way solution switching valves	Biochem Valve™ Inc series 075T3-MP-12-32	12 V from relay box	16 - Valve 1 ON 32 - Valve 2 ON 64 - Valve 3 ON 128 - Valve 4 ON

NB – Remaining hexadecimal code 0 not used, 256 – no power

To minimise the effect of power spikes, which can be common during shipboard analysis, an electronic smoothing circuit (RS In Line Filter Module, MAO5/1/2) was inserted into the common power feed to the FI-CL instrumentation. A second smoothing circuit (RS In Line Filter Module, MAO5/1/2) was inserted into the power line of the chart recorder to further reduce the risk of erroneous spikes on the recorder trace.

4.2.4 Solenoid Switching Valves

Automated switching of solutions streams was accomplished by 3-way solenoid valves (Biochem Valve™ Inc, series 075T3-MP-12-32, Figure 4.6). The wetted parts were machined from a PTFE block to prevent trace metal contamination. The Biochem valves utilised a 12 V DC signal to switch each from the rest position (normally open), although they were subsequently held in position (normally closed) by a reduced voltage (5 V) to prevent the solenoid overloading.

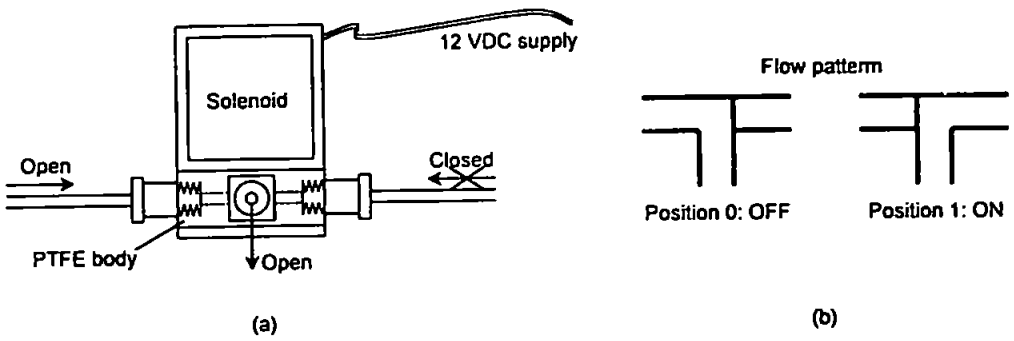

Figure 4.6 Biochem Valve™ Switching Valves (Biochem Valve™ Inc series 075T3-MP-12-32)

4.2.5 Software

4.2.5.1 Driver Files

In order to integrate the Quick BASIC code into the software routines, three files located in the Quick BASIC sub-directory were used.

- AD1200Q.QLB - This was a Quick Library file which enabled access to the to the range of Quanta driver routines contained in the Quick BASIC environment.
- AD1200Q.LIB - This was a Quanta Medium Model Library that provided calling conventions suitable for Quick BASIC, that contained the Quanta Driver routines that were used to compile the stand alone EXE.files and the DOS command line.
- AD1200.INC - This was an include file that provided the on-line HELP facility and for each of the Quanta routines contained in the AD1200Q.QLB and AD1200Q.LIB libraries, defined their syntax and parameters.

4.2.5.2 Compilation

The automation programs were compiled and validated within the Quick BASIC environment. The following syntax was included in the command line to enable use of the Quanta software driver when Quick BASIC was loaded;

- QB ANANLY1 / AD1210Q.QLB

At the start of each BASIC program compiled, a meta command was included for the AD1210 include library definitions.

- REM$INCLUDE:'AD1210.INC

Utilising the pull-down Run menu and BAS code, stand-alone .EXE programs were created within the Quick Basic Environment. During the compilation when utilising Quick BASIC, the

BC command line compiler is invoked. The output from this compiler has to be linked to the routines in the AD1210Q.LIB library.

4.2.5.3 Automation Programs

The operating code for the PC AD1210 card was written in Microsoft™ Quick BASIC, version 4.5 with the software routines run in a Microsoft Windows 3.1 environment. A sample program, "Quanta", included with the AD 1210 card supplied by Brainboxes®, formed the basis for the Quick BASIC code used to generate the TTL signals that drove the automation of the FI-CL manifold. The individual routines written were refined into seven programs that each controlled a specific sequence of operations (Table 4.3) of the FI-CL manifold and were icon driven from a Cu(II)-FI-CL operating window (Figure 4.7).

Table 4.3 Software Programs used to Automate the FI-CL Manifold

Operation Name	Description	Execution Filename
ANALTEST	Basic system test program - 10 s test of each automated component	ANALTEST.exe
ANAL3TEST	All operations ON for 10 s	ANALTEST3.exe
INSTRCLE	Cleaning sequence for FI-CL manifold	INSTRCLE.exe
ANY2SAMP	Seawater analytical sequence (n=4) without standard additions. 90 s column loading with UHP WATER column equilibration after elution, without column regeneration. Reagents switched ON/OFF	ANY2SAMP.exe
ANALY1	Seawater analytical sequence (n=4) with two standard additions. 60 s column loading. Column UHP WATER wash (20 s) only after elution.	ANALY1.exe
ANALY2	Seawater analytical sequence (n=4) with two standard additions. 90 s column loading, with column regeneration. Reagents switched ON/OFF	ANALY2.exe
ANYSTDAD	Seawater analytical sequence (n=4) with two standard additions. 90 s column loading without column regeneration or eqilibration. Reagents switched ON/OFF	ANYSTDAD.exe

Figure 4.7 PC Operating Screen Showing the Cu-FI-CL Operating Icons

Individual programs were required to develop the automation of the Cu(II) analytical cycle. The ANALTEST program was used to test the automated operation of each individual component of the FI-CL instrumentation, the hexadecimal code being changed as required for individual components. The ANAL3TEST program ran a full analytical cycle (n=1) without any standard additions, with each component ON for 10 s. The INSTRCLE program was used to acid clean (0.2 M HCl) and UHP water rinse the manifold at the cessation of analysis or if contamination of the manifold was present. The ANY2SAMP program was used to run a seawater analytical cycle (n=4) utilising a 90 s column loading time without any standard additions or column regeneration stage, but incorporating equilibration with UHP water after column elution. ANALY1 analysed a seawater sample as in ANY2SAMP but with a 60 s loading cycle and a 20 s UHP water rinse after elution (Chapter 3), whilst ANALY2 reverted to a 90 s sample loading with a full column regeneration cycle (60 s acid clean, 60 s UHP WATER equilibration cycle) with the reagents switched on as required 20 s prior to elution to minimise reagent use. ANYSTDAD analysed a sample including two standard additions as with ANALY 2 but without the column regeneration or equilibration cycles.

4.2.6 System Operation

The logic state of the automated components of the FI-CL manifold is shown in Figure 4.8 which represents the OFF (power off) or ON (power supplied) state of each component. For the solution switching Biochem™ valves, the flow pattern consisted of flow to a common outlet port from either the normally open inlet port (valve OFF position) or the normally closed inlet port (valve ON position) (Figure 4.6 b). The Anachem injection valve was in the column load position (ON) and switched to the reverse elution position in the OFF position.

4.2.7 Tamar Field Deployment

In order to validate the FI-CL instrumentation prior to oceanic deployment on an extended Atlantic Ocean cruise (AMT 9; see Chapter 5), it was deployed on local field trials to determine Cu(II) in the Tamar Estuary (Figure 4.11). These were undertaken on the research ship the 'John Dori' utilised for local coastal and estuarine studies, supplied by the University of Plymouth, and the 'Tamaris' used for estuarine and river research due to its shallow draft, supplied by Plymouth Marine Laboratorty (PML).

All samples were collected and analysed utilising trace metal clean protocols (see Chapters 3 and 5). Samples were acidified (pH 2, Q-HNO_3) and operationally defined by vacuum filtration (0.4 μm, Nuclepore, acid cleaned) utilising a Nalgene filtration unit (acid cleaned). A Perspex® cube (Figure 5.6) with double-bagged closed reagent and sample containers provided a clean environment in the absence of a clean room or portable laminar flow hood. A calibration utilising an open ocean Atlantic seawater (AMT 3) sample was performed onboard. Copper(II) levels were also determined in an unacidified and acidified (Q-HNO_3) Tamar Estuary sample in order to investigate the effect of acidification on the organically complexed copper. This unacidified sample was analysed onboard as soon as possible in order to minimise particle exchange and biological processes that can alter the concentration of Cu(II) in seawater. The ability to perform shipboard analysis with the FI-CL instrumentation made this possible. The method of standard additions was used for all seawater analysis in this study in order to eliminate the effect of changes in calibration sensitivity resulting from differences in the sample matrix as occurs in the Tamar Estuary.

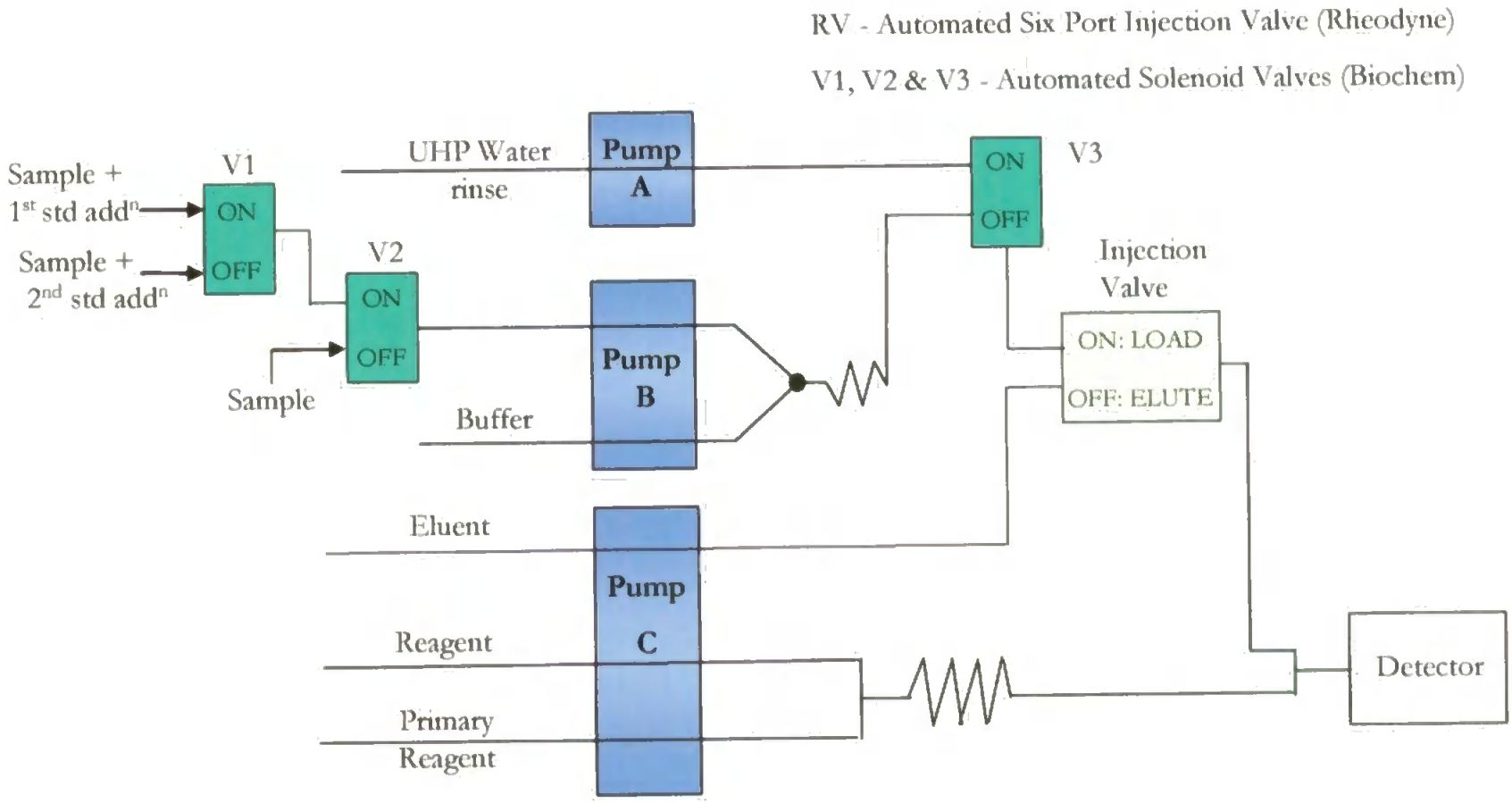

Figure 4.8 Logic State of Components During an Analytical Cycle. std addn – standard addition

4.3 Results and Discussion

4.3.1 Philosophy of Automation

The automation of FI-CL analytical instrumentation for Cu(II) could have taken one of two forms, namely using a text-based programming language such as Quick BASIC or Pascal or via a graphical programming approach utilising LabVIEW. The former is the more traditional route, although it does require a degree of programming skills to compile and modify the lines of program code, including the diagnostic routine for the data acquisition card (DAC) in the PC. The source code written in Quick BASIC enables the PC to control the instrumentation via the DAC card. This acts as an interface, supplying TTL signals (5 V, 1 mA) to the output. The low power of the TTL signals makes them unsuitable to drive the automated components directly. A relay-box controlled by the TTL signals is therefore required, from which sufficient power can be drawn (5, 12 or 240 V) to drive the automated instrumentation.

LabVIEW is a more contemporary approach, in which programs are created in block diagram form using the graphical programming language G. The programs are known as virtual instruments (VI) that often contain many sub-routines (sub-VIs), which are analogous to the lines of source code as found in a Quick BASIC program. Both approaches contain a set of libraries and examples for all simple tasks. LabVIEW requires a set of specialised virtual protocols to be written and requires relatively expensive hardware and software. Therefore, it was decided to use the traditional Quick BASIC approach to automation for this study.

4.3.2 Automation Programs

The automation programs written in the Quick BASIC environment were highly adaptable. The associated timings for each automated component with their individual hexadecimal codes for one analytical cycle are shown in Figure 4.9. The fully annotated Quick Basic code for this program including replicate injections is shown in Appendix A. By alteration of key lines of program source code it was possible to incorporate changes in the analytical cycle to enhance the analytical performance of the FI-CL instrumentation. For example, changing the hexadecimal code that designated the component(s) to be powered up enabled control of the individual phases of the analytical cycle. Alteration to the line of code that designates the time ON enabled control of the duration of operation

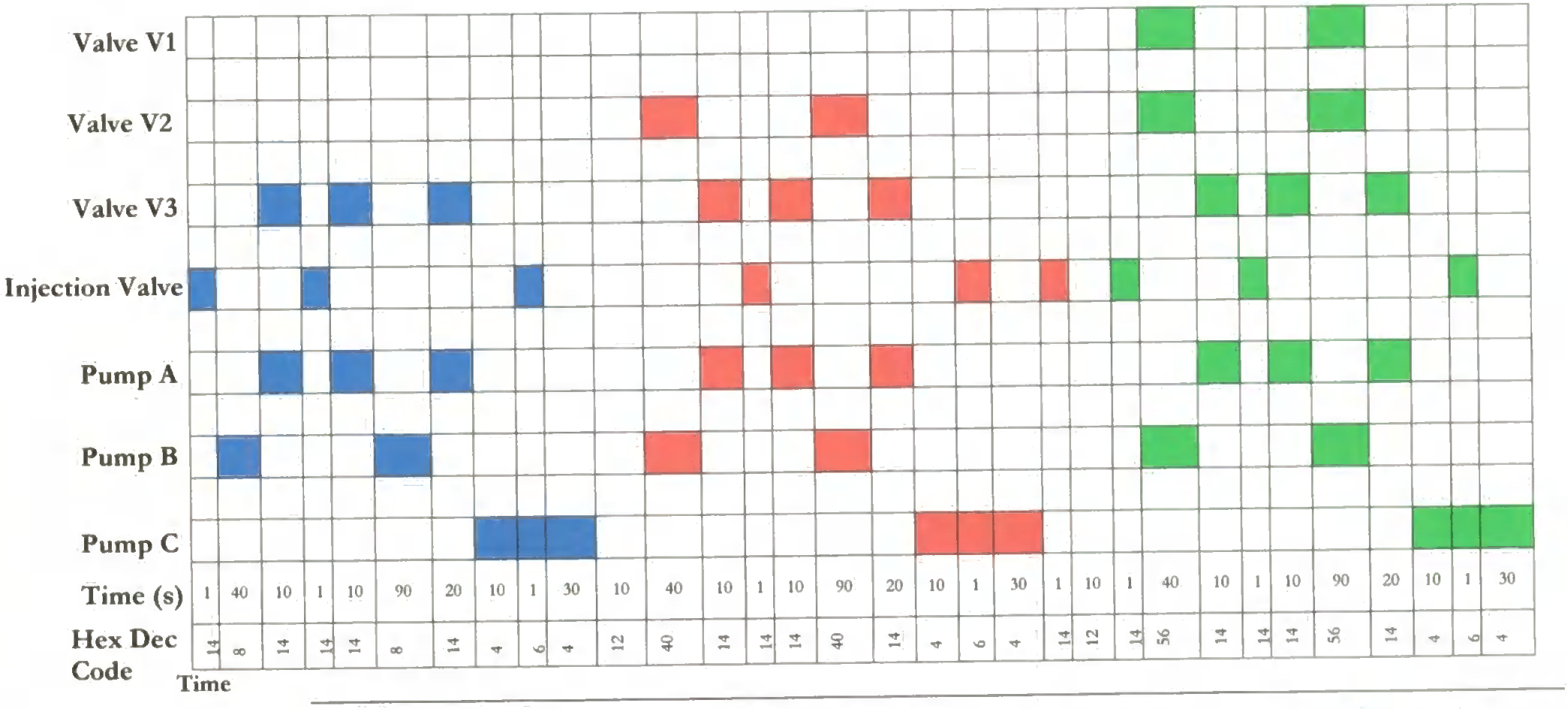

Figure 4.9 Timing Sequence for One Analytical Cycle of the FI-CL Manifold. Single Injection Sequence Shown for Sample ( ), First Standard Addition ( ), Second Standard Addition, ( ). Replicate Injections Not Shown.

of that component. Furthermore, the insertion of the REM or ' command at the beginning of a line of program code rendered that line inoperative, allowing removal of phases of the analytical cycle.

The ability to fine-tune the programs in association with the introduction of the machined acrylic column (Sections 3.2.3.2 and 3.3.1), enabled the removal of the mini-column regeneration phase (acid clean and UHP water equilibration cycles). This sequence was originally put in place after column elution, when the push fit mini-columns were originally incorporated into the manifold. The principal aim of this program alteration was to reduce the total analytical cycle time by shortening or removing these two stages and the results are shown in Table 4.4.

Table 4.4 Modification of Automation Software Program

Expt No	UHP Rinse post Loading	Acid Clean	UHP Rinse	Signal (mV)	RSD (%)
1	60	60	60	4.1	9.8
2	30	60	60	3.9	6.5
3	30	0	60	3.7	1.5
4	30	0	0	3.8	2.6

Whereas the CL signal was not significantly affected by the removal of the column regeneration cycles, the time for a single injection was reduced from 6 to 2.6 min and thus the time for 4 replicate injections (n=4) fell from 24 to 10.4 min. Therefore, the time for a full analytical protocol, including sample exchange and column and line rinsing phases prior to sample analysis, (including a two point standard addition), was significantly reduced from 75 to 35 min. This more than doubled the frequency of sample analysis. The ability to modify the automation programs also offered other advantages. For example, reduction of the column loading time enabled the determination of Cu(II) at concentrations in excess of the linear range, whereas increasing the sample loading time would increase the sensitivity of the manifold. For this study these modifications were not implemented since the sensitivity of the optimised FI-CL instrument was appropriate for the determination of Cu(II) in seawater (0.1 – 6 nM, Coale and Bruland, 1988). However, in other situations such as an estuarine flux study, where the concentrations of Cu(II) can be considerably higher and more variable, these modifications would be particularly useful.

The FI-CL manifold without a separate column equilibration stage resulted in a simpler and more efficient manifold. These improvements were a significant benefit during field deployment with its inherent time constraints. The time saving also halved the amount

of eluent required by reduction of the elution time to 30 s, removed altogether the requirement for the acid clean solution and reduced the amount of UHP water required. These represent real savings in cruise preparation time, reagent usage, storage and transport which are all precious commodities prior to and during field deployment. These aspects clearly demonstrated the flexibility of the automation software and the adaptability of the programs written in the Quick BASIC environment.

4.3.3 Power Requirements

The power consumption of any in-situ instrumentation is an important consideration for field deployment, due to possible limitations in power or safety issues associated with high power requirements. The power consumption of the automated FI-CL instrumentation is shown in Table 4.5.

Table 4.5 Power Consumption of FI-CL Analyser for Cu(II)

Component	Power Consumption (W)
Desktop PC – computer	200
monitor	50
Pumps - Gilson Minipuls 3 (2 x 45 W)	90
Ismatec 820	2.5
Anachem Switching Valve	50
PMT Detector	50
Biochem Switching Valves (4 x 4 W)	16
Chart Recorder	2
Relay Box	Negligible
Total	**460.5**

The power consumption of the FI-CL instrumentation, including the desktop PC was low (460.5 W), enabling it to be powered by a portable Honda generator (model EX 500). This aspect was important for field deployment, for example on local e.g. Tamar and extended cruises e.g. AMT 9, due to possible limitations on power supply onboard.

4.3.4 Analytical Performance

The automation of the FI-CL instrumentation enabled the shipboard monitoring of the Tamar for Cu(II) without the operator fatigue that can lead to analytical errors as can occur with a manually operated system. This is important where samples are limited in availability, preventing the loss of the analytical data. During the Tamar study the FI-CL instrumentation was deployed twice, for 8 h. It operated reliably each time, with only minimal downtime due to changing of the push fit style of 8HQ micro-columns then in use because of compaction of the resin and leakage. This problem was not experienced with

later instrument operation due to the incorporation of the machined design of micro-column. Once the instrument had been set up, samples were collected at 4 different locations selected as representative of differing salinity conditions.

Although precision prior to automation was good with typical RSD's of 5 – 8 %, automation further improved this aspect with typical RSD's falling to ~ 3 % or less (see Table 4.4). Onboard calibrations were highly linear (Section 4.3.5) with accurate determinations of Cu(II) (Section 4.3.5.4). The sampling and analytical time was reduced due to the time required to load, secure and set up the FI-CL instrumentation and the power requirements. Analytical time was also was also restricted by the time required for stabilisation of the PMT (2 – 3 h) after the high voltage was applied. Future familiarisation with protocols reduced the set up time although the latter could not be circumvented.

In addition, neither vessel had been used for shipboard analysis at trace levels or deployed such intricate instrumentation. This highlighted the lack of reliable and adequate shipboard power for such purposes, despite the low power consumption of the FI-CL instrumentation. This necessitated careful minimisation of power used onboard for other purposes, all other personnel onboard collecting samples for shore based analysis. On the second Tamar deployment a portable Honda generator was taken onboard and, after a major strip down to overcome starting problems, successfully powered the FI-CL instrumentation, highlighting the stand alone capacity of the FI-CL analyser. A further potential problem was the lack of trace metal clean facilities onboard. This was overcome by the use of clean protocols and the incorporation of the Perspex® cube, the latter providing a self contained clean space for reagents and samples.

4.3.5 Onboard Calibration and Cu(II) in The Tamar Estuary

During the Tamar deployments, calibrations were performed using an Atlantic open ocean sample (South Atlantic Gyre, collected by Andrew Bowie on AMT 3, October 1996) to verify the shipboard performance of the FI-CL instrumentation. This sample had been acidified (pH 2, Q-HCl) but not filtered due to the low particle count found in the open ocean. This sample had been analysed for Cu(II) by FI-CL in the University of Plymouth clean room and found to be low in Cu(II) (3.7 +/- 0.22 nM) and with Cu(II) additions had been used successfully for shore based calibrations over the range 0.1 to 50 nM (R^2 0.9676). A typical onboard calibration is shown in Figure 4.10.

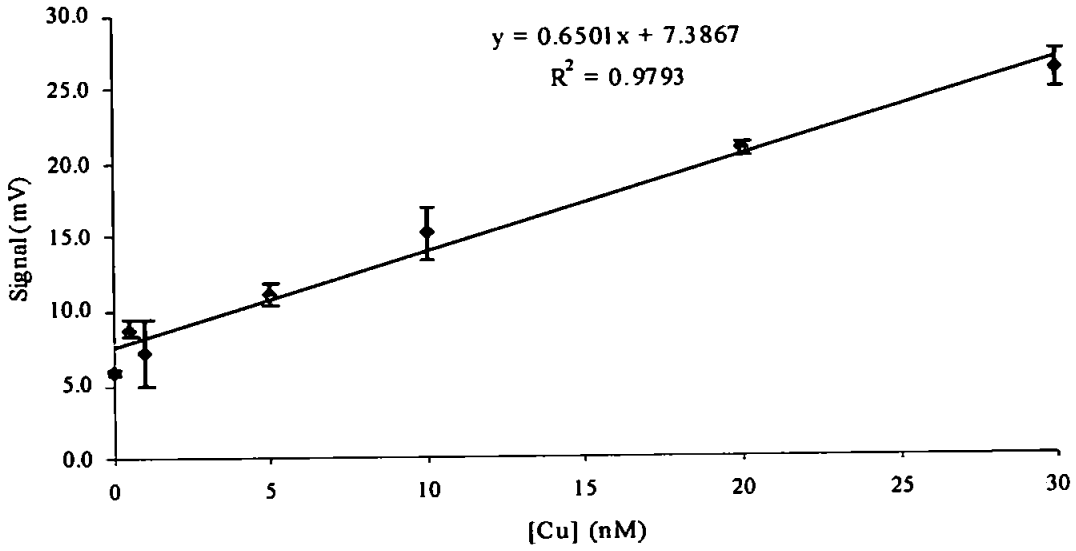

Figure 4.10 Onboard Calibration Using an Open Ocean Atlantic sample (AMT 3). Error bars are 3s.

During the shipboard calibration, the FI-CL instrumentation exhibited good sensitivity at 0.5 nM, the lowest Cu(II) addition, and a high degree of linearity (R^2 0.9793) over the Cu(II) concentration range of 0.5 to 30 nM. Reproducibility was also very good with typical RSD's of < 4 %.

4.3.5.1 Description of Tamar Estuary Field Site

Samples were collected and analysed for Cu(II) by FI-CL from the Tamar Estuary in the South West of England (Figure 4.11), a ria or flooded river system that forms part of the county boundary between Cornwall and Devon. The River Tamar flows southward for approximately 100 km, and the estuary is commonly defined as running from the seaward entrance at Plymouth Sound to the limit of the tidal incursion at Gunnislake weir, a distance of 31 km. Apart from a deep water channel (up to 40 m deep) from Plymouth Sound upstream to Torpoint, the estuary shallows progressively, especially from a point ~ 2 km above the Tamar Bridge, with typical depths being 5 m or less above chart datum. The catchment is largely rural covering approximately 1700 km^2. The Tamar experiences a variety of metal inputs from mine tailings, farming inputs, sewage treatment works effects, sedimentary regeneration and from the dockyards and urban areas towards the estuary mouth. The sampling sites in the Tamar Estuary and River Tamar represented a dynamic

Figure 4.11 Tamar Estuary and Field Deployment for the FI-CL Analyser - Sites A, B and C.

environment that had a seawater matrix composition with a variable concentration of Cu and other trace metals, a variable ionic composition, salinity and dissolved organic carbon (DOC) content. The Tamar is representative in length and characteristics of many UK estuarine systems and therefore represents a suitable local system in which to study biogeochemical processes whose trends should be also be found in other UK estuaries. The FI-CL instrumentation was deployed at the mouth of the River Tamar close to Drakes Island (Site A, Figure 4.11) which represented a seawater environment at high salinity (35) and at two other sites further upstream that represented a variable but lower salinity environment (sites B and C Figure 4.11).

4.3.5.2 Hydrography

The Tamar system is a partially mixed tidal estuary that has a dominant freshwater input from the River Tamar and collects the Rivers Tavy and Lyner enroute along with other minor tributaries. The River Tamar has a monthly average maximum flow in January of 38 $m^3 s^{-1}$ reducing to a minimum of 5 $m^3 s^{-1}$ in June (Uncles *et al.*, 1985), with an annual average of 30 $m^3 s^{-1}$ (Ackroyd *et al.*, 1986) although instantaneous flows can exceed 100 $m^3 s^{-1}$ (Morris *et al.*, 1987). The Rivers Tavy and Lyner contribute a further 30 % and 20 % of mean flow respectively, although alter the salinity by less than 2 units (Morris *et al.*, 1982). Estuarine tidal ranges vary at Devonport from 6.5 m at springs to 1.5 m at neaps, reducing to 1 – 2 m in the upper reaches. The estuary has a flushing time of approximately one week, although this can fall to one day in the lower salinity reaches (Miller, 1999). There exists a turbidity maximum zone (TMZ) at the saltwater/freshwater interface that migrates up and down the river with the tide (Millward *et al.*, 1992) and where the salinity is less than 0.5. The TMZ contains particles that are more reactive than from those up- or down-estuary due to their smaller particle size and increased specific surface area. The particles tend to originate from downstream and are relatively depleted in dissolved metals (Morris, 1986) and therefore tend to remove dissolved metals in the TMZ.

4.3.5.3 Analytical Methodology

Determination of Cu(II) in the Tamar samples was by FI-CL, with a comparative determination by voltammetry (CSV) in order to verify the analytical accuracy of the FI-CL instrument developed for this study. For the comparative study the sample was irradiated for 120 min to minimise the effect of the DOC on the voltammetric determination of Cu(II). In addition, the effect of the acidification (pH 2, Q-HNO_3) to stabilise the sample

on the organically complexed fraction of Cu, was investigated utilising the Tamar Estuary sample (salinity 35) collected close to Drakes Island (Figure 4.11, Site C). Sites A and B represented lower salinity sites further upstream in the Tamar estuary, due to the influence of freshwater from the Tamar River. The FI-CL Cu(II) data was also correlated to salinity and compared to literature values to aid a concise environmental interpretation of the observed Cu(II) concentrations.

4.3.5.4 Cu(II) Results

The Cu(II) concentrations as obtained by FI-CL and CSV are shown in Table 4.6.

Table 4.6 Concentration of Cu(II) in the Tamar Estuary by FI-CL and Voltammetry (CSV)

Tamar Site	[Cu(II)] (nM)				R^2
	FI-CL	+/-	CSV	+/-	FI-CL
A	18.1	0.9	16.2	0.9	1.000
B	18.4	0.6	18.6	0.5	0.9887
C	32.2	2.1	na		0.9989

For CSV analysis the sample was UV irradiated for 120 min to minimise the effect of DOC on the voltammetric determination. The sample from site B was analysed immediately upon return to shore, whereas the site A sample was stored in a fridge at 4 °C for two days. na – not analysed. All +/- values quoted are 3s.

The Cu(II) concentrations for samples from sites A and B as derived by FI-CL were in good agreement with Cu(II) data obtained by voltammetry (CSV). The close agreement with an established analytical technique for trace metals further validated the analytical accuracy of the FI-CL analyser The small difference between the FI-CL and voltammetric values was ascribed to storage processes e.g. particle reactivity scavenging the Cu(II), or deposition on the container walls over the storage time.

The Cu(II) concentration at site C was found to be 32.2 nM by FI-CL. The increase compared to sites A and B can be explained by the inverse correlation with salinity, this site having a salinity of 21.8, and the previously reported mid-estuary maximum for Cu(II) (van den Berg, 1991; Ackroyd *et al.*, 1986). These authors reported Cu ranges of 8 – 48 nM and 0.5 to 170 nM respectively, with the majority of observations at 7 – 60 nM Cu, and the highest Cu concentrations seen between a salinity of 1 – 10 %, commonly at a mid estuary sampling site. At site C further upstream, the salinity was reduced compared to sites B (salinity of 34.5) and A (salinity of 35.3). At the latter two sites the increased flocculation of Cu(II), that occurred upon mixing with seawater, lowered the Cu(II) concentration. The

Cu(II) concentration at site C may have been affected by the turbidity maximum as the incoming tide re-suspended the sediment, raising the suspended particulate material (SPM) content of the waters, although data for the SPM content of the samples was not available. A further factor at site C was the presence of the dockyards and the associated release of Cu from Cu based antifouling paint used to protect ships and yachts against marine growth on the immersed hull, which may have been transported upstream by the incoming tide.

Acidified (2 h equilibration) and unacidified aliquots of the Tamar sample from Site A were analysed by FI-CL for Cu(II). The acidified sample was also analysed by CSV and the results compared (Table 4.7).

Table 4.7 Cu(II) Concentrations in Unacidified and Acidified Tamar Estuary Samples by FI-CL and CSV

Sample	[Cu(II)] (nM)				R^2
	FI-CL	+/-	CSV	+/-	FI-CL
Unacidified	6.0	0.4	na		0.9523
Acidified	18.1	0.9	16.2	0.97	1

na – not analysed

The difference in Cu(II) concentrations between the unacidified and acidified aliquots was due to the acid (pH 2) digestion of the dissolved organic carbon (DOC) and the release of organically complexed Cu(II) by HNO_3, a strong oxidising acid that is more effective in oxidising DOC than HCl. The Tamar is a freshwater DOC-dominated estuary with a DOC range of 478 – 110 μM C that is consistent with the data from other riverine and coastal seawaters (Miller, 1999). The brown coloration of some Tamar tributaries testified to the DOC content derived from peat bogs and other organic sources in the Tamar catchment. During tidal cycles the DOC concentration has been reported as showing conservative behaviour with respect to salinity with an inverse correlation to turbidity (Miller, 1999). The DOC complexes up to 99 % of Cu in seawater (Buckley and van den Berg, 1986; Sunda and Huntsman, 1991) and therefore the difference in Cu(II) concentrations between the unacidified and acidified sample aliquots was attributed to the release of a fraction of the organically bound copper.

4.4 Conclusions

The manually operated FI-CL manifold was successfully automated resulting in a reliable, robust FI-CL instrument. This was accomplished using a commercially available

analogue to digital interface card (AD 1210) installed in a desktop PC, a transformer/relay box designed and constructed in house, three 3-way solenoid valves and an automated switching valve. Software programs were compiled in a Quick BASIC environment to drive the automation. The ability to modifiy key lines of source code enabled analytical protocols to be altered, increasing the flexibility of the instrument. For example during instrument development the time required prior to automation for one analytical cycle was almost halved, significantly increasing sampling frequency, an important consideration during field deployment as well as reducing reagent consumption. The ability to modify the loading time would also facilitate the determination of Cu(II) in waters that contained concentrations of Cu(II) outside of the linear range, enabling a wide range of Cu(II) concentrations in seawater to be determined.

Automation minimised operator error due to fatigue during sample analysis, freeing up time to complete other analytical tasks such as sample preparation prior to analysis. The FI-CL analyser demonstrated robustness and reliability as well as good analytical performance throughout the field trials in the Tamar Estuary. Onboard calibrations were highly linear, with shipboard Cu(II) determinations being in good agreement with those derived by shore based voltammetry (CSV). This validated the accuracy of the FI-CL instrumentation. The precision, which was already good for the manual system, was further improved by automation, with typical RSD's falling to < 3 %.

Instrument automation was achieved using many 'off the shelf' components e.g. the BrainBox DAQ card and the Biochem™ solution switching valves. The automated FI-CL instrument performed well for long periods (8 - 14 hrs a day for several weeks) without any reduction in performance, even under demanding sea conditions. Such conditions were experienced during the Tamar Estuary deployment when the FI-CL instrumentation was strapped on the open deck, with rough seas rolling the boat. Further extreme conditions were experienced during the AMT 9 research cruise (Chapter 5) during severe weather (two force 9 severe gales and storm force 10) at the outset of the cruise. The reliability and robustness of the automated FI-CL instrumentation is an important aspect when on research cruises, enabling continuous shipboard aquisition of near real time Cu(II) data and the ability to modify the protocols according to the observed data. This ensures that the considerable amount of pre-cruise preparation, the opportunity for collection of scientific data during the limited onboard research time and the financial investment were not lost.

The FI-CL results presented in this chapter clearly demonstrates the flexibility of the FI-CL instrumentation and the successful field deployment of the FI-CL analyser for shipboard Cu(II) determinations with minimal support. The automation of the FI-CL

instrumentation clearly aided the successful achievement of the research objectives as set out in the Introduction (Section 1.9).

Chapter Five

Deployment of FI-CL Analyser on Atlantic Meridional Transect 9

Chapter 5

5.1 Introduction

5.1.1 Overview

This chapter describes the shipboard validation of the flow injection chemiluminescence (FI-CL) instrumentation (Chapters 2, 3 and 4), on the Atlantic Meridional Transect 9 (AMT 9) research cruise, that spanned 50 ^{o}N to 50 ^{o}S and NE to SW through the Atlantic Ocean. Seawater samples were collected by daily CTD casts through the upper water column (0 to 250 m) at a number of strategic stations along the transect to create a comprehensive Atlantic data set for Cu(II). This enabled surface distributions and vertical profiles for Cu(II) as determined by FI-CL to be correlated with onboard hydrographic data, namely macro-nutrients (NO_3^-, NO_2^-, PO_4^{3-} and $Si(OH)_4$), temperature, salinity, chlorophyll *a* and irradiance, in order to characterise the different water masses. This also enabled the investigation of the biogeochemical cycling of Cu(II) through the upper water column (0 – 250 m), including biogenic and lithogenic processes and the fingerprinting of input mechanisms.

5.1.2 Atlantic Ocean

The Atlantic Ocean (Figure 5.1) lies between Western Europe, Africa, the Americas, the Arctic and Southern Oceans and covers an area of 81,500,000 km^2. It is relatively shallow (mean depth of 3,310 m), is divided east to west by the mid-Atlantic ridge which runs from the North Atlantic to the South Atlantic. Either side of the ridge lie the Eastern and Western Atlantic Troughs, which form elongated, deeper water sections (~5000 m), that are further divided into basins by transverse ridges. These consist of several semi-isolated areas, which receive water and sediment from riverine sources, and have large areas that are subject to significant aerosol deposition. A mixture of water masses and internal circulatory patterns can be found in the Atlantic (Pickard and Emery, 1990), an overview of which is presented in Section 5.3.3.1.

5.1.3 Atlantic Meridional Transect

5.1.3.1 Rationale and Objectives

Originally conceived by Plymouth Marine Laboratory (PML), the Atlantic Meridional Transect 9 (AMT 9, Robins and Aiken, 1996) oceanographic research programme was operated in collaboration with the University of Plymouth (UoP) and Southampton Oceanography Centre (SOC). To date all but one of the AMT research

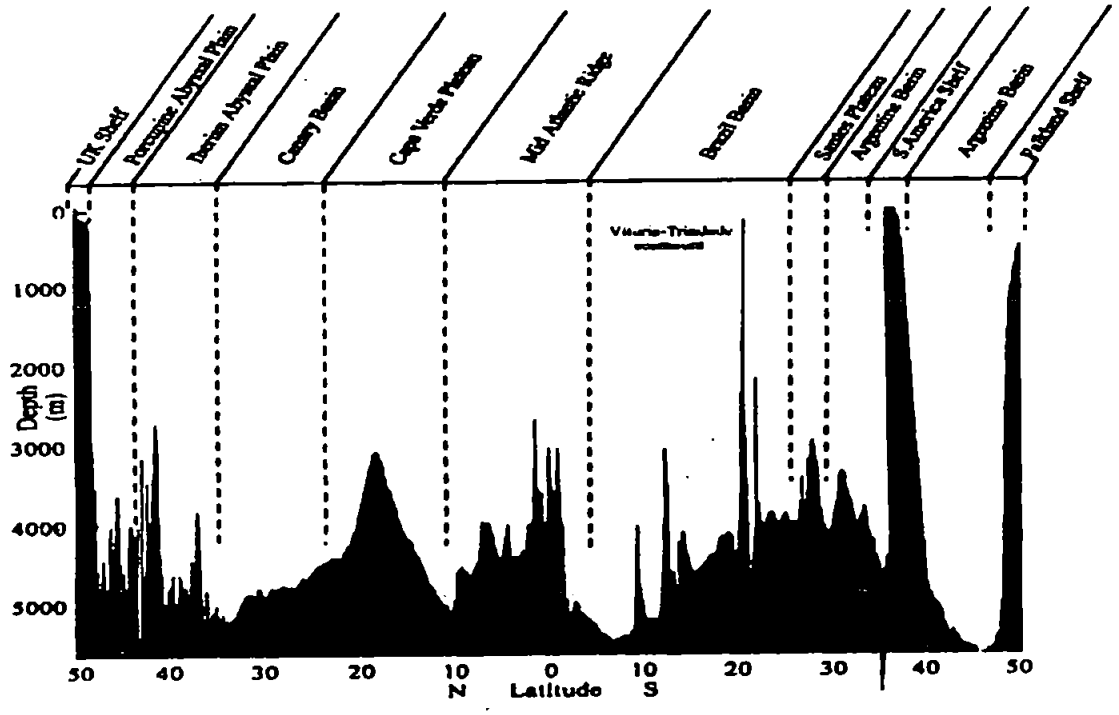

Figure 5.1 Atlantic Basin Bottom Topography Based on Typical AMT Transect (Aiken *et al.*, 2000)

cruises have utilised the passage of the British Antarctic Survey (BAS) operated NERC vessel, the *Royal Research Ship,* (RRS) *James Clark Ross* (JCR) enroute to re-supply Antarctic BAS bases and conduct marine research during the austral summer. Funding from the NERC Centre for Coastal and Marine Science (CCMS), NASA for SEAwifs validation (sea viewing Wide Field of view Scanner) and University of Plymouth (UoP) supported scientific objectives and enabled additional ship time to be purchased for course deviations and station work.

The core scientific objectives of the AMT programme form a holistic strategy to acquire a series of oceanographic, biological, chemical and optical data over broad spatial and temporal scales. More specifically, the objectives were to calibrate remotely sensed (satellite) measurements (primary validation) (NASA SeaWifs and NASDA ADEOS/OCTS programmes), secondary validation of remotely sensed products (e.g. chlorophyll levels) and the development of models to interpret satellite imagery in terms of total water column properties. Further core objectives were to evaluate basin scale remote sensing observations, interpret the interaction between physical processes and biological production and to identify, define and quantify latitudinal changes in biogeochemical provinces. Additional aims were to characterise phytoplankton community structure and photosynthetic parameters, to identify nutrient regimes and their role in biogeochemical cycles and to relate partial pressure of CO_2 in surface waters with biological production.

The AMT programme will enhance our understanding of biogeochemical processes, biogenic gas exchange, air sea exchanges, the role of the world's oceans in global carbon cycles and plankton community structure over latitudinal scales in order to predict the effects on and responses of oceanic ecosystems to climatic change. The AMT programme also contributes to the implementation of Sensor Intercomparison and Merger for Biological Interdisciplinary Ocean Studies (SIMBIOS), a programme to develop a methodology and operational capability to combine data from the various oceanic satellite missions. A longer-term aim is to contribute to the modelling of the global (basin scale) primary production and to ecosystem dynamics models.

The AMT 9 transect traversed a range of ecosystems and physio-chemical regimes from 50 ^{o}N to 52 ^{o}S, (~ 13,500 km). The track crossed the UK continental margin, the Porcupine and Iberian Plain, the Canary basins, and the Cape Verde plateau in the N.E. Atlantic and the Brazil basin, Argentine Basin and the South American Continental Margin in the SW Atlantic (Aiken *et al.*, 2000). Environmental conditions varied from sub-polar to tropical and from eutrophic shelf seas and upwelling zones to oligotrophic mid-ocean gyres. The outgoing passage from the UK (September 1999) surveyed the North Atlantic during the boreal fall and the South Atlantic during the austral spring (BFAS cruises). The return passage (April) surveyed the South Atlantic during the austral fall and spring in the Northern Hemisphere (AFBS cruises).

Commissioned in May 1991, the JCR (Figure 5.2) is a 90 m long, fully equipped multi-role vessel, purposely designed for long term operation (55 days) in Antarctic waters. It provided an ideal research platform to validate the FI-CL instrumentation and map Cu(II) levels, in conjunction with the ongoing research into the oceanographic responses of distinct ecosystems and coupled marine atmosphere to natural and forced environmental change. A berth was obtained on AMT 9 (September 1999), a southbound cruise that finished at Montevideo, Uruguay.

5.1.3.2 AMT 9 Cruise Track

AMT 9 left Grimsby on 15th September 1999 (0900), stopping at Portsmouth (16th September) to load aviation fuel, steering a course upon departure from Portsmouth (17th September, 1200) to arrive at 47 ^{o}N 20 ^{o}W, a Joint Global Ocean Flux Study (JGOFS) time series station. Unfortunately, due to a storm force 10 and two violent gales (force 9), a

Figure 5.2 RRS James Clark Ross on Station. The CTD was deployed from the remotely operated arm seen on the port side of the vessel.

more south-westerly course was required and the JCR reached 20 °W at 45.57 °N. The vessel then steamed due south along the 20 °W longitude, sampling parallel to the Spanish and African coasts and the periphery of the Mauritanian upwelling. At 13 °N 20 °W (29th September, 0248 GMT) the JCR altered course to south-southwest toward South America, shaping a course to run parallel to its east coast. The ship remained outside Brazilian and Uruguayan waters, arriving at a waypoint 200 nautical miles east of Montevideo, Uruguay in the R. Plate entrance on October 12th, 1999 and docking in Montevideo on October 13th (am). All core AMT hydrographic measurements were completed en-route (Figure 5.3).

5.1.3.3 Biogeochemical Oceanic Provinces

Traditional biophysical partitioning of oceans into regional ecosystems, designated here as biogeochemical provinces, has used physical, e.g. circulation, gyres, fronts and upwelling zones and biological parameters e.g. productivity, phytoplankton assemblages to define their boundaries. Longhurst *et al.*, (1995) furthered this concept by incorporating remotely sensed measurements of ocean colour and using global hydrographic data

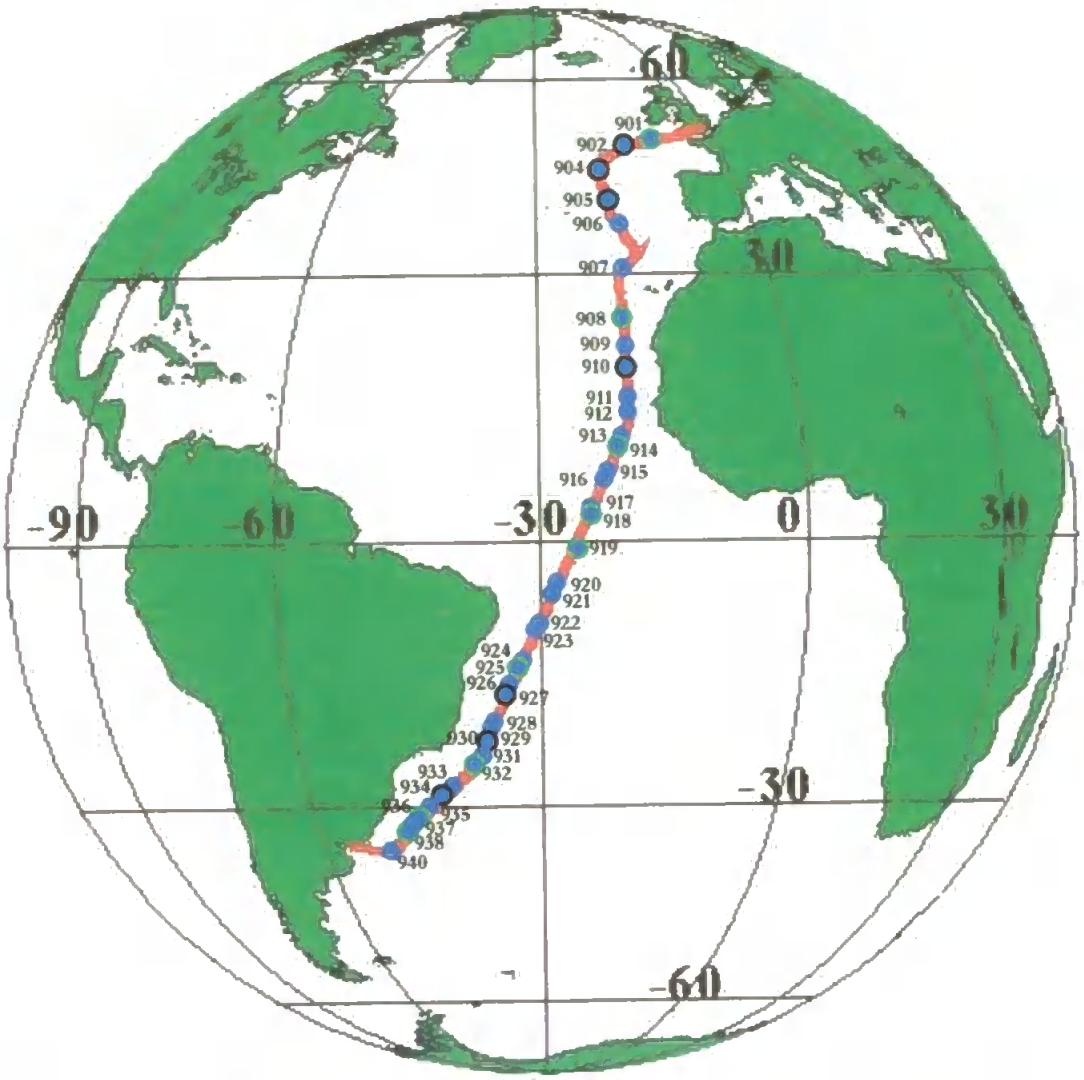

Figure 5.3 AMT 9 Cruise track with stations (Peters projection) All stations deployed CTD apart from AMT 930 and 939. ● CTD stations for surface and vertical Cu(II) profiles. ● CTD stations for vertical Cu(II) profiles only.

(emphasising biogeochemical aspects to evaluate basin scale productivity) and identified five main biogeochemical provinces along the AMT track (Table 5.1). The large scale smoothing required made it difficult to reproduce this methodology for smaller regions with higher resolution data.

Hooker *et al.*, (2000) identified Atlantic provinces with large-scale resolution utilising a more reproducible methodology based on near and sub-surface temperature and salinity (expressed as near surface density) during AMT 1 and 2. The province boundaries have since been validated by remotely sensed sea surface temperature (SST) coupled with

measurements of climatologically driven salinity and observations of bio-optical ocean colour (e.g. CSCZ[1], and SeaWIF[2], Figure 5.4). These are summarised in Table 1, together with a simplified classification used on AMT 3 (1996) by Bowie (1999).

Along track AMT pigment data has shown that the biological provinces are in broad agreement with the geographical boundaries (Aiken *et al.*, 2000). Each biogeochemical province represents an area of similar chemical, biological and physical oceanographic features that have discrete boundaries, distinct flora and fauna and may encompass more than one water mass. Although province boundaries can exhibit small-scale seasonal variation, province assignment for AMT 9 was in agreement with previous AMT cruises.

5.1.3.4 Copper Analytical Objectives

Cruise objectives for Cu(II) along the AMT 9 transect were;

1. To validate the FI-CL instrumentation through field deployment in contrasting coastal, shelf and open ocean waters.
2. To map Cu(II) levels utilising the FI-CL instrumentation developed for this study.
3. To investigate the distribution and vertical profile of Cu(II) through the upper water column through contrasting biogeochemical provinces via daily CTD casts.
4. To fingerprint Cu(II) inputs (e.g. wet and dry aeolian deposition, benthic regeneration, upwelling zones, frontal systems, and fluvial plumes) in conjunction with onboard hydrographic data.
5. To correlate Cu(II) levels with high resolution hydrographic and biological data to further define its biogeochemical cycling.

The cruise objectives were underpinned by the scarcity of high quality, trace metal data for the Atlantic Ocean with good temporal (seasonal) and spatial resolution. This emphasises the clear need for synoptic field studies to clarify the trace metal input and removal mechanisms to oceanic surface waters (0 – 250 m), which have commonly only

---

[1] Coastal Zone Color Scanner; http://daac.gsfc.gov/data/dataset/CZCS/

[2] Seaviewing Wide Field-of-View Sensor; http://daac.gsfc.gov/data/dataset/SeaWifs/

Table 5.1 Summary of Biogeochemical Provinces Encountered on AMT 9

Hooker *et al.*(2000)		Longhurst *et al.* (1995)		Bowie (PhD Thesis 1999)	
Oceanic Province	Latitude	Oceanic Province	Latitude	Oceanic Province	Latitude
EU Continental Shelf Water	ECSW 50°–47.5 °N	N. Atlantic Drift	NADR, 60°-40 °N	S.W Approaches - Continental Shelf	SWApp 50°-47 °N
N. Atlantic Drift	NAtD 47.5°-37 °N				
N. Atlantic Subtropical Gyre –East (NASEa)	NASE 37°–26.7° N (35 ° –26.7° N)	N.Atlantic Subtropical Gyre	NAST, 40° – 25 °N	N.E. Atlantic Oligotrophic Gyre - Open Ocean gyre	NEAOG 43°-24 °N
Canary Current	CanC –26.7°–20.5 °N	N. Atlantic Tropical Gyre	NATR, 25° – 10 °N	N.W Africa Upwelling -Open Ocean Upwelling	NWAUp 20 °N
Canary Current Upwelling	CCUp 20.5°–15.7° N				
North Equatorial Current	NEqC 15.7°–12.4 °N			S. of Upwelling/N of Equator – North Equatorial region	Sup/Neq 17° N - 3 °S
Guinea Dome	GDom 12.4°–7.9 °N				
North Equatorial Counter Current	NECC 7.9°-1 °N	Western Tropical Atlantic	WTRA, 10° N – 5 °S	Equator –Equatorial upwelling	Eq 2° N – 3 °S
South Equatorial Current (SeqCa)	SeqC 1° N–14.6 °S (SeqCa 7° S–14.6 °S)	S. Atlantic Tropical Gyre	SATL, 5° – 40 °S	South Atlantic Oligotrophic Gyre	SAOG 6° S – 30 °S
S. Atlantic Tropical Gyre (SATGa)	SATG 14.6° – 30 °S (SATGa 14.6°- 26 °S)				
Brazil Current	BraC 30° – 35° S			Brazilian and Falklands Currents Confluence –SW Atlantic mixing zone	BFCC 32° S – 48 °S
S. American Shelf	SASh 35°- 39.6 °S				

Sub provinces in parenthesis e.g. (NASEa) represent regions within the principal designated hydrographic boundaries with a distinct pigment signature.

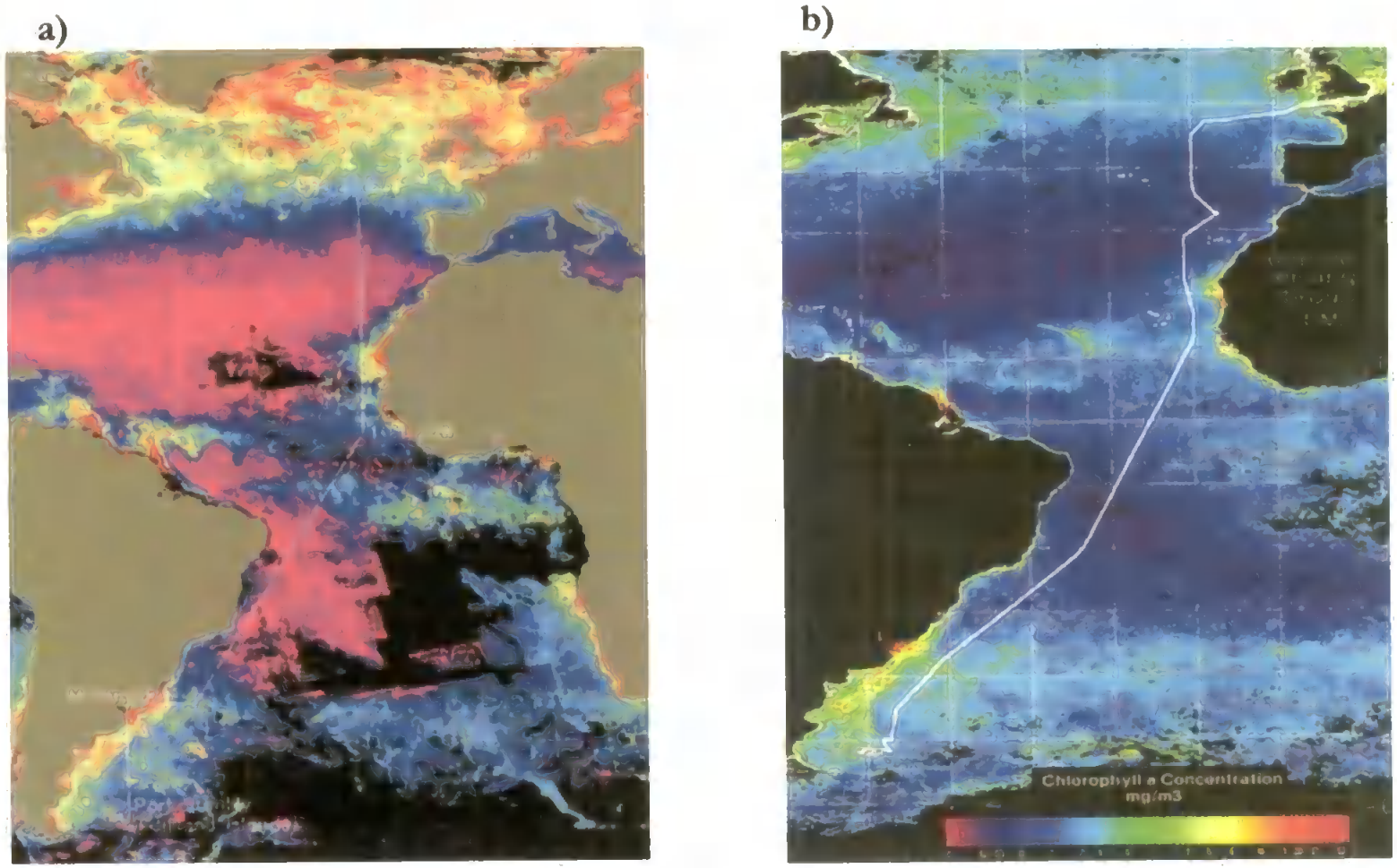

Figure 5.4 a) CZCS Composite of Chlorophyll Levels in the Atlantic Ocean for September. Ocean colours represent the diversity of province productivity, ranging from high chlorophyll levels – yellow through orange, red, blue, to mauve low chlorophyll levels (Aiken *et al.*, 2000). Typical AMT transect shown in white.

b) SeaWIFS Composite of Chlorophyll Concentration for Atlantic Ocean for AMT 5 Transect (shown in white), September/October 1997 (Aiken *et al.*, 2000).

been subjected to discrete sampling protocols. The ability to provide high quality, shipboard measurements of Cu(II) by the low cost, sensitive FI-CL instrumentation would avoid the analytical artefacts that may occur due to sample preservation, storage and subsequent land based analysis in conjunction with the other advantages discussed in Section 1.6. The correlation to the high quality biological and physical oceanographic parameters provided on AMT 9, enabled mapping of Cu(II) distribution to further the understanding of oceanic Cu distributions and its biogeochemical cycling.

5.1.4 Historical Cu Data for the Atlantic Ocean/Worlds Oceans

Long distance Atlantic transects undertaken by van de Loeff *et al.*, (1997), Boyle, (1981), Helmers *et al.*, (1993) indicate that Cu has no particular geographical trend and is subject to aerosol, fluvial and benthic inputs. Biological uptake of Cu(II) in surface waters leads to fairly constant oceanic surface water values with variation in concentration through the upper water column due to biological uptake, regenerative and sink mechanisms. Historically riverine fluxes were presumed to be far in excess of atmospheric deposition, although more recent evidence has suggested the aerosol flux to be of much greater importance than previously thought (Jickells, 1995). Duce *et al.*, (1991) reported atmospheric inputs of Cu to the global ocean to be 0.03 – 0.11 10^9 moles yr^{-1} and riverine fluxes to be 0.16 10^9 moles yr^{-1}. Sedimentary regeneration and hydrothermal venting are also known to play a role in determining surface concentrations. Table 5.2 summarises the previously reported Cu observations from a very similar surface water transect to AMT (van der Loeff *et al.*, 1997) and also from geographically similar waters where discrete samples have been collected for shore based determination for Cu.

5.2 Experimental

5.2.1 Sampling

5.2.1.1 Sampling Equipment

All sample collection whilst on station was performed using a Sea Bird SBE 32 Carousel Water Sampler (Figure 5.5), with an epoxy coated, high quality stainless steel

Table 5.2 Historical Data for Cu Concentrations in the Atlantic

Oceanic Province (Hooker *et al.*, 2000)	Latitude	AMT Stations	Cu(II)(nM) Clean Room	Cu(II) (nM) Shipboard	van der Loeff *et al.*, (1997) (nM)	Kremling & Pohl (1989) (nmol kg^{-1})	Boyle *et al.*, (1981) (nM)	Discrete Stations with Sources (nM)
EU Cont. Shelf Water (ECSW)	50–47.5 ^{O}N	901 902	3.0 4.7	1.7 2.8	1.8-2.8 (> 38 ^{O}N)	1.8-2 1.1-1.5		1-2 Le Gall 1.4 Danielsson
N. Atlantic Drift (NatD)	47.5-38.5 ^{O}N	904	3.7	1.5		1-1.3		
N. Atl. Subtropical Gyre East (NASE)	38.5-26.7 ^{O}N	905	2.8	1.7	0.9-1.3 (20-38 ^{O}N)	0.9-1.2	1.4	0.5-1.2 Land. (1995)
Canary Current (CanC)	26.7-20.5 ^{O}N	908	3.9				1.0	0.7-1.5 Yeats
Canary Current Upwelling (CCUp)	20.5-15.7 ^{O}N	910	2.6		0.5-1.0 (10-20 ^{O}N)		1.0	
N. Equatorial Current (NeqC)	15.7-12.4 ^{O}N							
Guinea Dome (Gdom)	12.4-7.9 ^{O} N	914	1.4				0.8	
N. Equatorial Counter Current (NECC)	7.9-1 ^{O}N	918	1.0		0.5-0.7 (5-9 ^{O}N)		1.1	
S. Equatorial Current (SeqC)	1^{O} N-14.6 ^{O}S	919 925	1.0 0.9				0.6 0.8	
S. Atlantic Tropical Gyre (SATG)	14.6-30 ^{O}S	929 932	1.1 1.3		0.6 (10-35 ^{O}S)	.		
Brazil Current (BraC)	30-35 ^{O}S	936 938	0.7 1.4					
S. American Shelf (SASh)	35-39.6 ^{O}S				1.1-2.2 (>35 ^{O}S)			

van der Loeff *et al.*, (1997); Boyle *et al.*, (1981), Kremling and Pohl (1989); Le Gall *et al.*, (1999); Danielsson *et al.*, (1985); Landing *et al.*, (1995), Yeats *et al.*, (1995)

Figure 5.5 Sea Bird SBE 32 Carousel Water Sampler on the deck of the JCR with conductivity-temperature-depth (CTD) instrumentation fitted.

carousel frame. The conductivity-temperature-depth (CTD) carousel was fitted with 12 grey poly(vinyl) chloride (PVC), Teflon® lined, free flushing water sampler bottles (Ocean Test Equipment Inc., model 110, 12 l capacity), fitted with latex tubing spring closures, silicone 'O' rings and seals and HDPE plastic drain valves to minimise metal contamination.

Prior to first use on AMT 9 each sampler was cleaned with 5% micro-detergent (Decon®, Merck, BDH), UHP water rinsed, followed by 5% Q-HCl, rinsed with UHP water and with copious amounts of seawater. Ten samplers were regularly fired for sample collection leaving two bottles to evaluate sample integrity by duplicate sampling. This was also evaluated by comparison of the CTD bottle fired at 7 m with the all Teflon® pumped supply. Any sampler bottles that resulted in outliers to the data were cleaned again using the protocol described above. The results are presented in the Section 5.3.1.4.

The first station was performed on Sunday 19th September (1100 GMT) with the first expendable bathythermographs (XBTs, model T7) deployed (1224 GMT). The deployment at stations AMT 901 - 905 was dictated by storms after which and wherever possible, stations were timed to coincide with SeaWiFS overpass window (~1300 GMT) to sea-truth the satellite imaging. A full station list is shown in Table 5.3.

Table 5.3 Station List for AMT 9

Biogeochemical Province	Station	Date	Julian Day	GMT	Latitude (°N / °S)	Longitude (°W)
Pumped JCR supply	A900	18/09/99	261	n/a	n/a	n/a
50 °N - S.W.	A901	19/09/99	262	11:00:00	48.512 °N	11.475
Approaches 47°N	A902	20/09/99	263	13:30:00	47.753 °N	16.443
43 °N –	A904	22/09/99	265	13:30:00	43.243 °N	20.984
N.E. Atlantic	A905	23/09/99	266	11:00:00	38.78 °N	20
Oligotrophic	A906	24/09/99	267	11:30:00	33.763 °N	17.789
Gyre	A907	25/09/99	268	11:30:00	30.024 °N	19.973
24 °N	A908	26/09/99	269	11:30:00	25.331 °N	20
20 °N.W.African. Upwell	A909	27/09/99	270	09:30:40	20.91 °N	20
17 ° N -N Equat	A911	28/09/99	271	09:33:51	16.357 °N	20
Region (S of Upwell,	A913	29/09/99	272	09:30:42	11.729 °N	20.61
N of Equator)	A915	30/09/99	273	09:32:03	7.525 °N	22.543
3 °N	A917	01/10/99	274	09:37:25	3.506 °N	24.438
2 °N to 3 °S	A919	02/10/99	275	11:30:00	0.842 °S	26.446
Equat. Upwelling						
	A920	03/10/99	276	10:31:31	4.917 °S	28.341
6 °S	A922	04/10/99	277	10:30:43	9.129 °S	30.298
	A924	05/10/99	278	10:31:56	13.209 °S	32.224
South Atlantic	A926	06/10/99	279	10:33:36	16.606 °S	33.841
Oligotrophic	A928	07/10/99	280	10:30:13	20.245 °S	35.617
Gyre	A931	08/10/99	281	10:28:17	24.094 °S	37.535
30 °S	A933	09/10/99	282	10:29:42	27.507 °S	40.905
32 °S to 48 °S	A936	10/10/99	283	16:00:31	30.606 °S	44.554
Brazilian/Falklands	A938	11/10/99	284	16:00:40	33.801 °S	48.33
Current Confluence						

n/a – data not available

5.2.1.2 Sample Collection Protocol

The CTD sampler firing (Table 5.4) was at pre-selected depths in accordance with chlorophyll *a* levels as indicated by fluorescence and the temperature/salinity profiles recorded by the CTD as it descended. Seawater samples were collected by deployment of the CTD to the maximum depth (250 m) with samplers open, the closures then being tripped electronically after 3 minutes at each of the selected depths.

Table 5.4 CTD Deployment Protocol

Depth (m) Comments	Bottle No	Depth (m) Comments	Bottle No	Depth (m) Comments	Bottle No
250 max. depth	1	Chlorophyll *a* max	5	7 m surface	9
Thermocline base	2	Transmissometer minimum	6	2m surface	10
In thermocline	3	Mixed layer base	7		
Chlorophyll min	4	In mixed layer	8		

The 7 m bottle correlated with the Teflon® lined non-toxic underway pumped supply drawn from below the JCR. 10 sampler bottles regularly fired.

5.2.1.3 Shipboard Procedures

Wherever possible reagents and stock standards were prepared using trace metal clean protocols in the class 1000 clean room at the UoP. Clean protocols were strictly adhered to onboard with a designated clean area constructed in the shipboard laboratory. A laminar flow hood (class 100) was lined with plastic and used for all sample and solution manipulation onboard. An initial batch of 1,10-primary reagent was prepared, which previous work in this study (Section 2.3.3.3) had shown to be stable for 3 weeks. The components of the 1,10-primary reagent were also carefully weighed out/prepared using clean protocols in the UoP clean room, with the further stock 1,10-primary reagent (60 μM, Section 2.2.1) prepared in the onboard laminar flow hood. Sample acidification (pH 2) was achieved with Q-HNO_3 and elution of 8-Hydroxquinoline (8-HQ) micro-column with Q-HCl; both prepared in the UoP clean room. Cu(II) determinations were performed using the FI-CL analyser (Figure 5.6, manifold - Figure 3.2).

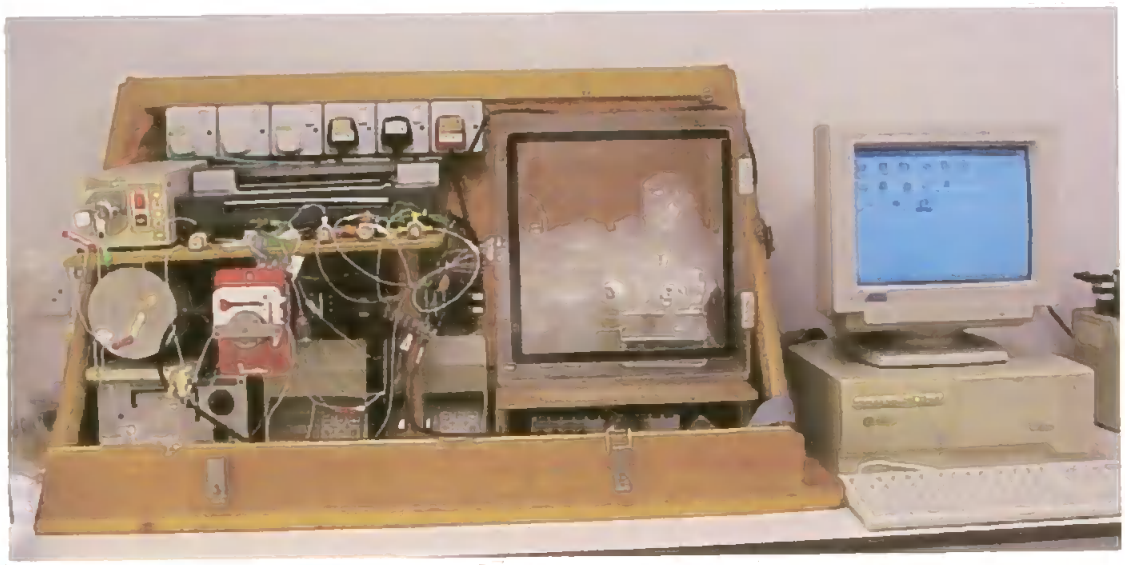

Figure 5.6 FI-CL Instrumentation Onboard the JCR

The FI-CL analyser was housed in a custom designed wooden box, secured to the laboratory bench. A sealable Perspex® cube was incorporated as a clean area that housed the reagents and sample in closed HDPE containers, double bagged in plastic bags to prevent contamination. All HDPE containers and sample bottles were prepared using trace metal clean, acid washing procedures according to Plymouth protocols (Section 2.2.5). HDPE sample bottles were taken on-board to return samples to the UK for subsequent analysis in the UoP clean room. Analysis of aliquots of acidified UHP water blank in 3 separate bottles was not statistically different (*t* test, p=0.05) from a contamination free blank prepared in the UoP clean room in an identical manner. Therefore, the acid cleaning protocols were sufficiently rigorous for Cu(II) determination at sub-nanomolar levels.

5.2.1.4 Sample Pre-treatment

Once the CTD had been retrieved using clean techniques the HDPE sample bottles were rinsed three times with sample, filled and resealed in zip lock plastic bags. These were immediately transferred to the dedicated onboard clean facility, vacuum filtered (Nalgene, 500 ml, acid cleaned, Figure 5.7) through acid cleaned and UHP rinsed polycarbonate membrane filters (Nuclepore, 0.4 µm) to minimise the exchange of acid leachable Cu(II) from suspended particulate material (SPM).

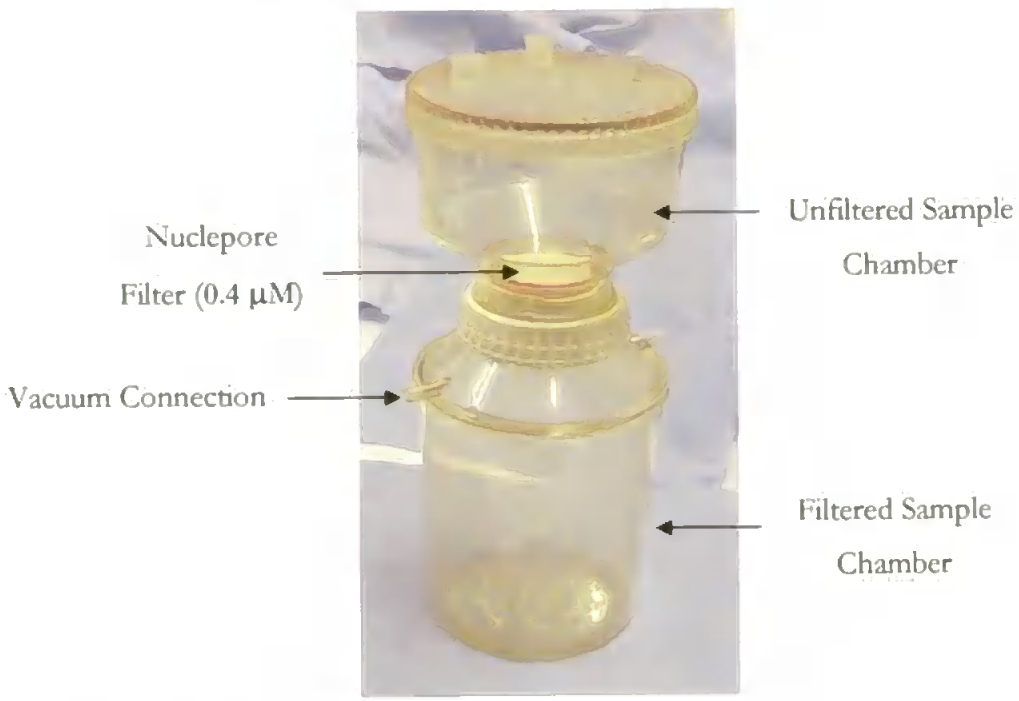

Figure 5.7 Nalgene Vacuum Filtration Unit. The hand vacuum pump is not shown.

The filter was preconditioned with seawater before first use, and the first 50 ml of the filtrate was discarded to minimise any possible trace metal leaching from the filter and the remaining sample acidified to pH 2 (Q-HNO_3, 80 µl 100 ml^{-1}). The filtration process operationally defined the Cu fraction determined as dissolved Cu(II) and that associated with colloidal species and weakly bound to organic complexes. Samples for shore based analysis were also filtered, acidified and stored in the dark at 4 ^{o}C.

5.2.2 Cu(II) Determinations

All analyses for Cu(II) were performed using a two point standard addition. In the clean facility, three 10 ml aliquots were pipetted into acid cleaned, polystyrene screw capped vials (Sterilin, Merck BDH). One sub-sample was analysed without further treatment, sub-samples 2 and 3 had aliquots (20 – 70 µl) of Cu(II) delivered by pipette to achieve standard additions that ranged from 0.5 to 7 nM. Analysis was then performed in order of increasing concentration. All results (mV) were blank subtracted to account for the blank signal generated by residual Cu in the UHP water, citrate buffer and acid used for acidification and elution (Section 3.3.8).

Utilising the automated FI-CL analyser, each aliquot required 10.6 min (n=4), totalling 31.8 min for the 2 point standard addition at each depth, making a total of 35 min including cleaning of the automated analyser between successive depths. A set of FI-CL peaks from a two point standard addition to an Atlantic Ocean sample is shown in Figure 5.8.

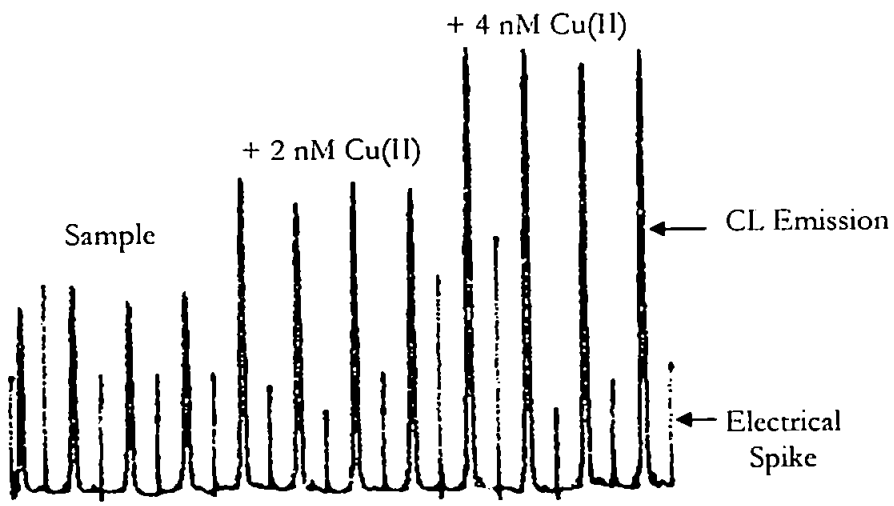

Figure 5.8 Detector Output from a Typical Two Point Standard Addition of Cu(II) to an Atlantic Ocean Seawater Sample. (n=4) with 2 and 4 nM standard additions of Cu(II).

5.2.3 Ancillary AMT 9 Measurements

5.2.3.1 Macro-nutrients

Station depth profiles for nitrate (NO_3), phosphate (PO_4) and silicate ($Si(OH)_4$) were determined by Vassilis Kitidis (University of Newcastle) on a 4-channel, Technicon® segmented flow Auto-Analyser® using standard colorimetric methodologies (Woodward *et al.*, 1999). Near surface nutrient concentrations were below the LOD (0.02 μM) at many stations with the exception of the European and South American shelf waters and the Brazilian/Falkland Current confluence, although an increase in concentration was observed at depth.

5.2.3.2 Phytoplankton Abundance and Pigments

Seawater samples were collected (1.0 – 2.5 l) from the underway, all Teflon® non-toxic seawater supply (~ 7m depth) at 2 h intervals whilst on passage, and at CTD stations from the Ocean Test 110 sampler bottles (2.0 l). This enabled the pigment distribution through the North-South surface waters and the vertical station profiles to be determined. The phytoplankton were harvested by positive filtration (0.7 μm, GF/F glass microfibre, Whatman, 25 mm diameter), the filter papers were transferred to a vial and stored frozen in liquid nitrogen (-196 ^{o}C) which has been shown to arrest pigment degradation for up to one year (Mantoura *et al.*, 1997). At PML, analysis by reverse phase high performance liquid chromatography (HPLC) identified a range of chemotaxonomic pigments e.g. chlorophyll *a* (CHL*a*), generally indicative of biomass, carotenoids (e.g. fucoxanthin), a biomarker for diatoms, and butanoyloxyfucoxanthin, a biomarker for chrysophytes.

Onboard analysis for CHL*a*, indicative of phytoplankton biomass, was conducted by Hester Wilson (PML) on filtered sub-samples to provide near real time data for validation of bio-optical models and remote sensing algorithms. The pigment in the filtered samples was immediately extracted (90 % acetone for 12-18 h) and analysed by fluorescence on a Turner Designs 10-AU fluorimeter (calibrated using CHL*a* pigment standards, Sigma Chemical Co.).

5.2.3.3 Hydrographic Data Acquisition

On AMT 9, North-South surface water and vertical sampling protocols were implemented to produce integrated, high quality hydrographic data over oceanic scales along the AMT cruise track with good seasonal/annual resolution provided by comparison to previous AMT cruises. High quality vertical resolution (0 – 250 m) was

provided by CTD casts even in the tropical and equatorial regions where the thermocline can be deep e.g. > 100 m (Hooker *et al.*, 2000). The surface water samples (7 m) also provided good horizontal resolution (~ 250 miles at an average steaming speed of 12 knots).

The CTD carousel was fitted with a PC compatible Sea-Bird 911 Plus CTD, which enabled real time data acquisition with high quality vertical resolution of conductivity, temperature and depth. Also fitted were a Fast Repetition Rate Fluorimeter (FRRF), which recorded vertical distribution of chlorophyll *a* by fluorescence, and upwelling and downwelling radiometers which provided measurement of photosynthetically available radiation (PAR). Transmissometer readings provided a measurement light intensity and therefore particle distribution through the water column.

Hydrographic data was also gathered via underway sampling of near-surface water at 5 s intervals. Salinity from a Sea-Bird flow through thermosalinograph (TSG), temperature, fluorescence and photosynthetically available radiation (PAR) were obtained using flow through sensors located in the all Teflon® non-toxic seawater supply (intake through hull at 7 m). All data was interfaced with the ships Ocean Logger. The deployment at 4 h intervals of T 7 XBTs provided vertical temperature resolution of the mixed layer depth (MLD) down to 760 m. Salinity and temperature data from the CTD and TSG was verified through use of salinity bottles at three depths and from the salinometer outlet, measured with a precision laboratory salinometer (Guideline 'Autosal') and with certified ISO reversing digital thermometers. The XBT data was validated by intercomparison of temperature (T) with the CTD data during its deployment as the JCR departed station.

5.3 Results and Discussion

5.3.1 Instrument Analytical Performance

During AMT 9 and on local field trials the FI-CL instrumentation was very reliable, functioning well even during the storm force 10 conditions experienced early in the cruise, which laid low most of the scientific personnel.

5.3.1.1 Quality Control Procedures

During AMT analysis only three samples were rejected due to a lack of precision (>15 %) during replicate (n=4) sample analysis, or a high degree of scatter on oceanic depth profiles. Contamination of CTD sampler degraded analytical accuracy and gave abnormally high Cu(II) values. Rigorous cleaning of the sampler, using the acid washing

procedure outlined in Section 5.2.1.1, restored the accuracy of Cu(II) determinations. Dixons Q-test (p = 0.05) was applied to replicate injections (n=4) and any possible outliers rejected from the data set. During the land based analyses 3 HDPE sample bottles were rejected due to possible contamination.

5.3.1.2 Certified Reference Material

The precision and accuracy of the FI-CL analyser was validated by determination of Cu(II) in NASS 5, a North Atlantic Surface Seawater certified reference material (CRM, Newfoundland site, 10 m depth) on 4 separate occasions at sea and again in the clean room at UoP prior to shore based Cu(II) analysis of stored AMT 9 samples. The FI-CL results (Table 5.5), show good agreement with the certified Cu(II) values and none were found to be statistically different (*t* test, p = 0.05) from the certified value.

Table 5.5 NASS 5 CRM Results

Certified Cu(II) value (nM)	Shipboard Cu(II) value (nM)
4.68 +/- 0.72	4.70+/- 0.33
	4.95 +/- 0.21
	4.39 +/- 0.20
	4.24 +/- 0.21
	Mean CRM 4.57 +/- 0.64
	Clean room Cu(II) value (nM)
	4.41 +/- 0.21
	4.63 +/- 0.15
	4.34 +/- 0.14
	4.37 +/- 0.21
	Mean CRM 4.41 +/-0.26

All data mean concentration +/- 2s

5.3.1.3 Sampling System Validation

The integrity of the water samples from the Ocean Test water sampler was ascertained by comparison of surface (7 m) seawater samples from the CTD with samples collected from the non-contaminated, all Teflon® supply. The latter were collected after CTD retrieval and once the JCR was underway to allow for flushing of the pumped supply. All samples were filtered and analysed for Cu(II) by FI-CL and the results are presented in Table 5.6, with a correlation between the two sources presented in Figure 5.9.

A good correlation (R^2 0.91) for Cu(II) was found between samples from the Ocean Test Samplers and a *t* test (p = 0.05) showed that there was no significant

Table 5.6 Comparison of Cu(II) (nM) from CTD Samplers with Underway Supply

Sample	Ocean Sampler	Date & Julian Day	GMT	Lat (°)	Long (°)	Cu(II) (nM)
A901	11	19 Sept	12.02	48.51	11.48	1.7
Underway	n/a	1999 – 262	12.35	48.42	11.37	1.8
A902	11	20 Sept	14.32	47.75	16.44	2.8
Underway	n/a	1999 - 263	15.10	47.68	16.35	2.6
A904	11	22 Sept	14.31	43.24	20.98	1.5
Underway	n/a	1999 - 264	15.06	43.70	20.75	1.3
A905	11	23 Sept	12.17	38.78	19.99	1.7
Underway	n/a	1999 - 265	12.52	37.95	19.72	1.9

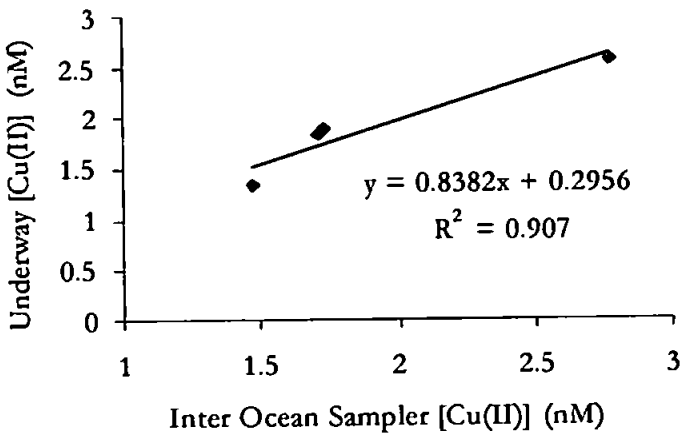

Figure 5.9 Correlation of Cu(II) from Samples Collected from Inter Ocean Sample Bottles on the CTD and the PTFE Lined Underway Supply, Pumped Onboard the JCR.

difference between the results. This demonstrated that the CTD samplers were contamination free and the good reproducibility of the FI-CL analyser.

On two separate occasions 2 CTD samplers on the same cast were fired at identical depths and analysed for Cu(II) and the results compared (Table 5.7) in order to investigate inter-sample reproducibility of the FI-CL analyser. A *t* test (p =0.05) indicated that there was no significant difference between the FI-CL determined Cu(II) values, demonstrating good inter-sample reproducibility when using the FI-CL analyser and showing that the CTD cleaning protocol was efficient.

Table 5.7 Comparison of Cu(II) (nM) from Replicate Firing of CTD Samplers

Sample	Ocean Sampler	Date-Julian Day	GMT	Lat (°N)	Long (°W)	Cu(II) (nM)
A901	11	19 Sept	12.02	48.51	11.48	1.7
	12	1999 – 262				1.6
A905	11	23 Sept	12.17	38.78	19.99	1.7
	12	1999 - 265				2.0

5.3.1.4 Replicate Sub-Sample Analyses

The FI-CL analyser and the sampling protocols were also validated by replicate shipboard analysis of acidified sub-aliquots taken from the same Inter-Ocean 110 sampler at 3 different stations (Table 5.8) and stored in separate acid cleaned HDPE sample collection bottles. Replicate analysis of sub-aliquots from the same HDPE sample collection bottles, performed in the UoP clean room provided further validation of the analytical performance of the FI-CL analyser.

Table 5.8 Comparison of Cu(II) (nM) – Replicate CTD Samplers at Same Depth

Analysis	Shipboard[a]			Clean Room (UoP)[b]		
Station	A902	A904	A905	A902	A904	A905
Date	20 Sept-1999	22 Sept-1999	23 Sept-1999	20 Sept-1999	22 Sept-1999	23 Sept-1999
Julian Day	263	264	265	263	264	265
GMT	13.30	13.30	11.00	13.30	13.30	11.00
Latitude	47.75	43.24	38.78	47.75	43.24	38.78
Longitude	16.44	20.98	19.99	16.44	20.98	19.99
Depth (m)	50	20	7	50	20	7
Cu(II) (nM)						
Replicates						
1	1.70	1.15	1.73	2.66	1.75	2.81
2	1.62	1.08	1.90	2.42	1.82	2.69
3	1.79	1.20	1.82	2.53	1.59	2.6
Mean Cu(II)	1.70	1.14	1.82	2.53	1.72	2.7
Std. Dev.	0.085	0.060	0.085	0.120	0.012	0.105
R.S.D. (%)	5.0	5.3	4.7	4.7	6.8	3.9

[a] Shipboard replicate analysis of sub-aliquots from same Inter Ocean Sampler bottle, collected in different HDPE sample bottles. [b] Clean Room replicate analysis of sub-aliquots from the same HDPE sample collection bottles.

5.3.2 Nature of Reported Trace Metal Determinations

In contrast to open ocean regimes low in suspended particulate matter (SPM), shelf areas receive enhanced continental aeolian dust, fluvial and benthic inputs that raise nutrient and trace metal levels and leads to increased biomass. Fluvial processes have been reported as contributing significant trace metal inputs to the global ocean (Chester, 2000 and references therein), although atmospheric fluxes can be of a similar magnitude (Jickells, 1995). Duce *et al.*, (1991) reported riverine Cu fluxes of 0.16 10^9 moles yr^{-1} and atmospheric Cu inputs of 0.03 – 0.11 10^9 moles yr^{-1}, the range of the latter reflecting the

variability of atmospheric inputs and their possible effect on oceanic Cu chemistry (Buat-Ménard and Chesselet, 1979).

Yeats *et al.*, (1995), in a trace metal study in the Eastern central and South Atlantic, concluded that Cu levels were higher in unfiltered compared with filtered surface layer samples. The fraction of Cu exchangeable with biogenic or lithogenic SPM can therefore be important, especially in waters with enhanced SPM e.g. those underlying offshore winds or biologically productive upwelling zones.

The AMT 9 cruise crossed coastal zones, shelf areas, upwelling zones and open ocean waters with varying SPM content and therefore, to enable a valid comparison of Cu(II) levels, an operational definition was made by sample filtration (Section 5.2.1.4) prior to acidification (Q-HNO_3 pH 2). The filtration approach yielded dissolved Cu(II) plus copper associated with colloidal species and weakly organically complexed Cu(II) that was released by acidification (Q-HNO_3) and the competitive retention during matrix separation by the 8HQ micro-column during analysis by FI-CL. This hypothesis was supported by the shore based FI-CL analyses after sample storage (Section 5.3.4.4), which resulted in higher Cu(II) concentrations due to its release after sample acidification over storage (up to 9 months).

The presence of SPM along the AMT 9 track was indicated by the light intensity readings from the transmissometer, with the majority of the particulate matter in open ocean environments being biogenic in origin (Helmers, 1996). The strong relationship between the transmissometer values and chlorophyll *a* concentration (R^2 0.758) in the surface waters (Figure 5.10) support this hypothesis.

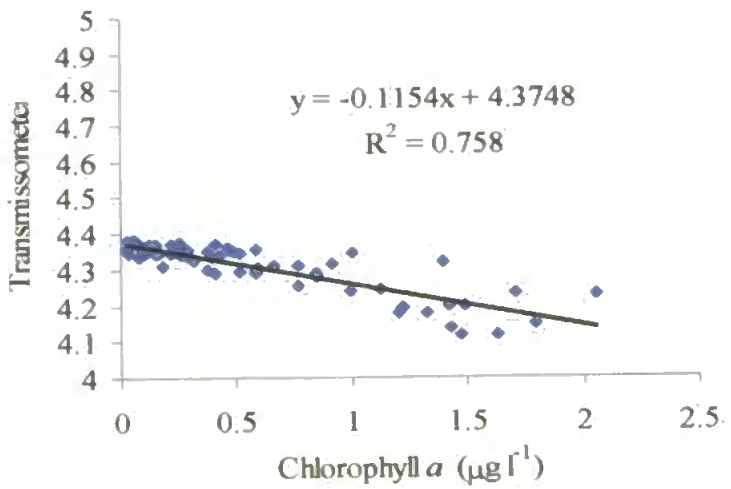

Figure 5.10 Relationship Between Surface Chlorophyll *a* and Transmissometer Readings

The presence of such particles would therefore be expected to affect the distribution of micronutrients through the euphotic zone, further supporting the adoption of a filtration protocol for this study.

5.3.3 Water Column Structure

5.3.3.1 Historical Review

Through the upper water column (0 – 500 m) of the Atlantic four dominant water masses have been identified (Emery and Meincke, 1986), underlain by five intermediate waters of varying salinity originating from a variety of latitudes. On a basin scale perspective the AMT track traverses 4 major circulatory features; 1) the North Atlantic Gyre (NAG) (50 – 20 ^{o}N) (1); 2) the tropics and equatorial regions (TER) (25 ^{o}N - 15 ^{o}S) (2); 3) the South Atlantic Subtropical Gyre (SATG) 15 – 35 ^{o}S; and 4) the Sub Antarctic Convergence Zone (SACZ) (35 – 50 ^{o}S).

The AMT 9 track passed through two of the upper water masses; namely Eastern North Atlantic Central Water (ENACW) which extended from 50 ^{o} to ~ 20 ^{o}N, and the South Atlantic Central Water (SACW) a stable water mass extending from ~20 ^{o}N – 37 ^{o}S. Each underwent modification through the tropics and equatorial regions (TER). The vertical distribution of the water masses encountered as a function of latitude is shown in Figure 5.11, with their geographical distribution and the principal Atlantic circulatory patterns shown in Figure 5.12.

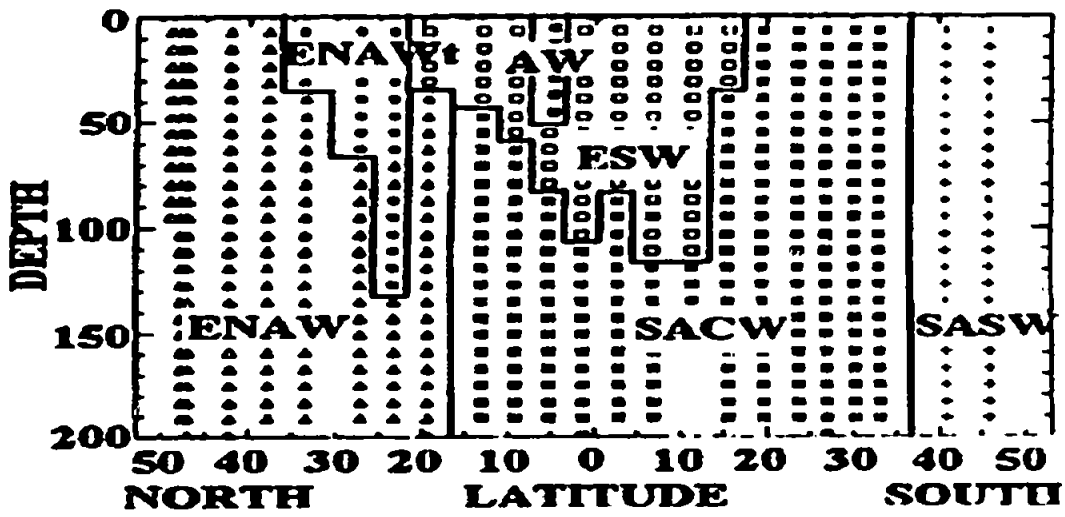

Figure 5.11 Vertical Distribution of Water Masses as a Function of Latitude During AMT 1 (Aiken *et al.*, 2000)

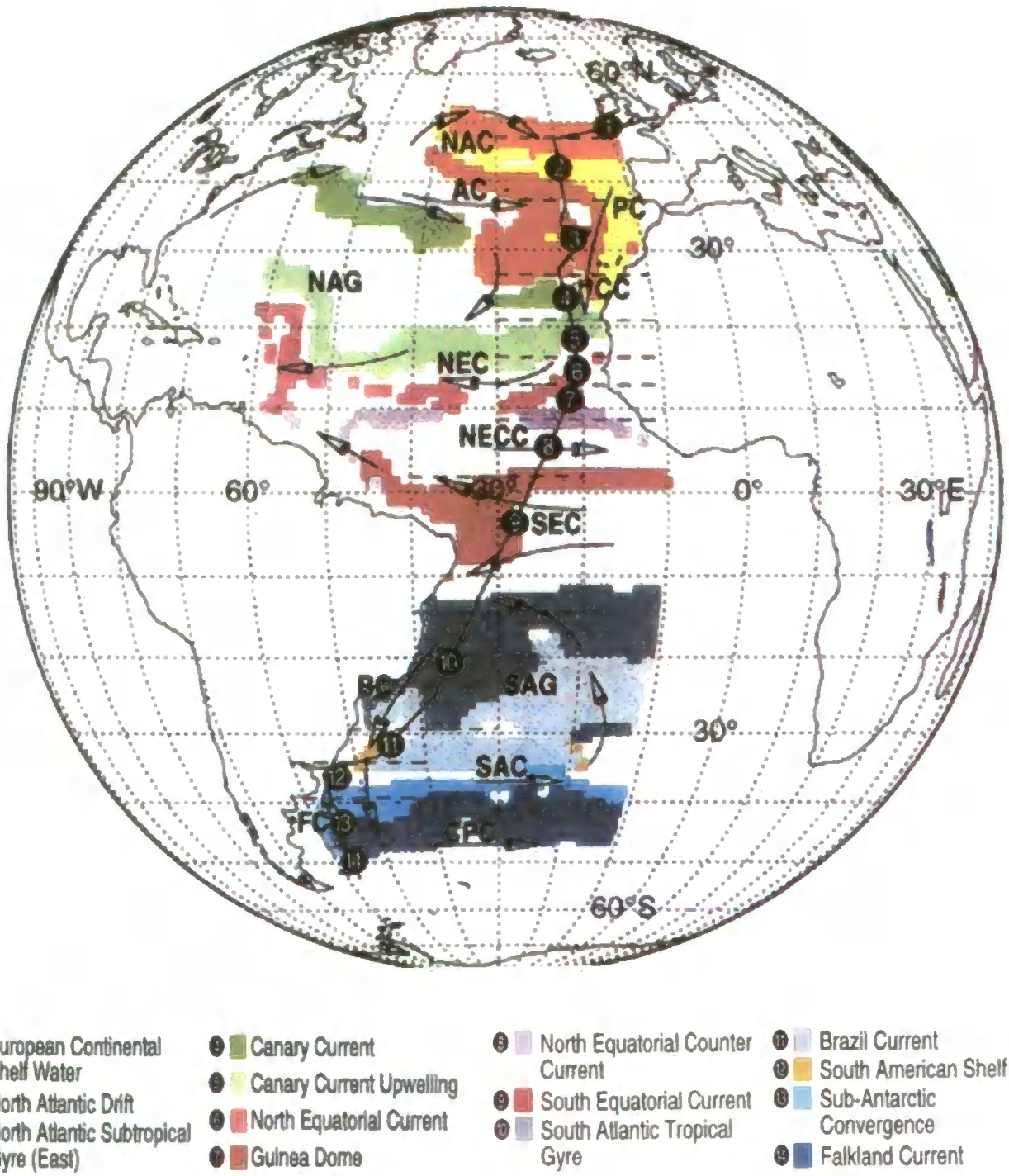

Figure 5.12 Geographical Distribution of Upper Water Masses (0 – 500 m) and Circulatory Patterns of the Atlantic Ocean. Compiled from Hooker et al., (2000).

The upper water column of the north-eastern Atlantic basin was dominated by the ENAW mixing with Western North Atlantic Water (WNAW). The latter is carried northwards from the Sargasso and Caribbean Seas by the Gulf Stream and across the

North Atlantic in the North Atlantic Current (NAC) and Azores Current (AC), forming ENAWt when mixed with the former (Hooker *et al.*, 2000). The salinity in ENACW is higher than in WNAW due to increased winter convection and Mediterranean outflow. Further south on the AMT 9 transect SACW flows northward across the equator, mixing with ENAW at a North-South Atlantic transitional front at ca. 1500 km north of the equator (15 ^{o}N) in the Western Atlantic. The SACW had a similar temperature but slightly lower salinity than ENAW due to the mixture of water moving northward and not being returned.

Modification of the hydrographic properties of the SACW surface waters to form Equatorial Surface Water (ESW) occurred through the tropical and equatorial region (TER) due to precipitation and strong equatorial surface water exchange in the opposing eastward and westward currents (Tomczak and Godfrey, 1994). ESW was characterised on previous AMT cruises by a salinity reduction down to ~100 m due to the rain induced dilution of SACW and mixing with Amazon Water (AW), which was carried eastward by the North Equatorial Counter Current (NECC). AW was characterised during the Boreal Autumn AMT 9 cruise as warm (~25 ^{o}C), low salinity (~ 35.0) water down to 22 m centred at ~5 ^{o}N (AMT 916) (Aiken *et al.*, 2000). The Brazil Current (BC) flowed poleward along the Brazilian coast to 44 ^{o}S (but was limited to 50 – 55 ^{o}W with lower temperatures west of its eastern limit (45 ^{o}W), and advected the SACW into the western South Atlantic. Here the SACW was characterised by a temperature > 10 ^{o}C (up to 26 ^{o}C in surface waters) and a salinity > 35.0 (up to 37.3). The SACW southern boundary was formed by the Subtropical Front (STF).

Sub Antarctic Surface Water (SASW) (=/<10 ^{o}C, salinity < 34.3) part of the circumpolar waters of the Southern Ocean, was advected northward by the Falklands Current (FC) along the S. American continental shelf, in the upper 500 m up to 36 ^{o}S, the southerly limit of AMT 9 and where its influence was observed mixing with the SACW (Figures 5.14 and 5.15).

5.3.3.2 Temperature and Salinity (AMT 9)

Temperature (T) and salinity (S) characteristics were used to identify the water mass types encountered along AMT 9 through the upper water column (0-250 m by CTD, Figure 5.13). Their principal characteristics are shown in Table 5.9, and their vertical distribution as a function of latitude shown in Figure 5.14. This enabled correlation of Cu(II) levels as determined by FI-CL with the various water masses encountered en-route.

Table 5.9 Temperature and Salinity of Principal Waters (< 500 m) on AMT 9

Water Mass	Temperature (°C)	Salinity
Eastern North Atlantic Water (ENACW)	8.0 - 18.0	35.2 – 36.7
South Atlantic Central Water (SACW)	5.0 – 18.0	34.3 – 35.8
Sub-Antarctic Surface Water (SASW)	3.2 – 15.0	34.0 – 35.5

Reproduced from Bowie (1999) PhD thesis

Figure 5.13 T-S Plot for Water Masses for AMT 9 through the Upper Water Column (0 – 250 m). AW – Amazon Water, ESW - Equatorial Surface Water, ENAW – Eastern North Atlantic Water (ENAWt - ENAW with Azores Current influence), SACW – South Atlantic Central Water, SASW - Sub-Antarctic Surface Water.

A distinct geographical distribution of temperature-salinity (T-S) in the near-surface layer (0 – 250 m) was identified during AMT 9, reflecting transitions in the structure of the upper water column (Section 5.3.3.1). These were in close agreement with previous AMT cruises (Aiken *et al.*, 2000) after allowing for seasonal solar forcing of the North-South distribution and episodic events. The T-S distribution supported the hypothesis that the different geographical zones have distinct physical characteristics and boundaries and enabled Hooker *et al.*, (2000) to further refine the biogeochemical provinces as described by Longhurst *et al.*, (1995).

Along AMT 9 the temperature distribution (Figure 5.14) showed a weak thermal stratification and a shallower thermocline (~ 50 m) in the Northern Hemisphere, in comparison to a deeper thermocline (~ 150 m) in the South Atlantic. Excluding regions of aerosol deposition and upwelling zones, the macro-nutrient profile also followed this pattern, with a nutrient maximum at 50 – 80 m in the North Atlantic compared to ~ 150 m in the South Atlantic. Between 20 – 9 °N in the North Atlantic, upwelling of colder

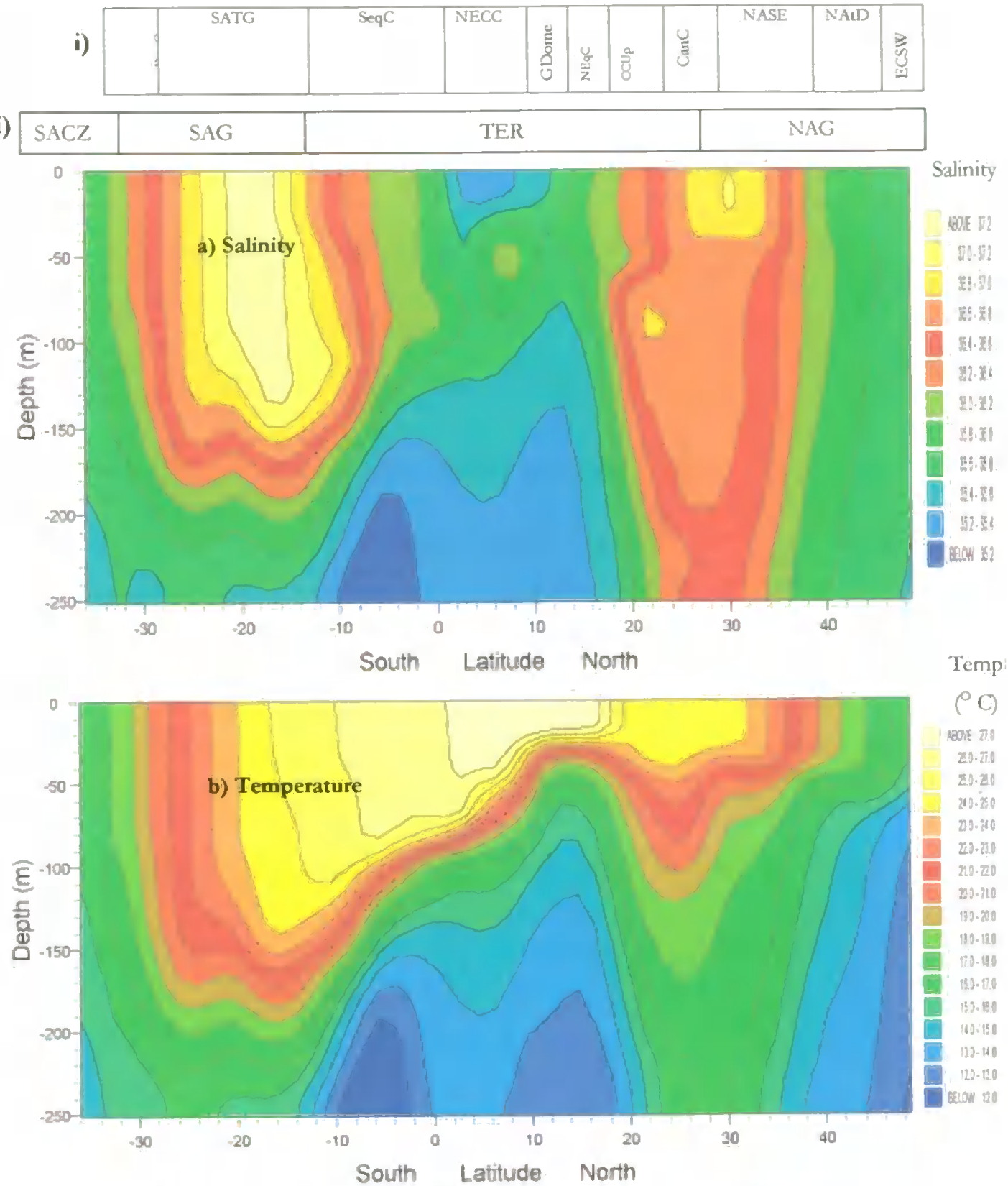

Figure 5.14 Latitudinal Distribution of a) salinity b) temperature through the Upper Water Column (0 – 250 m) of the Atlantic Ocean during September/October 1999 (AMT 9). The biogeochemical partitioning as defined by Hooker et al., (2000) (i), and the four major near-surface circulatory zones (NAG, TER, SAG and SACZ) (ii), are at the head the temperature and salinity plots.

subsurface waters, which also extended towards the equator, reduced the depth of the thermocline in the upper mixed layer and formed the Guinea Dome centred at 14 ^{o}N, 22 ^{o}W. This was a cyclonic, sub-tropical gyre driven by the North Equatorial Undercurrent and a portion of the North Equatorial Counter Current (NECC) which was largely prevented from flowing northwards by the east-west orientation of Africa.

During AMT 9 in both hemispheres, near-surface salinity increased from the high latitudes to the sub-tropics within the open ocean gyres and was closely related to increased temperature and therefore evaporation at lower latitudes (Figure 5.14). Increased precipitation in the tropical-equatorial (TER) zone, associated with equatorial weather systems, reduced the salinity (especially noticeable at the equator, Figure 5.14 a) producing the Equatorial Surface Water (ESW). This had a distinct temperature- salinity (T-S) relationship (higher T and lower S) distinguishing it from South Atlantic Central Water (SACW) which had a relatively consistent slope to the T-S relationship.

Through the TER zone (~25 ^{o}N – ~15 ^{o}S) the complex banded current distribution (Figures 5.14 and 5.16 b) was evident as fluctuations in the T-S relationship. The southern extent of the Canary Current (CC) was characterised by a relatively stable temperature coupled to a slow reduction in salinity (25 – 20 ^{o}N); the North Equatorial Current (NEC, 20 – 12 ^{o}N) was defined by a slow reduction in salinity with a rise in temperature; the North Equatorial Counter Current (NECC, 9 – 2 ^{o}N) as relatively constant temperature with a dip in salinity at ~5 ^{o}N; the South Equatorial Current (SEC, 2 ^{o}N – 15 ^{o}S) was characterised by a small decrease in temperature coupled to a rise in salinity to a surface maximum for the Southern Hemisphere. Differences in near-surface temperature and salinity as reported for AMT 1 and 2 through 15 ^{o}N to 10 ^{o}S, suggested some seasonal variability in latitude for this banded structure.

In the Southern Atlantic Gyre salinities were higher, extended over greater latitudes and to a greater depth compared to the Northern Hemisphere. The influence of cold, low salinity Sub-Antarctic Surface Water (SASW, 36 – 52 ^{o}S) was indicated on AMT 9 by a parallel reduction in temperature and salinity (33 – 36 ^{o}S) as it mixed with South Atlantic Central Water (SACW). The confluence of the southerly flowing, warm Brazilian Current (temperature > 15 ^{o}C, salinity 35 - 36) and the cold Falkland Current (temperature 5 – 10 ^{o}C and salinity ~ 34) at the South Atlantic Convergence Zone (SACZ) formed a heterogeneous water mass with a number of eddies. The eddies created from the two currents are separated by a subset of distinct temperature-salinity relationships (Aiken *et al.*, 2000).

5.3.4 Cu(II) Determination on AMT 9

The results of the FI-CL determination of Cu(II) on AMT 9 are now presented. Throughout this discussion, the Cu(II) distribution was correlated wherever possible with onboard hydrographical data, namely nutrient, chlorophyll *a*, temperature and salinity observations. Each of the stations presented was selected to represent each of the biogeochemical provinces as designated by Hooker *et al.*, (2000). In order to demonstrate oceanographic consistency, the AMT 9 Cu(II) data was compared with van der Loeff et al., (1997) on a geographically very similar Cu(II) surface transect and with other shorter research cruises or from discrete stations in waters close to the AMT transect.

The Cu(II) results are prefaced by a short discussion of the biogeochemical processes encountered on AMT 9, followed by a comparison of the analytical methodologies of the authors reported in order to demonstrate oceanographic consistency of the FI-CL Cu(II) data. This is followed by an overview of the distribution of surface Cu(II) along AMT 9, a discussion of the effects of storage on the Cu(II) concentrations as shown by comparing shipboard and University of Plymouth clean room Cu(II) data and then a detailed discussion of Cu(II) in surface waters at each of the selected stations. An overview of the vertical profile (0 – 250 m) of Cu(II) at the selected AMT 9 stations is then presented, followed by a detailed discussion of each of selected vertical profiles. A three dimensional surfer plot of the distribution of AMT 9 Cu(II) data is then presented.

5.3.4.1 Characterisation of Biogeochemical Provinces

Surface waters on the European and South American Shelves were subject to continental and coastal influences and were characterised by increased Cu(II), NO_3^- and PO_4^{3-} and therefore chlorophyll *a* concentrations, due to inputs from shelf regeneration and the anthropogenic/lithogenic aerosol veil over this region (Church *et al.*, 1990; Arimoto *et al.*, 1990; Duce *et al.*, 1991; Jickells, 1995). Aerosol inputs were fingerprinted by increased Cu surface and phosphate concentrations, e.g. off the West African coast at 25 – 20 ^{o}N. Increased $Si(OH)_4$ indicated a freshwater input e.g. $Si(OH)_4$ peak at 5 ^{o}S in the surface waters. Similar trends were also observed on AMT 3 (Autumn 1996) as reported by Bowie (PhD, 1998).

The relationship between Cu, biomass and physical oceanography is not fully understood due to its complex and dynamic nature (Gledhill *et al.*, 1997; Sunda and Huntsman, 1998; 1995, 1996; Gonzalez-Davila, 1995; Moffett *et al.*, 1997, 1996, 1995, 1990; Moffett, 1998, Bruland *et al.*, 1991; plus Section 1.2.5 and references therein). At many AMT 9 stations a correlation was found between Cu(II) and macro-nutrients as also

reported by Nolting *et al.*, (1991) for the Southern Ocean, although for AMT 9 this correlation was not strong, in agreement with van der Loeff *et al.*, (1997) for the same waters. This was possibly due to particulate scavenging of Cu(II), particularly in areas of high SPM (Boyle *et al.*, 1977; Bruland, 1980). On AMT 9 biolimitation due to surface water depletion of Cu(II) was not observed, although uptake and organic complexation influences were indicated, especially in the open ocean gyres, by a correlation of reduced Cu(II) concentrations with higher chlorophyll *a* levels. Cu(II) is strongly organically complexed in surface waters (Coale and Bruland, 1988; Sunda and Huntsman, 1991) with organic complexation in seawater accounting for 98 – 99 % of Cu (Coale and Bruland, 1988, 1990; Gerringa *et al.*, 1996; Moffett *et al.*, 1990). Xue and Sigg (1990) reported that exudation of extracellular ligands by phytoplankton reduces the concentration of Cu(II) in seawater, acting as a Cu(II) buffering mechanism to reduce the toxicity of Cu when above the optimum biotic concentrations.

Evidence of antagonistic interactions of Cu(II) with other trace metals in biological processes has been reported, e.g. Cu uptake inhibited by Co, Ni, Cd and Mn (Mierle, 1983) and of interaction of Cu(II) with Mn(II), (Sunda and Huntsman, 1986, Murphy *et al.*, 1983) and Cu(II) with Fe(III) (Murphy *et al.*, 1983), the latter two interactions inhibiting phytoplankton growth. This has been hypothesised (Sunda and Gessner, 1989; Sunda, 1986) to be the mechanism whereby upwelled waters have been observed to inhibit phytoplankton growth. The stimulation of phytoplankton growth rates by addition of Fe(III) (Martin and Fitzwater, 1988, 1989; Brand, 1991) may increase the low Fe(III):Cu(II) ratios in seawater (Gonzalez-Davila, 1995). Gonzalez-Davila (1995) also reported that added Cu(II) could displace iron from organic ligands, making it available to phytoplankton and that the adsorption of Cu onto algal surfaces subsequently released of Mg, Na and Ca.

The provinces will therefore be described in relation to the complex nature of these influences in conjunction with the physical oceanography of the AMT 9 transect from north to south.

5.3.4.2 Comparison of Methodologies for Cu Data

The small variation between Cu(II) on AMT 9 and the data used to demonstrate oceanographic consistency was attributed primarily to storage effects and the use of different sampling and analytical methodologies (Table 5.10). Other factors that may also have contributed to the differences were the collection of samples at different seasons and geographical locations and thus being subject to dynamic marine processes e.g. increased biological uptake and organic complexation of Cu(II) in spring and summer. Samples

representative of surface waters were also collected from different depths e.g. van der Loeff *et al.*, (1997) at 12 m, Landing *et al.*, (1995) and Yeats *et al.*, (1995) at 25 m whereas for AMT 9, 7 m represented surface water. It is worth noting that compared to the 7 m values, Cu(II) concentrations at AMT 902, 908 and 910 fell between 7 and 20 m (Figures 21, 22 and 23). On AMT 9 Q-HNO_3 (80 µl 100 mL^{-1}) was used for sample acidification, a

Table 5.10 Comparison of Analytical Methodologies for Cu in North East Atlantic

Research Cruise	Season	Depth (m)	Filtration	Acidification	Storage (months)	Extraction	Analysis
AMT 9	Autumn	7	0.4 µm	HNO_3	9	8HQ	FI-CL
van der Loeff *et al.*, (1997)	Autumn	12	No	HCl	1 - 4	None	DPASV
Kremling and Pohl (1989)	Spring & Summer	7	0.4 µm	HNO_3	5	Dithiocarbamate freon	ETAAS
Saager *et al.*, (1997)	Spring & Summer	10	Filtered	HCl & HNO_3	n/a but analysed ashore	APDC/DDDC freon	ETAAS
Yeats *et al.*, (1995)	Spring	25	Filtered & Unfiltered	HCl	n/a but analysed ashore	Dithiocarbamate	ETAAS
Landing *et al.*, (1995)	Spring	25	Filtered & Unfiltered	Acidified Ashore	n/a but analysed ashore	8HQ or Dithiocarbamate	1
Boyle *et al.*, (1981)	Varied	n/a	Unfiltered	HCl (after a few days)	n/a but analysed ashore	APDC coprecipitation	ETAAS

Yeats *et al.*, (1995) vertical profiling at only 2 relevant stations. 1 - variety of analytical methods used - ETAAS, hydride generation, X-ray fluorescence, DPASV and FI/spectrophotmetric analysis. n/a – data not available.

stronger oxidant than the HCl used by van der Loeff *et al.*, (1997) and others. The HNO_3 would therefore release a larger proportion of the organically bound and colloidal Cu.

Differences in the timing of acidification e.g. ashore for Landing *et al.*, (1995) and (Yeats *et al.*, (1995)}, has implications for losses through deposition onto bottle walls, particulate scavenging, especially in unfiltered samples, and biological uptake as opposed to immediate shipboard acidification on AMT 9. Some authors utilised filtration, as on AMT 9 when all samples were filtered (0.4 µm Nuclepore), and as did Kremling and Pohl (1989) on samples from the continental shelf and South West Approaches. There were also inconsistencies in the time between sample collection and analysis (1 to 9 months). The use of different extraction techniques has implications for Cu losses or contamination e.g. dithiocarbamate-freon requires additional chemicals and three steps, as opposed to direct extraction by 8HQ. Furthermore, the use of different analytical methods may result in the

determination of a different fraction of Cu e.g. van der Loeff et al., (1997) used differential pulse anodic stripping voltammetry (DPASV), Landing *et al.*, (1995) and Yeats *et al.*, (1995) used ETAAS, whereas on AMT 9 FI-CL was used.

Saager *et al.*, (1997) reported ~ 15 % interlaboratory reproducibility, with up to 25 % interannual reproducibility being typical of a large part of published global trace metal dataset (Yeats *et al.*, 1995). Therefore, due to the differences above, it was anticipated that the Cu(II) data from the comparative authors would be lower. These differences should be noted in the following discussions on both the surface and vertical distribution of Cu(II) that follow.

5.3.4.3 Overview of Surface Cu(II) Concentrations

The north-south distribution of surface water (~ 7 m) Cu(II) concentrations along the AMT 9 transect is shown in Figure 5.15 a). Shipboard and UoP clean room determinations are shown for five stations to show the effects of storage on Cu(II) concentrations, with clean room Cu(II) data for the remaining stations. Also shown is hydrographic data collected en-route, namely chlorophyll *a* (Figure 5.15 b), nitrate and silicate (Figure 5.15 c). Figure 5.16 a) illustrates the surface water distributions of nitrite and phosphate, with the surface temperature and salinity profiles shown in Figure 5.16 b, and a temperature-salinity plot (Figure 5.16 c) that describes the surface water masses encountered during AMT9. The north-south surface distributions of Cu(II), temperature, salinity and nutrients will be discussed by reference to these Figures and to the province boundaries shown in Table 5.1.

Due to the limited number of onboard Cu(II) determinations, the clean room Cu(II) data is discussed for both the surface and vertical profiles at selected stations for the whole transect. The Cu(II) clean room concentrations were higher than shipboard data due to storage (Section 5.3.4.4) and differences in analytical methodologies (Section 5.3.4.2). This effect was more pronounced in regions of higher biomass and DOM e.g. European Shelf Waters and North Atlantic Drift due to increased organic and colloidal complexation of Cu(II).

5.3.4.4 Effect of Storage on Cu(II) Concentrations

The effects of acidification and subsequent storage on the Cu(II) concentrations can be seen by the comparison of shipboard with University clean room data (Table 5.11). The shipboard and clean room Cu(II) concentrations exhibited the same distribution profile, although the clean room values were consistently higher. Sample filtration (0.4 μm,

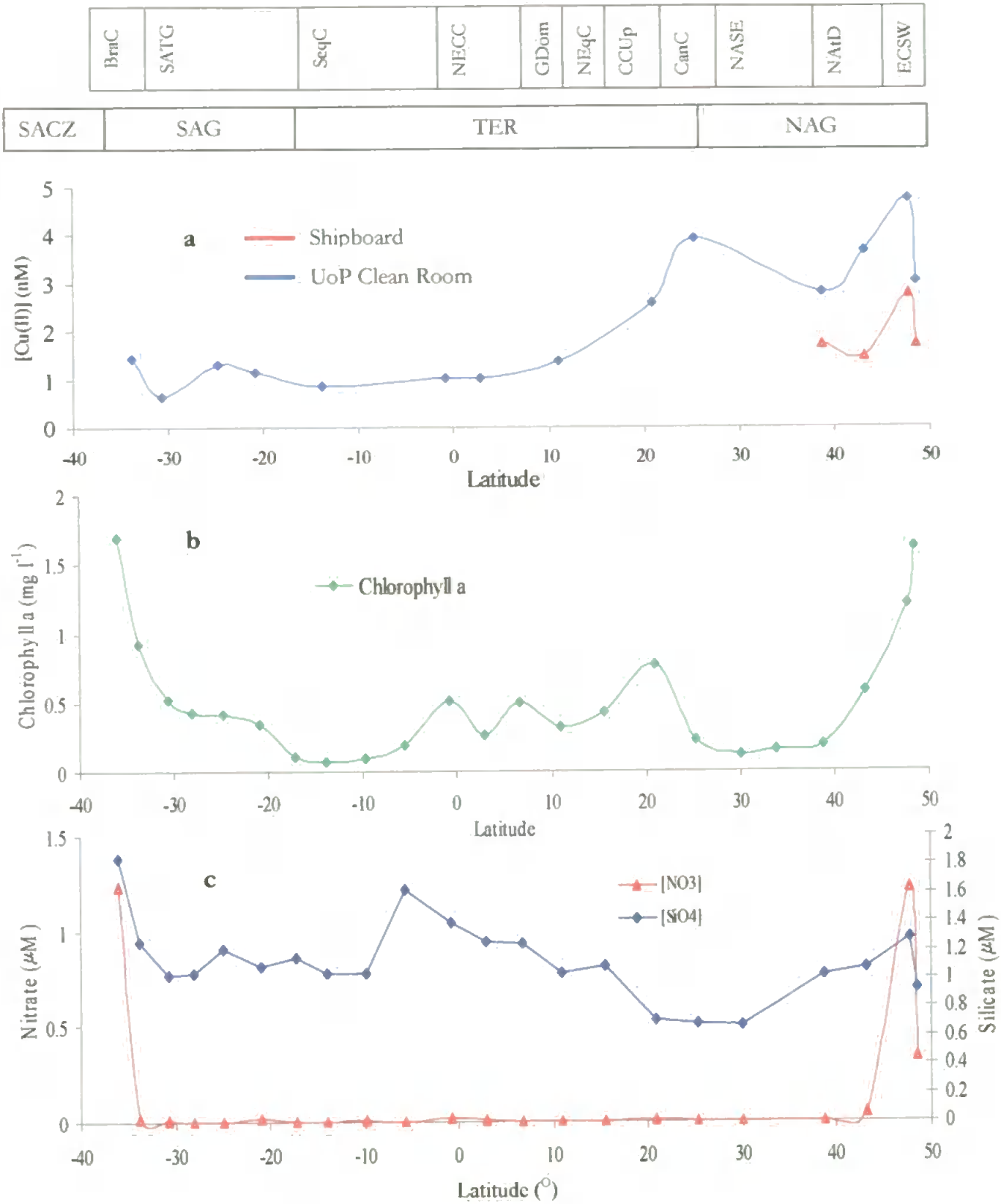

Figure 5.15 AMT 9 Surface (7m), Distributions along AMT 9 Track of a) Cu(II), (shipboard and UoP clean room) b) chlorophyll a, c) nitrate and silicate.

$[Si(OH)_4]$

N

S

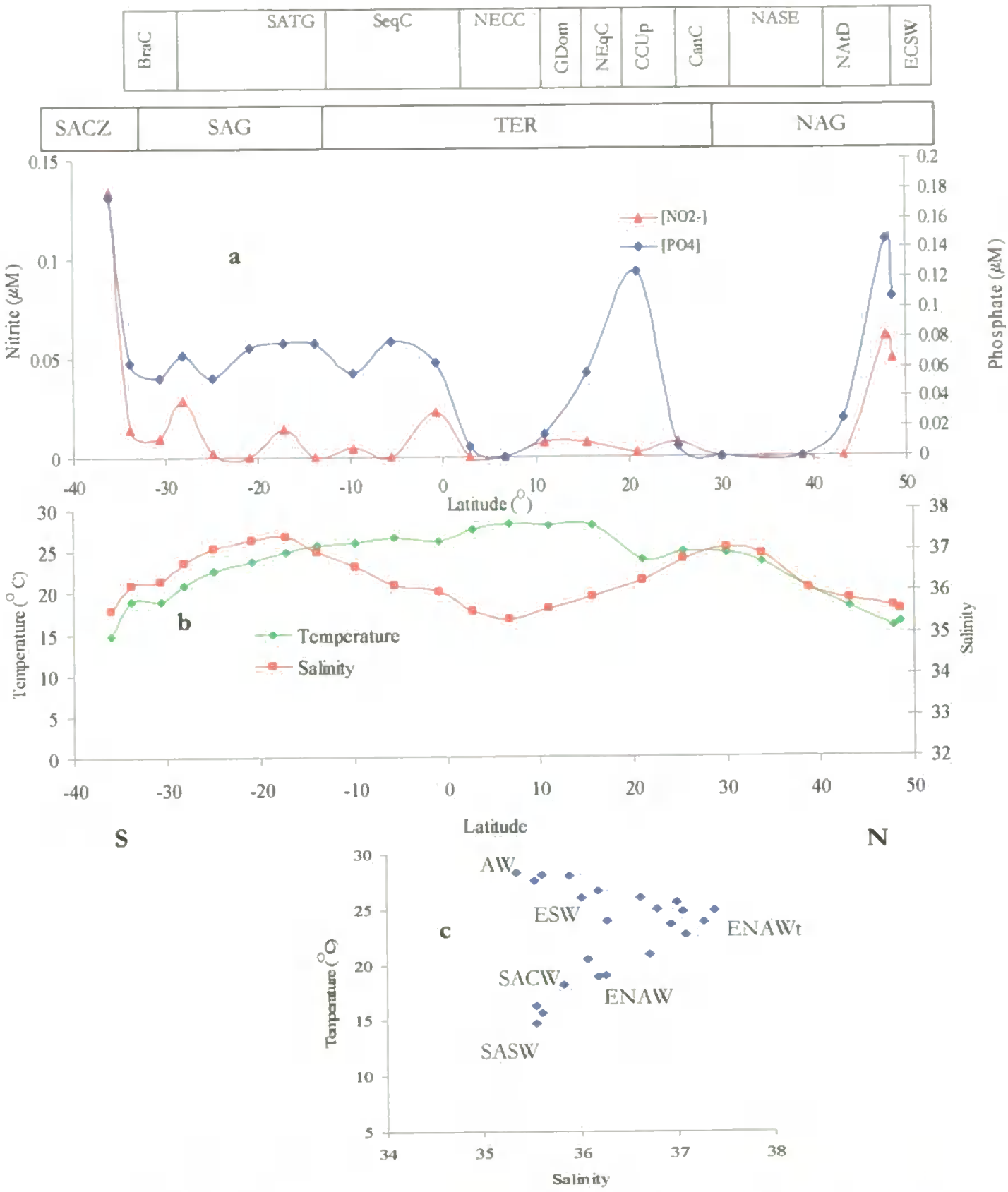

Figure 5.16 AMT 9 Surface (7m) Distributions along AMT 9 Track of a) NO_2, PO_4, b) surface temperature and salinity profiles, c) temperature vs. salinity plot

Table 5.11 Effect of Storage on Cu(II) Concentrations (nM)

AMT Station	Surface - Shipboard [Cu(II)]	Surface - Clean Room [Cu(II)]
901	1.7	3.0
902	2.77	4.7
904	1.5	3.7
905	1.7	2.8
AMT Station	**Vertical Profile - Shipboard [Cu(II)]**	**Vertical Profile - Clean Room [Cu(II)]**
901	4.0	5
902	2.0	3.3
904	2.92	2.67
905	1.92	2.7

Data presented for surface Cu(II) concentration was from 7 m with the mean Cu(II) concentration shown for the vertical profile.

Section 5.2.1.4) on AMT 9 yielded the dissolved Cu(II), the colloidal and the weakly organically complexed fractions of Cu(II). The increase in clean room Cu(II) concentrations compared to shipboard Cu(II) data was due to sample acidification, (Q-HNO_3) breaking down the colloidal and organic complexes during the storage (up to 9 months), and after competitive retention of Cu(II) during matrix separation by the 8HQ micro-column during Cu(II) determination by FI-CL. The shipboard and clean room data for the vertical Cu(II) profiles was in better agreement, a factor attributed to the lower concentration of DOM below surface waters (7 m).

5.3.4.5 Overview of Surface Water Distribution of Cu(II)

The surface (7 m) distribution of Cu(II) showed a high degree of spatial variability along the AMT 9 transect, with enrichments being superimposed on a horizontal gradient that decreased with departure south and then south-west away from the European coastal regions, through the open ocean gyres before climbing again at the South American Shelf. At the outset of the transect in European Shelf Waters, enhanced surface Cu(II) concentrations of 3.0 nM (AMT 901, 48.5 ^{o}N) and 4.7 nM (AMT 902, 47.8 ^{o}N) were observed. Cu(II) surface concentrations were lower in the North Atlantic Drift (NatD, 47.5 – 38.5 ^{o}N) at 3.7 nM (AMT 904, 43.2 ^{o}N) and decreased again to 2.8 nM (AMT 905, 38.8 ^{o}N) in the North Atlantic Subtropical Gyre East (NASE, 38.5 - 26.7 ^{o}N). A distinct Cu(II) enrichment to 3.9 nM was observed at AMT 908 (25.3 ^{o}N) off the West Coast of Africa, the highest open ocean, surface Cu(II) concentration observed on AMT 9.

Cu(II) concentrations gradually declined through sub-tropical waters to 2.6 nM in the Canary Current (AMT 910, 20.6 ^{o}N), 1.4 nM at the Guinea dome (AMT 914, 10.9 ^{o}N), ~1.0 nM across and immediately south of the equator (AMT 918, 919 2.8 ^{o}N and 0.8 ^{o}S), reaching 0.8 nM (AMT 925, 13.9 ^{o}S) at the northern edge of the open ocean South Atlantic Tropical Gyre (SATG, ~22.5 ^{o}S). Through the South Atlantic Gyre a slight increase in surface Cu(II) was observed between 20 - 26 ^{o}S to 1.1 nM (AMT 929, 20.9 ^{o}S) and to 1.3 nM (AMT 932, 24.8 ^{o}S), before falling to 0.6 nM (AMT 936, 30.6 ^{o}S), the lowest surface Cu(II) level observed on AMT 9. At the end of the AMT 9 transect, surface Cu(II) rose again to 1.4 nM (AMT 938, 33.8 ^{o}S), the highest South Atlantic surface concentration observed.

The distribution of surface Cu(II) along AMT 9 was in good agreement, both in concentration and distribution profile, with that reported by Rutgers van der Loeff *et al*,. (1997) on a geographically similar Atlantic transect from Bremerhaven, Germany to Punta Arenas, Chile during Oct-Nov 1990 (Figure 5.17) and thus subject to the same seasonal influences. This aspect is discussed further in the individual stations that represent the surface Cu(II) concentrations for each province.

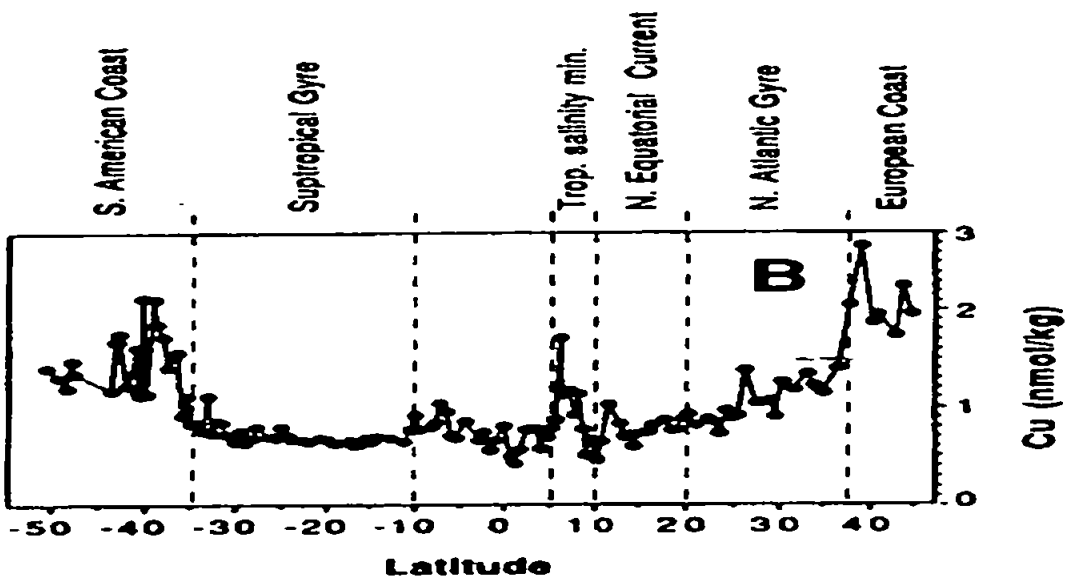

Figure 5.17 Surface (12 m) Distribution of Cu from Bremerhaven to Punta Arenas, Chile (Oct/Nov 1990, ANT IX/I) (van der Loeff *et al*,. 1997).

Table 5.12 shows the surface water concentrations of Cu(II) and other onboard hydrographic data for each province.

Table 5.12 Surface Water Cu(II) (7m) and Hydrographic Data (7m) for AMT 9

Oceanic Province (Hooker *et al.*, 2000)	Latitude	J. Day	Station	Cu(II) (nM)	Temp (°C)	Salinity (PSU)	NO_3 (μM)	NO_2 (μM)	PO_4 (μM)	$Si(OH)_4$ (μM)	Chlor *a* (μg l^{-1})
EU Cont. Shelf Water (ECSW)	50–47.5 °N	262-263	901	3.0	16.3	35.5	0.34	0.05	0.1	0.92	1.62
			902	4.8	15.7	35.6	1.23	0.06	0.14	1.28	1.20
N. Atlantic Drift (NatD)	47.5-38.5 °N	265-266	904	3.7	18.2	35.8	0.05	#	0.20	1.07	0.58
N. Atl. Subtropical Gyre East (NASE)	38.5-26.7 °N	267-268	905	2.8	20.4	36.1	#	#	0.03	1.02	0.18
			906		23.6	36.9	#	n/a	0.04	n/a	0.16
			907		24.8	37.1		#	#	0.68	0.12
Canary Current (CanC)	26.7-20.5 °N	269	908	3.9	24.9	36.8	#	0.007	0.007	0.69	0.22
Canary Current Upwelling (CCUp)	20.5–15.7 °N	270	910	2.6	24.0	36.3	0.014	0.003	0.12	0.71	0.77
N. Equatorial Current (NeqC)	15.7-12.4 °N	271	912		28.0	35.9	#	0.007	0.06	1.09	0.43
Guinea Dome (Gdom)	12.4- 7.9 °N	272	914	1.4	28.1	35.6	#	0.007	0.01	1.04	0.32
N. Equatorial Counter Current (NECC)	7.9-1 °N	273	916		28.3	35.3	#	#	#	1.24	0.49
			918	1.0	27.6	35.5		#	0.007	1.26	0.26
		274									
S. Equatorial Current (SeqC)	1° N–14.6 °S	275	919	1.0	26.1	36.0	0.02	0.023	0.06	1.39	0.51
			925	0.9	25.6	37.0	#	#	0.08	1.04	0.07
		278									
S. Atlantic Tropical Gyre (SATG)	14.6 – 30 °S	279	927 to	1.1	23.8	37.3	0.021	#	0.07	1.09	0.34
		282	934	1.3	22.7	37.1	#	0.002	0.05	1.21	0.41
Brazil Current (BraC)	30– 35 °S	283	936	0.7	19.0	36.3	0.09	0.01	0.05	1.02	0.51
		284	938	1.4	18.9	36.2	0.022	0.02	0.06	1.25	0.92
S. American Shelf (SASh)	35- 39.6 °S	285	940		14.8	35.5	1.24	0.13	0.17	1.84	1.69

The Cu(II) data presented in Table 5.12 was obtained in the UoP clean room after 9 months storage, and which by reference to the effect of storage on Cu(II) (Table 9) represents a larger fraction of total Cu(II) than was truly labile in seawater. Sample acidification during storage digested a substantial fraction of the organically complexed and colloidal Cu releasing it. # - data below instrumental LOD. n/a – data not available.

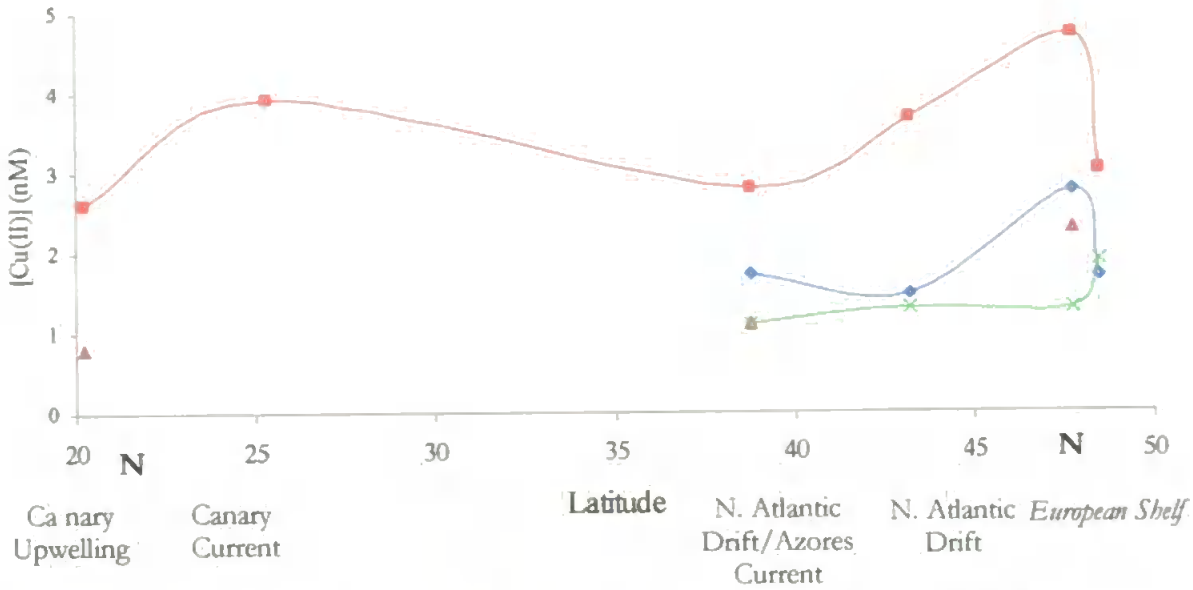

Figure 5.18 Comparison of Surface Water Cu Concentrations —— AMT 9 UoP Clean Room, —— AMT 9 Shipboard, ▲ van der Loeff *et al.*, (1997), —— Kremling and Pohl (1989).

5.3.4.6 European Shelf Waters

European Shelf waters (50 – 48 °N, AMT 901, 902) exhibited higher surface Cu(II) concentrations compared to more southerly AMT stations (Table 5.12). The AMT 9 shipboard Cu(II) concentrations compared well with van der Loeff *et al.* (1997) and Kremling and Pohl (1989) (Figure 5.18, Table 5.13). However, the University of Plymouth clean room values were higher than these authors at the European Continental Shelf, Canary Current and African Upwelling (Figure 5.18, Table 5.13, and Figures 5.16 a) and 5.17).

In the open-ocean further south, AMT 9 clean room Cu(II) values were in very good agreement with reported data e.g. van der Loeff *et al.*, (1997) due to the lower level of colloidal and dissolved organic material (DOM) and therefore a smaller fraction of organically complexed Cu(II) to be released upon acidification and storage. The surface Cu(II) level (7m) found on AMT 9 in the European Shelf and Western Approaches originated in part from the anthropogenic aerosol present down to latitudes of ~36/37 °N, that is variable in density and composition (Chester, 2000; Jickells, 1995; Duce *et al.*, 1991; Church *et al.*, 1990; Arimoto *et al.*, 1989). Helmers and Schrems (1995) also reported anthropogenic releases of Cu (and Pb, Mn, Zn) as heavily influencing the natural circulation patterns, global pathways and transport dynamics between the atmosphere and hydrosphere of these elements. Furthermore, Cu in urban generated aerosols has a higher solubility in seawater (32 +/- 16 %) than in lithogenic aerosols (25 % +/- 10 %) (unpublished data, Medway, 2001, University of Plymouth). A further influence on Cu(II)

concentrations were a series of deep depressions that crossed directly over the AMT 9 transect at its outset, their very strong anti-clockwise winds extending this aerosol veil further south and westward.

In European shelf waters, concentrations of NO_3, NO_2, PO_4, $Si(OH)_4$ and therefore chlorophyll *a* were also raised. Surface nitrate concentrations were above the LOD (> 0.05 μM) only in the European and South American Shelf areas.

5.3.4.7 North Atlantic Drift (NAD)/Subtropical Gyre East (NASE)

This region (48 - 26.7 °N) was characterised by a sharp fall in surface Cu(II) to 3.7 nM (AMT 904, 43.2 °N) and 2.81 nM (AMT 905, 38.8 °N) and a substantial reduction in surface macro-nutrients and chlorophyll *a*. Surface salinity concentrations rose through both of these provinces, although the dip in temperature between AMT 901 (48.5 °N) and AMT 902 (47.7 °N) suggested a permanent frontal system at ~47 °N (also reported by Bowie, 1999) resulting in poor lateral mixing of the water masses. Shipboard surface Cu(II) concentrations (AMT 9) through this province were in good agreement with previously reported data for this region (Table 5.13), although the clean room Cu(II) data were higher due to storage effects (Table 5.11).

Table 5.13 Surface Cu Concentrations in NAD and NASE Provinces

Province & AMT Station	AMT 9 (nM) Shipboard	UoP Clean Room (nM)	van der Loeff *et al.*, (nmol kg) (1997)	Saager *et al.*, (1997) (nM)	Kremling and Pohl (1989) (nM)	Yeats *et al.*, (1995) (nM)	Landing *et al.*, 1995 (nM)
NAD 904	1.5	3.7	1.8 - 2.8	1.0	1 - 2	n/a	0.8 - 1.2
NASE 905	1.7	2.8	0.9 - 1.3	1.2		0.7-1.5	

n/a –data not available

A *t* test ($p = 0.05$) showed that the differences were not significant between the Cu(II) as determined by FI-CL and other reported data, demonstrating the oceanographic consistency of the FI-CL Cu(II) results. The higher AMT 9 surface Cu(II) values through this region compared to stations further south could be attributed to the dynamic nature of marine systems coupled to the advection south of Cu rich waters in the North Atlantic Current (NAC, Figure 5.12) (van der Loeff *et al.*, 1997). Kremling and Pohl (cruise area ~ 38 – 50 °N, 0 – 25 °W, 1989), identified the importance of the relatively high fluvial and atmospheric inputs of Cu into North East Atlantic Surface waters, which receive a higher atmospheric metal loading than other Atlantic shelf areas e.g. the North American shelf.

5.3.4.8 Canary Current and Canary Upwelling

In the Canary Current (26.7 – 20.5 ^{o}N) at AMT 908 (25.33 ^{o}N) ~ 650 km west of the Mauritanian coast, the highest open ocean, AMT 9 surface (7 m) Cu(II) concentration of 3.9 nM was observed, with raised Cu(II) (2.6 nM) also found further south at AMT 910 (20.2 ^{o}N) in the Canary Upwelling section (20.5 – 15.7 ^{o}N) of the Guinea Dome (~22 – 9 ^{o}N).

The Cu(II) enrichment at AMT 908 was also observed by van der Loeff *et al.*, (1997) although at a lower concentration. The enrichment was most probably due to a high lithogenic particulate loading from the episodic and the highly variable (both seasonally/daily and in intensity), dust storms in N. W. Saharan and Southern Sahara/Sahel. The dust was transported westward in the North East Trades and the strong African Easterly Jet stream respectively that characterise this region. The subsequent release of particulate exchangeable Cu was superimposed on the Cu(II) rich waters that were advected south. Dust maximums have been recorded at ~3000 m between 17 – 21 ^{o}N, with the highest aerosol deposition to surface waters occurring north of 20 ^{o}N (Helmers and Schrems, 1995). This aerosol reaches a maximum in the summer months (Kremling and Streu, 1993; Husar *et al.*, 1997). Saharan dust was present in the air at this AMT station indicating the high aerosol particulate flux also present on AMT 9.

Kremling and Streu (1993), using sediment traps off the North African coast, identified atmospheric sources as dominating the trace metal fluxes through this region, although lithogenic aerosol Cu has reduced solubility in seawater compared to anthropogenic origin (Jickels, 1995). Maring *et al.*, 2000 also reported dust concentrations exceeding 4000 μg m^{-3} close to the Canary Islands (~27 ^{o}N), with reduced concentrations (200 μg m^{-3}) further south at the Cape Verde Islands. Chester (2000) also concluded that in near coast regions, solubilisation from atmospheric particulates can play a significant role in governing the trace metal burden of the surface water. The increase in surface PO_4, a particulate associated element, seen at this station supports the hypothesis of dry depositional input. Effects on concentration have been reported over a short, but variable time scale following deposition (Quetel *et al.*, 1993). This implies that a non steady state behaviour must be taken into account when assessing the impact of pulsed atmospheric inputs on particle trace element concentrations and fluxes in the water column.

In addition to atmospheric deposition, the Cu peak at AMT 908 was due to the integrated effect of Cu inputs over a longer time period due to advection south (Canary Current) of Cu rich waters from the NAD/SATG, combined with the slow biological removal of Cu compared to other trace metals. Van der Loeff *et al.*, (1997) also found

elevated Cu values from 40 – 15 ^{o}N and ascribed it to Cu having a residence time in seawater 25 times longer than Al due to lower particle scavenging activity in the surface waters of the Canary and North Equatorial Currents.

Further south, AMT 910 (20.2 ^{o}N) was influenced by surface filaments from the main upwelling drifting offshore as indicated by a steady increase in onboard fluorescence (chlorophyll *a*) through the afternoon, peaking at 1830 GMT. A corresponding open ocean, surface chlorophyll *a* maximum for AMT 9 was found. At AMT 910, the Canary Current Upwelling zone was also identified by a significant increase in surface PO_4, and a small rise in surface NO_3/NO_2, although still demonstrating surface depletion.

Cu(II) surface (7 m) concentrations were still elevated at AMT 910 (2.6 nM) due in part to the still raised aerosol particulate level and Cu in the Canary Current, although these were both reduced compared to AMT 908. This was consistent with the observation of Helmers (1996), who also reported elevated concentrations of SPM bound Cu (and other trace metals) at 20 – 15 ^{o}N and increased particulate organic carbon (POC) over 20 – 8 ^{o}N.

5.3.4.9 North Equatorial Current/Guinea Dome

Both provinces had skies still hazy with Saharan dust although at a lower level as the JCR changed course toward Montevideo (0248 GMT on JD 272 - AMT 914, 10.9 ^{o}N), departing the African coast. The North Equatorial Current (NEC, 15.7 – 12.4 ^{o}N) was identified by an AMT 9 surface salinity minimum and a rise in temperature (Section 5.3.3.2). The southern boundary of the Guinea Dome (12.4 – 7.9 ^{o}N) was indicated by a deepening of its compacted isothermals at ~ 10 ^{o}N, in the north of the Inter Tropical Convergence Zone (ITCZ) (~ 10 – 0 ^{o}N). The ITCZ was characterised by wet deposition due to the convergence of the dominant trade winds that transported West African dust and induced intense shower activity (up to 2000 mm yr^{-1}, Helmers and Schrems, 1995). These were often short lived and extended over a small area e.g. on JD 273/AMT 916 (coinciding with the salinity minima at ~ 5 ^{o}N (Figure 5.17).

The concentration of surface Cu(II) (7 m) continued the previously noted decreasing trend as the JCR departed coastal influences towards the open ocean. A Cu(II)concentration of 1.4 nM was observed at AMT 914 reflecting reduced dry Saharan atmospheric deposition coupled with biological uptake, organic complexation and particulate scavenging. Helmers (1996) identified a shift in Cu adsorption towards higher particulate concentration in this province. Through the ITCZ, on AMT Cu(II) concentrations remained at ~1.0 nM reflecting wet atmospheric scavenging of Cu from particulate material solubilised in cloud processes or in the surface seawater (Spokes *et al.*,

1996). Wet deposition dominates over dry for Cu in the tropical North Atlantic with raised Cu in the high annual rainfall (Cu - 0.91 μg l^{-1} (4 °N 20 °W); 0.40 μg l^{-1} (5 °N 28 °W)), strongly influencing the trace metal budget and surface water chemistry in the ITCZ (Helmers and Schrems, 1995). Church *et al.*, (1990) also reported the predominant wet scavenging of Cu, Cd, Ni, Pb and Zn from the troposphere in the ITCZ. Shelf and riverine inputs were also identified between 5 – 9 °N by van der Loeff *et al.*, (1997) as contributing Cu, $Si(OH)_4$, NO_3, and POC.

In these provinces, raised onboard surface fluorescence indicated surface filaments from the main Mauritanian upwelling advected south in the NEC. Surface and mean water column concentrations of chlorophyll *a* reached a maximum in the NEC, coincident with the raised Cu(II) concentrations, prior to declining slowly through these provinces to reach ~ 0.35 μg l^{-1} at 11 °N (AMT 914), the southern boundary zone of the Guinea Dome. Through these provinces surface PO_4^{3-} concentrations were sharply reduced from the previous peak observed at 20 °N in contrast to increasing surface $Si(OH)_4$ values.

5.3.4.10 North Equatorial Counter (NECC) and South Equatorial Currents (SeqC)

Equatorial surface Cu(II) concentrations were consistently low at 1.0 nM at both AMT 918 (2.8 °N) in the NECC (7.9 – 1 °N) and AMT 919 (0.8 °S) in the SEqC (1 °N – 14.6 °S), Cu(II) declining further to 0.85 nM (AMT 925, 13.9 °S). The pronounced rise in surface PO_4, NO_2, and $Si(OH)_4$ between AMT 918 and 919 and further rise in $Si(OH)_4$ at AMT 921, the increase in subsurface Cu(II) (AMT 918 and 919) together with the lower salinity in the NECC (Figures 5.15 and 5.16) suggested a freshwater Cu and nutrient input through these provinces. North of the equator, this was due to wet deposition in the ITCZ/NEC. South of the equator the $Si(OH)_4$ signature strongly indicated the surface influence (down to ~ 100m) of lenses of Amazon Water (AW) advected eastward in the NECC (Dessier and Donguy, 1994), with the residual freshwater signatures of $Si(OH)_4$ nutrients, Cu, POC and Cd also reported in this province by van der Loeff *et al.*, (1997).

The fluctuations in surface chlorophyll *a* values observed through the NECC - 0.5 μg l^{-1} at AMT 916 (6.7 °N) falling to 0.26 μg^{-1} l at AMT 918 (3 °N) and then rising to 0.5 μg l^{-1} at AMT 919 (~ 1 °S, Figure 5.15 b), were a response to the reduced surface macro-nutrient concentrations observed between AMT 916 and 918 and the subsequent rise nutrients at AMT 919. Onboard fluorescence rose (p.m. of JD 274) prior to crossing the equator (JD 275, 0647 GMT), which indicated the equatorial upwelling and preceded the surface chlorophyll *a* peak at station AMT 919 (0.5 μg l^{-1}). Surface chlorophyll *a*

concentrations then declined through the SEC to reach an open ocean minima (0.07 μg l^{-1}) between AMT 925 – 927, despite PO_4 (0.06 μM), NO_2 (0.025 μM), and $Si(OH)_4$ (0.8 μM) being present. Surface $Si(OH)_4$ across the equatorial region continued the rise first observed at 20 ^{o}N, rising further through the SEC prior to falling sharply at AMT 923 in the SeqC.

5.3.4.11 South Atlantic Tropical Gyre (SATG)

The SATG (14.6 to 30 ^{o}S, encompassing AMT 927 - 17.2 ^{o}S, 929 - 20.9 ^{o}S, 932 - 24.8 ^{o}S and 934 - 28.0 ^{o}S, was the most remote province encountered on AMT 9, with much reduced continental influences. In the absence of upwelling or significant wet deposition, this region was dominated by long range dry aerosol deposition (Chester, 2000) as typified by Cu, associated as it often is with particulates < 1 μM, that therefore travel long distances and contribute to open ocean surface concentrations. Surface Cu(II) at 1.1 and 1.3 nM at AMT 929 and 932 respectively, were higher than the previous NECC/SEqC region, probably due to dry aerosol deposition and reduced biological uptake in this low chlorophyll *a* province.

Surface $Si(OH)_4$, PO_4 and NO_2 concentrations fluctuated in the SATG, although still raised as observed in the SeqC and compared to more northerly AMT stations. $Si(OH)_4$ was consistently > 1 μM. Nitrite and PO_4 fell between AMT 927 -932 (~17 – 25 ^{o}S,) before rising at ~28 ^{o}S (AMT 934) due to a pulsed input from the Brazilian Current (BC). The BC forms the western boundary current (down to ~ 44 ^{o}S and to a depth of ~ 200 m) of the SATG, and advects southwards, along the continental margin into the western South Atlantic, both SACW and South American aerosol and fluvial inputs. These inputs may have contributed to the rise in Cu(II) at AMT 932. Surface (and mean upper water column) salinity values reached a maximum for AMT 9 due to high temperatures and lack of rain in this province. NO_3 exhibited surface depletion (<LOD) throughout the SATG. Mean chlorophyll *a* concentrations through this region were correspondingly low (~0.35 μg l^{-1}), typical of an open ocean gyre despite raised nutrients suggesting other biolimiting influences. Surface concentrations rose further south ~ 24 – 28 ^{o}S (AMT 929 – 934).

5.3.4.12 Brazil and Falklands Current Confluence (BFCC)

This province encompassed the confluence of the southern extremity of the warm, saline BC (30 – 35 ^{o}S) and the northern limit of the cold, less saline sub-Antarctic waters

advected north in the Falkland Current (FC). The BC separates from the South American coast at ~ 33 - 38 ^{o}S, forming the sub-Antarctic front with the FC, which itself separates from the South American Shelf break at ~ 38 ^{o}S.

The BC and FC surface waters undergo transitional mixing within a 300 km wide confluence zone, that is characterised by seasonal variability and intense eddies that form large areas of water that travel long distances into opposing water masses prior to dispersal (Olson *et al.*, 1988). The confluence is at its northern extreme during the winter. AMT 936 (30.6 ^{o}S), 938 (33.8 ^{o}S) and 940 (36.0 ^{o}S) were at the northern and southern boundaries of the South American Shelf and in the Sub-Antarctic Convergence zone respectively.

At AMT 936 surface (7 m) Cu(II) concentrations fell to the AMT 9 open ocean surface minimum of 0.7 nM, probably due to reduced Cu input coupled to increased biotic uptake and organic complexation resulting from the nutrient stimulated chlorophyll *a* increase (see below). Further south at AMT 938, Cu(II) rose again to 1.4 nM, due to upwelled waters at the South American shelf, shelf regeneration processes, and fluvial and aerosol Cu(II) inputs advected south in the BC. These may have been combined with the influence of Cu(II) advected north in the FC and Cu(II) in the Rio de la Plata plume, the latter indicated by raised $Si(OH)_4$ and a fall in salinity that suggested a freshwater input. Surface water temperature fell between AMT 938 – 940 signifying mixing of the cold FC with the BC and resulting in convergence circulation that concentrated material along the front.

Surface PO_4, NO_2 and $Si(OH)_4$ concentrations rose at AMT 934, situated in the BC on the BFCC's boundary with the SATG, due to the processes described above. The nutrients stimulated sharp increases in chlorophyll *a* to ~ 1.75 μg l^{-1} at AMT 940 (36 ^{o}S), a surface level only observed in European Shelf surface waters. At AMT 936 the raised chlorophyll *a* subsequently depleted the PO_4, NO_2 and $Si(OH)_4$, which began to rise again by AMT 938 (~34 ^{o}S). All nutrients rose very sharply to European Shelf concentrations at AMT 940 (36 ^{o}S), where the increase in surface NO_3 was especially noteworthy.

The raised chlorophyll *a* indicated the South Atlantic austral bloom, also observed on AMT 3 (1996), particularly the increased diatom population in these temperate waters (Maranon and Holligan, 1999). This hypothesis was supported by the reduction between AMT 932 - 934 of the previously consistently elevated $Si(OH)_4$, a prerequisite for diatom growth and the depletion of PO_4 and NO_2.

For AMT 936, 938 and 940, a good correlation was found between reduced salinity and increases in both chlorophyll *a* and macronutrients (Figures 5.19 & 5.20). This implied a conservative mixing of the less saline FC with the BC and supported the hypothesis that

the FC and the Rio de Plata supplied nutrient rich waters to this province, promoting chlorophyll *a*. A low correlation (0.07, Figure 5.19) was found between salinity and Cu(II) for this province suggesting that other influences besides mixing of water masses were dominant for Cu(II).

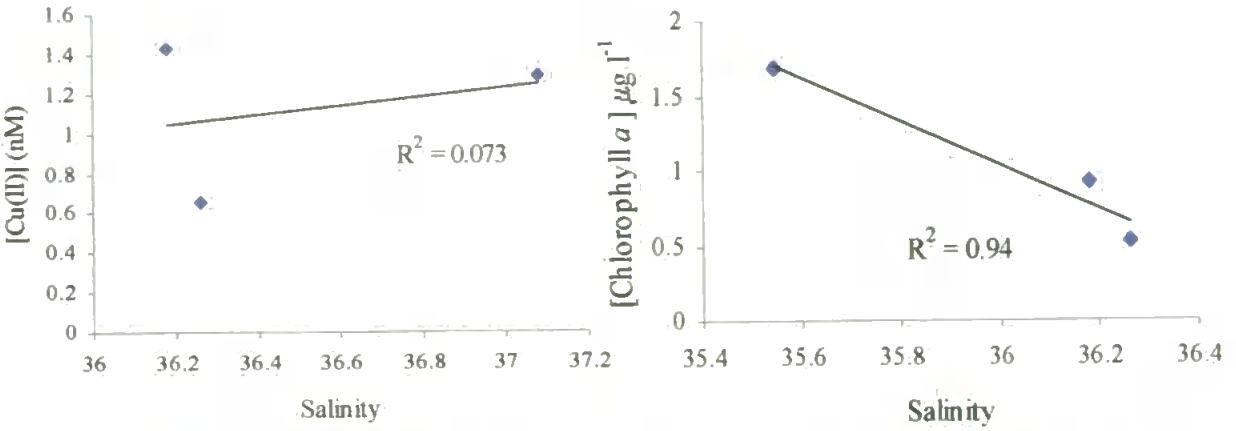

Figure 5.19 Correlation between Salinity and Cu(II) and Salinity and Chlorophyll *a* for AMT 932, 936 and 938

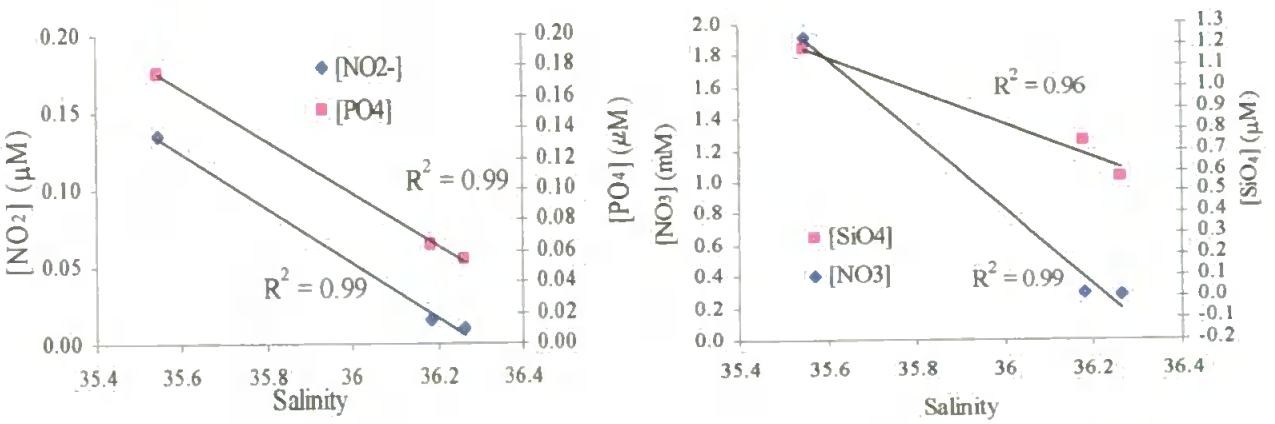

Figure 5.20 Correlation between Salinity and NO_2/ PO_4 and Salinity and NO_3/$Si(OH)_4$ for AMT 932, 936 and 938

In summary the increased and variable concentration of nutrients and Cu(II) at the southernmost AMT 9 stations in this province were due to strong coastal and internal advective and upwelling processes combined with mixing of the BC with the FC.

5.3.5 Vertical Profiles of Cu(II)

5.3.5.1 Overview

The vertical distribution (0 – 250 m) of Cu(II), the nutrients NO_3, NO_2, PO_4 and $Si(OH)_4$ the hydrographic data for temperature (T), salinity (S) (with a T-S plot describing the structure of the upper water column) and transmissometer readings with biological

(chlorophyll *a*) observations are presented for 10 selected AMT 9 stations (Figures 5.22 – 5.31). Each depth profile represents an Atlantic biogeochemical province based on the designation of Hooker *et al.*, (2000), as far south as the northern boundary of the South American shelf province, the limit of Cu(II) determinations on AMT 9 and for which no vertical profiles are shown. For discussion purposes, the Canary Current and Canary Upwelling are combined under one heading. The data is summarised in Table 5.14.

The range of diverse input, removal and physical oceanographic processes imposed fluctuations in the depth profile of Cu(II) during AMT 9, with an interpretation of these interrelated mechanisms also presented. The depth profiles show Cu(II) behaving as a bio-intermediate element displaying nutrient type surface depletion due to biotic uptake and complexation, removal in the upper water column due to these same processes and SPM scavenging, with a gradual regeneration of Cu(II) through the lower water column water resulting from biomass degradation and benthic regeneration (Chester, 2000). Precision of the FI-CL analyser during determination of Cu(II) in sub-aliquots from the same Inter-Ocean sampler bottle and the same HDPE sample bottle was 7 % r.s.d. (n=4).

5.3.5.2 European Continental Shelf Waters (ECSW) (AMT 901)

This station (Figure 5.21) was situated close to the steeply shelving continental shelf break (500 m) and represented a dynamic transition zone between oceanic and shelf regimes. It was a nutrient rich zone with the dominant currents moving up the continental slope. In the surface and subsurface water (0 – 40 m), concentrations of all macro-nutrients were relatively high (Figure 5.21) in contrast to open ocean provinces further south where concentrations were generally < LOD (0.02 μM). The significant increase in nutrients (nutricline) and decrease in temperature (thermocline) and slight rise in salinity at ~ 50 m suggested a strongly stratified mixed layer at a shallow depth and also provided evidence of upwelled waters. The temperature-salinity plot indicated little mixing of water masses with a front indicated at ~ 47 ^{o}N.

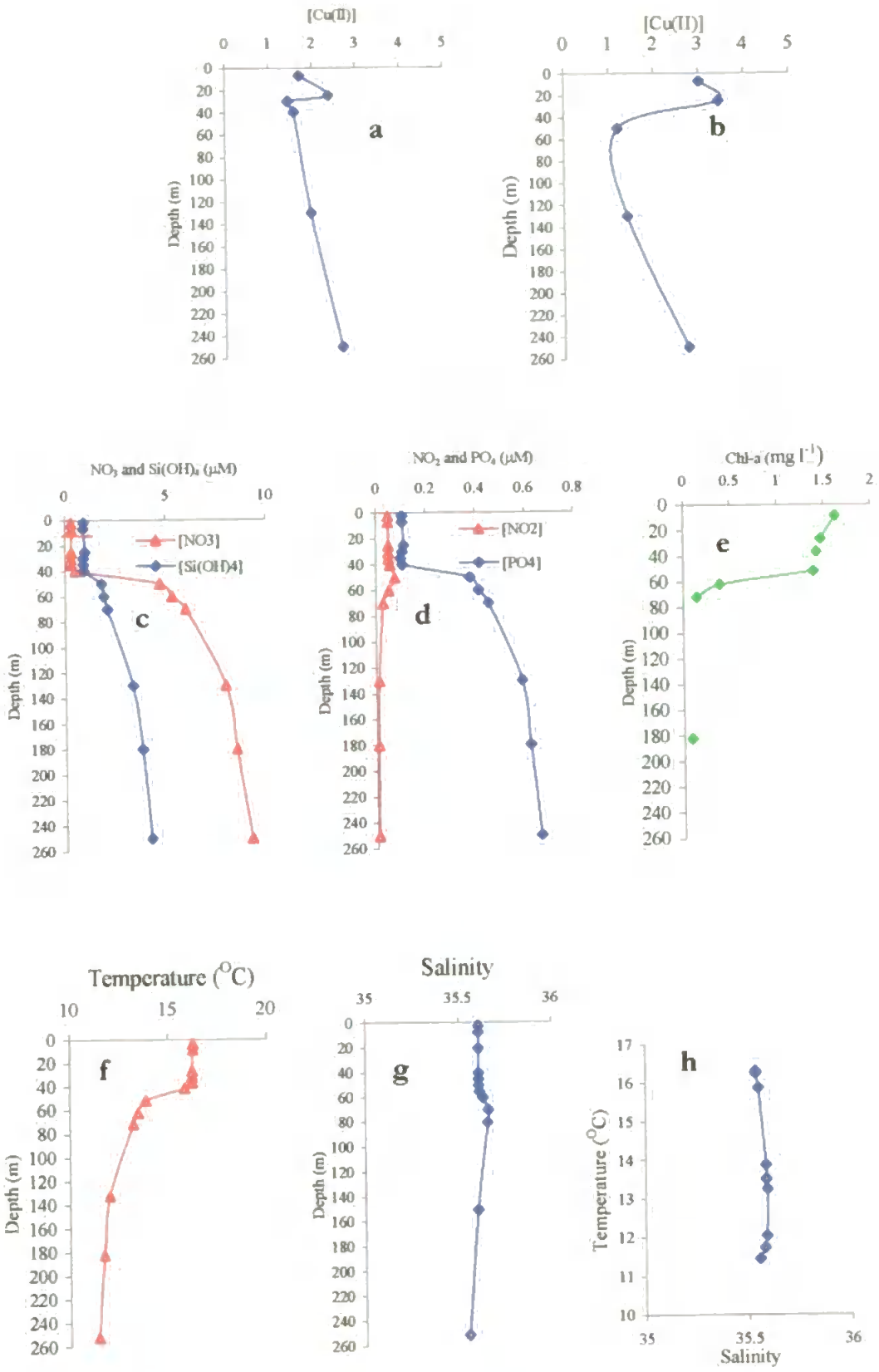

Figure 5.21 Vertical Profiles at AMT 901 for Cu(II) a) Shipboard b) Clean Room c) NO_3 and $Si(OH)_4$, d) NO_2 and PO_4, e) Chlorophyll *a*, f) Temperature, g) Salinity, h) Salinity /Temperature.

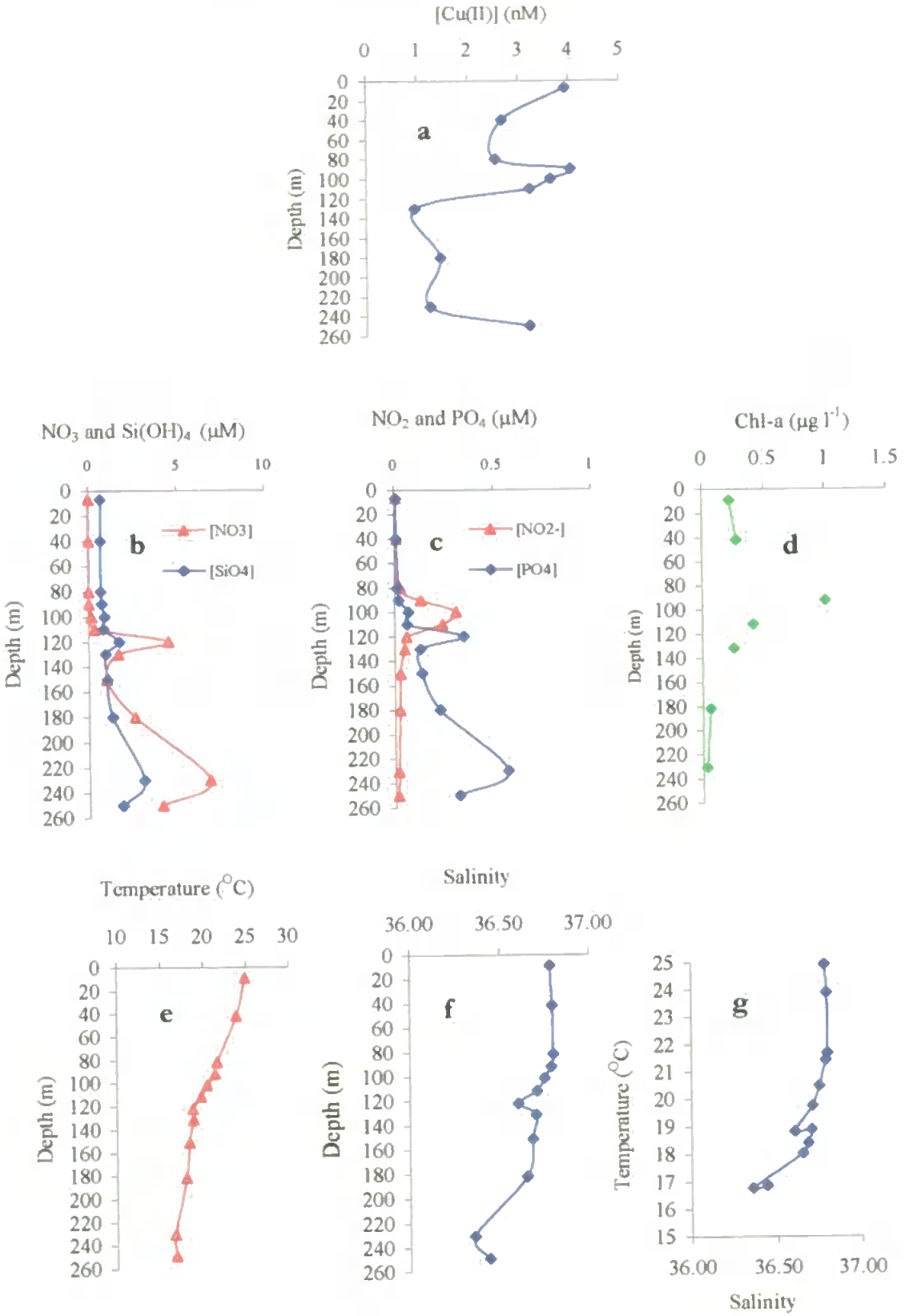

Figure 5.22 Vertical Profiles at AMT 908 for a) Cu(II) (clean room), b) NO_3 and $Si(OH)_4$, c) NO_2 and PO_4, d) Chlorophyll *a*, e) Temperature, f) Salinity, g) Salinity/Temperature.

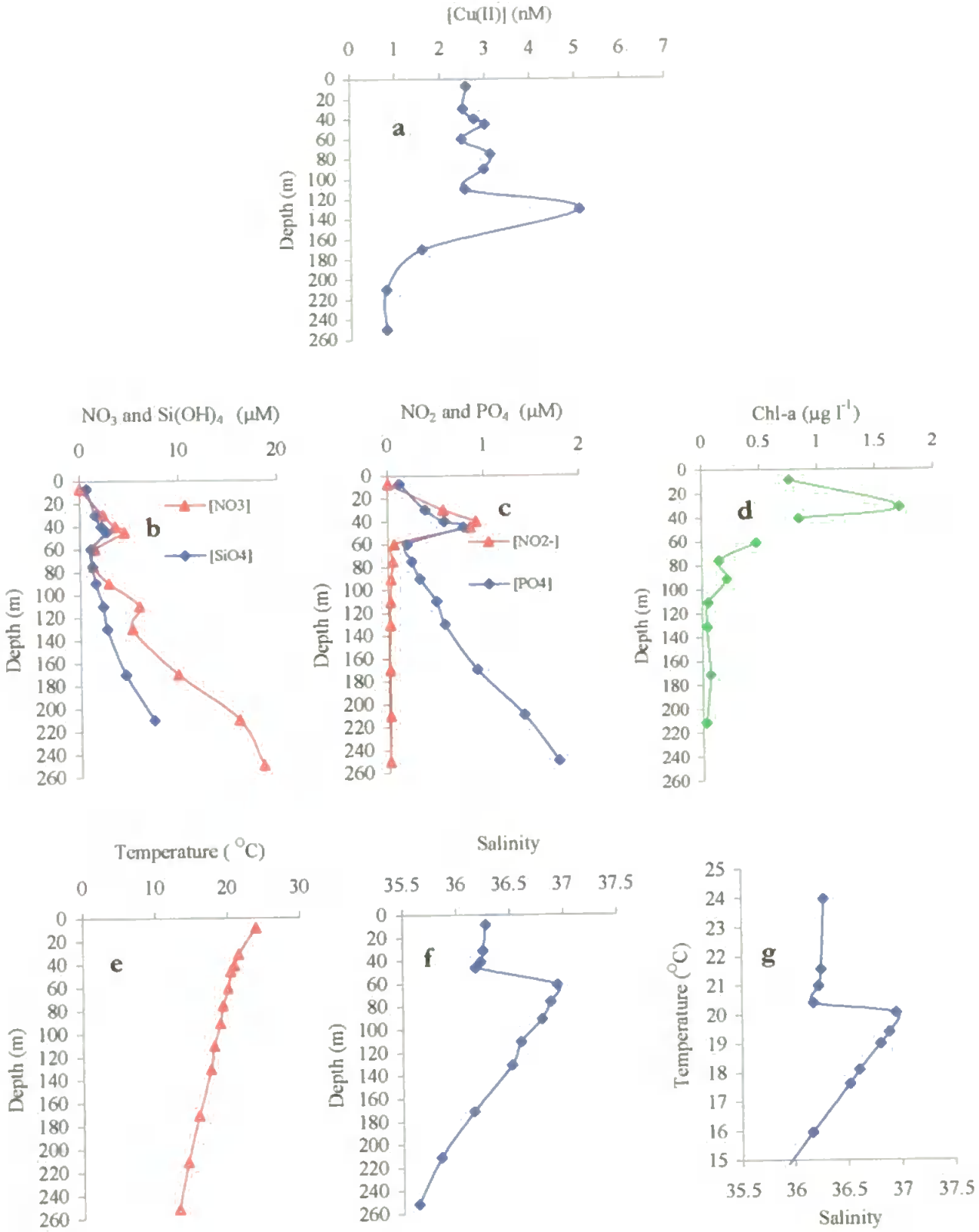

Figure 5.23 Vertical Profiles at AMT 910 for a) Cu(II) (clean room) b) NO_3 and $Si(OH)_4$, c) NO_2 and PO_4, d) Chlorophyll *a*, e) Temperature, f) Salinity, g) Salinity/Temperature.

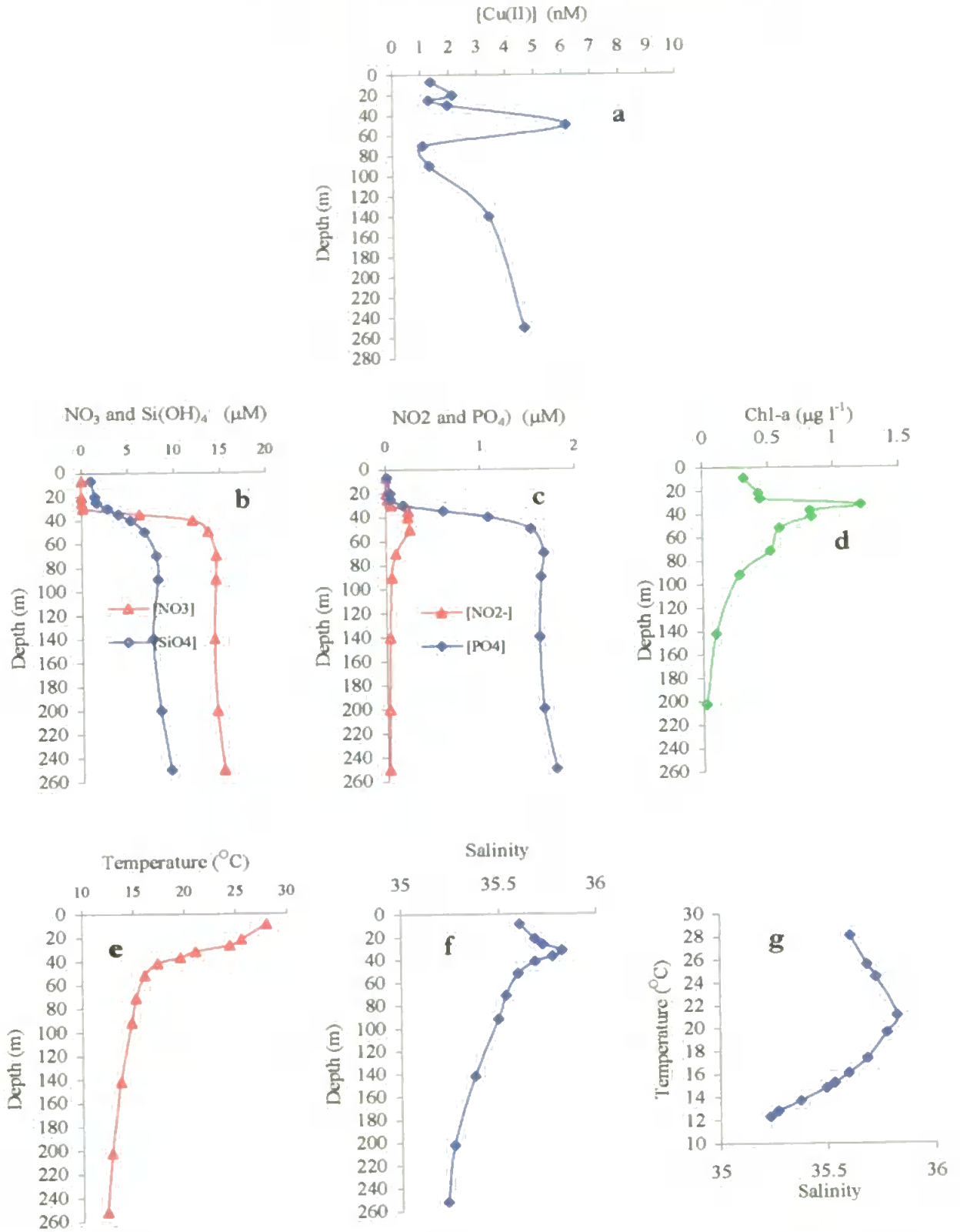

Figure 5.24 Vertical Profiles at AMT 914 for a) Cu(II) (clean room) b) NO_3 and $Si(OH)_4$, c) NO_2 and PO_4, d) Chlorophyll *a*, e) Temperature, f) Salinity, g) Salinity/Temperature

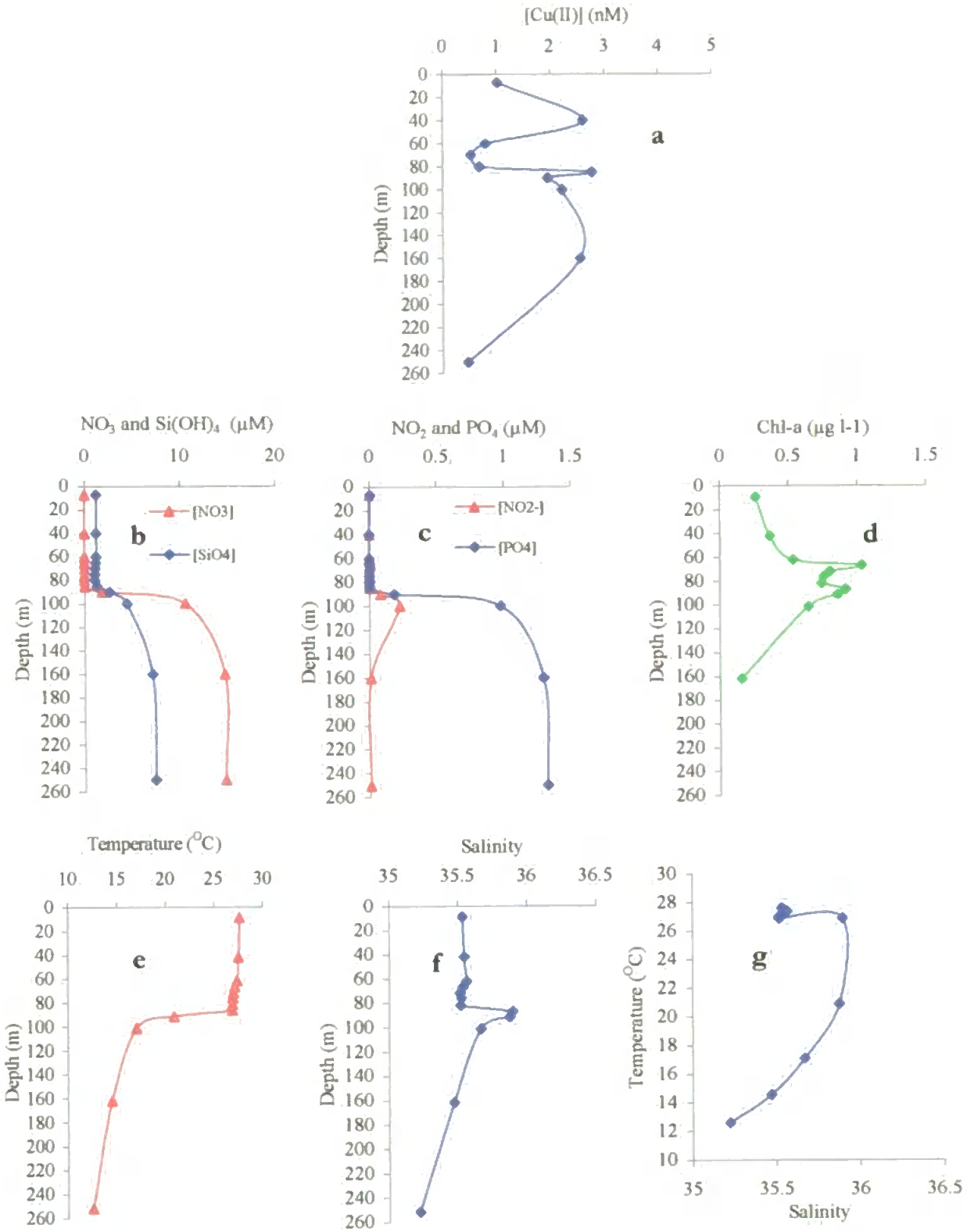

Figure 5.25 Vertical Profiles at AMT 918 for a) Cu(II) (clean room) b) NO_3 and $Si(OH)_4$, c) NO_2 and PO_4, d) Chlorophyll *a*, e) Temperature, f) Salinity, g) Salinity/Temperature

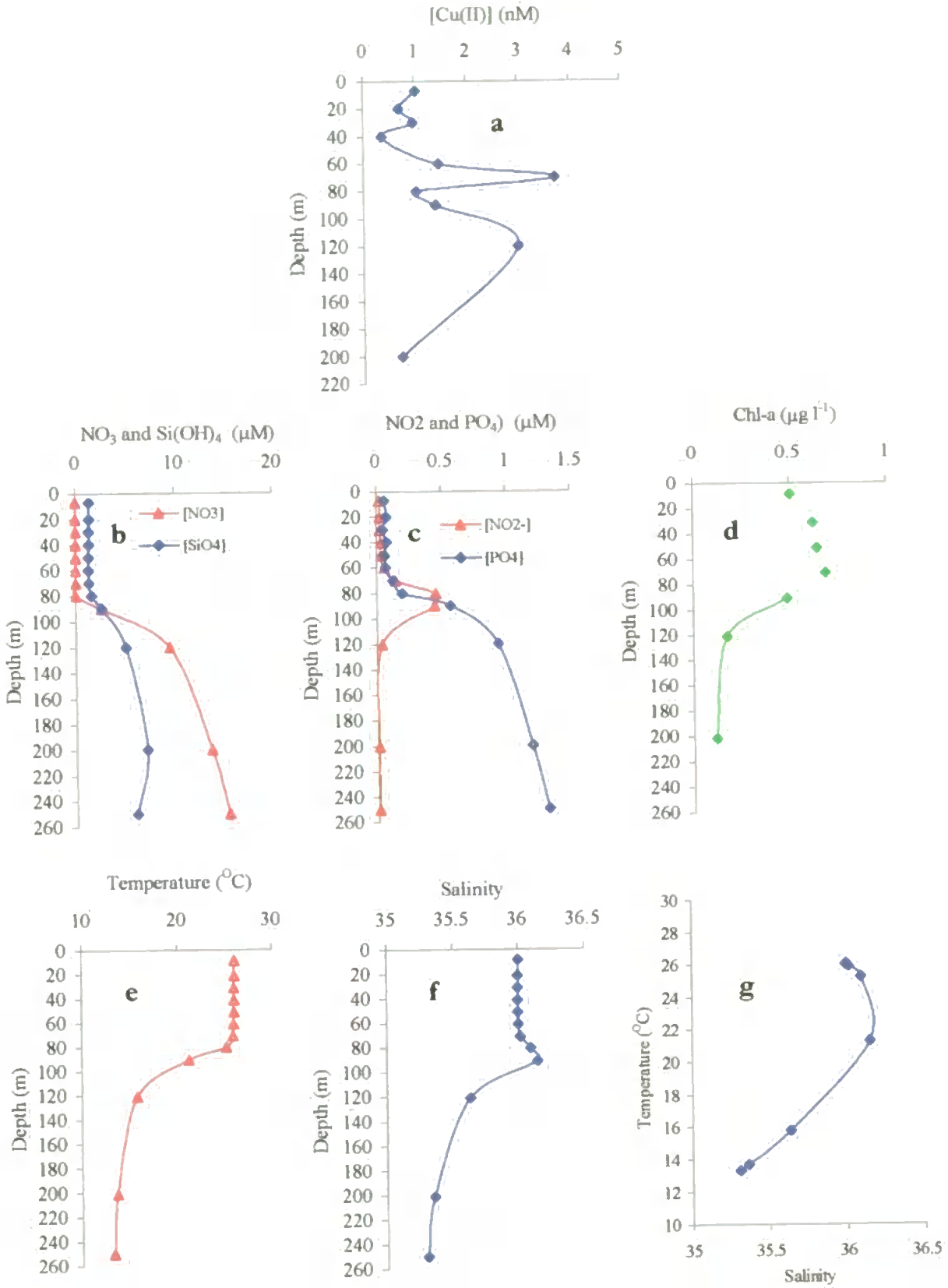

Figure 5.26 Vertical Profiles at AMT 919 for a) Cu(II) (clean room) b) NO_3 and $Si(OH)_4$, c) NO_2 and PO_4, d) Chlorophyll *a*, e) Temperature, f) Salinity, g) Salinity/Temperature

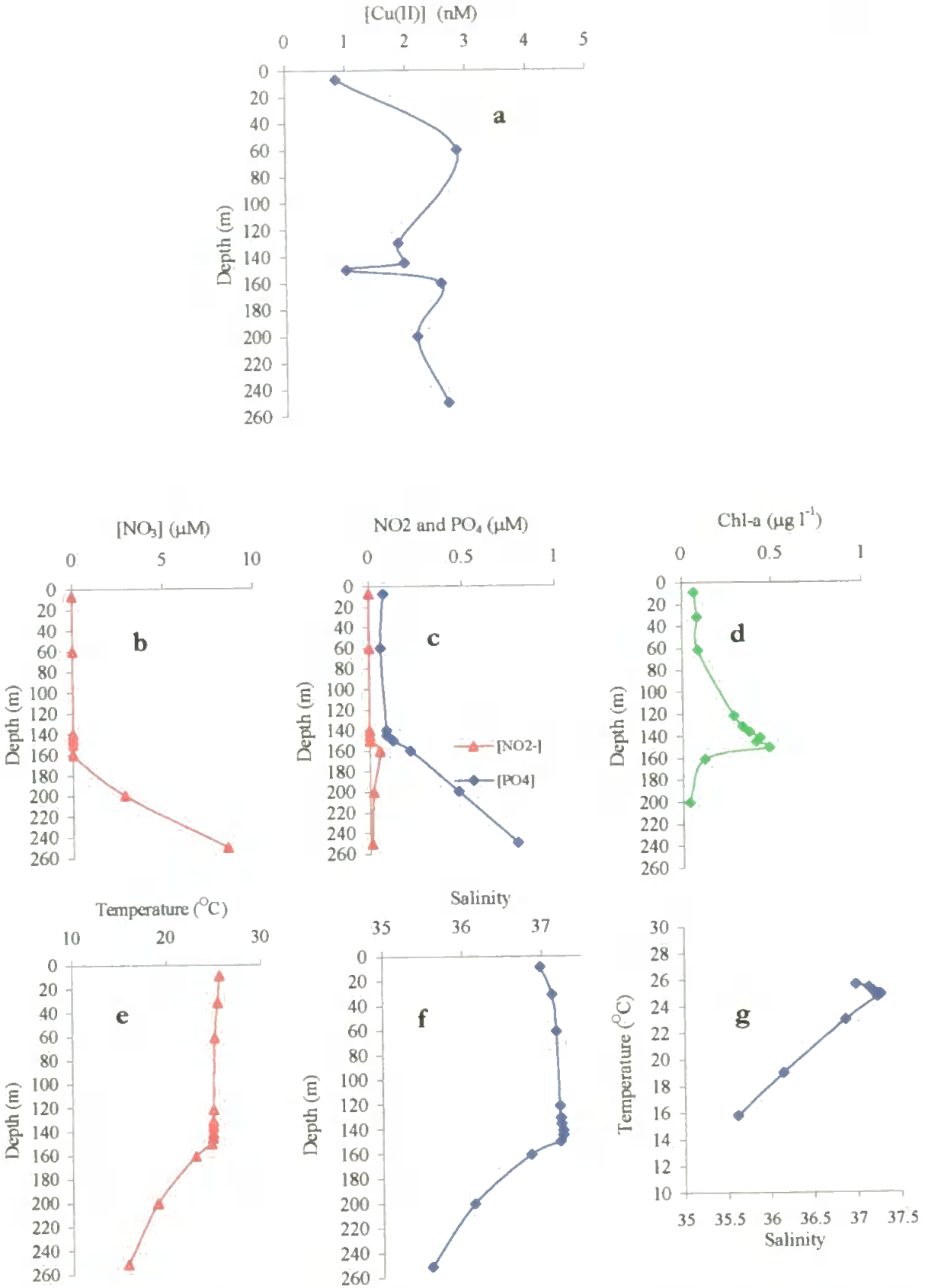

Figure 5.27 Vertical Profiles at AMT 925 for a) Cu(II) (clean room) b) NO_3 and $Si(OH)_4$, c) NO_2 and PO_4, d) Chlorophyll *a*, e) Temperature, f) Salinity, g) Salinity/Temperature

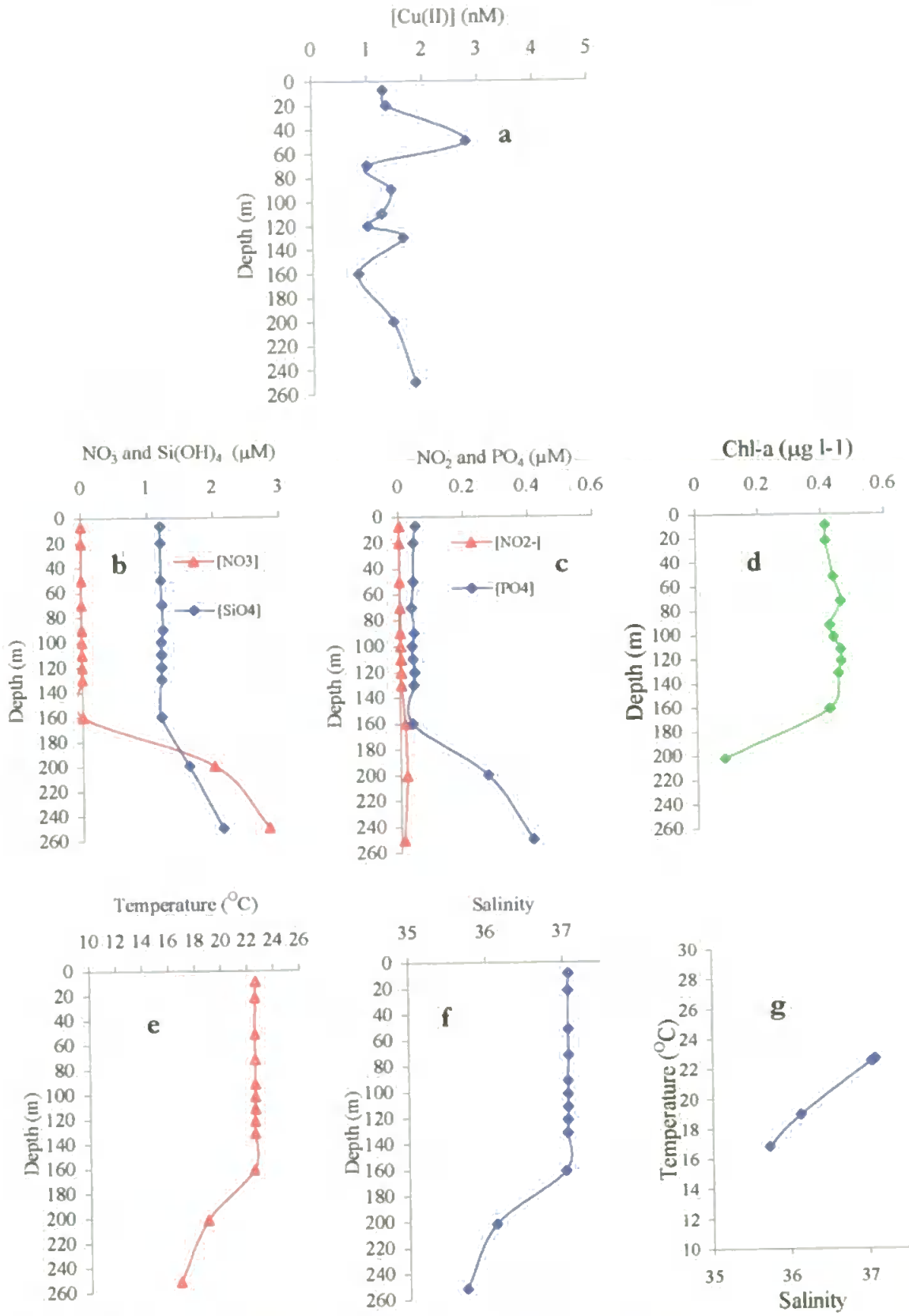

Figure 5.28 Vertical Profiles at AMT 932 for a) Cu(II) (clean room) b) NO_3 and $Si(OH)_4$, c) NO_2 and PO_4, d) Chlorophyll *a*, e) Temperature, f) Salinity, g) Salinity/Temperature

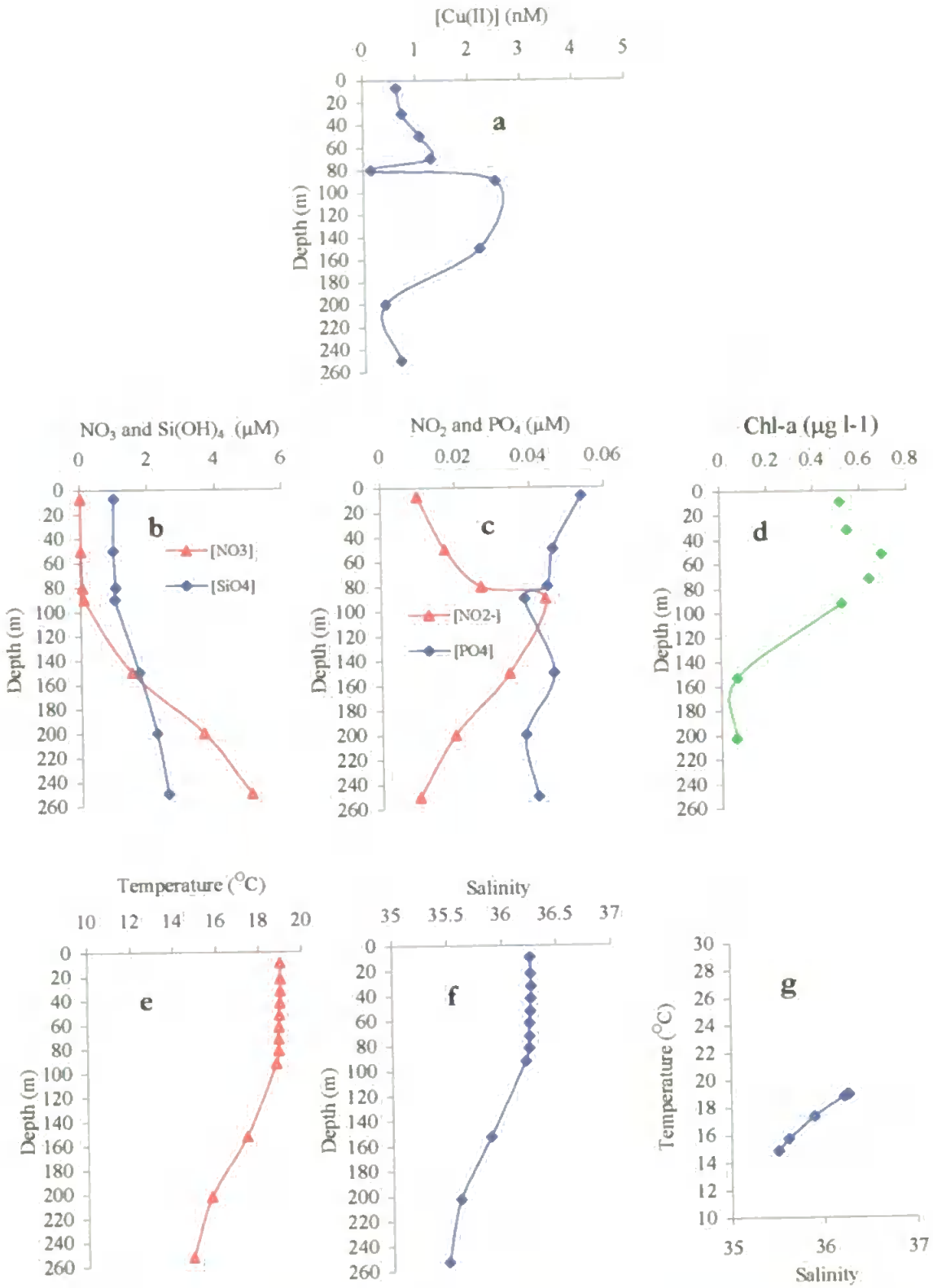

Figure 5.29 Vertical Profiles at AMT 936 for a) Cu(II) (clean room) b) NO_3 and $Si(OH)_4$, c) NO_2 and PO_4, d) Chlorophyll *a*, e) Temperature, f) Salinity, g) Salinity/Temperature

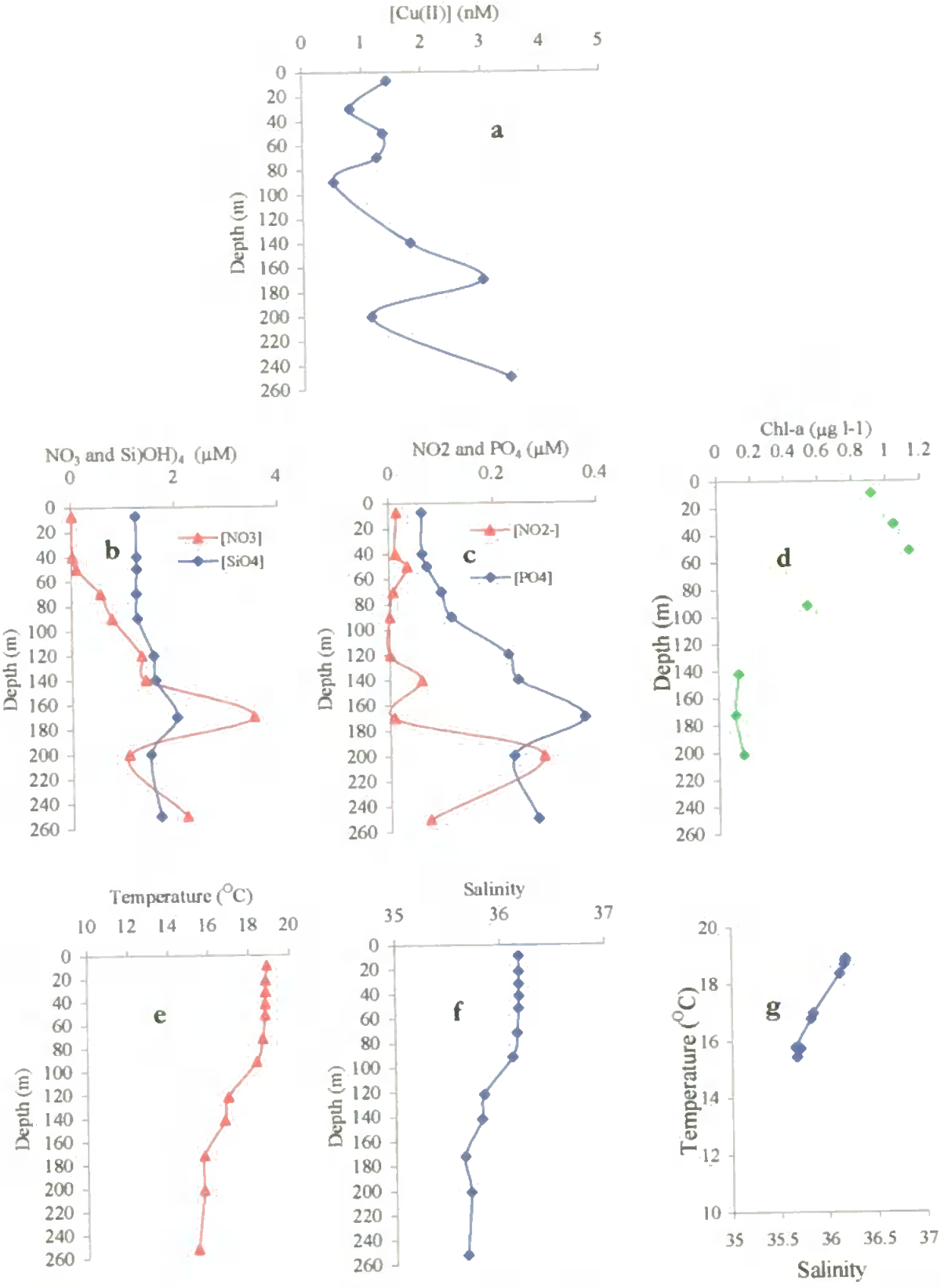

Figure 5.30 Vertical Profiles at AMT 938 for a) Cu(II) (clean room) b) NO_3 and $Si(OH)_4$, c) NO_2 and PO_4, d) Chlorophyll *a*, e) Temperature, f) Salinity, g) Salinity/Temperature

Table 5.14 Mean Upper Water Column (0 – 250 m) Parameters Along AMT 9 Transect

Oceanic Province (Hooker *et al.*, 2000)	Latitude	J. Day	Station	Temp (°C)	Salinity	Cu(II) (nM)	Chlr *a* (μg L^{-1})	PO_4 (μM)	NO_3 (μM)	NO_2 (μM)
EU Cont. Shelf Water (ECSW)	50–48 °N	262-263	901 902	14.6	35.6	5.0 3.3	1.03	0.32	3.92	2.10
N. Atlantic Drift (NatD)	48-37 °N	265-266	904 905	16.3	36.0	2.7 2.7	0.35	0.20	2.71	1.86
N. Atl. Subtropical Gyre East (NASE)	37-26.7 °N	267-268	906 907	19.4	36.6	No Data	0.26	0.04	0.51	0.85
Canary Current (CanC)	26.7-20.5 °N	269	908	20.0	36.7	2.7	0.32	0.16	1.77	1.22
Can. Current Upwelling (CCUp)	20.5–15.7 °N	270	910	18.7	36.4	2.5	0.43	0.66	6.01	2.56
N. Equatorial Current (NeqC)	15.7-12.4 °N	271	912	18.2	35.6	No Data	0.77	0.96	8.03	3.78
Guinea Dome (Gdom)	12.4- 7.9 °N	272	914	18.4	35.6	2.6	0.51	0.99	8.8	5.14
N. Equatorial Counter Current (NECC)	7.9-1 °N	273-274	916 918	22.5	35.7	 1.6	0.64	0.44	3.81	3.21
S. Equatorial Current (SEqC) (SeqC)	1° N–14.6 °S	275-278	919 925	22.5	36.3	919 - 2.8 925- 2.0	0.42 0.32	0.46 0.35	3.55 1.27	3.20 5.27
S. Atlantic Tropical Gyre SATG	14.6 – 30 °S	279-282	927 934	22.2 20.8	36.8 36.6	932 - 1.9	0.33 0.38	0.22 0.13	0.81 0.88	1.52 1.57
Brazil Current BraC	30– 35 °S	283, 284	936 938	17.7	36.1	936 - 1.1 938- 1.2	0.51	0.11	1.29	1.50
S. American Shelf SASh	35- 39.6 °S	285	940	14.5	35.5	No Data	0.89	0.78	3.13	2.53

Cu(II) concnetraions and the hydrographic data presented are mean values for the upper water (0 – 250 m) column

Shipboard and land based determination of Cu(II) gave similar vertical profiles although concentrations were higher in the latter due to acidification and storage (Section 5.3.4.4). The clean room values are discussed for all the selected depth profiles. Surface (7 m) Cu(II) at 3.0 nM suggested a strong continental anthropogenic contribution resulting in raised Cu concentrations as also reported by van de Loeff (1.8 – 2.8 nM, 1997), with a small Cu(II) peak at 25 m (3.45 nM). This was followed by a reduction in Cu(II) due to biomass uptake and complexation by exudation of organic ligands to reduce the free Cu(II) ion and thus its toxicity.

A lower Cu(II) concentration (2.3 nM) was seen at the nutricline/thermocline (50 m) due to increased SPM scavenging, biomass uptake and organic complexation. Below the stratified layer a slow rise in Cu(II) occurred due to regenerative release of particulate bound and intracellular Cu coupled with a further rise at 250 m due to shelf sedimentary regeneration (Kremling, 1983, Westerlund *et al.*, 1986, Pohl *et al.*, 1993). The latter process was aided by strong bottom water currents at the European continental margin (Tappin *et al.*, 1993). Mean upper water column Cu(II) declined to 2.7 nM at AMT 904 and 1.9 nM at 905 (NAD).

At this station the chlorophyll a_{max} (1.7 $\mu g\ l^{-1}$) was found at the surface (8 m), the shallowest chlorophyll a_{max} observed on AMT 9, with raised subsurface values (~ 1.4 $\mu g\ l^{-1}$) in the strongly stratified layer down to 52 m, just below the nutricline/thermocline. Chlorophyll *a* then exhibited rapid reduction with depth, due principally to light limitation. A similar chlorophyll *a* profile was found on the South American Shelf (AMT 938 and 940).

5.3.5.3 North Atlantic Subtropical Gyre East (NASE) (AMT 908)

At this station (Figure 5.22) on the northern boundary of the Canary upwelling zone, ENAW was overlain to a depth of ~ 90 - 100 m by ENAWt (Section 5.3.3), as indicated by the thermocline and halocline at 90 – 120 m. Further significant decreases in salinity were observed at ~ 120 m and 230 m. The sharp disconformity in the temperature-salinity plot indicated the presence of two water masses.

Cu(II) concentrations were higher in ENAWt than in the underlying ENAW. An open ocean surface maximum at 3.9 nM (Section 5.3.4.8) identified a surface enrichment followed by subsurface depletion to ~ 2.5 nM due to biological uptake and/or biomass complexation of Cu(II). Cu(II) peaked at the thermocline/nutricline ($Cu(II)_{max}$ 4.0 nM) due to slow diffusion of seawater elements across the stratified boundary and therefore

collection of these elements just above the stratified boundary. At greater depths Cu(II) fell rapidly to ~ 1.2 nM due to scavenging and transition to ENAW. At 230 m, close to the profile bottom, Cu(II) rose substantially (3.2 nM) due to Cu in a filament of upwelled waters as indicated by a change in salinity and steadying of temperature at this depth. At this station the mixing of water masses was very influential in determining Cu(II) concentrations (Le Gall *et al.*, 1999), with atmospheric inputs and the advection south of Cu rich waters (Section 5.3.4.8) also contributing to the raised concentrations observed in this profile.

Mean upper water column Cu(II) concentrations continued to decline to 1.8 nM in NASE due to the reduction in aerosol flux with increasing distance from the continental anthropogenic source, the absence of shelf inputs (water column >/= to 3 km) in conjunction with biological uptake and a small amount of particle scavenging.

Chlorophyll *a* concentrations were low in surface and subsurface waters (~0.2 –0.3 $\mu g\ l^{-1}$) with a deeper chlorophyll a_{max} (~ 1.0 $\mu g\ l^{-1}$) at 92 m, coincident with the rise in nutrient concentrations at the thermocline and the change in water masses. Chlorophyll *a* values reduced rapidly below the thermocline to less than the LOD at 230 m.

This station also exhibited surface water (< 80 m) depletion of macro-nutrients with NO_3, NO_2 and PO_4, below the LOD (< = 0.02 µM, although a low level of $Si(OH)_4$ was found) in conjunction with elevated surface salinity (36.8) and temperature which were all typical of an oligotrophic gyre. The significant rise in nutrient concentrations at 90 - 120 m was probably due to slow diffusion of seawater elements through the stratified layer and therefore the retention of material at this deep halocline. Nutrient concentrations rose slowly between 120 and 230 m with a second nutricline at 230 m, probably due to a filament of upwelled water as indicated by temperature and salinity data.

5.3.5.4 Canary Current/Canary Upwelling (AMT 910)

Located off the West African coast this station (Figure 5.23) received inputs from episodic atmospheric deposition and seasonal upwelling of enriched sub-surface water. The physical structure of the upper water column was complicated, consisting of a shallow, well defined surface layer with a sharp salinity discontinuity between 45 – 62 m (halocline) and weaker thermocline at ~ 30 – 50 m. The temperature-salinity plot clearly showed Equatorial Surface Water influenced by the North Equatorial Current, overlying ENAW of increased salinity at 40 m.

Surface Cu(II) were higher than at many other AMT 9 stations due in part to the advection south of Cu enriched waters. This implied that Cu concentrations were the

integrated effect of long term Cu inputs (van der Loeff *et al.*, 1997). A further Cu(II) input was aeolian Saharan dust (Section 5.3.4.8) as evidenced by very hazy skies on AMT 9. Concentrations of Cu(II) were relatively constant at 2.6 nM in the upper 110 m due to the Cu(II) removal processes of SPM scavenging, a pronounced mixed layer effect retaining SPM in the upper 50/60 m, bio-uptake and organic complexation. The Cu(II) fluctuations correlated with the salinity profile.

Upwelled waters could also have raised Cu(II) values at AMT 910, since upwelled water with lower concentrations of organic ligands may increase the free Cu(II) concentration without significantly affecting total Cu (Saager, 1994, from van der Loeff, 1997). The upwelled waters had not recently passed over shelf sediments (water column > 3.6 km) and therefore a Cu input from sedimentary regeneration processes was unlikely.

Below 110 m the Cu(II) distribution reflected the influence of ENAW with a distinct subsurface Cu(II) maxima (5.1 nM) at 130 m, probably due to the slow diffusion of chlorophyll a_{max} across the stratified boundary and the subsequent release of intra-cellular Cu. Thereafter Cu(II) fell sharply to 1.6 nM and then to consistently sub-nanomolar values at the base of the vertical profile (250 m), due probably to biogenic particle scavenging.

The Canary Current Upwelling zone was identified by a significant increase in surface and mean upper water column (0 – 250 m) of PO_4, a small rise in surface NO_3/NO_2 although still demonstrating surface depletion, and a significant rise in mean upper water column (0 – 250 m) of NO_3/NO_2 and $Si(OH)_4$ indicative of fluvial inputs. Strong evidence of upwelled waters was provided by a sharp fall in salinity and temperature at the nutricline at 30 – 40 m, which itself indicated nutrients collecting at the stratified layer due to a low rate of advective mixing across the halo/thermocline. Macronutrients then declined to low concentrations at 60 m below the stratified layer. Thereafter concentrations of NO_3, PO_4, and $Si(OH)_4$ (although not NO_2) rose sharply, reaching a subsurface maximum at 250 m and also suggesting upwelled, nutrient rich water.

Mean upper water column chlorophyll *a* concentrations rose at AMT 910 compared to AMT 908, with a shallow but elevated chlorophyll a_{Max} (1.7 $\mu g\ l^{-1}$) at ~ 30 m, coincident with the rise in nutrient concentrations through the photic zone, and in contrast with the oligotrophic gyre to the north. Chlorophyll *a* was also high due to surface filaments from the main upwelling drifting offshore, indicated by the rise in onboard fluorescence (p.m. of JD 270). Deeper than 30 m chlorophyll *a* reduced rapidly to low concentrations of 0.1 and 0.2 $\mu g\ l^{-1}$ at 75 to 250 m respectively. The chlorophyll *a* did not rise in correlation with the steady increase in nutrient concentrations in the upwelled waters indicating a further bio-limiting aspect, most probably light.

5.3.5.5 Guinea Dome (AMT 914)

Located in the Guinea Dome on the northern boundary of the ITCZ (10 – 0 ^{o}N), AMT 914 (Figure 5.24) exhibited reduced surface salinity (0 – 25 m 35.6) compared to AMT 910 (36.3) due to shower activity of the ITCZ. The shallow (32 m), well defined halocline and thermocline indicated the Guinea Dome (see also Figure 5.14) which consisted of Equatorial Surface Water (0 - 30 m) overlying the markedly less saline and colder South Atlantic Central Water. The presence of two water masses was also indicated by the change in temperature-salinity plot (Figure 5.24, g).

Surface Cu(II) concentrations fluctuated between 1.4 nM (7 m) to 2.2 nM (20 m) and back to 1.2 nM (30 m) due to biogenic surface depletion followed by particle exchange processes. The vertical Cu(II) profile was generally lower than at AMT 910 due in part to a reduction in Saharan aerosol inputs (Section 5.3.4.9), although the skies were still hazy with Saharan dust. The mean upper water column Cu(II) (2.57 nM) was similar to the Canary Current and Upwelling zone (AMT 910) reflecting similar Cu inputs and regeneration mechanisms.

Cu(II) rose sharply to 6.1 nM beyond the stratified layer (30 to 50 m), the highest AMT 9 Cu(II) concentration and which coincided with the rapid reduction in chlorophyll *a*. This rise in Cu(II) was most probably due to intra and extra-cellular regeneration of Cu(II) from SPM that had slowly diffused across the sharp, stratified boundary, coupled with the transition to SACW with its inherently higher Cu concentrations. After the chlorophyll max, Cu(II) values fell sharply to ~ 1 nM at 70 m due to particle scavenging, with a rise to 4.6 nM at 250 m due to regenerative processes and the influence of upwelled waters which became the dominant water mass at > 80 m (Guinea Dome, Figure 5.14). The lower concentration of dissolved organic carbon (DOC) in the upwelled waters may have contributed to the level of the free Cu(II) ion without altering the total Cu value (Saager, 1994, van der Loeff *et al.*, 1997).

The mean, upper water column, macronutrient values continued the rise first seen at AMT 910, reaching a maximum at the southern boundary of the Guinea Dome. After surface depletion, the sharp increases in NO_3, PO_4, and $Si(OH)_4$ between 30 – 40 m were due to the transition to SACW with its raised nutrient concentrations, coupled to upwelled nutrient rich waters observed through the remaining depth profile. This resulted in a nutrient profile that was consistently raised at depth in contrast to the slow increase with depth observed at AMT 910. Surface chlorophyll *a* was low, rising sharply to a maximum at

32 m, correlating with the well defined nutricline, thermocline and halocline. Chlorophyll *a* thereafter declined sharply limited by light rather than nutrient concentrations.

5.3.5.6 Equatorial Inter Tropical Convergence Zone (ITCZ) (AMT 918)

Situated close to the equator in the ITCZ, AMT 918 (~ 3 ^{o} N, figure 27) exhibited a complex water column structure with salinity fluctuations between 65 – 100 m. Compacted isothermals (Figure 5.14) indicated a strongly stratified layer of Equatorial Surface Water overlying South Atlantic Central Water, with a sharp thermocline and halocline, deeper than at previous AMT stations at ~ 90 m. Reduced surface salinity (35.5) due to recent rain events indicated this station's location in the ITCZ (Helmers and Schrems, 1995; Church *et al.*, 1990) coupled to the influence of the freshwater plume of the River Amazon (Dessier and Donguy, 1994, van der Loeff *et al.*, 1997), which was also indicated by the raised surface $Si(OH)_4$ (Figure 5.15 (c). Mean upper water column (0 – 250 m) salinity concentrations remained low (35.7) in the North Equatorial Counter Current due to rainfall although this value rose in the South Equatorial Current (SeqC - 36.3). The temperature-salinity plot (Figure 5.25, (g)) again indicated a change of water masses.

Mean upper water column Cu(II) concentrations fluctuated at this and subsequent equatorial stations and south to the South Atlantic Gyre compared to the relatively stable mean Cu(II) concentrations (~ 2.6 nM) from 48 ^{o}N to 8 ^{o}N. Through the ITCZ mean upper water column Cu(II) declined to 1.56 nM at AMT 918, rising to 2.75 nM at AMT 919 in the SEC and then falling to 2 nM at AMT 925 on the northern boundary of South Atlantic Gyre.

The complex vertical Cu(II) distribution ranged from ~ 1 nM (7m), climbing steeply to 2.6 nM (40 m) due to Cu inputs from rain events (Helmers and Schrem, 1995; Church *et al.*, 1990) and the Amazon River (Dessier and Donguy, 1994, van de Loeff, 1996) (Section 5.3.4.3 - North Equatorial Current/Guinea Dome and N. & S Equatorial Currents). A sharp fall in Cu(II) to ~ 0.7 nM (60 – 80 m) coincided with this station's chlorophyll *a* max at 66 m, and was due to biological uptake and complexation by organic exudates and increased particulate scavenging. At 85 m, Cu(II) rose sharply due to the transition to South Atlantic Surface Water with its higher Cu(II) content and due to regenerative release of Cu from material that has diffused across the stratified boundary. Cu(II) concentrations then varied between ~ 2 nM and 2.6 nM, before decreasing to 0.5 nM at the profile base because of particulate processes.

Surface nutrients were depleted with the equatorial upwelling indicated by the sharp nutricline at 90 m, the stratified boundary. Although still low, nutrients then rose sharply

due to the transition to SACW and the nutrient rich upwelled waters. In the North Equatorial Counter Current (NECC) and South Equatorial Current (SeqC) flowing through this province, the mean upper water column nutrient and chlorophyll *a* concentrations fell substantially approaching the oligotrophic SATG, apart from nitrite in the latter part of the SeqC.

Increasing on-board fluorescence concentrations through p.m. of JD 274 indicated the equatorial upwelling, the equator being crossed at 0647 on JD 275. Surface (7 m) chlorophyll *a* concentrations of 0.26 μg l^{-1} were similar to those in the North Atlantic Subtropical Gyre East (37 – 26.7 ^{o}N), but lower than found at AMT 910 and 914. At AMT 918 chlorophyll a_{max} deepened to 66 m, concentrations remaining raised down to the thermocline/nutricline (~ 90 m) suggesting a retention of nutrients at the stratified boundary which increased the chlorophyll *a* concentration. Chlorophyll *a* then fell sharply despite raised nutrient concentrations suggesting photo-limitation.

5.3.5.7 South Equatorial Current (AMT 919)

At this first South Atlantic station (0.8 ^{o}S, Figure 5.26) the vertical distribution of nutrients, temperature and salinity were similar to AMT 918 and can be explained by the same oceanographic processes. However, salinity concentrations rose due to departure from the ITCZ and the thermocline, halocline and nutricline were less pronounced. Cu(II) concentrations fluctuated between 1.0 to 0.4 nM (8 – 40 m) in the mixed layer with a sharp sub-surface maxima of 3.7 nM at the thermocline/nutricline (70 m) probably due to retention of material at the boundary. Past the boundary, Cu(II) concentrations declined sharply to ~ 1 nM, before rising to 3.0 nM (120 m) and then falling to sub-nanomolar concentrations at the profile base.

Onboard fluorescence increased overnight which corresponded to higher surface chlorophyll *a* values (~ 0.5 μg l) than just north of the equator (AMT 918). At AMT 919 thereafter concentrations remained constant at ~ 0.5 μg l^{-1} from 8 to 71m, a lower level than at AMT 918 with no sharp subsurface peak observed, possibly due to the absence of Amazon Water. The chlorophyll maximum (DCM) was deeper at 71 m than at AMT 918.

5.3.5.8 South Equatorial Current (AMT 925)

Located in the South Equatorial Current in the northwest of the South Atlantic Tropical Gyre (SATG), this remote station (Figure 5.27) did not receive any shelf upwelling or any significant dry deposition. The upper water column (0 – 250m) was characterised by

a deep stratified layer (~150 m) of Equatorial Surface Water overlying South Atlantic Central Water, with a distinct thermocline and halocline. Surface salinity was high (37.0) compared with more northerly stations, due to the high water temperature through this equatorial region.

The vertical distribution of Cu(II) was complex with 0.85 nM at 7 m, a sub-surface maxima of 2.9 nM (60 m) before falling to ~1.9 nM at 140 m (thermo/halocline) because of SPM scavenging. Long distance dry atmospheric deposition of Cu(II), which has a long residence time in seawater compared with Al, was integrated into the anti-clockwise circulatory pattern of the SATG, and combined with trace metal rich rain (Cu 0.28 to 0.45 $\mu g\ l^{-1}$), this region receiving rainfall of increased intensity (Helmers and Schrems, 1995).

A good correlation (R^2 0.7246) was found between Cu(II) and chlorophyll *a* at AMT 925 (Figure 5.31) suggesting a coupling of biological activity to Cu(II) concentrations.

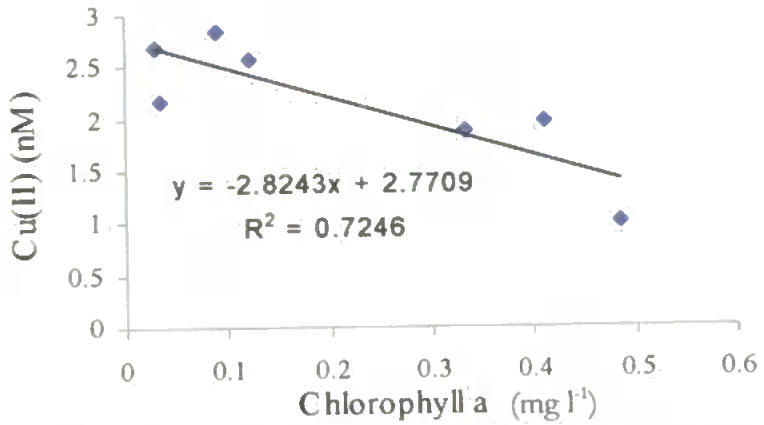

Figure 5.31 Relationship Between Cu(II) and Chlorophyll *a* Through the Upper Water Column at AMT 925 in the South Atlantic Oligotrophic Gyre.

The chlorophyll a_{max} (0.48 $\mu g\ l^{-1}$, 150 m) coincided with a sharp reduction in Cu(II) due to biological uptake, biogenic organic complexation and particle scavenging (see also AMT 914, 918) at the stratified boundary. At 160 m, Cu(II) values rose quickly to 2.6 nM due to the transition to Cu(II) rich SACW and Cu(II) regeneration from biogenic particles that had diffused across the stratified boundary. Sunda and Huntsman, (1995) also reported phytoplankton uptake and regeneration as dominating open ocean Cu concentrations. Through the remaining profile Cu(II) concentrations varied little (2.2 – 2.7 nM), any variance being due to particle exchange processes.

At AMT 925 macro-nutrients were depleted with only PO_4 being > LOD (0.02 µM) above 160 m, with a less well defined nutricline due to greater advective mixing across the stratified boundary. Nutrients rose steadily through the remaining profile due to the higher concentrations in the SACW, although remained lower than at AMT 918 and 919.

Surface chlorophyll *a* concentrations were the lowest yet observed on AMT 9, with a deep but low concentration chlorophyll *a* max (0.48 μg l^{-1}) at the thermocline (150 m). This was made possible by light penetrating the clear pristine waters, which, with the low nutrient and chlorophyll *a* levels was characteristic of the oligotrophic South Atlantic Tropical Gyre (SATG).

5.3.5.9 South Atlantic Tropical Gyre (AMT 932)

This station in the west of the SATG, ~ 400 km east of the South American coast, received intensive rainfall (~ 1000 mm a^{-1}, Helmers and Schrems, 1995) and dry continental deposition. The upper water column (Figure 5.28) was physically homogenous with steady but (compared to other AMT stations) raised temperature (22.5 ^{o}C) and salinity (37.1) profiles down to 160 m, with a distinct deep-water thermocline/halocline and stratified waters. Both parameters then fell quite sharply to 16.8 ^{o}C and 35.7 (250 m). This indicated the intrusion of colder less saline waters, e.g. Antarctic waters.

At AMT 932, the mean upper water column Cu(II) concentration was generally low (1.9 nM). Surface Cu(II) (1.2 nM, open ocean) was consistent with those encountered southwards from 914 (0.9 ^{o}N), reaching a subsurface maximum (2.9 nM) at 50 m, probably due to episodic wet and dry atmospheric Cu deposition and subsequent particulate exchange. Reductions in Cu(II) correlated with two deep chlorophyll *a* maximums at 72 and 122 m suggesting biological coupling e.g. uptake or complexation of Cu(II). Cu(II) then fell at 160 m, the stratified boundary, rising at the profile base due to particle regenerative processes and the possible intrusion of Antarctic waters with elevated Cu concentrations.

Down to ~160 m NO_3 and NO_2 were below the LOD (< =0.02 μM), PO_4 was low (0.04 μM) although $Si(OH)_4$ at 1.2 μM suggested a South American fluvial or rain input. The low nutrient level and the deep-water stratification were typical of an oligotrophic gyre. At depths greater than 160 m, PO_4, $Si(OH)_4$ and especially NO_3 increased sharply, indicative of the intrusion of nutrient rich Antarctic waters. was consistently low (~ 0.43 μg l^{-1}) down to the stratified boundary (160 m), with the two deep chlorophyll *a* maximums (72 and 122 m). Chlorophyll *a* then fell sharply after the stratification to 0.08 μg l^{-1}.

5.3.5.10 Brazilian Current (AMT 936)

Trends similar to AMT 932, but at shallower depths were observed at AMT 936 (Figure 5.29) with a more physically homogenous water column (Figure 5.14). Salinity and temperature were reduced due to increased departure from the tropics, with a stratified

boundary and nutricline at ~ 90 m. Nutrients were generally low in the mixed layer, with $Si(OH)_4$ (as at AMT 932) and NO_2 being the highest. In the mixed layer chlorophyll *a* concentrations were slightly higher than at AMT 932, although consistent at ~ 0.5 μg l^{-1}, with a broad chlorophyll *a* maxima at 52 m (~ 0.7 μg l^{-1}) and raised concentrations down to 72 m, coincident with the collection of nutrients above the stratified layer. Chlorophyll *a* concentrations declined sharply beyond the stratification (90 m).

Surface and sub-surface (< 30 m) Cu(II) were sub-nanomolar (0.7, 0.8 nM) rising to 1.3 nM at 70 m, prior to a significant depletion to 0.14 nM (80 m) the lowest Cu(II) level observed on AMT 9 and which coincided with the raised chlorophyll *a* concentrations. This was probably due to biological uptake, organic complexation through biomass exudates (a toxicological response), coupled with biogenic SPM scavenging. At the stratified layer (90 m), Cu(II) values rose significantly again (2.52 nM) due to the release of intra and extra-cellular Cu from particulate regenerative processes. At greater depths Cu(II) concentrations fell to 2.2 nM, followed by a sharp fall to 0.4 nM (200 m) prior to rising again at 250 m (0.7 nM), possibly due to sedimentary regeneration from the South American Shelf.

5.3.5.11 Brazilian Current/Falklands Current/South American Shelf (AMT 938)

Located in the vicinity of the Brazil and Falklands Currents Confluence (Section 5.3.3.2), an intense mixing zone several degrees of latitude wide, and on the South American Shelf, this station (~ 34 ^{o}S, Figure 5.30) had a broadly temperate, non-stratified, homogenous upper water column of South Atlantic Central Water. Halo and isothermals (Figure 5.14) had a vertical orientation down to 130 m, after which they became compacted and horizontally orientated, notably so between 150 m and 220 m. The narrow range of mean temperature and salinity were reduced due to departure from the sub-tropics and mixing with the less saline, colder sub-Antarctic water advected north by the FC. However, the range indicated the dominance of the warmer, more saline Brazilian Current (BC). The steady subsurface temperature and salinity (< 90 m) fell between 90 – 120 m and between 120 – 170 m, thereafter showing consistency to 250 m.

The mean upper water Cu(II) was 1.2 nM. Surface Cu(II) (1.5 nM) was higher than at the previous station, probably due to advection south in the BC of continental fluvial and atmospheric inputs coupled to local deposition. Concentrations of Cu(II) then fluctuated between ~ 0.7 – 1.5 nM to past the chlorophyll maximum (small Cu(II) repletion) due to biological and particle exchange processes. Deeper than this Cu(II) correlated to NO_3 and PO_4, Cu(II) rising substantially between 90 - 170 m (3.2 nM) due to

mixing with Cu and nutrient rich Antarctic water advected north in the FC, prior to Cu(II) falling back sharply to ~ 1 nM (200 m). Cu(II) then rose to a station maximum of 3.8 nM at 250 m due to Shelf regeneration and further mixing with Antarctic waters. At this station Cu(II) concentrations were no longer dominated by biological processes as found in the oligotrophic gyres (Sunda and Huntsman, 1995), but more influenced by mixing of water masses as also observed in the European Shelf waters.

Nutrients at < 40 m were low, although $Si(OH)_4$ (1.2 μM) and PO_4 were higher than at AMT 925 and 932 in the South Atlantic Tropical Gyre, probably due to advection south in the BC of continental fluvial and atmospheric inputs. At depths > 40 m NO_3 and PO_4 rose substantially reaching a maximum at ~ 160 m, with a smaller rise in $Si(OH)_4$ from 80 m, after which the nutrient profile became complex. At 200 m NO_3, PO_4 and $Si(OH)_4$ fell whilst NO_2 rose rapidly. At greater depths, NO_2 fell in contrast to the other nutrients. Chlorophyll *a* (< 50 m) was raised (~ 0.9 μg l^{-1}) compared with the latter AMT stations with a maximum at 52 m (1.1μg l^{-1}), echoing a trend from AMT 932 (SATG) of higher chlorophyll *a* concentrations at shallower depths as the JCR approached Montevideo. Chlorophyll *a* concentrations then declined quite rapidly to 0.1μg l^{-1} at 140 m, remaining constant to the profile base.

5.3.6 Latitudinal Distribution through the Upper Water Column

The good vertical resolution coupled with the large spatial scale of AMT 9 (48 ^{o}N to 38 ^{o}S) obtained through the daily CTD sampling protocol enabled an along track latitudinal/depth plot of Cu(II) through the upper water column (0 – 250 m) of the Atlantic to be constructed (Figure 5.32). The variation in Cu(II) reflected many of the biogeochemical processes described above. Cu inputs were fingerprinted and attributed to a variety of mechanisms including dry (e.g. Saharan) and wet (e.g. ITCZ) aerosol inputs, both lithogenic (African) and anthropogenic (European) in origin, shelf regeneration (European and S. American), upwelling (W. African coast) and biogenic influences. Onboard hydrographic data enabled identification of the water masses of the upper water column as the JCR passed through the provinces along the AMT transect. The oceanographic profile of the Atlantic on AMT 9 was found to be very much in agreement with previous Autumnal/Boreal Fall AMT cruises.

Copper(II) concentrations were higher in the North East Atlantic than in the South West Atlantic reflecting the increased anthropogenic influences in the Northern Hemisphere. Copper(II) enriched waters were found at the European Shelf and to a lesser

extent at the South American break, with a decreasing Cu(II) gradient from coastal provinces to the Atlantic Gyres, reflecting the reduced inputs and ongoing particulate scavenging of Cu(II). Enrichment to the upper waters was observed at ~45 °N and 30 °N due to anthropogenic and aerosol/fluvial inputs respectively. Raised Cu(II) concentrations

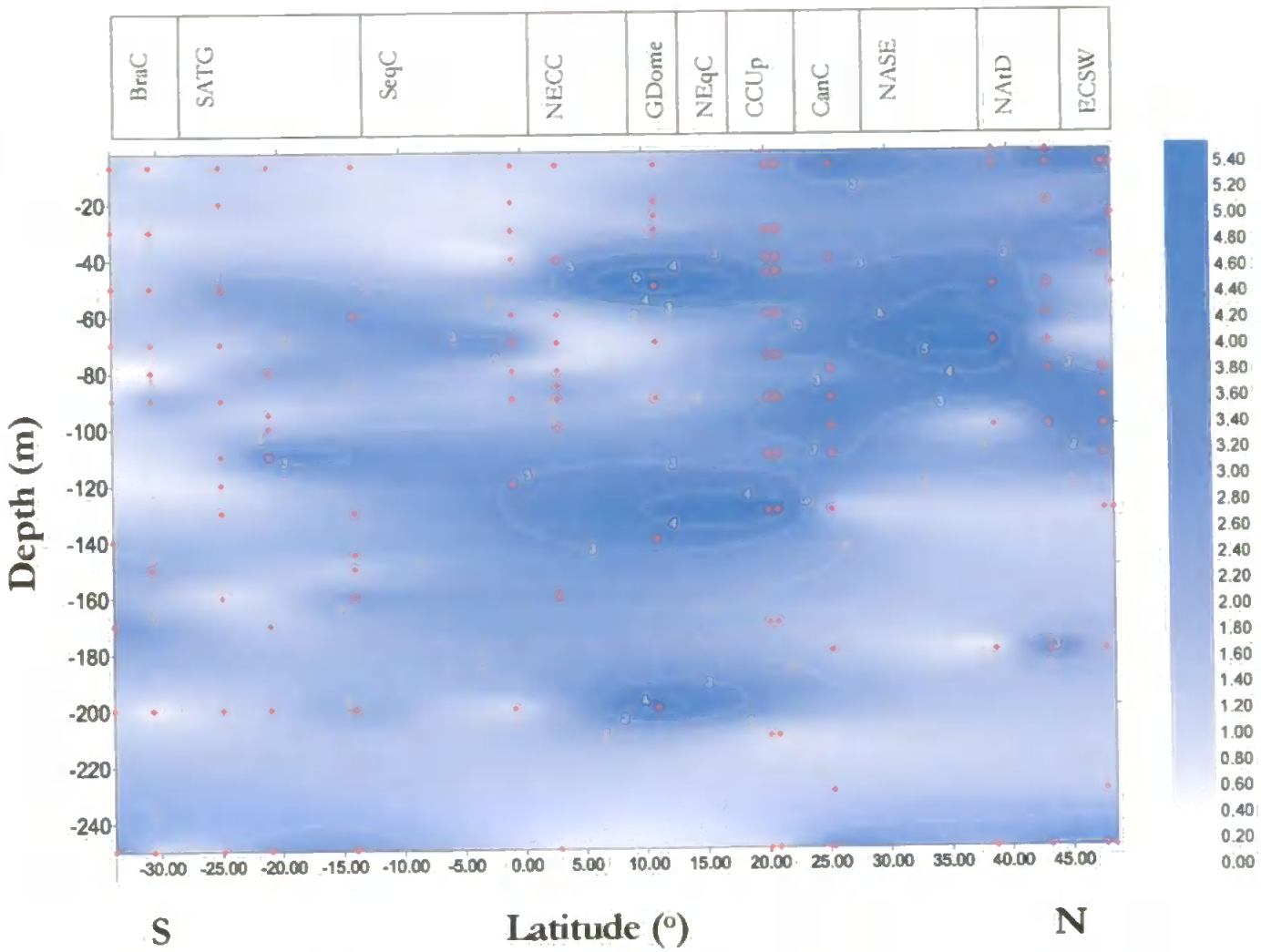

Figure 5.32 Combined Latitudinal and Depth Plot of Cu(II) Concentrations Along the AMT 9 Track

were observed at mid depth in the North Atlantic. The elevated concentrations, especially in the surface waters of the North East Atlantic Drift (AMT 904) and Canary Current (AMT 908) provinces, reflected the advection south of Cu rich waters and Saharan dust inputs. Copper(II) exhibited less variation through the equatorial and subtropical regions of 11 °N to 21 °S. Surface levels declined to ~ 1 nM and upper water column (0 –250 m) values ranged between ~ 1 to 4 nM through this region due to hydrographic, biological and particulate processes. The Cu(II) reached two subsurface maxima. The lowest Cu(II) concentrations were found in the South Atlantic Oopen ocean gyre. The pattern observed

on AMT 9 reflected the highly variable nature of Cu fluxes in terms of frequency, duration and intensity combined with seasonal influences.

5.4 Conclusions

Participation in the AMT 9 validated the FI-CL instrumentation, in adverse weather conditions and through a variety of water masses ranging from nutrient and SPM rich shelf and coastal zones to pristine, open ocean oligotrophic regions. Cu(II) data along the AMT 9 transect exhibited good precision with typical RSD's of 5 – 8 % (n=4). Instrument sensitivity and linear range easily encompassed the range of Cu(II) found on AMT 9. During determination of Cu(II) all possible precautions were taken to minimise contamination and ensure analytical accuracy.

A trace metal data set must show oceanographic consistency (Boyle *et al*, 1977), which has been demonstrated for the Cu(II) data obtained by FI-CL on AMT 9. The Cu(II) surface distribution on AMT 9 was in good agreement with previously reported trans-Atlantic surface Cu data from van de Loeff *et al.*, (1997) obtained on a geographically similar transect and with Boyle (1981) who sampled at many similar locations. The Cu(II) surface distribution on AMT 9 also agreed with that derived by discrete sampling at selected locations or over shorter cruises closer to the UK e.g. Kremling and Pohl (1989). The small differences can be attributed to the different analytical methodologies used and reflected variance due to sampling in a dynamic oceanographic regime. coupled to seasonal and episodic events. During AMT 9, Cu(II) data was operationally defined by filtration (0.4 μM) to minimise the SPM exchangeable fraction of Cu determined which otherwise, especially for regions underlying high lithogenic input e.g. off the African coast, could increase the level of Cu(II) observed. Operational definition also included acidification (Q-HNO_3) to preserve samples and which, as shown in Chapter 6 of this study, can release a fraction of the organically complexed and colloidal Cu(II). During AMT 9, the FI-CL instrumentation exhibited high sensitivity and it was possible to distinguish between water masses of differing Cu(II) content.

Surface water concentrations of Cu(II) during AMT 9 exhibited a high degree of spatial variability due to a number of oceanographic influences, with higher concentrations in the North East Atlantic compared to the South West Atlantic. Enrichments were superimposed on an otherwise decreasing NE - SW gradient of Cu(II) concentrations. Elevated surface Cu(II) concentrations were observed in European Shelf Waters due to anthropogenic, riverine and sedimentary regeneration processes. A rapid decline in Cu(II)

concentrations was observed through the NEAG region although concentrations were still higher than stations further south e.g. in the SATG, due to advection south of Cu(II) rich waters and the slow rate of Cu(II) scavenging. Copper(II) enrichment (3.9 nM, 25.3 ^{o}N) was observed off the West Coast of Africa due to enhanced lithogenic aerosol particle deposition e.g. Saharan dust and low rate of removal.

Copper(II) concentrations gradually declined along the AMT 9 transect largely due to reduced inputs coupled to biological uptake and slow scavenging through tropical and equatorial waters. Concentrations of 2.6 nM were observed in the Canary Current (20.6 ^{o}N), 1.4 nM in the Guinea dome (10.9 ^{o}N) and ~1.0 nM across the equator. The narrow range of surface Cu(II) observed between the equator and ~ 20 ^{o}S indicated Cu fluxes were in a steady state equilibrium through this region. The low concentrations of surface Cu(II) observed through the oligotrophic SATG were largely governed by long range atmospheric fluxes. South of 25 ^{o}S Cu(II) concentrations fluctuated due to variable South American aerosol dust, rain and fluvial inputs, shelf regeneration and Rio de Plata influences. This situation was complicated by the intense mixing zone of the BC/FC under the influence of the coastal and internal advective processes.

The vertical profiles (0 – 250 m) of Cu(II) obtained for the AMT 9 transect represented a unique Cu(II) data set and exhibited oceanographic consistency. Copper(II) exhibited significant spatial variation ranging from 0.1 nM to 6.2 nM. In subsurface waters the distribution of Cu(II) was influenced by particle scavenging, both of lithogenic and biogenic origin, coupled to biological uptake and/or organic complexation. Through the oligotrophic gyres, the biological mechanisms became dominant as illustrated by the high degree of correlation of chlorophyll *a* to Cu(II) through these regions. Copper (II) did not become depleted through the gyres and thus was not biolimiting due to less than optimum levels, although the toxicological response of the biomass to Cu(II) was not clear.

Cu(II) inputs were fingerprinted by the interpretation of geographical factors e.g. European and South American shelf influences, upwelling zones, fluvial inputs, wet and dry anthropogenic and lithogenic aerosol deposition in conjunction with hydrographic data (temperature, salinity and nutrient (N, P, and Si)). Through careful interpretation, it was possible to ascribe much of the subtle variations in Cu(II) concentration to biogeochemical responses such as variation of input mechanisms, oceanographic features and/or biological activity, rather than sampling or analytical artefacts. However, the same interpretation was not possible with all data points reflecting the uncertainty that still exists regarding the complete biogeochemical cycling processes of Cu(II). This highlights the need to include

shipboard trace metal analysis in future research cruises incorporating high resolution sampling over a long-term temporal and large spatial scale.

Chapter Six

Development of a UV Photo-oxidation Stage for the Determination of Total Cu(II) in Seawater by FI-CL

Chapter Six

6.1 Introduction

Organic complexation of Cu plays an important but as yet not fully defined role in the biogeochemical cycling of Cu. This chapter describes the development of an on-line UV photooxidation system to break down dissolved organic matter (DOM) in seawater, releasing organically complexed Cu and enabling the determination of total Cu using the FI-CL analyser described in Chapters Two and Three. A new UV photooxidation system was designed as an on-line stage and fabricated with the aims of enabling near real time analysis for total dissolved Cu(II), whilst promoting reproducible performance and maximising operational lifetime. Further objectives were to produce a robust on-line system to use in place of fragile conventional UV irradiation systems e.g. silica coils and to aid safe field deployment by containment of the ozone commonly produced during the operation of UV lamps. The oxidant hydrogen peroxide was added to accelerate DOC breakdown efficiency, and the effect of heat was investigated. Humic acid (Aldrich) was used as a model organic compound, representing a high molecular weight organic compound, rich in aromatics, which is well known for its refractory nature (Schnitzer, 1972). Tamar River and Celtic Sea samples were also collected and analysed for labile Cu(II) and total dissolved Cu(II) using the newly designed on-line UV photooxidation unit and hydrogen peroxide with FI-CL detection. The efficiency of DOC breakdown by the new on-line UV system was verified by comparison with a humic acid sample that had undergone 4 h batch UV irradiation thereby ensuring complete breakdown of the DOC. Further verification was supplied by the comparison of Cu(II) recoveries as determined by FI-CL with those by adsorptive cathodic stripping voltage (AdCSV) for an organic rich seawater sample from the Tamar Estuary.

6.2 Experimental

6.2.1 Reagents

Reagents for the determination of the Cu(II) in seawater by FI-CL were as described in Chapter Three. All samples were acidified to pH 2.0 by the addition of 80 µl of Q-HNO_3 to 100 mL^{-1} of sample. Humic standards were prepared in UHP water by adding 0.5 mg L^{-1} of humic acid (Aldrich), resulting in a 194 mg C L^{-1} stock solution. A 15 mg C L^{-1} (76.1 ml $L^{-1}$of 194 mg C L^{-1} stock) and a 3 mg C L^{-1} (15.2 ml L^{-1} of 194 mg C L^{-1} stock) working humic standard were prepared by serial dilution. The humic acid standards were refrigerated and found to be stable for 3 months. The humic acid had an elemental

ratio of 36.7 % C, 4.7 % H and 1.7 % N as determined using a CHNS analyser (CE instruments EA 1110). A 10 mM H_2O_2 addition to the samples was achieved by adding 400 µl of 1 M hydrogen peroxide stock solution (2.83 ml of 8.8 M reagent to 20 ml of UHP water, prepared daily) to a 40 ml sample.

Total organic carbon (TOC) analysis was performed on a Shimadzu TOC 5000 A analyser for which a 1000 µg L^{-1} potassium phthalate ($C_6H_4(COOK)(COOH)$) standard was prepared in low carbon UHP water (0.2125 g per 100 ml) and 10, 5, 2, 0.5 and 0.2 µg L^{-1} standards were prepared by serial dilution.

6.2.2 Instrumentation

6.2.2.1 UV Instrumentation

The UV irradiation for this study was produced by a 400 W, medium pressure mercury vapour lamp (Photochemical Reactors, model 3040, Figure 6.1), with a typical spectral output shown in Figure 6.2. The lamp was encapsulated in a quartz immersion chamber, purpose designed for this study and positioned in an in-house designed aluminium housing as shown in Figures 6.3 to 6.5.

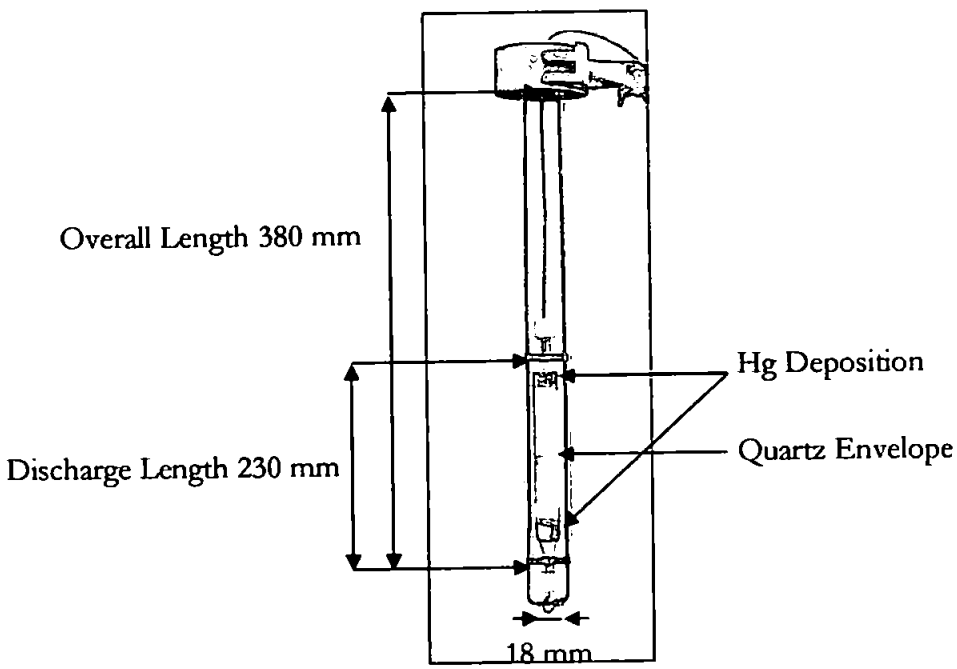

Figure 6.1 400 W Medium Pressure Mercury Lamp – Lamp Only – Figure 6.1 shows a previously used lamp, with a new lamp used for this UV study.

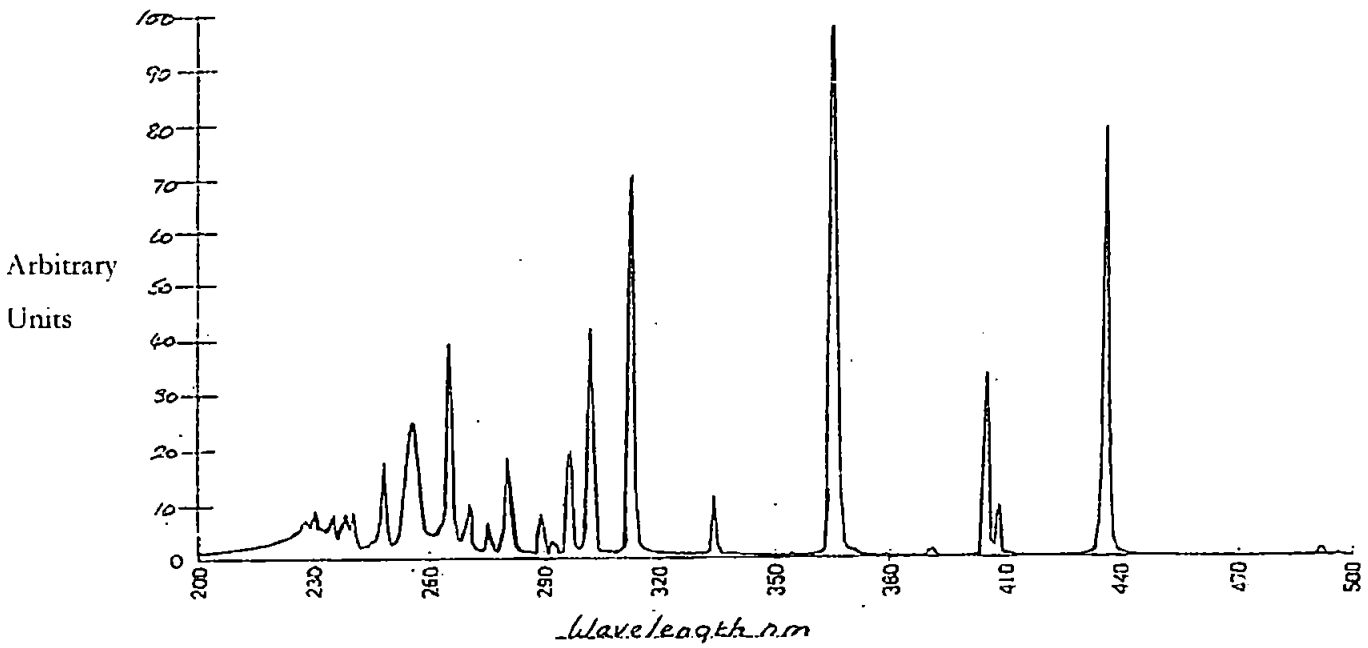

Figure 6.2 Spectrum of 400 W Medium Pressure Mercury Lamp

The 400 W UV lamp had a radiant output of 5 x 10^{19} photons per molecule as measured by ferrioxalate actinometry (Photochemical Reactors). The Hg deposition at the ends of the quartz envelope, caused by unequal cooling can be clearly seen (Section 6.3.1). The 400 W medium pressure lamp emitted predominately 365 – 366 nm radiation with lower intensities at the shorter UV wavelengths of 254, 265, 270, 280, 289, 297, 302, 313 and 334 nm. Also present were the visible bands at 405 – 408, 436, 546 and 577 – 579 nm. An essential component of the new on-line UV irradiation system was a purpose designed quartz immersion well consisting of a double walled quartz water jacket surrounding the UV irradiation system (Figures 6.4 and 6.5), which was fabricated in-house.

A photoreactor coil was designed using fluoro-ethylene polymer (FEP) tubing (0.8 mm i.d., 1.6 mm o.d., 9 m length, 3.98 ml volume) wound around the quartz water jacket to enable on-line irradiation of the sample pumped through it. Both innovative design features are fully discussed in the Results and Discussion (Section 6.3). When used in batch irradiation mode, 8 quartz UV digestion tubes (30 ml volume, 18 mm i.d.), loosely closed with PTFE collars and screw caps, were placed in a ring around the UV lamp, with a 5 cm distance between the lamp and digestion tube centres. A short on-line UV irradiation study was also conducted using a quartz, spiral photoreactor coil (1.0 mm i.d., ca. 3.5 m coiled length, 2.8 ml volume, consisting of 16 loops, each approximately 7 cm diameter) mounted in place of the quartz sample vials. A light-tight lid was fitted over the lamp, immersion well, photoreactor coil and batch digestion tubes. Two safety micro-switches were

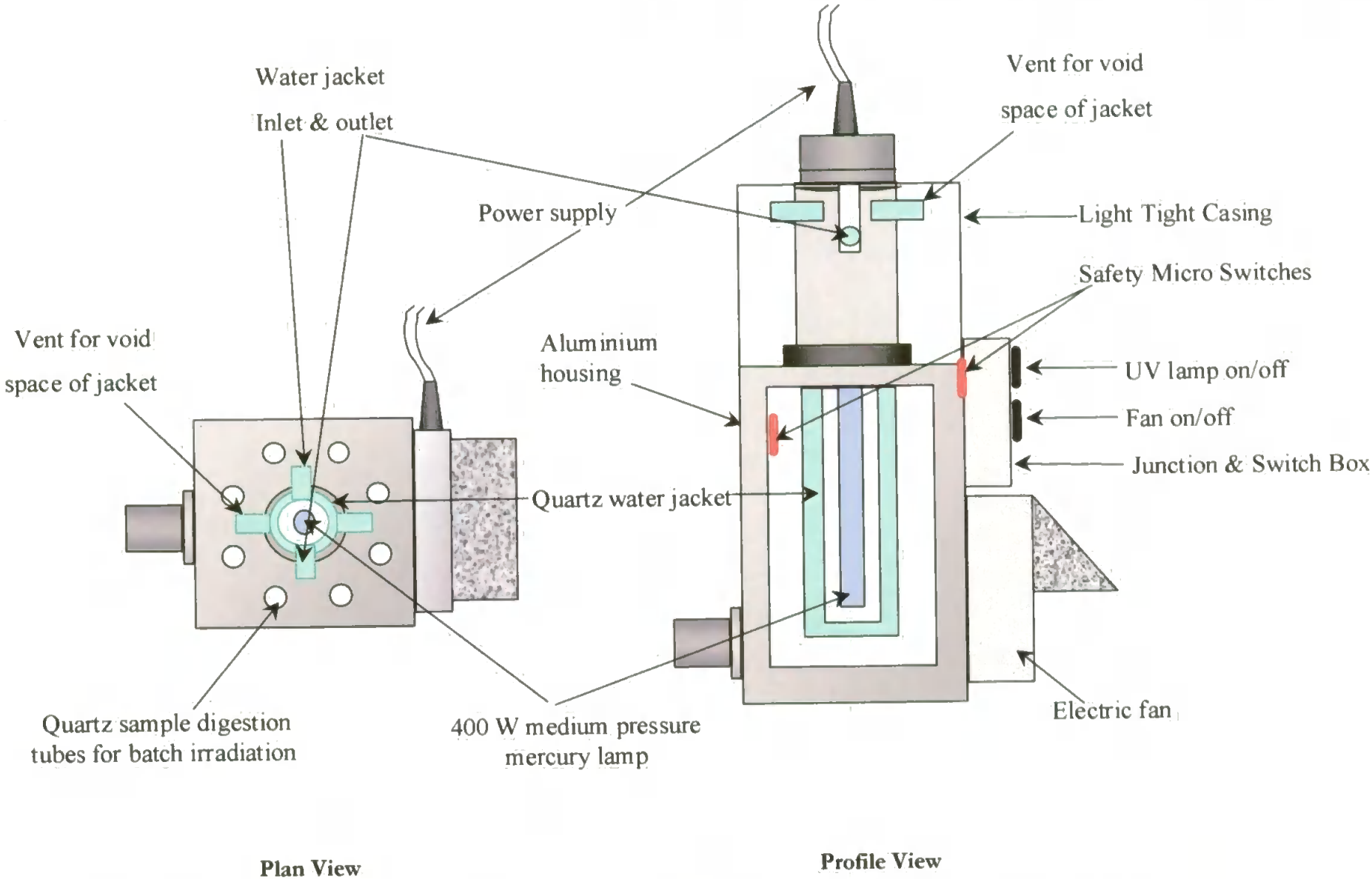

Figure 6.3 Schematic of UV Photooxidation System Incorporating a 400W medium pressure Hg lamp and quartz water jacket.

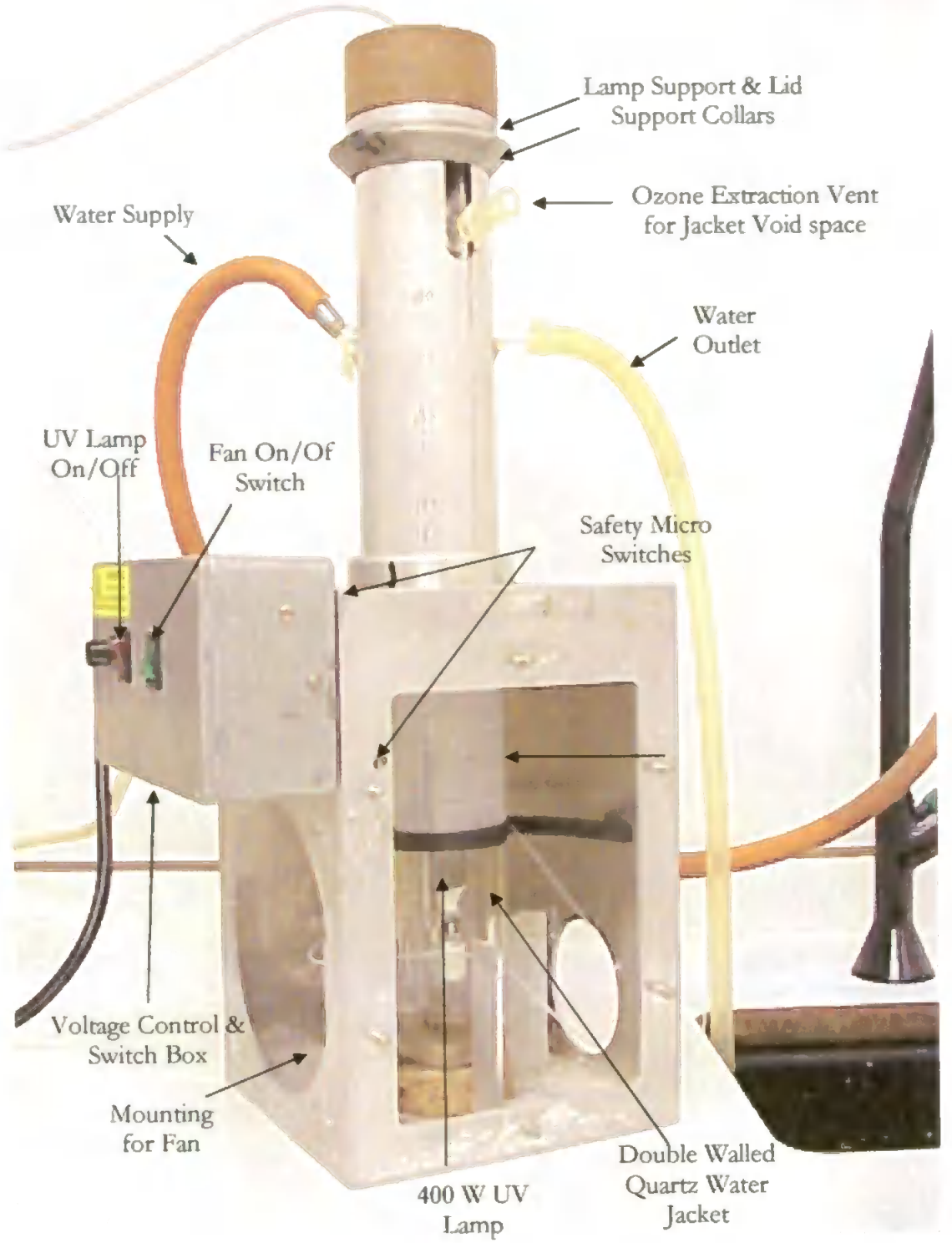

Figure 6.4 UV Photooxidation Lamp incorporating a 400W medium pressure Hg lamp and quartz cooling jacket, with thermocouple, light tight lid, side access plate and fan removed.

were incorporated for on/off operation of the UV lamp and fan. Control of fan operation enabled a 180 s lamp burn-in time to be used in batch irradiation mode and the fan ro be switched off when in on-line mode. Due to the negative voltage-current characteristics of arc sources, conventional low-impedance power supplies were not suitable. High voltage

power for the lamp was provided by a 400 W reactive type supply with a large inductance (Photochemical Reactors, model 3140). This provided the high power required to initiate the arc of the lamp, the power then being reduced for operation.

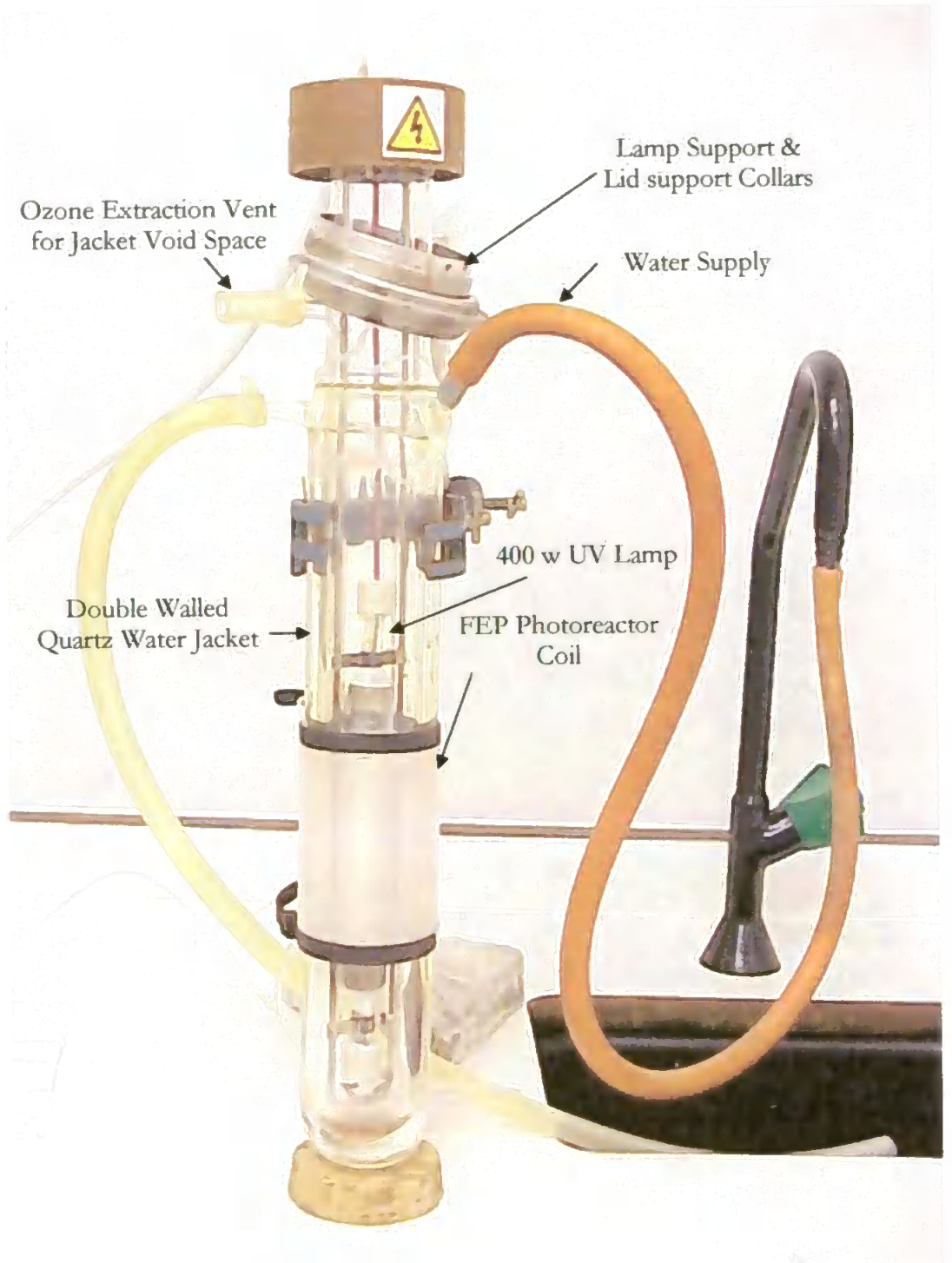

Figure 6.5 Double Walled Quartz Water Jacket with FEP Photoreactor Coil and Water Supply.

6.2.2.2 Organic Carbon Instrumentation

Analysis for total organic carbon (TOC) in the humic acid and seawater samples was conducted on a TOC-5000A analyser fitted with an ASI 5000A autosampler (Figure 6.6). The fraction of organic carbon measured was operationally defined as dissolved organic carbon by filtration (0.4 μM, Nuclepore) The Shimadzu instrument utilises a high temperature catalytic oxidation (HTCO) process to fully oxidise the DOC to CO_2, which was precisely measured by an infrared gas analyser (IRGA). The operational parameters for the TOC instrument are shown in Table 6.1.

Figure 6.6 Shimadzu TOC 5000A Analyser with ASI 5000A Auto Analyser and PC.

Table 6.1 Shimadzu TOC 5000 A Operating Conditions

Operating mode	NPOC		Air Sparging	10 min @150 p.s.i.
Catalyst	High Sense TC 0.5 % Pt on AL_2O_3		Carrier air stream flow rate	150 ml min^{-1}
Syringe injection vol	266 μl		Grubbs outlier test	yes
No of injections	5		Bubble removal	Off
Injection Speed	Standard		Line wash	3
No of washes	3			

NPOC – non purgeable organic carbon mode of operation (see below)

A carrier air stream was purified by passing it through hydrocarbon and organic filters (Fisons, UK) followed by a moisture trap, prior to delivery to the instrument at a regulated flow rate of 150 mL min^{-1}. The instrument was operated in the high sensitivity mode using the high sensitivity TC Shimadzu column catalyst (0.5 % Pt on Al_2O_3 housed in a quartz tube), which has over 98 % efficiency for converting total hydrocarbons and CO to CO_2 under net oxidising conditions (Bauer *et al.*, 1993).

All high sensitivity measurements were conducted in the non-purgeable organic carbon (NPOC) mode, during which inorganic C was purged prior to analysis for DOC. An aliquot of sample was injected into the TOC-5000 A column catalyst and combusted at 680 ^{o}C. The combustion products (CO_2, H_2O and radicals e.g. nitric oxide) were then passed through a H_3PO_4 solution (25 %) in the inorganic reaction vessel, which prevented the CO_2 from being absorbed by the water vapour. The gas stream then passed through a halogen scrubber to remove the halogens that effect the infrared gas analyser (IRGA) during its detection of CO_2. The signal count was integrated and recorded in a PC driven environment.

6.2.2.3 Voltammetric Analysis

Verification of the accuracy of the FI-CL Cu(II) data for the Celtic Sea samples, was achieved by parallel determination of Cu(II) by adsorptive cathodic stripping voltammetry (AdCSV), using a voltammetric analyser (Autolab PGSTAT 10, Ecochemie) connected to a hanging drop mercury electrode (663 VA Stand, Metrohm). A CHNS analyser (CE instruments EA 1110) was used to determine the elemental composition of the Aldrich humic acid.

6.2.3 Procedures

6.2.3.1 Humic Standards

Acidified (Q-HNO_3, pH 2) and unacidified humic acid standards (3 and 15 mg C L^{-1}, Aldrich) were compared to investigate the effect of sample acidification, commonly used to preserve metal species, on DOC complexation of Cu. Aliquots were also compared from the batch (4 h) and the on-line UV photo-oxidation system (100 - 600 s sample irradiation, achieved by alteration of sample flow rate) utilising a 400 W medium pressure mercury lamp (Section 6.2.2). The humic standard at 15 mg C L^{-1} represented an organic rich aquatic system, the 3 mg C L^{-1} humic acid equating to the maximum DOM level typically found in surface seawater (0.5 – 2 mg C L^{-1} (40 to 160 µM C), Mopper and Kieber, 2000).

6.2.3.2 Hydrogen Peroxide and FEP Photoreactor Coil Temperature

The effect of adding the oxidant H_2O_2 (10 mM) on the efficiency of DOC breakdown by UV irradiation and the release of Cu(II), was investigated utilising batch and on-line UV modes. The temperature of the FEP photoreactor coil and thus the heating effect on the sample was regulated by control of the flow rate of the cooling water through the jacket. The temperature was monitored during both lamp burn-in time and operation using a Comark 2001 thermocouple attached to the mid position of the FEP photoreactor coil.

6.2.3.3 Voltammetric Analysis

For the voltammetric analysis 100 µl of *N*-hydroxyethylpiperazine-*N'-2'*-ethanesulphonic acid (HEPES) pH buffer (1 M ; pH 7.7) (final concentration 10 mM, pH 7.7) and 25 µL of salicylaldoxime (SA, 0.1 M) as the AdCSV ligand was added to an aliquot of sample (10 mL). Quartz distilled ammonia (Q-NH_3) was added for final pH adjustment of the sample. Standard solutions of Cu(II) in the range 10^{-6} - 10^{-7} M were prepared by serial dilution of an atomic absorption standard solution (Spectrosol, 10,000 mg L^{-1}) and acidified to pH 2 (Q-HCl).

6.2.3.4 Cleaning Protocols

All UV studies utilised the FEP photoreactor coil or batch UV method as indicated, with the exception of a preliminary UV study with a Tamar estuarine sample, which used an on-line quartz coil, described in Section 6.2.2. All glass labware used for the TOC analysis was rigorously cleaned using a hot Decon™ detergent wash for 24 h, a UHP water rinse, followed by an acid clean (50 % Aristar HCl) for 5 days, rinsed again with UHP water followed by ashing at 400 °C in a muffle furnace. All plastic labware was rigorously cleaned using trace metal clean protocols (Section 2.2.5).

6.2.3.5 Sample Collection

Samples (35 PSU) from the Tamar Estuary were collected using trace metal clean sampling protocols. This entailed the use of polythene gloves, sampling upstream of the boat into trace metal free, acid cleaned high density polyethylene (HDPE) bottles (Section 2.2.5), immediately vacuum filtered (acid cleaned Nalgene, 500 ml volume) through acid cleaned polycarbonate membrane filters (0.4 µm, Nuclepore, 47 mm). The first 50 mL of filtrate was discarded to minimise the effects of leaching from the filter, followed by sample

acidification to pH 2 (Q-HNO_3) and storage in the dark at 4 ^{o}C. The samples were analysed using a two point standard addition immediately after batch irradiation (4 h) and again 50 min later to evaluate the effect on the 1,10-phenanthroline CL reaction of photochemical species, e.g. free radicals, produced during UV irradiation.

Celtic Sea samples were also collected, using trace metal clean protocols, during the PROPHEZE cruise on-board the *RRS Discovery* from 15th–30th May 2000. A CTD, mounted on a stainless steel rosette frame and fitted with acid cleaned Teflon® lined Niskin™ sample bottles was used for sampling. The samples were vacuum filtered on board (Nalgene, acid cleaned, 500 ml capacity) through acid cleaned polycarbonate membrane filters (0.4 μm, Nuclepore) into trace metal free, acid cleaned (Section 2.2.5) HDPE sample bottles (250 ml; Nalgene) and stored frozen at – 20 ^{o}C. To prevent airborne contamination all samples were thawed in a class 1000 clean room (University of Plymouth) and processed in a laminar flow hood (Bassaire, model A3VB).

6.3 Results and Discussion

6.3.1 UV Irradiation System Design

The UV lamp was housed in a purpose built aluminium housing (Section 6.2.2). Deficiencies in the design of UV instrumentation can reduce UV lamp efficiency, reproducibility of sample irradiation and effective operating life of the UV lamp. Fume hoods are required to meet health and safety requirements to contain the ozone produced from UV photolysis of the oxygen in the air. Fans are also commonly used to cool the sample tubes to prevent boiling. However, these can result in uneven cooling of the UV lamp, establishing a temperature gradient over its length, which causes Hg deposition at the ends of its quartz jacket. The automatic and continuous operation of the fan can also prevent the lamp reaching its optimal burn-in and operating temperatures, creating inefficient and irreproducible sample irradiation and causing further mercury deposition on the lamps quartz jacket.

A quartz well reactor consisting of a double walled quartz water jacket (Figure 6.5) was designed and constructed to overcome these deficiencies and promote easier and safer use, particularly during shipboard deployment, of the on-line UV system alongside the shipboard FI-CL analyser. The jacket design rather than an immersive design removed the contamination aspect that can occur with the latter design. Quartz (vitreous silica) was selected because it has a low coefficient of expansion, making it resilient to thermal shock, preventing the heat output of the mercury vapour UV lamp fracturing the jacket. Quartz

also has a transmittance range down to 180 nm, allowing the passage of the full UV spectrum in comparison to ordinary silicate glass (transmittance down to 380 nm) (Skoog *et al.*, 1992), which would effectively filter out a significant portion of the UV spectral output of the Hg lamp at wavelengths of ca. 365 nm and below (Section 6.2.2, Figure 6.2).

For batch irradiation, the new UV lamp design incorporated a switch to prevent fan operation for the first three minutes, thereby allowing the UV lamp to complete its burn-in time and reach the correct operating temperature. When used in on-line mode with the water jacket, the cooling water was not flowing for the first 180 s to achieve the burn in time, after which the flow through the jacket was regulated to maintain a pre-selected optimum temperature over the whole length of the FEP photoreactor coil. These actions minimised the deposition of Hg at the lamp ends thereby extending its effective operating life, promoted the maximum radiant output of the UV spectrum and enabled reproducible sample irradiation to take place so removing the need to irradiate for long periods to ensure DOC breakdown.

6.3.2 Photoreactor Temperature

In the on-line mode the temperature of the FEP photoreactor coil was monitored using a Comark 2001 thermocouple fixed to the mid length point of the photoreactor coil (Table 6.2).

Table 6.2 Temperature of FEP Photoreactor Coil

UV Irradiation Time (s)	FEP Temperature (°C)	UV Irradiation Time (s)	FEP Temperature (°C)
0	22	360	96
30	28	390	96
60	70	420	96
90	86	480	96
120	96		Sample Flowing
150	106	500	85
180 - Water on	115	540	81
185	119	600	81
210	115	660	82
240	110	720	82
270	103	780	82
300	100	840	82
330	97		

After a 180 s burn in time for the UV lamp an FEP temperature of 119 °C was recorded, and the water flow through the jacket was turned on. The water flow was regulated to maintain an FEP temperature of 96 °C after 360 s lamp operating time. The

sample was pumped (1 mL min^{-1}, Gilson MiniPuls 3 pump) through the FEP photoreactor coil after 480 s lamp operating time, resulting in a 15 ^{o}C drop in the temperature due to the cooling action of the sample stream. The temperature stabilised at ca. 82 ^{o}C after 540 s.

Variation of the cooling water flow enabled the FEP photoreactor coil to be operated over a range of temperatures, up to a maximum of 137 ^{o}C, as shown in Table 6.3. Again, a 180 s UV lamp burn in time was used.

Table 6.3 Temperature of FEP Coil (sample on) at 0.5 mL min^{-1}

UV Irradiation Time (s)	FEP Temperature (^{o}C)	UV Irradiation Time (s)	FEP Temperature (^{o}C)
180	110	300	132
210	115	330	133
240	119	360	135
270	125	390	137

At a FEP temperature of 140 ^{o}C the water in the quartz jacket boiled. For all subsequent UV studies, the temperature of the FEP photoreactor coil was maintained at 98 ^{o}C, thereby heating the sample during its passage through the FEP coil, which aided organic breakdown. Kolb *et al*, (1992) reported an optimum temperature of 94 ^{o}C =/- 2 ^{o}C. Heating of the sample increased the reaction rate of the auto-oxidation reactions that are the main pathways for UV degradation of DOC.

6.3.3 UV Irradiation time

Altering the flow rate (Gilson MiniPuls 3 pump) of the sample through the FEP photoreactor coil enabled the residence time and therefore the photooxidation time of the sample to be varied (Table 6.4).

Table 6.4 Sample Irradiation Time (s) in FEP Reactor Coil

Flow Rate (mL min^{-1})	UV Irradiation Time (s)		Flow Rate (mL min^{-1})	UV Irradiation Time (s)
0.4	600		1.0	300
0.6	500		1.2	200
0.8	400		1.4	100

The FEP photoreactor coil significantly increased the robustness of the UV lamp for field deployment in comparison to the very fragile silica coil previously used and was considerably cheaper. FEP is an inert and corrosion resistant copolymer of tertrafluoroethene and hexafluoropropene and has been used extensively in the food

industry for irradiation purposes due to it allowing the passage of UV light and being resistant to UV degradation (Batley, 1984).

6.3.4 Ozone Production

Oxygen in the air surrounding the UV light undergoes photolysis at 184 nm to produce free oxygen, which combines with oxygen to produce toxic and explosive ozone (O'Neill, 1993).

$$O_2 \xrightarrow{UV\ (184\ nm)} 2O^{\bullet}$$

$$O^{\bullet} + O_2 + M \longrightarrow O_3 + M^{\bullet}$$

M = a molecular species

Due to the continuous and unconfined production of O_3, UV lamps commonly require a fume hood ducted to the outside to comply with health and safety regulations. The water in the quartz jacket of the new design of lamp filtered wavelengths less than 200 nm, so containing the formation of ozone to the void space between the lamp and the inner wall of the water jacket encapsulating the lamp. The 400 W UV lamp had a λ max at 366 nm with lower intensities at 254, 265, 270, 280, 289, 297, 302, 313 and 334 nm (Figure 6.2) and therefore the amount of effective UV radiation reaching the sample was not reduced by the water jacket. The void space was designed with vents to allow ozone extraction or flooding with an inert gas to minimise secondary photochemical reactions or products. These actions were not required and the vents were sealed, containing the O_3 to the void space and therefore removing the need for a fume hood. The new design of the UV system thus significantly enhanced the safe use of the photooxidation system, particularly during field deployment, a considerable advantage for shipboard determination of total Cu(II) and promoted its incorporation as an on-line UV stage for the FI-CL instrumentation.

6.3.5 Sample Acidification

Sample treatment protocols prior to trace metal determination commonly use inorganic acidification (pH 2) to preserve the metal species in solution. The effect of acidification on DOC breakdown was investigated by comparing acidified and unacidified (Q-HNO_3, pH2) humic standards (3 and 15 mg C L^{-1} without UV irradiation or a chemical oxidant, e.g. H_2O_2. Residual TOC (Figure 6.7) was determined using the Shimadzu TOC-5000A instrument with the high sense catalyst in non-purgeable organic carbon (NPOC) mode. This removed the inorganic C present in the sample prior to TOC determination.

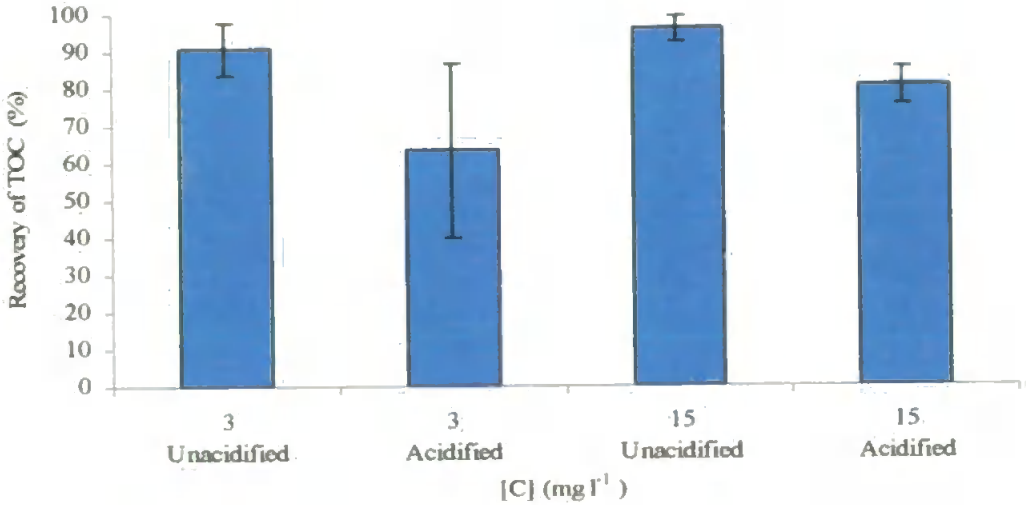

Figure 6.7 Acidification Study (Q-HNO_3) The effects of sample acidification on DOC breakdown (15 & 3 mg C L^{-1} humic standards), conducted without UV irradiation or an added oxidant (H_2O_2). Error bars are 3s.

The recovery of DOC was reduced for both of the 3 and 15 mg C L^{-1} acidified aliquots in comparison with the unacidified aliquots. Acidification to pH 2 (Q-HNO_3) therefore does degrade the weaker DOC complexes. In addition, acidified and unacidified aliquots of a filtered (Nuclepore 0.4 µm polycarbonate membrane, acid cleaned) Tamar Estuary sample were analysed for TOC without a Cu(II) addition, UV irradiation or the addition of hydrogen peroxide. A significant reduction in the TOC recovered was seen for the acidified Tamar sample, supporting the hypothesis that DOC in seawater is broken down through acidification.

In a further investigation the humic sample (3 mg C L^{-1}) was also spiked with 10 and 5 nM Cu(II) additions and allowed to equilibrate for 24 and 40 h respectively to promote complexation of the Cu(II). After equilibration, acidified (pH 2, Q-HNO_3) and unacidified aliquots were analysed for Cu(II) using the FI-CL analyser. UV irradiation or hydrogen peroxide were not used. The acidified samples had a 40 % (24 h) and 35 % (40 h) greater recovery of Cu(II) indicating acid degradation of the weaker DOC complexes and release of the complexed Cu(II). At pH 2, the H^+ ions were in stoichiometric excess and protonation of the humic acid also occurred, displacing the organically complexed Cu(II).

As a control, acidified and unacidified aliquots of humic acid (3 mg C L^{-1}, without UV irradiation or a Cu(II) spike) were analysed for Cu(II) and showed no significant difference. As a further control experiment, an acidified and unacidified Cu(II) (10 nM) standard in UHP water without UV irradiation showed no significant difference in recovery of Cu(II). Therefore, the increase in Cu(II) seen with acidified and UV irradiated samples containing DOC did not originate from the acid used for sample acidification or the humic

complex itself but resulted from breakdown of the DOC releasing the complexed Cu(II). The increase in Cu(II) seen with acidification has implications for the determination of trace metals that have an operational definition of sample preservation by inorganic acidification to ca. pH 2.

Investigations of the direct effect of UV irradiation or the indirect action of the photo-reactive species produced e.g. free radicals, on either the loading of Cu(II) onto the 8HQ micro-column or on the 1,10-phenanthroline CL reaction itself were also conducted. For the both 5nM and 10 nM Cu(II) standards in UHP water, analysed for Cu(II), no significant difference (*t* test, p = 0.05) was seen between irradiated and non-irradiated aliquots indicating that neither column loading nor the CL reaction were affected by UV photooxidation.

6.3.6 UV Irradiation

6.3.6.1 Batch UV study

To ascertain the efficiency of batch UV irradiation when combined with sample acidification on the breakdown of DOC, acidified and unacidified humic acid standards (15 and 3 mg C L^{-1}) were batch UV irradiated (4 h). These were then analysed for TOC using the Shimadzu TOC 5000A in NPOC mode, without the oxidant H_2O_2. The results are presented as efficiency of DOC breakdown (Figure 6.8) by subtracting the fraction of DOC recovered in TOC mode from the original DOC concentration.

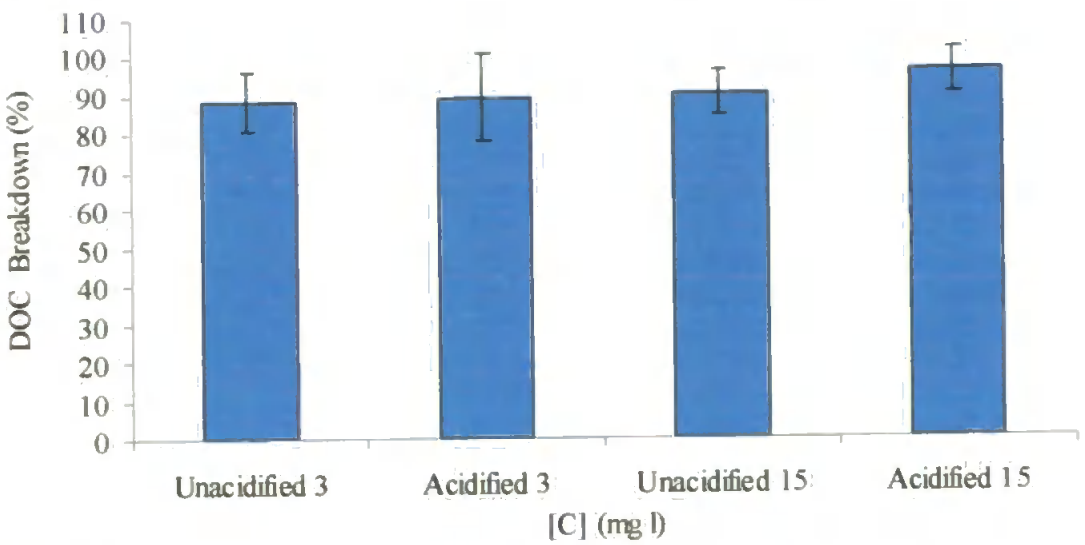

Figure 6.8 Batch UV Irradiation (4 h) and Acidification Study (Q-HNO_3), 3 & 15mg C L^{-1} humic standards,) without oxidant (H_2O_2). Error bars are 3s.

For both humic standards, batch UV irradiation (4 h) alone resulted in efficient breakdown (ca. 90 %) of the DOC, with a small but highly refractory component remaining. Acidification improved the degradation of the DOC for both humic standards, breaking down a further fraction of the refractory component remaining after UV irradiation alone.

6.3.6.2 Effect of H_2O_2 on Efficiency of UV Photo-oxidation

Although batch UV photooxidation (4 h) with acidification was efficient for DOC digestion, a refractory DOC fraction still remained which could retain and re-complex Cu released from weaker ligands. In order to improve the efficiency of DOC digestion, an oxidant (H_2O_2, 10 mM) was added to acidified 3 and 15 mg C L^{-1} humic acid samples which were then batch UV irradiated (4 h). The results are expressed as a percentage breakdown of the DOC (Figure 6.9).

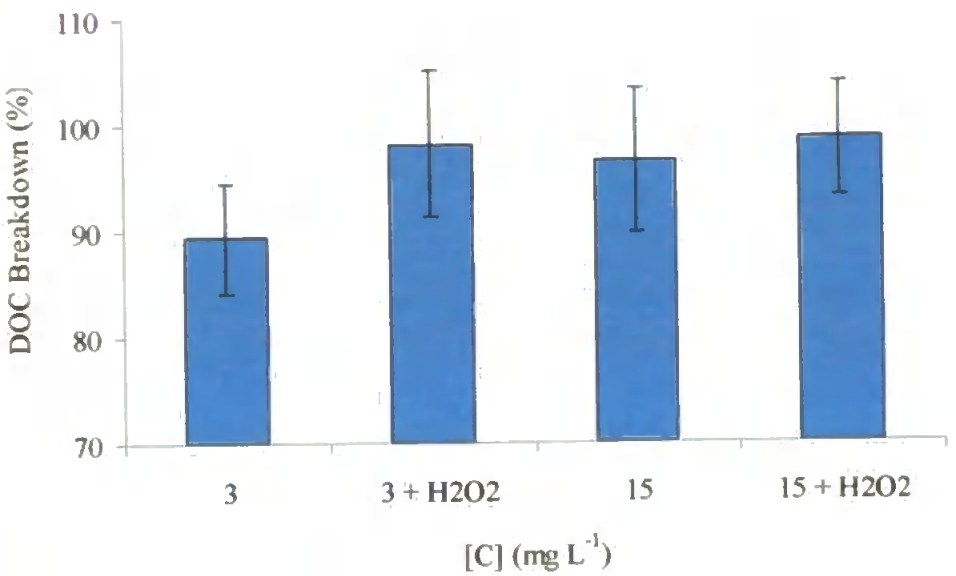

Figure 6.9 Effect of an Added Oxidant H_2O_2 (10 mM) on Acidified (Q-HNO_3), 3 & 15 mg C L-1, Humic Acid Standards with Batch UV Photooxidation (4 h). Error bars are 3s.

The addition of the H_2O_2 improved the efficiency of DOC breakdown (especially for the 3 mg L^{-1} humic standard) of the acidified humic standards to 98 - 99 % after a 4 h batch UV irradiation. This compared well with the improved breakdown (88 - 99 %) when H_2O_2 was used (Worsfold *et al.*, 2000). UV irradiation degrades DOC by auto-oxidation reactions (Section 1.8), reducing oxygen in the process, with the hydroxyl radical being the most reactive of the suite of radicals involved. When exposed to UV light a direct photolytic cleavage of the H_2O_2 occurs, and $OH^{\bullet}$ radicals are produced that initiate the

auto-oxidative chain reactions. The addition of the $OH^{\bullet}$ radical to aromatic ring structures promotes subsequent oxidation reactions, which often produce more radicals in the process (Achterberg and van den Berg, 1994).

$$OH^{\bullet} + RH \longrightarrow R^{\bullet} + HOH$$

$$R^{\bullet} + O_2 \longrightarrow ROO^{\bullet}$$

$$Ar^{\bullet} + O_2 \longrightarrow Ar\,OO^{\bullet}$$

$$ROO^{\bullet} + RH \longrightarrow ROOH + R^{\bullet}$$

Hydrogen peroxide was selected as the added oxidant for this study due to the undesirability of introducing additional chemicals, it also being present as a CL reagent for the FI-CL analyser.

6.3.6.3 On-line UV Study

The efficiency of UV irradiation using the new on-line UV system incorporating the quartz water jacket and FEP photoreactor coil (Section 6.2.2) was investigated and compared with a batch UV study. The 3 mg L^{-1} humic standard was divided into acidified (pH 2, Q-HNO_3) and unacidified aliquots, each of which was analysed for DOC with and without H_2O_2 (10 mM) added prior to on-line UV irradiation (100 to 600 s, Figure 6.10 and Table 6.5). An FEP photoreactor coil temperature of 96 $^{\circ}$ C was used.

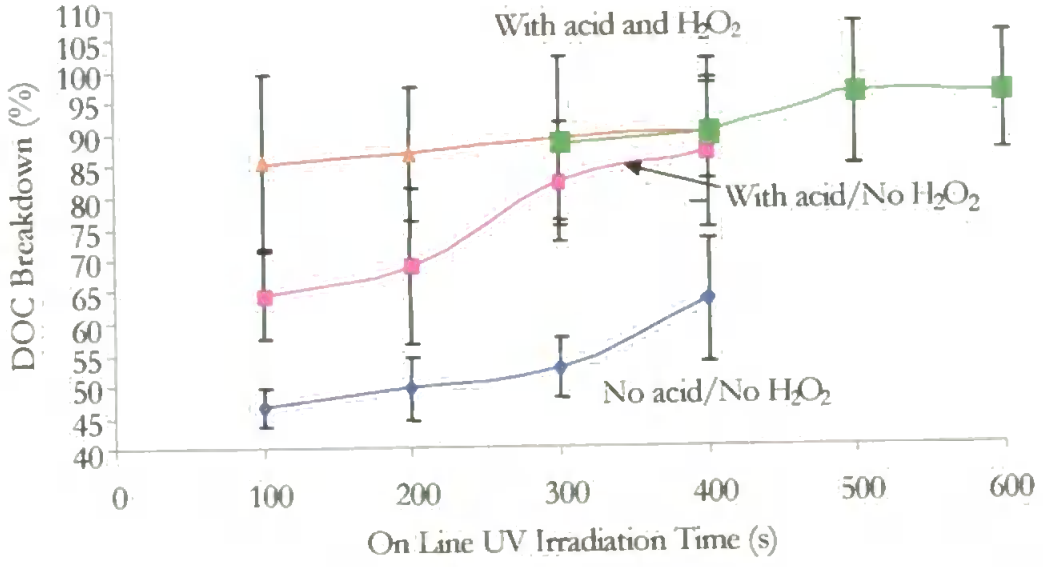

Figure 6.10 On-line UV Study. FEP Photoreactor Coil and Quartz Water Jacket Used. 3 mg L^{-1} C humic aid standard, with and without acidification and H_2O_2 (10 mM). Error bars are 3s.

Table 6.5 Efficiency of On-line UV Breakdown of DOC (%)

On-line Irradiation time (s)	No Acid No H_2O_2	With Acid No H_2O_2	With Acid With H_2O_2	With Acid With H_2O_2
100	47	64	85	
200	50	69	87	
300	52	82	89	88
400	63	87	90	90
500				96
600				96

The with acid and H_2O_2 investigation was conducted in two stages, each of which is shown to demonstrate the consistency of UV digestion with the new on-line system.

On-line UV irradiation alone for 100 s was 47 % efficient at digesting the DOC, rising to 63 % after 400 s UV irradiation. Sample acidification increased the breakdown efficiency to 87 % (400 s), correlating with the increase seen with sample acidification in the batch UV study (Section 6.3.6.1). The addition of the H_2O_2 enhanced the radical driven, auto-oxidative processes at the centre of UV digestion of DOC, increasing the efficiency at 400 s irradiation time to 90 %. Increasing the irradiation time in the FEP photoreactor coil to 500 s by slowing the flow rate of the sample stream raised the efficiency of DOC degradation to 96 %. Only a small further increase in efficiency (0.3 %) was obtained by extending the sample residence time to 600 s, indicating that a small, highly refractive DOC fraction remained. The on-line UV system required a much lower irradiation time to achieve efficient DOC breakdown when compared with batch irradiation. This can be explained by the increase in the ratio of surface area to volume with the FEP on-line photoreactor coil together with enhancement through diffusive radiative transfer and internal reflection of the UV radiation (Batley, 1984).

The determination of total Cu(II) for the Celtic Sea station 20/06 (Section 6.3.8.2), validated by 4 h batch irradiation and adsorptive cathodic stripping voltammetry (AdCSV) demonstrated that functional groups involved in organic complexation of Cu were fully digested, releasing the bound Cu. Thus, the new on-line UV system was suitable for digestion of DOC complexes in seawater, enabling determination of total dissolved Cu(II) by FI-CL.

6.3.6.4 On-line UV Study with an Organic Rich System

The DOC breakdown efficiency of the new on-line UV system utilising the quartz water jacket and FEP photoreactor coil was investigated with an organic rich system. A 15 mg C L^{-1} humic standard, known to be highly refractory, was acidified (pH 2, Q-HNO_3)

and H_2O_2 (10 mM) added prior to 300, 400, 500 and 600s on-line UV irradiation (Figure 6.11).

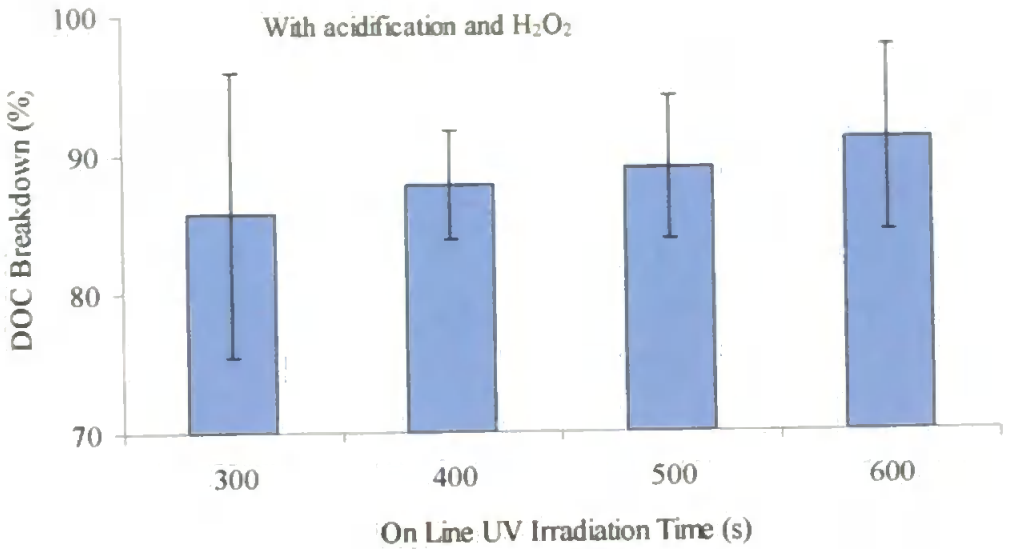

Figure 6.11 On-line UV Study. FEP Photoreactor Coil and Quartz Water Jacket Used. 15 mg L^{-1} C humic acid standard, with acidification (Q-HNO_3) and with H_2O_2 (10 mM). Error bars are 3s.

The efficiency of DOC breakdown with acidification and H_2O_2 addition for the 15 mg C L^{-1} humic standard rose with increasing UV photooxidation time, reaching 91 % at 600 s. Seawater samples rarely contain DOC at as a high a concentration as the humic standard used here and therefore the efficiency of the on-line UV system could be expected to be higher with real samples. The new on-line UV irradiation system therefore enabled determination of total dissolved Cu(II) by FI-CL in organic rich aquatic systems.

6.3.7 Copper Reference Material

Prior to determination of Cu(II) using the FI-CL instrument, NASS 5, an open ocean certified reference seawater was analysed for Cu(II) to verify the accuracy of the FI-CL method. All samples where prepared in a Class 100 clean room, analysed using a two point standard addition (Cu(II) 5 and 10 nM additions to 10 mL of sample) with blank subtraction. A typical NASS 5 result is shown in Figure 6.12.

By calculation, using the equation best fit straight line the concentration of Cu(II) in NASS 5 was found to be;

$$[Cu(II)] = C/M = 273.48/61.67 = 4.43 \text{ nM } (+/- 0.28 \text{ nM})$$

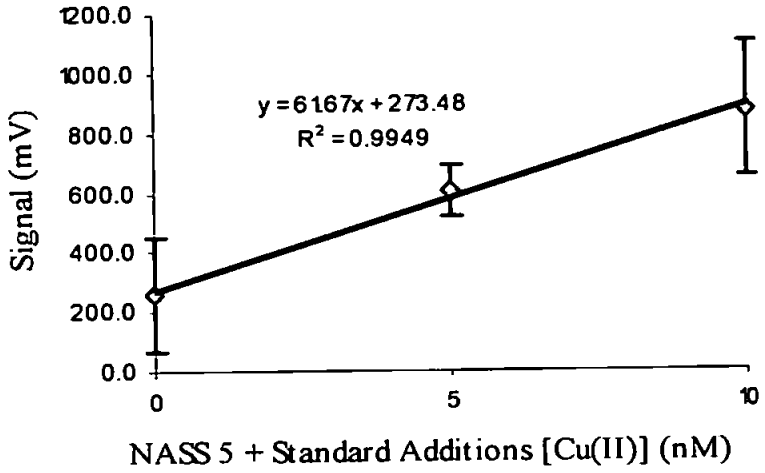

Figure 6.12 Determination of Cu(II) in NASS 5 by FI-CL

The Cu(II) value of 4.43 nM (+/- 0.28 nM) as determined by FI-CL was in very good agreement to the NASS 5 certified value of 4.68 (+/- 0.70 nM) with statistically no significant difference found (*t* test; p = 0.05). This verified the accuracy of the FI-CL method for Cu(II).

6.3.8 Seawater UV Studies

6.3.8.1 Tamar Estuary

Seawater (35 PSU) from the DOC rich Tamar Estuary (ca. 3 mg L^{-1} (Achterberg *et al.*, 2001) was collected using trace metal clean sampling protocols, immediately filtered through acid cleaned polycarbonate membrane filters (0.4 µm, Nuclepore) and acidified to pH 2 (Q-HNO_3). An aliquot of this was UV irradiated on–line utilising the quartz immersion jacket and FEP photoreactor coil system with H_2O_2 (10 mM). This was analysed for Cu(II) immediately, and again 50 min later, to evaluate the effect of photochemically produced species e.g. free radicals, on the CL reaction, using the FI-CL analyser with a two point standard addition. An aliquot of the same Tamar sample was also batch UV irradiated (4 h) with H_2O_2 (10 mM) and analysed using FI-CL and adsorptive cathodic stripping voltammetry (AdCSV) (Achterberg *et al.*, 2001) to further verify the good performance of the new on-line UV system and of the FI-CL analyser with UV irradiated seawater samples in DOC rich seawater.

The Cu(II) concentration as determined by FI-CL analysis immediately after UV irradiation was 18.4 nM (+/- 0.46 nM (3s), r^2 0.9887, RSD < 3 %, n=4) and after 50 minutes 17.6 nM (+/- 0.67 nM (3s), r^2 0.9951, RSD < 4 %, n=4). These values were in good agreement with the batch irradiated (4 h) AdCSV method, namely 18.6 nM (+/- 0.48

nM) verifying the efficiency of digestion of DOC by the new on-line UV system. The close agreement in Cu(II) concentrations by the two methods also validated the accuracy of the FI-CL method for total dissolved Cu(II). This also showed that, due to their short-lived nature or volatilisation, photochemical species produced by the UV irradiation did not affect the 1,10-phenanthroline CL reaction.

6.3.8.2 Celtic Sea

Seawater samples were also collected using trace metal clean protocols from the Celtic Sea, a moderately DOC rich system, south of Ireland during the PROPHEZE cruise on-board the *RRS Discovery* 15th to 30th May 2000. This was organised principally by Dynamics of Marine Ecosystems (DYME) group of Plymouth Marine Laboratory (PML). The rationale underpinning the PROPHEZE cruise was the scarcity of knowledge of the scale and dynamics of biogeochemical cycling within fine spatial scales of major shelf oceanographic discontinuities. Such features are most prominent at upwellings or fronts at the shelf edge and at tidal fronts on the shelf e.g. Central English Channel, Southern Irish Sea and within the strongly stratified thermocline of the Celtic Sea.

Sampling was thus conducted at an Irish Sea Front and within the oligotrophic, stratified Celtic Sea, the core site for the PROPHEZE cruise, to investigate the physical controls, including turbulence, on primary productivity and biogeochemical cycling. Samples were collected at station 18/06 (18th May, 2000, CTD cast 6, 51° 49' 16" N, 5° 41' 49" W), representative of the Southern Irish Sea front, and at station 20/06 (22nd May, 2000, CTD cast 6, 51° 48' 34" N 5° 40' 34" W), representative of the stratified Celtic Sea, to investigate the effect of the on-line UV irradiation on the organic complexation of Cu. The CTD depth profiles were vacuum filtered onboard (Nalgene, acid cleaned polysulphone, 500 ml, through acid cleaned polycarbonate membrane filters (0.4 µm, Nuclepore, 47 mm diameter) to remove the suspended particulate material (SPM) and enable determination of the dissolved labile and total dissolved complexed Cu(II) fraction by FI-CL as described in Chapter 3. The samples were collected in acid cleaned HDPE sample bottles (500 mL; Nalgene) and immediately frozen at –20 °C for storage and transport back for shore based analysis at the University of Plymouth. To prevent airborne contamination all samples were thawed and analysed in a class 1000 clean room (University of Plymouth) and processed in a laminar flow hood (Bassaire, model A3VB).

Station 18/06

Once defrosted in the clean room, sub-samples of the depth profile from station 18/06 underwent three different sample treatments prior to determination of Cu(II) using the FI-CL analyser. One sub-sample was left unacidified (1), and a second was acidified (pH 2, Q-HNO_3) to ascertain the effects of acidification on the organic complexes present (2). A third sub aliquot was acidified (pH 2, Q-HNO_3) and then UV irradiated with H_2O_2 (10 mM) using the new 400 W on-line UV system (600 s, 3) incorporating the quartz immersion jacket and FEP photoreactor coil to determine the total dissolved Cu(II) after digestion of the organic complexes. The results are shown in Figure 6.13 and Table 6.6 along with CTD hydrographic data (temperature (^{o}C), salinity (PSU), fluorescence (V, indicative of chlorophyll *a*) and dissolved oxygen (μM).

Table 6.6 Celtic Sea - Station 18/06

Depth (m)	[Cu] (nM) Unacidified (1)	[Cu] (nM) Acidified (2)	[Cu] (nM) Acid + UV (3)
4	1.5	4.0	5.0
6	2.9	3.0	4.2
11	2.9	2.6	3.1
21	0.8	2.7	2.8
32	0.9	3.0	3.6
36	1.9	3.8	4.6
52	1.4	3.0	3.4

Although the Cu(II) concentration profiles follow each other for most of the depths sampled, a divergence was seen at 4 m between the unacidified or labile fraction, and the acidified and acidified/UV irradiated aliquots. The concentration of the labile Cu(II) fraction (4 m) fell to 1.4 nM, whilst that of the organically complexed fraction rose to 4.0 (acidified) and 5.0 nM (acidified and UV irradiated). These results indicated biomass uptake of Cu(II) in surface waters and/or ligand production by the biomass which complexed the Cu(II) as a protective function against toxicological effects. (Section 1.3.4). A convergence of Cu(II) concentration for all three sample treatments was seen at 6 - 11 m, where the increase in the labile (unacidified) fraction was complemented by a decrease in the both profiles representing the complexed fraction. This suggested biomass use of the complexed fraction of Cu(II).

Between 11 and 21 m the labile fraction fell to 0.8 nM, whilst both complexed fractions remained constant at ca. 2.5 nM, suggesting biomass uptake and regulation of Cu(II) concentration correlating with a chlorophyll *a* max at 11 m and a transition to

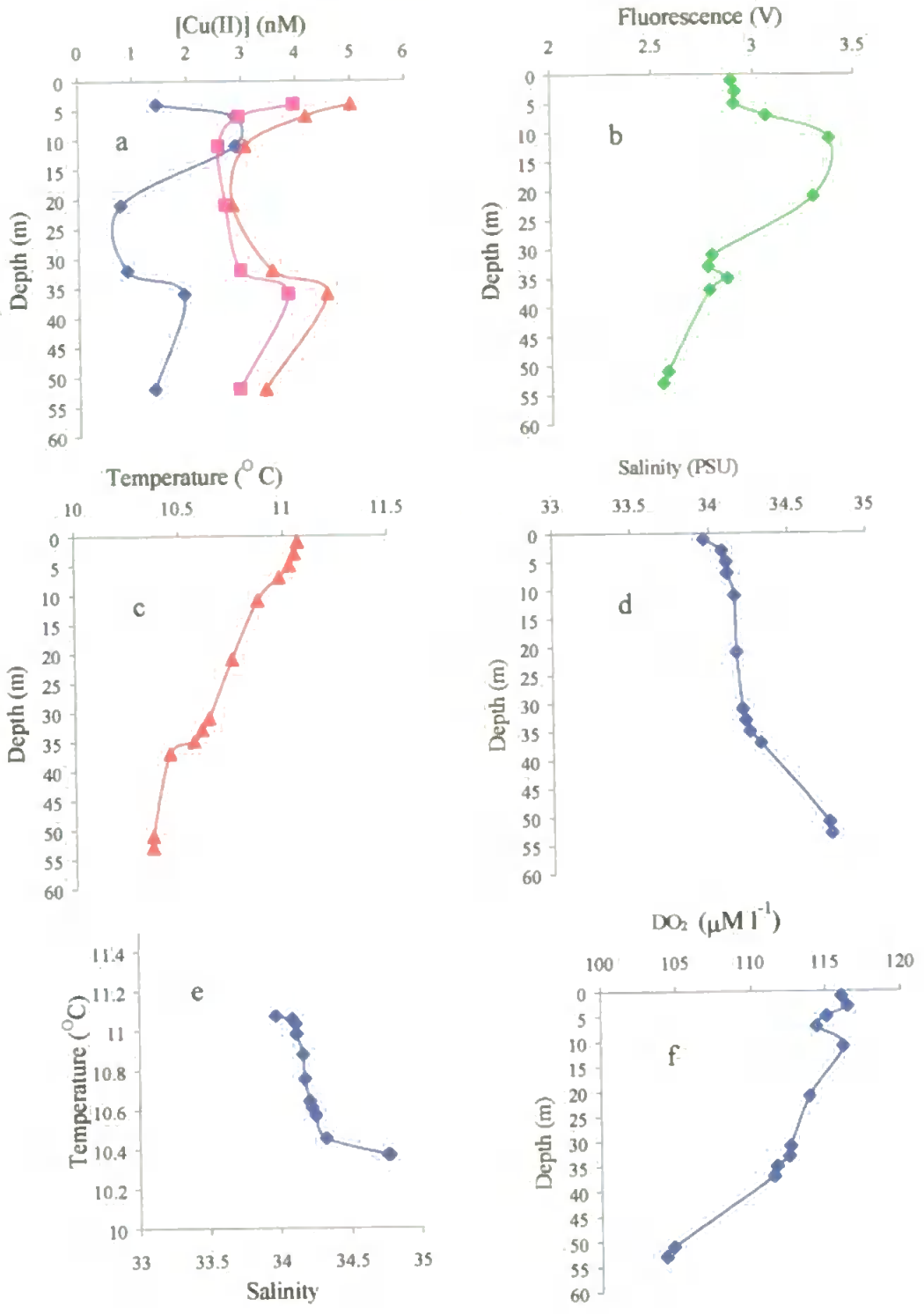

Figure 6.13 Celtic Sea Sample – Station 18/06 (18th May, 2000, CTD cast 6, 51O 49' 16" N, 5O 41' 49" W a) Cu(II) depth profiles - Unacidified , Acidified (Q-HNO_3) , Acidified with on-line UV/H_2O_2 (10 mM) , b) Fluorescence (V), c) Temperature (°C), d) Salinity (PSU), e) Temperature (° C)/Salinity (PSU), f) Dissolved Oxygen (μM).

different water mass as indicated by the temperature and salinity profiles. At depths greater than 21 m the Cu(II) profiles for the three different sample treatment protocols generally mirror each other. More specifically at 20 - 30 m the labile Cu(II) concentration fell to ca. 1 nM whilst the complexed Cu(II) remains constant at ca. 2.5 (acidified) to 3 nM (acidified with UV) indicating biomass activity. All Cu(II) depth profiles showed a significant increase in Cu(II) concentration at 35 m with the labile fraction rising to 1.9 nM and the complexed fraction rising to 3.8 (acidified) and 4.6 nM (acidified with UV digestion). The thermocline and halocline at 35 m suggested a stratified layer with colder, less saline water below the mixed layer. The dissolved oxygen also decreased steeply at 35 m, possibly due to biomass decay and oxygen uptake. The rise in Cu(II) in all 3 profiles at this depth was attributed to cellular release of Cu(II) and accumulation of material at the stratified boundary due to slow diffusion across it. At 52 m the Cu(II) levels fell again due to particle scavenging.

Comparison of the Cu(II) depth profiles from the different sample treatment protocols showed the Cu(II) concentration to be lowest for the unacidified sub-sample, which represented the labile fraction of Cu(II) in seawater. A raised Cu(II) level was found with the acidified sub-sample with a further rise in Cu(II) seen with the UV irradiated/H_2O_2 treatment. Clearly the Cu(II) levels rose in accordance with more DOC destructive sample treatment protocols. Acidification (pH 2, Q-HNO_3) resulted in digestion of the weak organic complexes, liberating the weakly bound Cu(II). On-line UV treatment with H_2O_2 (10 mM) resulted in more efficient digestion of the organic complexes, releasing the strongly complexed fraction of Cu(II) through the depth profile.

As shown by the on-line UV study (Section 6.3.6.3), the new on-line UV digestion system (600 s with H_2O_2 (10 mM)) was very efficient (96.3 %) at the breakdown of the humic acid (Aldrich) used as a model compound and known for its refractory nature. Therefore, these values represent total dissolved Cu(II) through the depth profile. This supposition was supported by the TOC results for the MEMOSEA study (Achterberg *et al.*, 2001) at the same Celtic Sea station (20/06), which found that the seawater DOC was more easily digested than the humic acid (Aldrich).

Celtic Sea Station 20/06

Samples from a second Celtic Sea CTD cast (station 20/06, 51°48' 16" N, 5 ° 41' 49" W) situated in a coastal region, away from direct land-derived run-off, were collected, filtered and frozen as described above and analysed for Cu(II) by FI-CL and for DOC. Sub-samples were acidified to pH 2 (Q-HCL) and batch UV irradiated (4 h, 400 W UV lamp without quartz water jacket and FEP photoreactor coil) with and without H_2O_2 (15

mM) to investigate the enhancement of the UV digestion of the organically complexed Cu with an added oxidant. The samples were analysed for TOC using the Shimadzu TOC 5000A analyser (Section 6.2.2.2) and for Cu(II) by FI-CL (Figure 6.14, Table 6.7).

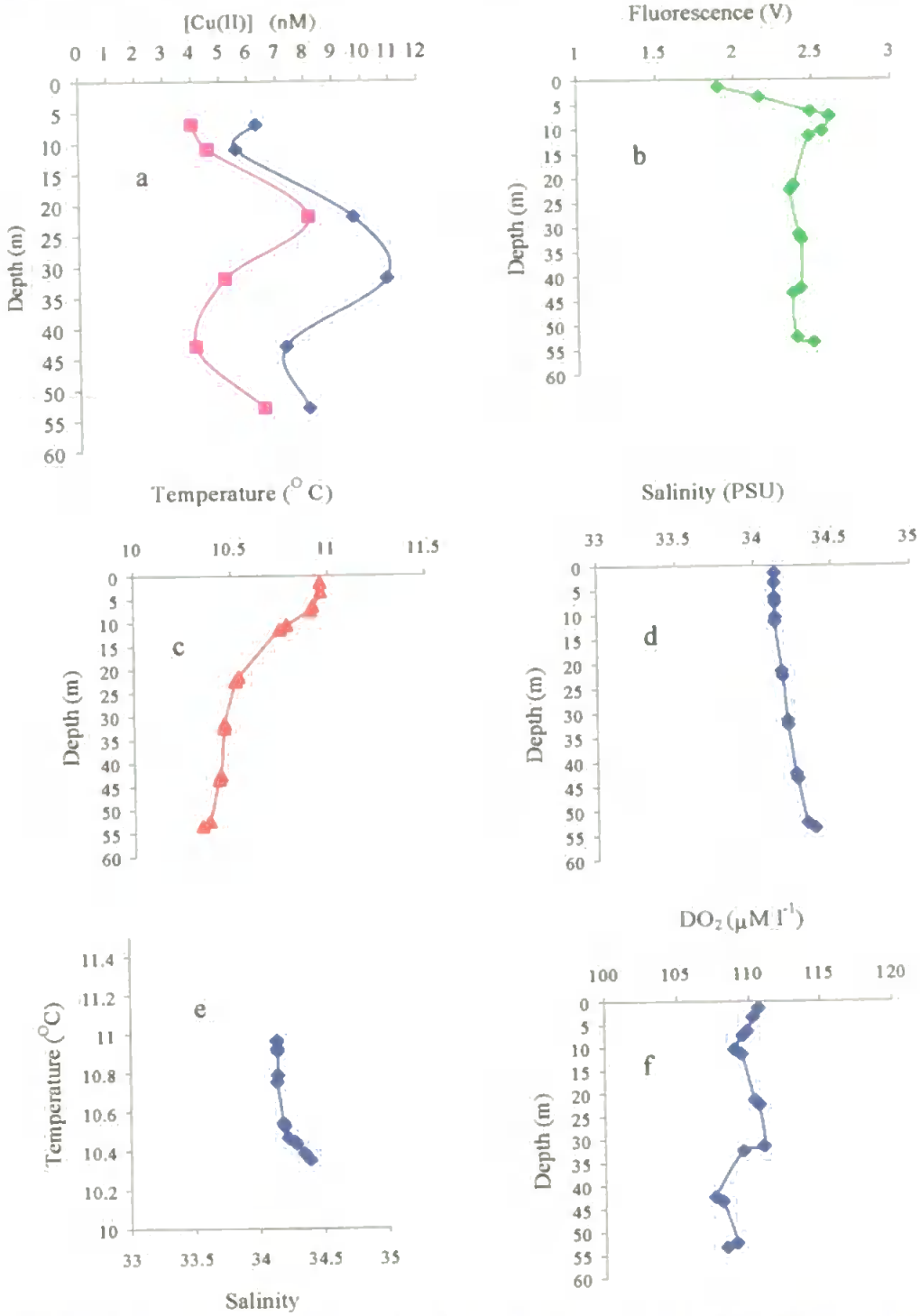

Figure 6.14 Celtic Sea - Station 20/06 (20th May 2000, CTD cast 6, 51O 48' 34" N, 5O 40' 34" W) a) Cu(II) depth profiles–Acidified (Q-HCl) + batch (4h) UV, , Acidified + batch (4 h) UV/H_2O_2 (15 mM) , b) Fluorescence (V), c) Temperature (°C), d) Salinity (PSU), e) Temperature (°C) /Salinity (PSU), f) Dissolved Oxygen (μM).

Table 6.7 Celtic Sea - Station 20/06

Depth (m)	[Cu(II)] (nM) Without H_2O_2	[Cu(II)] (nM) With H_2O_2
7	4.0	6.3
11	4.6	5.6
22	8.1	9.7
32	5.2	10.9
43	4.1	7.3
53	6.5	8.1

The Cu(II) levels ranged from ca. 4 to 11 nM, which compared well with levels observed in other Irish/Celtic regional coastal seas (5-7 nM - Western Irish Sea (Kremling and Hydes, 1988); 7-18 nM, - Irish Sea/Liverpool Bay (Achterberg and van den Berg, 1996); 3.5-24 nM - Irish Sea/Liverpool Bay (Laslett, 1995). The The Cu(II) concentration for both samples have similar profiles although they diverge at 7 m and 32 m, where the labile/weakly complexed Cu(II) fraction (UV irradiation without H_2O_2) both fell correlating with the chlorophyll *a* max and a reduction in dissolved oxygen at 32 m. The rise in the more refractory fraction of Cu(II) (UV irradiation with H_2O_2) 32 m suggested biogenic exudation of organic ligands from the biomass, in order to complex the Cu(II) as a protective function against its toxicological effects.

The two Cu(II) profiles from 11 to 22 m both rose rapidly, coincident with a shallow thermocline (Figure 6.14, c). The latter indicated a transition to a colder, slightly more saline waters. At 32 m the Cu(II) profiles showed the greatest difference with the sample without H_2O_2 falling to 5.2 nM compared to the H_2O_2 treated sample continuing to rise to 10.9 nM. This indicated ongoing biomass activity (chlorophyll *a* still close to the station maximum) with uptake and particle activity reducing the labile fraction coupled to biogenic release of organic complexing ligands, which resulted in a rise in the more strongly complexed fraction Cu(II). Dissolved oxygen fell at 32 m suggesting some cellular decay activity supporting the particle activity hypothesis. At 43 m Cu(II) concentrations for both treatment protocols fell and converged before rising and converging further at 53 m. This, coupled to the reduced dissolved oxygen levels suggested cellular decay and particle scavenging of Cu(II) at 43 m followed by Cu(II) particulate regenerative activity.

Most of the DOC in the Celtic Sea is biologically produced in-situ, and it is likely that this biogenic DOC is more susceptible to UV breakdown than humic acids. The DOC concentrations through the depth profile at station 20/06 ranged between 0.88 and 0.96 mg L^{-1} C. DOC analysis of station 20/06 of the UV digested samples (4 h, batch UV digestion, with and without added H_2O_2) conducted for the MEMOSEA study resulted in

DOC concentrations below the LOD of the TOC 5000A analyser, indicating the ease of breakdown of the organic matter in these seawater samples.

In further support of this a 100 % recovery of Cu(II), as determined by FI-CL, added to Celtic Sea station 20/06 was observed after on-line UV digestion utilising the silica coil and a sample residence time of 11.2 min (0.25 mL min^{-1} flow rate) for the MEMOSEA study. This indicated that it was the total dissolved Cu that was involved in complexing Cu were more susceptible determined using on-line UV irradiation despite a small highly refractive fraction of DOC remaining after on-line UV digestion, as indicated by the Shimadzu TOC 5000A analyser (Sections 6.3.6.3 and 6.3.6.4). This suggested that the functional groups of the organic compounds to UV digestion, releasing the complexed copper, than the refractory parts of the complexes.

The Q-HNO_3 used for acidification of station 18/06 was a stronger oxidising acid than the Q-HCl used for station 22/06. This explained the closer correlation seen between the acidified and UV/H_2O_2 treated aliquots in station 18/06 in comparison to station 22/06 in which a larger difference was seen for the acidified depth profile, with and without the H_2O_2 (the more destructive treatment).

6.4 Conclusions

A new on-line UV photooxidation instrument consisting of a double walled quartz water jacket and FEP photoreactor coil has been successfully designed, fabricated and used for the determination of Cu(II) in seawater, using organic rich Celtic Sea samples. The digestion efficiency of the new lamp was improved by heating the sample to a temperature of 96 °C (Kolb *et al.*, 1992) as it passed through the FEP photoreactor coil. This was achieved by regulation of the water flow through the cooling jacket and enabled the sample to be run up to 137 °C. DOC digestion efficiency was increased from ca. 90 % to ca. 99 % by the addition of the oxidant H_2O_2, which was used for all subsequent studies.

Ozone production was limited to the void space surrounding the UV lamp, thus substantially increasing safety and removing the need for a fume hood as with many conventional UV systems. The water jacket enabled an even temperature to be maintained over the length of the lamp, which prevented Hg deposition at either end of its quartz jacket, in contrast to previously used UV lamps. This should therefore extend its effective operational lifetime. The even cooling provided by the water jacked in conjunction with the provision of a 3 min lamp burn time enabled more efficient and reproducible photooxidation of samples.

Loading of Cu(II) onto the 8HQ column and the 1,10-phenanthroline CL reaction, both fundamental parts of the analytical protocol of the FI-CL analyser, were not affected by the UV irradiation process, enabling UV irradiation to be used with the FI-CL instrument for determination of total Cu(II). The new on-line UV system was found to be very efficient at DOC digestion when using a highly refractory model humic compound (96.3 %), comparing well with batch systems.

Investigation of sample acidification found DOC breakdown due to acidification (Q-HNO_3) and illustrated the need to define operational parameters for trace metal analysis. The recovery of total Cu(II) in a Tamar Estuary seawater sample utilising the new on-line UV system (600 s, + H_2O_2 (10 mM)) and FI-CL determination (18.4 nM, +/- 0.46 nM (3s)) was in good agreement with the value obtained by batch UV irradiation (4 h, + H_2O_2 (15 mM)) and AdCSV (18.6 nM, +/- 0.48 nM).

Cu(II) depth profiles were also determined by FI-CL for two Celtic Sea CTD stations from the PROPHEZE cruise (May 2000) and clearly demonstrated the difference between acidified and unacidified sample aliquots, and the digestion of DOC by UV photooxidation, with and without H_2O_2. The Cu(II) levels were found to increase in accordance with increasingly DOC destructive treatment protocols and the total Cu(II) to be in good agreement with those determined previously for areas close to the Celtic Sea.

In summary the new UV system promoted a more efficient and reproducible digestion of DOC, maximised operational lifetime and promoted near real time analysis for total dissolved Cu(II) as an in-line UV system. It also increased the robustness of the on-line system in comparison to conventional UV irradiation systems and promoted safe field deployment and ease of use, both considerable advantages during shipboard deployment in conjunction with the FI-CL analyser. The comparative determination of Cu(II) validated the efficiency of the new on-line UV system and the accuracy of the FI-CL analyser for the determination of total Cu(II) by UV digestion. Although the investigation suggested a trend, the results are inconclusive and further studies are required to clarify the issue of copper and DOC.

Chapter Seven

Conclusions and Future Work

Chapter 7

7.1 General Conclusions

The conclusions at the end of each chapter summarise the specific achievements presented in that chapter, although there are also several general conclusions that can be drawn from the work presented in this thesis. The first of these is the sutability of the flow injection (FI) approach coupled with the wet chemistry of the 1,10-phenanthroline chemiluminescence (CL) reaction and PMT detection for monitoring Cu(II) in marine systems. FI instrumentation is simple, robust and portable, which coupled with the rapid response (minutes) and the high sensitivity and thus excellent detection limits (sub-nanomolar) of the 1,10-phenanthroline CL based FI analyser, makes it ideally suited to shipboard determination of Cu(II). It has been demonstrated in this study that this methodology generates trace metal data at sea with high spatial and temporal resolution, validated by CRMs and electroanalytical metalogy. Its use also eliminates the need for expensive sampling procedures and minimises the risk of sample contamination and loss of sample integrity.

Copper(II) concentrations in the surface waters of the North and South Atlantic were in agreement with previously observed data (0.1 – 6.1 nM) but showed spatial variability and inter-province fractionation. Elevated Cu(II) surface concentrations (> 1.5 nM) were observed at latitudes greater than ~38 ^{o}N in the North Atlantic due to anthropogenic aerosol deposition, other coastal fluvial influences and upwelled European shelf waters. Elevated Cu surface levels (> 1.5 nM) were also observed in the Canary Current, due to high aerosol loadings from the Saharan and Sahel deserts and advection south of Cu rich waters, and at the South American continental shelf break due to upwelling events. Away from strong input mechanisms, Cu(II) concentrations were often subnanomolar. Copper input mechanisms were fingerprinted through correlation with onboard nutrients and hydrographic data e.g. salinity and temperature, which indicated the structure of the water column. High nutrient, chlorophyll *a* and suspended particulate matter concentrations were indicative of coastal influences or upwelled waters. Cu(II) vertical distributions through the upper mixed layer displayed a strong correlation with biological activity (indicated by chlorophyll *a* concentrations), especially in the open ocean gyres. Furthermore, a correlation of Cu(II) concentrations with the different water masses encountered, consistent with stratification of the upper mixed layer (as indicated by thermoclines and haloclines), was also observed.

On AMT 9 Cu(II) levels were above the lower end of the optimum biotic concentration and therefore not biolimiting, although they were observed at concentrations above those at which marine organisms, e.g. phytoplankton, operate protective organic exudation mechanisms to complex Cu(II).

7.2 Suggestions for Future Work

Future work arising from the research reported in this thesis can be divided into two separate areas: (i) the continued development of shipboard analytical monitors for trace elements, and (ii) research focussed on furthering the understanding of Cu(II) and total organically complexed Cu in marine biogeochemical cycles.

7.2.1 Analytical Developments

7.2.1.1 Effect of Sample Treatment Protocols on Cu(II) Determinations

The 1,10-phenathroline CL reaction reported in this thesis is selective towards Cu(II) species. As shown in this work sample acidification does effect the concentration of Cu(II) observed due to part digestion of organic complexes and the release of organically bound Cu. Therefore there is a need to conduct more shipboard studies to elucidate the true level of labile Cu(II) available to marine organisms. The FI-CL methodology developed for this study could be modified to enable determination of Cu(II) immediately upon retrieval of the sample and before acidification. This would involve modification of the FI-CL manifold to remove the buffer stream which could be easily accomplished.

7.2.1.2 In-line Ultraviolet Digestion of Organic Complexes

For this study dissolved Cu(II) and total Cu(II) measurements were performed, the latter after in-line UV digestion of the organic complexes binding the Cu(II). The cycling of Cu in marine systems is linked to both labile Cu(II) and the organically complexed species and therefore further Cu shipboard studies involving the UV digestion of the organic complexes would aid the resolution of the understanding of the effect of organic complexation of Cu in seawater. Modification of the FI-CL manifold to include extra solution switching valves and the compilation of additional lines of instrument automation code would enable this to be accomplished as an automated, on-line method.

The new design of UV lamp developed for this study can be operated as a stand-alone unit without the need for a fume hood, which greatly facilitates field deployment and

increases safety of operation. The UV unit could be automated to run in conjunction with the FI-CL instrumentation. A further improvement to the UV system would be the design of a light tight instrument container incorporating 'plug in' sample and coolant water supply lines and power lines. A flow meter to monitor the flow rate of the sample would enable irradiation times to be varied by alteration of the pump speed, a feature on the Gilson Minipuls pump which can be TTL, and therefore PC, driven.

7.2.1.3 In-line Standard Addition(s)

An integral part of the FI-CL technique reported in this thesis is the utilisation of the internal standard addition method for the determination of Cu(II) in natural waters. This was adopted in order to overcome any alterations in calibration sensitivity that may have resulted from changes in the sample matrix. This was especially relevant to analysis in an estuarine environment where the full salinity range (0 -35.5) can be experienced or during open-ocean analysis where changes in quantity of suspended particulate material (e.g. through the chlorophyll *a* maximum or atmospheric deposition of dust particles) may have altered the 8HQ mini-column extraction efficiency and / or sensitivity of the Cu(II) catalysed CL reaction. Therefore, the inclusion of a further solution line and mixing loop would enable automated in-line standard additions to be performed, reducing both operator time and error, and the risk of sample contamination.

7.2.1.4 Multi-element FI-CL Technique

The use of FI coupled to CL when deployed as a field monitor enables rapid analysis with high sensitivity, a portable and robust instrument, minimal sample handling, compatibility to automated operation and data acquisition facilities and low maintenance and running costs. CL-based analytical techniques for trace metals are ideally suited to marine applications as has been reported more recently, although their practical application for shipboard and in-situ analysis has yet to be exploited to any great degree. Novel CL chemistries can be used with the future generations of FI-CL monitors for a variety of trace metal species (e.g. Mn, Co, Cu, Cr) in seawater. The generic nature of FI-CL instrumentation would enable the adaptation of the current FI-CL monitor to the simultaneous, selective determination of two or more analytes, based on different reaction chemistries. However, an essential facet of this is the design of a sophisticated flow configuration to eliminate potential cross contamination or interference effects of one CL reaction to another.

7.2.1.5 FI-CL Instrument Upgrade

Recent research and development has led to a number of improvements in instrumental design for the for FI-CL monitor. Foremost amongst these is the next generation of CL detectors. Although the high voltage (typically 1000 V) PMT detector used in this study exhibited excellent sensitivity and has proved to be successful during field deployment reported in this study, they are fragile and have a relatively large power supply. The latter does not lend itself to scaling down of instrument size. The new generation of CL detectors are more robust in design, are considerably smaller and utilise a low voltage (typically 12 V). Their use will promote reduction in the size of the current FI-CL monitor, a requirement for commercial applications. In addition, due to the nature of the output signals from such detectors, they will aid the PC acquisition of CL data. This would remove the bulky chart recorder from the instrument. The reduction in size would be further aided by the use of miniature solenoid pumps as supplied by Biochem® in place of the bulky Gilson minipuls pumps.

Instrumental improvements could also include the investigation of the addition of a CL sensitiser e.g. fluorescein, to the 1,10-phenanthroline primary reagent to improve the CL yield. The FI line between the mixing T and the flow cell could also be further shortened using low dead volume connectors more recently available, which may improve sensitivity by improving the positioning of the fast CL reaction and also enable a reduction in reagent consumption by decreasing flow rates.

A further suggestion for future work would be the automation of the FI-CL analyser in a more flexible and user-friendly PC environment, using graphical programming operating and data acquisition systems (e.g. LabVIEW®, National Instruments). Such portable analytical monitors may then be easily and rapidly controlled through notebook computers, improving the response and flexibility of the FI-CL monitor to changes in the environmental sample matrix.

7.2.1.6 Clean Filtration Methods

Within the Worlds oceans there exists a dynamic Cu cycling mechanism between the dissolved and particulate phases, especially in regions which are heavily influenced by particle fluxes e.g. from the atmosphere or sediments or of biogenic origin. An important aspect of understanding the biogeochemical cycling of Cu is to be able to operationally distinguish between dissolved, total dissolvable e.g. the organic fraction and particulate Cu.

Such determinations can be performed at the sub-nanomolar level using the FI-CL technique reported in this thesis, although the validity of such a data set is heavily dependent on the adoption of trace metal clean sampling, filtration and UV digestion techniques. Surface sampling systems based on a continuous on-line pumped supply from a trace metal clean towed torpedo fish and vertical profiling utilising modified samplers e.g. Niskin bottles and Kevlar line, remain expensive, but should be utilised in future oceanographic trace metal studies in conjunction with shipboard analytical techniques such as FI-CL reported in this thesis.

7.2.1.7 In-situ FI-CL Units

A significant aspect of future FI-CL trace metal monitoring will lie with truly *in situ* (i.e. submersible) units. However, the further modification of the current generation of FI-CL monitors to enable the submersible determination of Cu(II) and other trace metals will pose a considerable research challenge. However, a successful design, based on spectrophotometric detection, and submersible deployment of such a monitor has already been accomplished for macro-nutrients (David *et al.*, 1998). The advantages of such a monitor are many-fold, including removal of the necessity for costly remote sample collection, minimisation of contamination and an increase in the temporal and spatial resolution of a real-time data set. It would be a considerable advantage for the monitor to possess a multi element capability by the incorporation of different chemistries in parallel, in association with sophisticated automation and communication technologies e.g. telemetric transmission of instrument commands from shore based laboratories and data transferal back to shorebased research institutions. Deployments could be buoy or CTD mounted or on remotely controlled submersible vehicles. One interesting application of such a unit would be the *in situ* deployment at km depths for mapping and tracing of species in hydrothermal vent plumes (e.g. Cu(II), Fe, Mn).

7.2.2 Biogeochemical Cycling of Cu(II) in Marine Environments

The production of truly reliable data sets for Cu(II) and other trace metals in marine environments has only been possible since the 1980's when peer reviewed analytical methods for trace metals were first reported. This was greatly supported by the development of trace metal clean sampling protocols and later the advent of shipboard techniques during the early 1990s. Clearly the late introduction of such techniques has meant that significant areas of marine chemistry and substantial oceanic and coastal regions

of the World's seas remain unresolved from the perspective of trace metal biogeochemistry. One such area is the Southern Ocean, the worlds largest high nutrient, low chlorophyll (HNLC) region, although other areas, e.g. the open ocean gyres, also urgently require further biogeochemical investigation to ascertain the role of trace metals in marine processes that greatly influence the worlds oceans e.g. regulation of phytoplankton growth. Although, as observed during this study, Cu(II) concentrations are generally above the lower biolimiting level, Cu may be a co-limiting factor at the higher levels encountered in conjunction with other trace metals e.g. Fe as discussed briefly in Chapter 5. Therefore, further research to establish the true nature of these aspects should be an important part of future oceanographic studies.

7.2.2.1 Effect of Atmospheric Deposition

One aspect of the biogeochemical cycling of Cu is the strong influence the atmospheric deposition of trace elements can have in remote open-ocean regions. However, the influence of such inputs on oceanic mechanisms, e.g. productivity, is poorly understood and shipboard and shorebased studies are required to investigate the solubility, mobility and reactivity of Cu received through such aerosol inputs. Shipboard studies would be focused on the acquisition of a suite of chemical, biological and physical measurements in the path of an aerosol plume of anthropogenic origin e.g. close to European or American industrialised areas and lithogenic origin e.g off the West African continent. This aspect could include a sequential leaching protocol of such dusts, which may be more conveniently conducted ashore.

7.2.2.2 Copper Distributions in Coastal Regions

The potential for anthropogenic inputs to greatly influence Cu concentrations in seawater highlights the importance of the highly productive coastal regions of the world's oceans in modifying, for example, fluvial or atmospheric inputs of Cu before they reach the open-ocean. However, there is a need to reinforce the current database of such inputs (e.g. reducing shelf sediments, riverine inputs) and uptake mechanisms of trace elements along shelf-slope margins and in upwelling systems. Shipboard research utilising FI-CL could be conveniently performed in these relatively accessible areas and, through a long-term series of short expeditions, provide the opportunity for the observation of seasonal changes.

7.2.2.3 Atlantic Meridional Transect Database

The Atlantic Meridional Transect (AMT) programme provided a unique opportunity to investigate longterm (decades) changes in trace element levels through several contrasting biogeochemical provinces of the Atlantic Ocean. Complementary onboard oceanographic data e.g. nutrients, chlorophyll *a*, temperature and salinity greatly aided the interpretation of the Cu(II) measurements reported in Chapter 5 of this thesis. The AMT cruise track enabled European anthropogenic influences on Cu(II) concentrations to be fingerprinted, and also the lithogenic aerosol deposition from the West African continent e.g. Saharan and Sahel dust plume to be investigated.

It is therefore clearly important to continue the shipboard deployment of trace metal monitors e.g. on future AMT cruises. FI-CL has a leading role to play in improving the temporal resolution of the trace metal oceanographic database and the observation of seasonal and annual changes. This will provide the baseline data that aids modelling predictions and the interpretation of marine processes in general.

References

References

CRC Physical Constants, 58 ed. 1978.

Photochemical Reactors Ltd. [1]. 1998. Blounts Farm, Blounts Court Road, Sonning Common, Reading, UK. RG4 9PA, Photochemical Reactors Ltd. Ref Type: Catalog

Achterberg, E. P. and Vandenberg, C. M. G., "In-line ultraviolet-digestion of natural-water samples for trace- metal determination using an automated voltammetric system," *Analytica Chimica Acta*, Vol. 291, 1994, pp. 213-232.

Achterberg, E. P. and Vandenberg, C. M. G., "Automated monitoring of Ni, Cu and Zn in the Irish Sea," *Marine Pollution Bulletin*, Vol. 32, 1996, pp. 471-479.

Achterberg, E. P., Braungardt, C. B., Sandford, R. C., and Worsfold, P. J., "UV digestion of seawater samples prior to the determination of trace metals using flow injection with chemiluminescence detection," *Analytica Chimica Acta*, Vol. 440, 2001, pp. 27-36.

Ackroyd, D. R., Bale, A. J., Howland, R. J. M., Knox, S., Millward, G. E., and Morris, A. W., "Distributions and behavior of dissolved Cu, Zn and Mn in the tamar estuary," *Estuarine Coastal and Shelf Science*, Vol. 23, No. 5, 1986, pp. 621-640.

Aiken, J., Rees, N., Hooker, S., Holligan, P., Bale, A., Robins, D., Moore, G., Harris, R., and Pilgrim, D., "The Atlantic Meridional Transect: overview and synthesis of data," *Progress in Oceanography*, Vol. 45, No. 3-4, 2000, pp. 257-312.

Andrew, R. W., Biesinger, K. E., and Glass, G. E., "Effects of inorganic complexation on the toxicity of copper to *Daphnia magna.*," *Wat.Res*, Vol. 11, 1977, pp. 309.

Apte S.C. and Batley, G. E., "Trace Metal Speciation of Labile Chemical Species in Natural Waters and Sediments: Non Electrochemical Approaches," *Metal Speciation and Bioavailability in Aquatic Systems*, edited by A. Tessier and D. R. Turner, Vol. 3, John Wiley & Sons Ltd, Chichester, 1995, pp. 259-306.

Apte, S. C., Gardner, M. J., Ravenscroft, J. E., and Turrell, J. A., "Examination of the range of copper complexing ligands in natural waters using a combination of cathodic stripping voltammetry and computer simulation," *Anal.Chim.Acta, 235(2)*, Vol. 287-97, 1990.

Arimoto, R., Ray, B. J., Duce, R. A., Hewitt, A. D., Boldi, R., and Hudson, A., "Concentrations, sources, and fluxes of trace-elements in the remote marine atmosphere of new-zealand," *Journal of Geophysical Research-Atmospheres*, Vol. 95, 1990, pp. 22389-22405.

Bauer, J. E., Williams, P. M., and Druffel, E. R. M., "^{14}C activity of dissolved organic carbon fractions in the north- central Pacific and Sargasso Sea," *Nature*, Vol. 357, 1992, pp. 667-670.

Beinrohr, E., Tschöpel, P., Tölg, G., and Németh, M., "Flow-through anodic stripping coulometry and anodic stripping coulometry with collection for the simultaneous absolute

determination of copper, lead, cadmium and zinc," *Analytica Chimica Acta*, Vol. 273, 1993, pp. 13-25.

Benjamin, M. M. and Honeyman, B. D., "Trace Metals," *Global Biogeochemical Cycles*, edited by S. S. Butcher, R. J. Charlson, G. H. Orians, and G. V. Wolfe International Geophysics Series, Academic Press, London, 1992, pp. 317-352.

Benner, R., Pakulski, J. D., McCarthy, M., Hedges, J. I., and Hatcher, P. G., "Bulk chemical characteristics of dissolved organic matter in the ocean," *Science*, Vol. 255, No. 5051, 1992, pp. 1561-1564.

Bernhard, M. and George, S. G., "Importance of chemical species in uptake, loss and toxicity of elements for marine organisms," *The importance of chemical speciation in environmental processes*, edited by F. E. B. P. J. S. M.Bernhard Springer-Verlag, 1986, pp. 385-422.

Beynon, R. J. and Easterby, J. S., *Buffer Solutions*, Oxford University Press 1996.

Blough, N. V. and Zepp, R. G., "Efffects of Solar Ultraviolet Radiation on Biogeochemical Dynamics in Aquatic Environments," Woods Hole Oceanographic Institute, WHO 90-99, Woods Hole Oceanographic InstituteTechnical Report, 1990.

Bowie, A. R., Fielden, P. R., Lowe, R. D., and Snook, R. D., "Sensitive determination of manganese using flow-injection and chemiluminescent detection," *Analyst*, Vol. 120, 1995, pp. 2119-2127.

Bowie, A. R., Sanders, M. G., and Worsfold, P. J., "Analytical applications of liquid-phase chemiluminescence reactions - a review," *Journal Of Bioluminescence And Chemiluminescence*, Vol. 11, 1996, pp. 61-90.

Bowie, A. R.. Flow Injection With Chemiluminscence Detection for the Determination of Iron in Surface Atlantic Waters. 1999. University of Plymouth. PhD Thesis

Boyle, E. A., Sclater, F. R., and Edmond, J. M., "The distribution of dissolved copper in the Pacific," *Earth and Planetary Science Letters*, Vol. 37, 1977, pp. 38-54.

Boyle, E. A., Huested, S. S., and Jones, S. P., "On the distribution of copper, nickel, and cadmium in the surface waters of the north-atlantic and north pacific-ocean," *Journal of Geophysical Research-Oceans and Atmospheres*, Vol. 86, No. NC9, 1981, pp. 8048-8066.

Brand, L. E., "Minimum iron requirements of marine phytoplankton and the implications for the biogeochemical control of new production," *Limnology And Oceanography*, Vol. 36, 1991, pp. 1756-1771.

Bruland, K. W., "Oceanographic distributions of cadmium, zinc, nickel, and copper in the north Pacific," *Earth and Planetary Science Letters*, Vol. 47, 1980, pp. 176-198.

Bruland, K. W., Donat, J. R., and Hutchins, D. A., "Interactive influences of bioactive trace-metals on biological production in oceanic waters," *Limnology And Oceanography*, Vol. 36, 1991, pp. 1555-1577.

Buat-Menard, P. and Chesselet, R., "Variable influence of the atmospheric flux on the trace metal chemistry of oceanic suspended matter," *Earth and Planetary Science Letters*, Vol. 42, 1979, pp. 399-411.

Buckley, P. J. M. and Vandenberg, C. M. G., "Copper complexation profiles in the Atlantic Ocean - a comparative study using electrochemical and ion exchange techniques," *Marine Chemistry*, Vol. 19, No. 3, 1986, pp. 281-296.

Buffle, J., *Complexation Reactions in Aquatic Chemistry.*, Ellis Horwood/Wiley, Chichester, 1988.

Butcher, S. S., Charlson, R. J., Orians, G. H., and Wolfe, G. V., *Global Biogeochemical Cycles*, Academic Press, London, 1992.

Byrne, R. H., Kump, L. R., and Cantrell, K. J., "The influence of temperature and pH on trace-metal speciation in seawater," *Marine Chemistry*, Vol. 25, 1988, pp. 163-181.

Cabral, J. P. S., "Influence of organic-ligands on the toxicity of copper to pseudomonas-syringae," *Fems Microbiology Letters*, Vol. 117, 1994, pp. 341-344.

Campbell, A. K., *Chemiluminescence*, Ellis Horwood, Chichester, 1988.

Capodaglio, G., Toscano, G., Scarponi, G., and Cescon, P., "Copper complexation in the surface seawater of terra-nova bay (Antarctica)," *International Journal of Environmental Analytical Chemistry*, Vol. 55, 1994, pp. 129-148.

Caprioli, R. and Torcini, S., "Determination of copper, nickel, zinc, cobalt and manganese in seawater by chelation ion chromatography," *Journal of Chromatography*, Vol. 640, No. 1-2, 1993, pp. 365-369.

Chester, R., *Marine Geochemistry*, Second edition., Blackwell Science Ltd, Oxford, 2000.

Chester, R., *Marine Geochemistry*, 1st ed., Unwin Hyman, London, 1990.

Church, T. M., Veron, A., Patterson, C. C., Settle, D., Erel, Y., Maring, H. R., and Flegal, A. R., "Trace elements in the North Atlantic troposphere: shipboard results of precipitation and aerosols," *Global Biogeochemical Cycles*, Vol. 4, 1990, pp. 431-443.

Coale, K. H. and Bruland, K. W., "Copper complexation in the northeast pacific," *Limnology And Oceanography*, Vol. 33, 1988, pp. 1084-1101.

Coale, K. H. and Bruland, K. W.. Spatial and temporal variablity in copper complexation in the North Pacific. Deep-Sea Research 37[2a], 317-336. 1990. Ref Type: Journal (Full)

Coale, K. H., Johnson, K. S., Stout, P. M., and Sakamoto, C. M., "Determination of copper in sea-water using a flow injection method with chemiluminescence detection," *Analytica Chimica Acta*, Vol. 266, 1992, pp. 345-351.

Coastal Zone Color Scanner; http://daac.gsfc.gov/data/dataset/CZCS/

Cooper, W. J., Zika, R. G., Petasne, R. G., and Fischer, A. M., "Sunlight-induced photchemistry of humic substances in natural waters: major reactive species," *Aquatic Humic Substances:Influence on Fate and Treatment of Pollutants*, edited by I. H. Suffet and P. MacCarthy American Chemical Society, Washington DC, 1989, pp. 333-362.

Crompton, T. R., *Analysis of seawater*, Butterworth and Co Ltd. 1989.

Cutter, G. A. and Oatts, T. J., "Determination of dissolved sulphide and sedimentary sulphur speciation using gas-chromatography photoionization detection," *Analytical Chemistry*, Vol. 59, No. 5, 1987, pp. 717-721.

Daih, B. J. and Huang, H. J., "Determination of trace elements in seawater by flow-injection anodic stripping voltammetry preceded by immobilized quinolin-8-ol silica gel preconcentration," *Analytica Chimica Acta*, Vol. 258, 1992, pp. 245-252.

Danielsson, L. G., Magnusson, B., and Westerlund, S., "Cadmium, copper, iron, nickel, and zinc in the North-East Atlantic Ocean," *Marine Chemistry*, Vol. 17, 1985, pp. 23-41.

David, A. R. J., McCormack, T., Morris, A. W., and Worsfold, P. J., "A submersible flow injection-based sensor for the determination of total oxidised nitrogen in coastal waters," *Analytica Chimica Acta*, Vol. 361, 1998, pp. 63-72.

De Filippis, L. F., "The effect of heavy metal compounds on the pearmeability of chlorella cells.," *Z.Pflanzenphysio.*, Vol. 78, 1979, pp. 314-322.

dc Jong, J. T. M., Boye, M., Schoemann, V. F., Nolting, R. F., and de Baar, H. J. W., "Shipboard techniques based on flow injection analysis for measuring dissolved Fe, Mn and Al in seawater," *Journal of Environmental Monitoring*, Vol. 2, No. 5, 2000, pp. 496-502.

de Mora, S. J., Demers, S., and Vernet, M., *The effects of UV radiation in the marine environment*, Cambridge University Press 2000.

Dessier, A. and Donguy, R., "The sea surface salinity in the tropical Atlantic between 10 °S and 30 °N - seasonal and interannual variations (1977 - 1989) ," *Deep-Sea Res*, Vol. I 41, No. 1, 1994, pp. 81-100.

Donat, J. R. and Bruland, K. W., "A comparison of two voltammetric techniques for determining zinc speciation in Northeast Pacific waters," *Marine Chemistry*, Vol. 28, 1990, pp. 301-323.

Duce, R. A., Liss, P. S., Merrill, J. T., Atlas, E. L., Buat-Menard, P., Hicks, B. B., Miller, J. M., Prospero, J. M., Arimoto, R., Church, T. M., Ellis, W., Galloway, J. N., Hansen, L., Jickells, T. D., Knap, A. H., Reinhardt, K. H., Schneider, B., Soudine, A., Tokos, J. J., Tsunogai, S., Wollast, R., and Zhou, M., "The atmospheric input of trace species to the world ocean," *Global Biogeochemical Cycles*, Vol. 5, 1991, pp. 193-259.

Duinker, J. C. and Kramer, C. J. M., "An experimental study on the speciation of dissolved zinc, cadmium, lead and copper in river Rhine and North Sea water, by differential pulsed anodic stripping voltammetry," *Marine Chemistry*, Vol. 5, 1977, pp. 207-228.

Dyrssen, D., "Sulfide complexation in surface seawater," *Marine Chemistry*, Vol. 24, No. 2, 1988, pp. 143-153.

Electron Tubes Ltd.. Photomultipliers and Accessories. 1998. Electron Tubes Ltd. Ref Type: Catalog

Elliott, S., "Linear free energy techniques for estimation of metal sulfide complexation constants," *Marine Chemistry*, Vol. 24, 1988, pp. 203-213.

Emery, W. J. and Meincke, J., "Global water masses - summary and review," *Oceanologica Acta*, Vol. 9, 1986, pp. 383-391.

Esser, B. K., Volpe, A., Kenneally, J. M., and Smith, D. K., "Preconcentration and purification of rare-earth elements in natural- waters using silica-immobilized 8-hydroxyquinoline and a supported organophosphorus extractant," *Analytical Chemistry*, Vol. 66, 1994, pp. 1736-1742.

Fang, Z., *Flow injection separation and preconcentration*, VCH Verlagsgesellschaft, Germany, 1993.

Federova, O. S., Olkin, S. E., and Berdnikov, V. M., "The chemiluminescence mechanism in 1,10-phenanthroline oxidation during catalytic decomposition of hydrogen peroxide," *Zeitschrift fur Physikalische Chemie-Leipzig*, Vol. 263, No. 3, 1982, pp. 529-549.

Fletcher, P., Andrew, K. N., Calokerinos, A. C., Forbes, S., and Worsfold, P. J., "Analytical applications of flow injection with chemiluminescence detection - a review," *Luminescence*, Vol. 16, No. 1, 2001, pp. 1-23.

Florence, T. M. and Stauber, J. L., "Toxicity of copper-complexes to the marine diatom Nitzschia-*closterium*," *Aquatic Toxicology*, Vol. 8, No. 1, 1986, pp. 11-26.

Garcia, A. L., Gonzalez, E. B., and Sanzmedel, A., "Determination of trace-elements in seawater by electrothermal atomic- absorption spectrometry with and without a preconcentration step," *Mikrochimica Acta*, Vol. 112, 1993, pp. 19-29.

Garman, G. D., Pillai, M. C., and Cherr, G. N., "Inhibition of cellular events during early algal gametophyte development - effects of select metals and an aqueous petroleum waste," *Aquatic Toxicology*, Vol. 28, No. 1-2, 1994, pp. 127-144.

Gerringa, L. J. A., Rijstenbil, J. W., Poortvliet, T. C. W., Vandrie, J., and Schot, M. C., "Speciation of copper and responses of the marine diatom ditylum- brightwellii upon increasing copper concentrations," *Aquatic Toxicology*, Vol. 31, 1995, pp. 77-90.

Gerringa, L. J. A., Poortvliet, T. C. W., and Hummel, H., "Comparison of chemical speciation of copper in the Oosterschelde and Westerschelde estuaries, The Netherlands," *Estuarine Coastal and Shelf Science*, Vol. 42, 1996, pp. 629-643.

Gledhill, M., Nimmo, M., Hill, S. J., and Brown, M. T., "The toxicity of copper(II) species to marine algae, with particular reference to macroalgae," *Journal of Phycology*, Vol. 33, 1997, pp. 2-11.

Golimowski, J. and Golimowska, K., "UV-photooxidation as pretreatment step in inorganic analysis of environmental samples," *Analytica Chimica Acta*, Vol. 325, 1996, pp. 111-133.

Gonzalez-Davila, M., "The role of phytoplankton cells on the control of heavy-metal concentration in seawater," *Marine Chemistry*, Vol. 48, 1995, pp. 215-236.

Gorsuch.T.T., *The destruction of organic matter*, Pergamon Press, Oxford, 1970.

Grasshoff, K., Kremling, K., and Ehrhardt, M., *Methods of Seawater Analysis*, Third ed., Wiley-VCH, Weinheim, 1999.

Groschner, M. and Appriou, P., "3-Column system for preconcentration and speciation determination of trace-metals in natural-waters," *Analytica Chimica Acta*, Vol. 297, 1994, pp. 369-376.

Gueguen, C., Belin, C., Thomas, B. A., Monna, F., Favarger, P.-Y., and Dominik, J., "The effect of freshwater UV-irradiation prior to resin preconcentration of trace metals," *Analytica Chimica Acta*, Vol. 386, 1999, pp. 155-159.

Harrison, W. G., Eplley, R. W., and Renger, E. H., "Phytoplankton nitrogen metabolism, nitrogen budgets and observations on copper toxicity - a controlled ecosytem pollution experiment.," *Bull.Mar.Sci.*, Vol. 27, 1977, pp. 44-57.

Heissenberger, A. and Herndl, G. J., "Formation of high molecular weight material by free living marine bacteria," *Marine Ecology-Progress Series*, Vol. 111, No. 1-2, 1994, pp. 129-135.

Helmers, E. and van der Loeff, M. M. R., "Lead and aluminum in atlantic surface waters (50 °N to 50 °S) Reflecting anthropogenic and natural sources in the eolian transport," *Journal of Geophysical Research-Oceans*, Vol. 98, 1993, pp. 20261-20273.

Helmers, E. and Schrems, O., "Wet deposition of metals to the tropical north and the south-atlantic ocean," *Atmospheric Environment*, Vol. 29, 1995, pp. 2475-2484.

Helmers, E., "Trace metals in suspended particulate matter of Atlantic Ocean surface water (40 °N to 20 °S)," *Marine Chemistry*, Vol. 53, 1996, pp. 51-67.

Hojerslev, N. K., "Yellow substances in the sea," *The Role of Solar Ultraviolet Radiation in Marine Ecosystems*, edited by J. Calkins Plenum Press, New York, 1982, pp. 263-281.

Hooker, S. B., Rees, N. W., and Aiken, J., "An objective methodology for identifying oceanic provinces," *Progress in Oceanography*, Vol. 45, No. 3-4, 2000, pp. 313-338.

Huang, S. D. and Shih, K. Y., "Direct determination of copper in seawater with a graphite furnace atomic-absorption spectrometer.," *Spectrochimica Acta Part B-Atomic Spectroscopy*, Vol. 48, No. 12, 1993, pp. 1451-1460.

Huizenga, D. L. and Kester, D. R., "The distribution of total and electrochemically available copper in the Northwestern Atlantic Ocean," *Marine Chemistry*, Vol. 13, 1983, pp. 281-291.

Husar, R. B., Prospero, J. M., and Stowe, L. L., "Characterization of tropospheric aerosols over the oceans with the NOAA advanced very high resolution radiometer optical thickness operational product," *Journal of Geophysical Research-Atmospheres*, Vol. 102, 1997, pp. 16889-16909.

Imdadullah, I., "Development of new hybrid analytical methods based on the combination of solvent-extraction with reversed micellar-mediated chemiluminescence detection and their application to the trace determination of precious metals," *Bunseki Kagaku (Japan Analyst)*, Vol. 43, 1994, pp. 363-364.

Isildak, I., Asan, A., and Andac, M., "Spectrophotometric determination of copper(II) at low mu g L^{-1} levels using cation-exchange microcolumn in flow-injection," *Talanta*, Vol. 48, No. 1, 1999, pp. 219-224.

Jannasch, N. W. and Pritchard, P. H., "The role of inert particulate matter in the activity of aquatic microorganisms.," *Mem.Inst, Ital.Hydrobiol.*, Vol. 24, 1972, pp. 289-306.

Jickells, T. D., "Atmospheric inputs of metals and nutrients to the oceans - their magnitude and effects," *Marine Chemistry* , Vol. 48, 1995, pp. 199-214.

Kamidate, T., Ishikawa, A., and Watanabe, H., "Luminol chemiluminescence-delay method for determination of copper(Ii)," *Bulletin Of The Chemical Society Of Japan*, Vol. 65, 1992, pp. 1591-1594.

Katayama, A., Kamidate, T., and Watanabe, H., "Peroxidase-catalyzed chemiluminescence-delay of luminol for determination of traces of copper(Ii)," *Bulletin Of The Chemical Society Of Japan*, Vol. 65, 1992, pp. 2501-2504.

Kennish, M. J., *Practical Handbook of Marine Science*, 2nd ed., CRC Press 1994.

Kieber, D. J. and Blough, N. V., "Determination of carbon centred radicals in aqueous solution by liquid-chromatography with fluorescence detection," *Analytical Chemistry*, Vol. 62, No. 21, 1990, pp. 2275-2283.

Kieber, D. J., Jiao, J. F., Kiene, R. P., and Bates, T. S., "Impact of dimethylsulfide photochemistry on methyl sulfur cycling in the equatorial Pacific Ocean," *Journal of Geophysical Research-Oceans*, Vol. 101, No. C2, 1996, pp. 3715-3722.

Kolb, M., Rach, P., Schafer, J., and Wild, A., "Investigations of oxidative UV photolysis. 1. Sample preparation for the voltammetric determination of Zn, Cd, Pb, Cu, Ni and Co in waters," *Fres.J.Anal.Chem.*, Vol. 342, 1992, pp. 341-349.

Kremling, K., "Trace-metal fronts in European shelf waters," *Nature*, Vol. 303, No. 5914, 1983, pp. 225-227.

Kremling, K. and Hydes, D., "Summer distribution of dissolved Al, Cd, Co, Cu, Mn and Ni in surface waters around the british-isles," *Continental Shelf Research*, Vol. 8, 1988, pp. 89-105.

Kremling, K. and Pohl, C., "Studies on the spatial and seasonal variability of dissolved cadmium, copper and nickel in northeast atlantic surface waters," *Marine Chemistry*, Vol. 27, 1989, pp. 43-60.

Kremling, K. and Streu, P., "Saharan dust influenced trace-element fluxes in deep north-atlantic subtropical waters," *Deep-Sea Research Part I-Oceanographic Research Papers*, Vol. 40, 1993, pp. 1155-1168.

Lage, O. M., Parente, A. M., Soares, H. M. V. M., Vasconcelos, M. T. S. D., and Salema, R., "Some effects of copper on the dinoflagellates Amphidinium *carterae* and Prorocentrum *micans* in batch culture," *European Journal of Phycology*, Vol. 29, No. 4, 1994, pp. 253-260.

Lan, C. R. and Yang, M. H., "Synthesis, properties and applications of silica-immobilized 8-quinolinol. Part 1. Characterization of silica-immobilized 8- quinolinol synthesized via a Mannich reaction," *Analytica Chimica Acta*, Vol. 287, 1994, pp. 101-109.

Landing, W. M., Haraldsson, C., and Paxeus, N., "Vinyl polymer agglomerate based transition-metal cation chelating ion-exchange resin containing the 8-hydroxyquinoline functional group," *Analytical Chemistry*, Vol. 58, 1986, pp. 3031-3035.

Landing, W. M., Cutter, G. A., Dalziel, J. A., Flegal, A. R., Powell, R. T., Schmidt, D., Shiller, A., Statham, P. J., Westerlund, S., and Resing, J., "Analytical intercomparison results from the 1990 intergovernmental- oceanographic-commission open-ocean base-line survey for trace-metals - atlantic-ocean," *Marine Chemistry*, Vol. 49, 1995, pp. 253-265.

Landing, W. M.. Fractogel TSK-8HQ Resin Synthesis. 1996. Ref Type: Personal Communication

Laslett, R. E., "Concentrations of dissolved and suspended particulate Cd, Cu, Mn, Ni, Pb and Zn in surface waters around the coasts of England and Wales and in adjacent seas," *Estuarine, Coastal and Shelf Science*, Vol. 40, 1995, pp. 67-85.

Le Gall, A. C., Statham, P. J., Morley, N. H., Hydes, D. J., and Hunt, C. H., "Processes influencing distributions and concentrations of Cd, Cu, Mn and Ni at the North West European shelf break," *Marine Chemistry*, Vol. 68, No. 1-2, 1999, pp. 97-115.

Lewis, S. W., Price, D., and Worsfold, P. J., "Flow-injection assays with chemiluminescence and bioluminescence detection - a review," *Journal Of Bioluminescence And Chemiluminescence*, Vol. 8, 1993, pp. 183-199.

Liu, Z. S. and Huang, S. D., "Determination of copper and cadmium in sea-water by preconcentration and electrothermal atomic-absorption spectrometry," *Analytica Chimica Acta*, Vol. 267, 1992, pp. 31-37.

Longhurst, A., Sathyendranath, S., Platt, T., and Caverhill, C., "An estimate of global primary production in the ocean from satellite radiometer data," *Journal of Plankton Research*, Vol. 17, 1995, pp. 1245-1271.

Macdonald, A. M. G., Chan, L.-H., and Nieman, T. A., *Analytical Chemisty*, Vol. 51, 1979, pp. 2077-2082.

Mantoura, R. F. C., Wright, S. W., Jeffrey, S. W., Barlow, R. G., and Cummings, D. G., "Filtration and storage of pigments from maocroalgae," *Phytoplanton Pigments in Oceanography: Guidelines to Modern Methods*, edited by S. W. Jeffrey, R. F. C. Mantoura, and S. W. Wright Monographs on Oceanographic Methology, SCOR-UNESCO, 1997.

Mantoura, R. F. C., Dickson, A., and Riley, J. P., "The complexation of metals with humic materials in natural waters," *Estuar.Coast.Mar.Sci.*, Vol. 6, 1978, pp. 387-408.

Mantoura, R. F. C., "Organo-metallic interactions in natural waters. " *Marine Organic Chemistry*, edited by E. K. D. R. Duursma Elsevier Oceanography Ser. No 31, Elsevier, 1981.

Maranon, E. and Holligan, P. M., "Photosynthetic parameters of phytoplankton from 50 degrees N to 50 degrees S in the Atlantic Ocean," *Marine Ecology-Progress Series*, Vol. 176, 1999, pp. 191-203.

Maring, H., Savoie, D. L., Izaguirre, M. A., McCormick, C., Arimoto, R., Prospero, J. M., and Pilinis, C., "Aerosol physical and optical properties and their relationship to aerosol composition in the free troposphere at Izana, Tenerife, Canary Islands, during July 1995," *Journal of Geophysical Research-Atmospheres*, Vol. 105, No. D11, 2000, pp. 14677-14700.

Martin, J. H. and Fitzwater, S. E., "Iron-deficiency limits phytoplankton growth in the northeast pacific subarctic," *Nature*, Vol. 331, 1988, pp. 341-343.

Martin, J. H., Gordon, R. M., Fitzwater, S., and Broenkow, W. W., "VERTEX: Phytoplankton/iron studies in the Gulf of Alaska," *Deep-Sea Research Part A-Oceanographic Research Papers*, Vol. 36, 1989, pp. 649-680.

Mierle, G., "Studies on the uptake and toxicity of copper and other transition metal ions with a green algae *Scenedesmus acuminatus*," *Diss.Abstr.Int.*, Vol. 44, No. 03, 1983, pp. 663.

Miller, A. E. J., "Seasonal investigations of dissolved organic carbon dynamics in the Tamar Estuary, UK," *Estuarine Coastal and Shelf Science*, Vol. 49, No. 6, 1999, pp. 891-908.

Miller, J. N. and Miller, J. C., *Statistics and Chemometrics for Analytical Chemistry*, 4th ed., Prentice Hall; Pearson Education, Harlow, 2000.

Miller, W. L., "Recent advances in the photochemistry of natural dissolved organic matter," *Aquatic and Surface Photochemistry*, edited by G. R. Helz, R. G. Zepp, and D. G. Crosby Boca Raton, FL, 1994, pp. 111-127.

Miller, W. L. and Zepp, R. G., "Photochemical production of dissolved inorganic carbon from terrestial organic matter - significance to the oceanic organic carbon cycle," *Geophysical Research Letters*, Vol. 22, No. 4, 1995, pp. 417-420.

Miller, W. L. and Moran, M. A., "Interaction of photochemical and microbial processes in the degradation of refractory dissolved organic matter from a coastal marine environment," *Limnology And Oceanography*, Vol. 42, No. 6, 1997, pp. 1317-1324.

Millward, G. E., Glegg, G. A., and Morris, A. W., "Zn and Cu removal kinetics in estuarine waters," *Estuarine Coastal and Shelf Science*, Vol. 35, No. 1, 1992, pp. 37-54.

Moffett, J. W. and Zika, R. G., "Photochemistry of copper-complexes in seawater," *Abstracts Of Papers Of The American Chemical Society*, Vol. 189, 1985, pp. 2-GEOC.

Moffett, J. W. and Zika, R. G., "Reaction-kinetics of hydrogen-peroxide with copper and iron in seawater," *Environmental Science & Technology*, Vol. 21, 1987, pp. 804-810.

Moffett, J. W. and Zika, R. G., "Solvent-extraction of copper acetylacetonate in studies of copper(Ii) Speciation in seawater," *Marine Chemistry*, Vol. 21, 1987, pp. 301-313.

Moffett, J. W. and Zika, R. G., "Measurement of copper(I) in surface waters of the subtropical Atlantic and Gulf of Mexico," *Geochimica et Cosmochimica Acta*, Vol. 52, 1988, pp. 1849-1857.

Moffett, J. W., Zika, R. G., and Brand, L. E., "Distribution and potential sources and sinks of copper chelators in the sargasso sea," *Deep-Sea Research Part A-Oceanographic Research Papers*, Vol. 37, 1990, pp. 27-36.

Moffett, J. W., "Temporal and spatial variability of copper complexation by strong chelators in the sargasso-sea," *Deep-Sea Research Part I-Oceanographic Research Papers*, Vol. 42, 1995, pp. 1273-1295.

Moffett, J. W. and Croot, P. L., "Does a feedback loop control Cu speciation in seawater," *Abstracts Of Papers Of The American Chemical Society*, Vol. 209, 1995, pp. 112-GEOC.

Moffett, J. W. and Brand, L. E., "Production of strong, extracellular Cu chelators by marine cyanobacteria in response to Cu stress," *Limnology And Oceanography*, Vol. 41, 1996, pp. 388-395.

Moffett, J. W., Brand, L. E., Croot, P. L., and Barbeau, K. A., "Cu speciation and cyanobacterial distribution in harbors subject to anthropogenic Cu inputs," *Limnology And Oceanography*, Vol. 42, 1997, pp. 789-799.

Moffett, J. W., "Chemistry of toxic metals in coastal waters," *Abstracts Of Papers Of The American Chemical Society*, Vol. 216, 1998, pp. 6-SOCED.

Mopper, K. and Kieber, D. J., "Marine photochemistry and its impact on carbon cycling," *The effects of UV radiation in the marine environment*, edited by S. J. de Mora and M. Vernet Cambridge University Press, 2000, pp. 101-129.

Moran, M. A. and Zepp, R. G., "Role of photoreactions in the formation of biologically labile compounds from dissolved organic matter," *Limnology And Oceanography*, Vol. 42, No. 6, 1997, pp. 1307-1316.

Morris, A. W., Bale, A. J., and Howland, R. J. M., "Chemical Variability in the Tamar Estuary, South-West England," *Estuarine Coastal and Shelf Science*, Vol. 14, 1982, pp. 649-661.

Morris, A. W., "Removal of trace-metals in the very low salinity region of the tamar estuary, england," *Science of the Total Environment*, Vol. 49, 1986, pp. 297-304.

Morris, A. W., Bale, A. J., Howland, R. J. M., Loring, D. H., and Rantala, R. T. T., "Controls of the chemical composition of particle populations in a macrotidal estuary (Tamar Estuary, U.K.)," *Cont.Shelf Res.*, Vol. 7, 1987, pp. 1351-1355.

Mota A.M. and Correia Dos Santos, M. M., "Trace Metal Speciation of labile Chemical Species in Natural Waters: Electrochemical Methods," *Metal Speciation and Bioavailability in Aquatic Systems*, edited by A. Tessier and D. R. Turner, Vol. 3, IUPAC Series on Analytical and Physical Chemistry of Environmental Systems, John Wiley & Sons, Chichester, 1995, pp. 205-257.

Murphy l.S., Guillard, R. R. L., and Brown, J. F., "The effect of iron and manganese on copper sensitivity in diatoms: Differences in response of closely related neritic oceanic species.," *Biol.Oceanogr.* , Vol. 3, 1983, pp. 187-201.

Nakamura, T., Oka, H., shii, M., and Ato, J., "Direct atomisation atomic-absorbtion spectrometric determination of Be, Cr, Fe, Co, Ni, Cu, Cd, and Pb in water with Zirconium hydroxide coprecipitation.," *Analyst*, Vol. 119, No. 6, 1994, pp. 1397-1401.

Nelson, A., "Voltammetry of copper species in estuarine waters. Induced adsorption of copper on the hanging mercury drop electrode in complexing ligand/surfactant/chloride media," *Anal.Chim.Acta, 169*, Vol. 273-86, 1985.

Nickson, R. A., Hill, S. J., and Worsfold, P. J., "Solid-phase techniques for the preconcentration of trace-metals from natural-waters," *Analytical Proceedings*, Vol. 32, 1995, pp. 387-395.

Nimmo, M., van den Berg, C. M. G., and Brown, J., "The chemical speciation of dissolved nickel, copper, vanadium and iron in liverpool bay, irish sea," *Estuarine Coastal and Shelf Science*, Vol. 29, 1989, pp. 57-74.

Nolting, R. F., de Baar, H. J. W., Vanbennekom, A. J., and Masson, A., "Cadmium, copper and iron in the scotia sea, weddell sea and weddell scotia confluence (Antarctica)," *Marine Chemistry*, Vol. 35, 1991, pp. 219-243.

O'Neill, P., *Environmental Chemistry*, 2nd ed., Chapman and Hall, London, 1993.

Olson, D. B., Podesta, G. P., Evans, R. H., and Brown, O. B., "Temporal variations in the separation of Brazil and Malvinas Currents," *Deep-Sea Research*, Vol. 35, No. 12, 1988, pp. 1971-1990.

Palenik, B., Price, N. M., and Morel, F. M. M., "Potential effects of UV-b on the chemical environment of marine organisms - a review," *Environmental Pollution*, Vol. 70, 1991, pp. 117-130.

Paull, B., Foulkes.M, and Jones, P., "High performance chelation ion-chromatographic determination of trace metals in coastal seawater using dye impregnated resins," *Analyst*, Vol. 119, No. 5, 1994, pp. 937-941.

Perrin, D. D. and Dempsey, B., *Buffers for pH and metal ion control*, Chapman and Hall Laboratory 2002.

Pesavento, M. and Baldini, E., "Study of sorption of copper(II) on complexing resin columns by solid phase extraction," *Analytica Chimica Acta*, Vol. 389, 1999, pp. 59-68.

Pickard, G. L. and Emery, W. J., *Descriptive Physical Oceanography: An Introduction*, Fifth ed., Pergamon Press, Oxford, 1990.

Pohl, C., Kattner, G., and Schulzbaldes, M., "Cadmium, copper, lead and zinc on transects through Arctic and Eastern Atlantic surface and deep waters," *Journal of Marine Systems*, Vol. 4, No. 1, 1993, pp. 17-29.

Quentel, F., Elleouet, C., and Madec, C., "Determination of copper in seawater by adsorptive voltammetry with 1,2-dihydroxyanthraquinone-3-sulphonic acid," *Electroanalysis*, Vol. 6, No. 8, 1994, pp. 683-688.

Quetel, C. R., Remoudaki, E., Davies, J. E., Miquel, J. C., Fowler, S. W., Lambert, C. E., Bergametti, G., and Buatmenard, P., "Impact of atmospheric deposition on particulate iron flux and distribution in northwestern mediterranean waters," *Deep-Sea Research Part I-Oceanographic Research Papers*, Vol. 40, 1993, pp. 989-1002.

Rao, R. R. and Chatt, A., "Preconcentration neutron-activation analysis of trace elements in seawater by coprecipitation with 1-(2-thiazolylazo)-2-napthol, pyrrolidinedithiocarbamate and N-nitroso-phenylhydroxylamine," *Journal of Radioanalytical and Nuclear Chemistry-Articles*, Vol. 168, No. 2, 1993, pp. 439-448.

Raspor, B., Nurnberg, H. W., Valenta, P., and Branica, M., "Kinetics and mechanism of trace metal chelation in sea water," *Journal of Electroanalytical Chemistry*, Vol. 115, 1980, pp. 293-308.

Rijstenbil, J. W., Derksen, J. W. M., Gerringa, L. J. A., Poortvliet, T. C. W., Sandee, A., Vandenberg, M., Vandrie, J., and Wijnholds, J. A., "Oxidative stress-induced by copper - defense and damage in the marine planktonic diatom ditylum-brightwellii, grown in continuous cultures with high and low zinc levels," *Marine Biology*, Vol. 119, 1994, pp. 583-590.

Robards, K. and Worsfold, P. J., "Analytical applications of liquid-phase chemiluminescence," *Analytica Chimica Acta*, Vol. 266, 1992, pp. 147-173.

Robins, D. B. and Aiken, J., "The Atlantic Meridional Transect - an oceanographic research program to investigate physical, chemical, biological and optical variables of the Atlantic Ocean," *Underwater Technology*, Vol. 21, 1996, pp. 8-14.

Robinson, M. G. and Brown, L. N., "Copper complexation during a bloom of Gymnodinium sanguineum Hirasaka (Dinophyceae) measured by ASV," *Marine Chemistry*, Vol. 33, 1991, pp. 105-118.

Rueter, J. G. and Morel, F. M. M., "The interaction between zinc-deficiency and copper toxicity as it affects the silicic-acid uptake mechanisms in thalassiosira- pseudonana," *Limnology And Oceanography*, Vol. 26, 1981, pp. 67-73.

Ruzicka, J. and Hansen, E. H., *Flow Injection Analysis*, 2 ed., Wiley, New York, 1988.

Saager, P. M., de Baar, H. J. W., de Jong, J. T. M., Nolting, R. F., and Schijf, J., "Hydrography and local sources of dissolved trace metals Mn, Ni, Cu, and Cd in the northeast Atlantic Ocean," *Marine Chemistry*, Vol. 57, 1997, pp. 195-216.

Saitoh, K., Hasebe, T., Teshima, N., Kurihara, M., and Kawashima, T., "Simultaneous flow injection determination of iron(II) and total iron by micelle enhanced luminol chemiluminescence," *Analytica Chimica Acta*, Vol. 376, 1998, pp. 247-254.

Sanders, B. M., Jenkins, K. D., Sunda, W. G., and Costlow, J. D., "Free cupric ion activity in sewater - effect on metallothionein and growth in crab larvae," *Science*, Vol. 222, No. 4619, 1983, pp. 53-55.

Seaviewing Wide Field-of-View Sensor; http://daac.gsfc.gov/data/dataset/SeaWifs/

Scarano, G., Morelli, E., Seritti, A., and Zirino, A., "Determination of copper in seawater by anodic stripping voltammetry using ethylenediamine," *Analytical Chemistry*, Vol. 62, 1990, pp. 943-948.

Scarponi, G., Capodaglio, G., and Cescon, P., "Anodic stripping voltammetric determination of the contamination of seawater samples by cadmium, lead, and copper during filtration and storage.," *Analytica Chimica Acta*, Vol. 135, No. 2, 1982, pp. 263-276.

Schnitzer, M. and Khan, S. U., *Humic substances in the environment*, Marcel Dekker, New York, 1972.

Segawa, T., Ishikawa, H., Kamidate, T., and Watanabe, H., "Micelle-enhanced fluorescein chemiluminescence catalyzed by horseradish-peroxidase for the determination of hydrogen-peroxide," *Analytical Sciences*, Vol. 10, 1994, pp. 589-593.

Sharp, D. W. A., *Dictionary of Chemistry*, Second ed., Penguin 1993.

Shio, Y., Tamai, H., and Sasaki, K., "Inhibition of phtosystem II in the green algae *Ankistrodesmus falcatus* by copper," *Physiol.Pl*, Vol. 44, 1978, pp. 434-438.

Sillen, L. G., *Stability Constants of Metal-Ion Complexes, Special Publications no. 17*, 2nd ed., The Chemical Society, London, 1964, pp. 598.

Skoog, D. A., West, D. M., and Holler, F. J., *Fundamentals of analytical chemistry*, 7th ed., Saunders College Publishing 1996.

Slavin, W., Carnrick, G. R., and Manning, D. C., "Chloride interferences in graphite furnace atomic absorption spectrometry," *Analytical Chemistry*, Vol. 56, 1984, pp. 163-168.

Sperling, M., Yin, X. F., and Welz, B., "Determination of ultra-trace concentrations of elements by means of online solid sorbent extraction graphite-furnace atomic absorbtion spectrometry.," *Fresenius Journal of Analytical Chemistry*, Vol. 343, No. 9-10, 1992, pp. 754-755.

Spokes, L. J., Campos, M. L. A. M., and Jickells, T. D., "The role of organic matter in controlling copper speciation in precipitation," *Atmospheric Environment*, Vol. 30, 1996, pp. 3959-3966.

Stumm, W. and Morgan, J. J., *Aquatic Chemistry: Chemical Equilibria and Rates in Natural Waters*, 3rd ed., Vol. 5, Wiley-Interscience, New York, 1996.

Sunda, W., "Citation classic - the relationship between cupric ion activity and the toxicity of copper to phytoplankton," *Current Contents/Agriculture Biology & Environmental Sciences*, 1986, pp. 24.

Sunda, W. G. and Gillespie, P. A., "The response of a marine bacterium to cupric ion and its use to estimate cupric ion activity in seawater," *Journal of Marine Research*, Vol. 37, 1979, pp. 761-777.

Sunda, W. G. and Guillard, R. R. L., "The relationship between cupric ion activity and the toxicity of copper to phytoplankton," *J.Mar.Res.*, Vol. 34, 1976, pp. 511-529.

Sunda, W. G., Barber, R. T., and Huntsman, S. A., "Phytoplankton growth in nutrient rich seawater - importance of copper-manganese cellular interactions," *Journal of Marine Research*, Vol. 39, 1981, pp. 567-586.

Sunda, W. G. and Huntsman, S. A., "Relationships among growth-rate, cellular manganese concentrations and manganese transport kinetics in estuarine and oceanic species of the diatom thalassiosira," *Journal of Phycology*, Vol. 22, 1986, pp. 259-270.

Sunda, W. G. and Gessner, R. V., "The production of extracellular copper-complexing ligands by marine and estuarine fungi," *Chemical Speciation and Bioavailability*, Vol. 1, 1989, pp. 65-70.

Sunda, W. G. and Huntsman, S. A., "The use of chemiluminescence and ligand competition with EDTA to measure copper concentration and speciation in seawater," *Marine Chemistry*, Vol. 36, 1991, pp. 137-163.

Sunda, W. G. and Huntsman, S. A., "Regulation of copper concentration in the oceanic nutricline by phytoplankton uptake and regeneration cycles," *Limnology And Oceanography*, Vol. 40, 1995, pp. 132-137.

Sunda, W. G. and Huntsman, S. A., "Antagonisms between cadmium and zinc toxicity and manganese limitation in a coastal diatom," *Limnology And Oceanography*, Vol. 41, 1996, pp. 373-387.

Sunda, W. G. and Huntsman, S. A., "Interactive effects of external manganese, the toxic metals copper and zinc, and light in controlling cellular manganese and growth in a coastal diatom," *Limnology And Oceanography*, Vol. 43, 1998, pp. 1467-1475.

Sunda, W. G. and Huntsman, S. A., "Interactions among Cu2+, Zn2+, and Mn2+ in controlling cellular Mn, Zn, and growth rate in the coastal alga Chlamydomonas," *Limnology And Oceanography*, Vol. 43, 1998, pp. 1055-1064.

Tappin, A. D., Hydes, D. J., Burton, J. D., and Statham, P. J., "Concentrations, distributions and seasonal variability of dissolved Cd, Co, Cu, Mn, Ni, Pb and Zn in the English Channel," *Continental Shelf Research*, Vol. 13, No. 8-9, 1993, pp. 941-969.

Tappin, A. D., Millward, G. E., Statham, P. J., Burton, J. D., and Morris, A. W., "Trace metals in the Central and Southern North Sea," *Estuarine Coastal and Shelf Science*, Vol. 41, 1995, pp. 275-323.

Tomczak, M. and Godfrey, J. S., *Regional Oceanography; an introduction*, Pergamon 1994.

Townshend, A., *Encyclopedia of Analytical Science*, Academic Press 1995, pp. 852.

Tranvik, L. J., "Microbial transformation of labile dissolved organic matter into humic like matter in seawater," *Fems Microbiology Ecology*, Vol. 12, No. 3, 1993, pp. 177-183.

Valcarcel, M. and Luque de Castro, M. D., *Flow Injection Analysis: principles and applications*, Ellis Horwood, Chichester, 1987.

van den Berg, C. M. G., "Monitoring of labile copper and zinc in estuarine waters using cathodic stripping chronopotentiometry," *Marine Chemistry*, Vol. 34, 1991, pp. 211-223.

van den Berg, C. M. G., Boussemart, M., Yokoi, K., Prartono, T., and Campos, M. L. A. M., "Speciation of aluminum, chromium and titanium in the nw mediterranean," *Marine Chemistry*, Vol. 45, 1994, pp. 267-282.

van der Loeff, M. M. R., Helmers, E., and Kattner, G., "Continuous transects of cadmium, copper, and aluminium in surface waters of the Atlantic Ocean, 50oN to 50oS: Correspondence and contrast with nutrient-like behaviour," *Geochimica et Cosmochimica Acta*, Vol. 61, No. 1, 1997, pp. 47-61.

Vandenberg, C. M. G., Buckley, P. J. M., Huang, Z. Q., and Nimmo, M., "An electrochemical study of the speciation of copper, zinc and iron in 2 estuaries in england," *Estuarine Coastal and Shelf Science*, Vol. 22, 1986, pp. 479-486.

Westerlund, S. and Öhman, P., "Cadmium, copper, cobalt, nickel, lead, and zinc in the water column of the weddell sea, antarctica," *Geochimica et Cosmochimica Acta*, Vol. 55, 1991, pp. 2127-2146.

Woodward, E. M. S., Rees, A. P., and Stephens, J. A., "The influence of the south-west monsoon upon the nutrient biogeochemistry of the Arabian Sea," *Deep-Sea Research Part Ii-Topical Studies in Oceanography*, Vol. 46, 1999, pp. 571-591.

Worsfold, P. J., Achterberg, E. P., Bowie, A. R., Sandford, R. C., and Mantoura, R. F. C., "Flow injection with chemiluminescence detection for ship-board monitoring of trace metals," *Sensors in Oceanography*, edited by M. S. Varney Gordon and Breach Science Publishers , Amsterdam; 2000, pp. 49-71.

Wu, X. Z., Yamada, M., Hobo, T., and Suzuki, S., "Uranine sensitized chemi-luminescence for alternative determinations of copper(ii) and free cyanide by the flow- injection method," *Analytical Chemistry*, Vol. 61, 1989, pp. 1505-1510.

Xue, H. and Sigg, L., "Binding of Cu(II) to algae in a metal buffer," *Water Research*, Vol. 24, 1990, pp. 1129-1136.

Yamada, M. and Suzuki, S., "Micellar enhanced chemi-luminescence of 1,10-phenanthroline for the determination of ultratraces of copper(II) by flow injection method," *Analytical Letters Part A-Chemical Analysis*, Vol. 17, 1984, pp. 251-263.

Yamada, M., Kanai, H., and Suzuki, S., "Flavin mononucleotide chemi-luminescence for determination of traces of copper(ii) by continuous-flow and flow-injection methods," *Bulletin Of The Chemical Society Of Japan*, Vol. 58, 1985, pp. 1137-1142.

Yamada, M. and Suzuki, S., "Cyclic flow injection determination of copper with hexadecyltrimethylammonium bromide micelle-enhanced, fluorescein- sensitized chemi-luminescence detection," *Analytica Chimica Acta*, Vol. 193, 1987, pp. 337-341.

Yeats, P. A., Westerlund, S., and Flegal, A. R., "Cadmium, copper and nickel distributions at 4 stations in the eastern central and south-atlantic," *Marine Chemistry*, Vol. 49, 1995, pp. 283-293.

Yokoi, K., Tomisaki, T., Koide, T., and van den Berg, C. M. G., "Effective UV photolytic decomposition of organic-compounds with a low-pressure mercury lamp as pretreatment for voltammetric analysis of trace-metals," *Fresenius Journal of Analytical Chemistry*, Vol. 352, 1995, pp. 547-549.

Zafiriou, O. C., Joussot-Dubin, J., Zepp, R. G., and Zika, R. G., "Photochemistry of natural waters," *Envir.Sci.Technol.*, Vol. 18, 1984, pp. 358A-371A.

Zhou, X. and Mopper, K., "Determination of photochemically produced hydroxyl radicals in seawater and freshwater," *Marine Chemistry*, Vol. 30, 1990, pp. 71-88.

Zhuang, Z. and Hong, H., "A flow injection/atomic absorption spectrometry system with C sub(18)-bonded silica gel column online for the concentration and determination of trace metals in seawater," *Oceanol.Limnol.Sin.Haiyang.Yu.Huzhao.*, Vol. 23, 1992, pp. 264-269.

Zika, R. G., "Marine organic photochemistry," *Marine organic chemistry*, edited by E. K. Duursma and R. Dawson Elsevier, Amsterdam, 1981, pp. 299-325.

Zuehlke, R. W. and Kester, D. R., "Development of shipboard copper analyses by atomic-absorption spectroscopy,", edited by Z. Alberto Americal Chemical Society, Washington D.C., 1985, pp. 117-137.

Appendices

ELSEVIER

Analytica Chimica Acta 440 (2001) 27–36

ANALYTICA CHIMICA ACTA

www.elsevier.com/locate/aca

UV digestion of seawater samples prior to the determination of copper using flow injection with chemiluminescence detection

Eric P. Achterberg, Charlotte B. Braungardt, Richard C. Sandford, Paul J. Worsfold*

Department of Environmental Sciences, Plymouth Environmental Research Centre, University of Plymouth, Plymouth PL4 8AA, UK

Received 2 November 2000; received in revised form 28 December 2000; accepted 12 January 2001

Abstract

A purpose built UV digestion system was successfully used for the breakdown of Cu complexing organic ligands in seawater samples, prior to total dissolved Cu determination using flow injection with chemiluminescence detection (FI-CL) and on-line micro-column preconcentration/matrix removal. Residual dissolved organic carbon (DOC) was quantified using a DOC analyser. Humic acid (1.8–7.2 mg l^{-1} C) in ultra high purity (UHP) water was completely broken down within 4 h in all batch experiments (125 and 400 W lamps; with and without 15 mM H_2O_2 and, as expected, was more rapid with the 400 W lamp, in the presence of H_2O_2, and for lower humic acid concentrations. UV digestion experiments with seawater showed that the residual DOC concentration after batch UV treatment (4 h) was <0.08 mg l^{-1} C compared with >0.32 mg l^{-1} C after on-line irradiation (residence time 11.2 min). Therefore, the batch method was more efficient than on-line UV digestion at breaking down added humic acid and naturally present organic compounds in seawater. However, the release of Cu from metal complexing organic matter in seawater and estuarine water was the same using both on-line and batch UV digestion (sample irradiation residence time: 5.6 min and 8 h, respectively). UV digestion is, therefore, a contamination-free approach for seawater pretreatment prior to micro-column preconcentration and FI-CL determination of total dissolved Cu and should also be applicable to the selective determination of the total dissolved fractions of other trace metals in seawater (e.g. Co, Fe, Mn).

Keywords: UV digestion; Copper; Seawater; Preconcentration; Flow injection; Chemiluminescence detection; DOC

1. Introduction

Studies undertaken during the last two decades have shown that organic complexation is important for a number of trace metals in seawater. An important fraction (30–99.9%) of metals, including Co [1], Cu [2–4], Fe [5–7], Ni [8,9], Zn [10–12], is complexed by natural organic ligands in seawater. The organic complexation of metals is thought to prevent metal scavenging by suspended particulate matter and formation of insoluble inorganic metal complexes, thereby maintaining enhanced dissolved trace metal concentrations in seawater. The metal–organic complexes are strong, with reported conditional stability constants ($\log K_{MeL}$; where Me is the metal and L the ligand) for Co(II) (15.6–17.5) [1], Cu(II) (10–13) [4], Fe(III) (18.8–21.2) [5], Ni(II) (17.3–18.7) [13], and Zn(II) (10–10.5) [12]. For total dissolved trace metal determinations, it is necessary to release the trace metal from the metal–organic complex prior to analysis. Furthermore, the removal of dissolved organic matter (DOM) from samples is often preferable,

* Corresponding author. Tel.: +44-1752233009; fax: +44-1752233006.
E-mail address: p.worsfold@plymouth.ac.uk (P.J. Worsfold).

0003-2670/01/$ – see front matter
PII: S0003-2670(01)00824-8

as enhanced concentrations may interfere with the trace metal analysis. In some cases, DOM may cause fouling of the preconcentration column during trace metal determination using flow injection methods with on-line solid-phase preconcentration. In the case of stripping voltammetric methods, DOM may interfere with the physical and electrochemical processes occurring at the electrode surface and within its material. The nature of DOM in seawater is complex, but is thought to include humic acids, fulvic acids, glycollic acid, peptides, proteins, amino-acids, lipids and polysaccharides, and in coastal waters may also include EDTA, NTA, citric acid, tartaric acid and surfactants from anthropogenic sources [14].

Traditionally, wet digestion has been used as a method for the destruction of DOM in natural waters, thereby liberating trace metal ions, followed by total dissolved trace metal determination. Wet digestion methods use chemical oxidants such as sodium peroxodisulphate, nitric acid, sulphuric acid, perchloric acid or hydrogen peroxide to destroy organic matter [15]. A serious drawback of this approach is the addition of large concentrations of oxidants to the sample, and the often used open digestion/evaporation procedures, which can introduce contamination. As trace metal concentrations in marine waters are low (typically 10^{-11} to 10^{-8} M), wet digestion is not considered to be an acceptable sample preparation method. A preferred approach for the breakdown of dissolved metal–organic complexes and the removal of DOM involves treatment of the sample with ultra-violet (UV) radiation prior to trace metal determination [16–22]. UV digestion is a clean sample preparation method, as it does not require the addition of large amounts of oxidants. Furthermore, UV digestion is effective and can be readily incorporated in flow injection manifolds, allowing stand-alone trace metal analysis. A commonly used source of UV radiation for UV digestion methods is a Hg vapour lamp. The spectrum of a medium pressure Hg vapour lamp (used in our study) is rich in lines in the UV range (40–400 nm), with a pronounced signal at ca. 254 nm arising from with the transition of Hg atoms from their lowest excited state (6^3P_0) to the ground state (6^1S_0). In addition, lines are present at ca. 185 nm and correspond to the $6^1P_1 \rightarrow 6^1S_0$ transition. A relatively small number of Hg atoms are excited to atomic states higher than 6^1P_1, but their lines are weak. The main wavelengths involved in the breakdown of DOM during UV digestion of natural water samples are reported to be 185 and 254 nm [16,17,19].

Photo-degradation of organic matter in natural waters by sunlight is thought to proceed by mechanisms which involve singlet oxygen reactions and free radical auto-oxidation [23–26], and similar processes can be expected to take place during UV digestion of samples. The excited (singlet) $^1O_2$ state is formed by transfer of energy from sensitisers (organic molecules, e.g. humic acid), which have been excited through UV radiation capture, to molecular oxygen in the ground state (triplet; $^3O_2$). Singlet oxygen is highly reactive and thought to be an important intermediate product of DOM decomposition. Organic reactants susceptible to singlet oxygen attack include molecules with electron-rich centres (e.g. phenols) and those containing oxidisable functional groups [16]. Singlet oxygen is rapidly quenched by water, but the strong UV exposure of samples during UV digestion may result in an enhanced concentration of this reactive intermediate. The formation of hydroxyl radicals, produced by the action of UV radiation on H_2O, or H_2O_2 added to samples, and their subsequent reaction with organic matter is reported to play an important role in DOM breakdown [27]. The greater the number of hydroxyl radicals, the faster the UV breakdown of DOM proceeds because of their role in initiating radical chain reaction involving organic molecules. The direct breakdown pathway of DOM through exposure to UV radiation is thought to play a minor role during UV digestion of samples [27].

This paper reports on the effectiveness of batch and on-line UV digestion of samples prior to Cu analysis using flow injection with chemiluminescence detection (FI-CL). The FI-CL method is based on breakdown of 1,10-phenanthroline, which is catalysed by Cu in an alkaline medium [28,29]. The FI-CL method uses an on-line micro-column with 8-hydroxyquinoline (8-HQ) immobilised on a resin for preconcentration of trace metals and removal of matrix interference. Uncertainties exist about the extent of trace metal binding by the immobilised 8-HQ during preconcentration, due to the competition with the natural metal complexing organic ligands. Copper was chosen as a model metal, because more than 95% of dissolved Cu occurs in strong organic complexes in seawater [4], and hence, the binding of this element

by the micro-column may be thermodynamically or kinetically limited. Experiments on UV digestion efficiency have been conducted using samples (seawater and deionised water) with added DOM (humic acid), and natural seawater samples. The UV digestion efficiency has been evaluated by determination of dissolved organic carbon (DOC), fluorescence and Cu in the treated water samples.

2. Experimental

2.1. Sample collection and reagents

Low carbon seawater (LCSW) for UV digestion efficiency experiments involving the addition of humic acid was collected in the Western Approaches (coastal area near Plymouth, UK) from a depth below the thermocline (>37 m depth, salinity $S = 34.7$). The water was filtered on-line (peristaltic pump, Gilson Minipuls 3) using a filtration unit (47 mM diameter, Swinnex, Nalgene) fitted with a 0.45 μm pore size membrane filter (cellulose nitrate, Whatman) and passed through a Sep-pak C18 column (Millipore) in order to remove hydrophobic compounds. Subsequently, the water was UV digested for 12 h (batch UV treatment using 400 W Hg lamp; further details below) in the presence of H_2O_2 (15 mM). A seawater sample for UV digestion efficiency experiments investigating the release of Cu from natural Cu complexing organic ligands was collected in the Tamar Estuary (south-west UK, $S = 22$) in an acid-cleaned high density polyethylene (HDPE) container (10 l). The water was vacuum filtered using a filtration unit (polysulphone 500 ml, Nalgene) fitted with 0.45 μm pore size, cellulose nitrate membrane filters (47 mM diameter, Whatman). The Tamar sample was processed immediately upon sampling. Furthermore, seawater samples for similar experiments were collected from a coastal region south of Ireland (Celtic Sea) during the Propheze cruise on-board the *RRS Discovery*. Samples from different depths were collected using acid-cleaned Teflon™ lined Niskin™ samplers attached to a stainless steel rosette frame. The samples were vacuum filtered on-board ship using polycarbonate membrane filters (0.4 μm; Nuclepore) fitted in a filtration unit (500 ml, Nalgene), and stored frozen (−20°C) in acid-cleaned HDPE sample bottles (500 ml; Nalgene).

All reagents and standards were of analytical grade, supplied by Merck BDH, unless stated otherwise, and prepared in deionised (ultra-high purity; UHP) water. UHP water, which is low in carbon and trace metals, was obtained from an Elgastat Maxima system ($\geq 18.2\ \Omega\ m\ cm^{-1}$) fitted with UV treatment. A humic acid (250 mg l^{-1} HA) stock solution was prepared by dissolution of commercial HA (Aldrich) in UHP. HA solutions in UHP and LCSW used for the experiments were made by dilutions of the stock solution. The HA solutions were refrigerated and found to be stable for three months. Elemental analysis of the solid HA material using a CHNS analyser (CE instruments EA 1110), yielded the following composition: 36.7% C, 4.7% H and 1.7% N.

Standard solutions for the determination of DOC were prepared from potassium phthalate (KPH, 0.5–12.5 mg l^{-1} C, Shimadzu) in acidified (quartz distilled HCl (Q-HCl), pH 2) UHP. Standard solutions for the fluorescence determinations were prepared by dilution of HA stock solution in acidified (Q-HCl, pH 2) UHP and LCSW, respectively (0.5–2.0 mg l^{-1} HA). Solutions for FI-CL determination of dissolved Cu in seawater included hydrogen peroxide (0.7 M), 1,10-phenanthroline (60 μM; Fluka), sodium hydroxide (80 mM), cetyldimethylethylammonium bromide (CEDAB) (15 mM; Aldrich), tetraethylene pentamine (TEPA) (0.4 μM), citrate buffer (0.2 M, resulting in final pH 5.2 upon mixing with the acidified sample in FI-CL manifold) and 0.2 M Q-HCl for eluting preconcentrated Cu from the micro-column. Solutions for the determination of Cu in seawater using adsorptive cathodic stripping voltammetry (AdCSV) included *N*-hydroxyethylpiperazine-*N*′-2′-ethanesulphonic acid (HEPES) pH buffer (1 M, pH 7.7), salicylaldoxime (SA; 0.01 M) as AdCSV ligand and quartz distilled ammonia (Q-NH_3) for sample pH adjustment. Standard solutions of Cu(II) in the range 10^{-6} to 10^{-7} M were prepared from dilution of an atomic absorption standard solution (Spectrosol, 10,000 mg l^{-1}) and acidified to pH 2 using 6 M Q-HCl.

2.2. Labware, instrumentation and methods

For DOC and fluorescence determinations, quartz UV digestion tubes and other glassware were washed in a warm Decon solution (5% v/v) and rinsed with UHP [30]. Vials used in the autosampler of the DOC

analyser were ashed (450°C, >4 h) after washing. For Cu determinations, quartz UV digestion tubes were washed in Decon, followed by a two-step wash in HCl (1 M) and rinsed with UHP. High density polyethylene (HDPE) bottles (Nalgene) were washed in Decon, followed by a two-step wash in HCl (6 M) and HNO_3 (2 M), and thoroughly rinsed with UHP.

UV digestion of samples was effected by irradiation of solutions using 125 and 400 W medium pressure Hg lamps (Photochemical Reactors), positioned in a purpose-built aluminium lamp housing, which was cooled by a fan (RS, air flow 40 l min^{-1}). The power supply for the lamps (Photochemical Reactors) switched from a high output during the initiation of the Hg arc lamp to a reduced output for continuous operation. The housing was light tight to prevent exposure to harmful UV radiation and the power supply to the UV lamp was cut automatically upon opening the digestion unit. Medium pressure UV lamps produce ozone, and therefore, all UV digestion experiments were performed in a fume cupboard. Batch experiments were carried out by placing up to eight quartz glass UV digestion tubes (30 ml, 18 mM i.d.) fitted with PTFE caps in the unit. The centre-to-centre distance between the light source and the tubes was ca. 5 cm. For on-line UV digestion of samples, a quartz coil was positioned in the unit and solutions were pumped through the coil using a peristaltic pump (Gilson Minipuls 3). The light source was positioned in the centre of the coil, which has 16 loops of 7 cm diameter (length ca. 3.5 m) and 1.0 mM i.d., giving a volume of ca. 2.8 ml.

DOC was determined using a high temperature catalytic oxidation method (HTCO, Shimadzu; TOC analyser model 5000A, with model ASI autosampler) [30]. The analytical performance of the TOC analyser was verified by determination of the non-purgeable organic carbon concentration in a reference seawater (deep sea reference; DSR) prepared by the Bermuda Biological Station. During each DOC run a DSR sample was analysed in triplicate. The results of these analyses (44.4 μM C, 2σ = 5.6 μM C, n = 30) agreed well with the nominal value (44–45 μM C). A spectrofluorimeter (Hitachi, model F-4500) was used to measure fluorescence using excitation and emission wavelengths of 260 and 472 nm, respectively (Ex slit width 10 μM, Em slit width 20 μM, PMT voltage 700 V). DOC and FS were measured within hours of irradiation of the samples.

The FI-CL manifold for dissolved Cu analyses is shown in Fig. 1. Two peristaltic pumps (Gilson Minipuls 3) were used to deliver the sample and buffer, UHP water, eluent and reagents. All manifold tubing

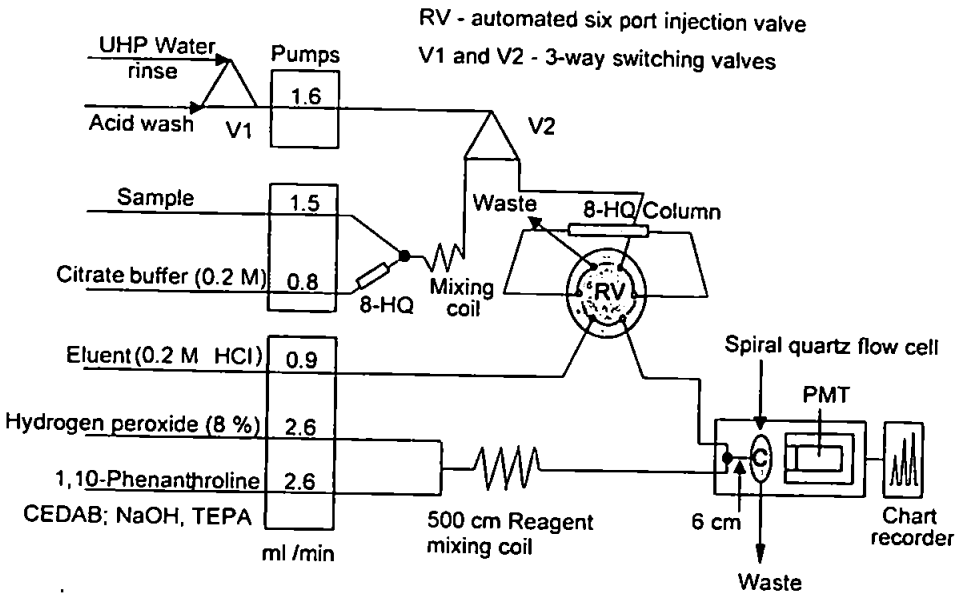

Fig. 1. FI-CL manifold for the determination of Cu in seawater.

was PTFE (0.75 mm i.d., Elkay) except for the peristaltic pump tubing, which was Tygon (Elkay). The preconcentration micro-column containing immobilised 8-HQ on a hydrophilic vinyl co-polymer was synthesised according to the method of Landing et al. [31] using Toyopearl HW-75F resin (TSK; 30–60 μm, fine, Toso-Haas, Anachem). The micro-column was constructed from Perspex® and the TSK-8HQ resin sealed inside using polyester pads and nylon frits. The column was installed in the six-port rotary injection valve and cleaned with 0.5 M quartz-distilled HCl for at least 4 h, followed by UHP water for 1 h, prior to use. A six-port PTFE rotary injection valve (Rheodyne, model 5020) was used to transport the sample to the detector. A quartz glass spiral flow cell (1.0 mM i.d., 130 μl internal volume) positioned behind a mirror in a sealed housing enabled the CL reaction to be monitored. The detection system consisted of an end-window photomultiplier tube (Electron Tubes, 9798QA) contained in a μ-metal shield for magnetic insulation (M552D), an ambient temperature shielded housing (B2F/RFI) and a 1.165 kV power supply (Electron Tubes, PM28B). Peak detection and quantification was achieved using a flatbed chart recorder (Kipp and, Zonen BD111). Computerised control of the FI-CL manifold was undertaken in a QuickBasic programming environment using a D/A device control interface card (Brainboxes) housed in a desktop PC. The analytical sequence for the FI-CL determination of Cu was as follows: the 8-HQ micro-column was loaded with sample (buffered to pH 5.2) for 90 s, followed by a 20 s rinse with UHP water to remove interfering major seawater ions. Copper was eluted (30 s) from the column using 0.2 M HCl and this stream was merged with the reagent streams (H_2O_2, 1,10-phenanthroline, CEDAB, NaOH, TEPA) and a CL signal was obtained. Samples were analysed four times and Cu in the samples was quantified by the standard addition method. The precision of the method was <5% at 1.0 nM Cu, with a linear range of 0.01–50 nM. Further details of this method will be described elsewhere.

Dissolved Cu was determined by AdCSV using a voltammetric analyser (Autolab PGSTAT 10, Ecochemie) connected to a hanging mercury drop electrode (663 VA Stand, Metrohm). To an aliquot (10 ml) of sample, 100 μl of HEPES buffer was added (final concentration: 10 mM, pH 7.7) and 25 μl SA (final concentration: 25 μM) [32]. In order to neutralise the pH value, Q-NH_3 (22 μl) was added to acidified samples. The following voltammetric conditions were used: sample purge time: 3 min (nitrogen gas); deposition time: 15 s; deposition potential: −0.12 V; scan form: square wave (50 Hz). Samples were analysed in duplicate, and quantification of the dissolved Cu concentration was undertaken using the standard addition method. The analytical precision of the Cu AdCSV method was typically below 5%.

Certified reference seawaters (SLEW-2 and NASS-4) were analysed to verify the accuracy of the FI-CL and AdCSV methods for Cu analysis, and in all cases a good agreement (*t*-test; $P = 0.05$) was obtained between measured and certified values. In order to reduce airborne contamination, all sample handling which involved waters to be analysed for dissolved Cu was performed inside a class-100 laminar flow hood (Bassaire, model A3VB).

2.3. Experiments

Solutions containing HA (UHP_{HA} and $LCSW_{HA}$) were irradiated using the 125 and 400 W lamps. The effect of the UV digestion on the HA breakdown was assessed by DOC and fluorescence measurements. In order to mimic conditions used for UV digestion prior to trace metal analysis, the UHP_{HA} and $LCSW_{HA}$ solutions were acidified to pH 2 (using Q-HCl) prior to UV digestion. Experiments were performed in the absence and presence of H_2O_2 (15 mM; final concentration). Batch experiments were carried out by placing the aliquots in quartz glass tubes and irradiating for up to 12 h. On-line experiments were carried out by pumping UHP_{HA} and $LCSW_{HA}$ solutions at specific flow rates (0.25–4 ml min^{-1}) through the quartz coil. During UV digestion, the sample temperature in the quartz tubes was ca. 92°C (400 W) and 80°C (125 W), and in the coil ca. 70–90°C, depending on the flow rate. UV digestion of acidified (pH 2) seawater samples from the Celtic Sea and Tamar Estuary was undertaken to investigate release of Cu from Cu complexing ligands in batch and flow modes using the 400 W Hg lamp. Acidification prior to UV digestion is necessary in order to prevent trace metal loss by adsorption onto the walls of the quartz tubes and coil. The effect of the UV digestion on the breakdown of naturally present Cu complexing organic ligands was

followed by determination of Cu using FI-CL for the Celtic Sea samples, and AdCSV and FI-CL for the Tamar sample aliquots.

3. Results and discussion

3.1. UV digestion of UHP_{HA} and $LCSW_{HA}$

Fig. 2(a) shows the results of batch UV digestion experiments of UHP with 20 mg l^{-1} of HA (7.2 mg C l^{-1}), in the presence and absence of H_2O_2, using 125 and 400 W lamps. The results are presented as the fraction of DOC remaining. The added HA concentration is high but such levels could be encountered in upper estuarine regions receiving large amounts of soil run-off [14]. In the presence of H_2O_2 (15 mM), the fraction of DOC remaining was <1% after 2 h of irradiation using 125 and 400 W lamps. For 5 mg l^{-1} of HA (1.8 mg C l^{-1}) the DOC remaining was <1% after 0.5 h with the 400 W lamp and < 1% after 1 h with the 125 W lamp. After 4 h DOC concentrations in all solutions (even without H_2O_2) were close to the limit of detection (LOD) of the TOC analyser

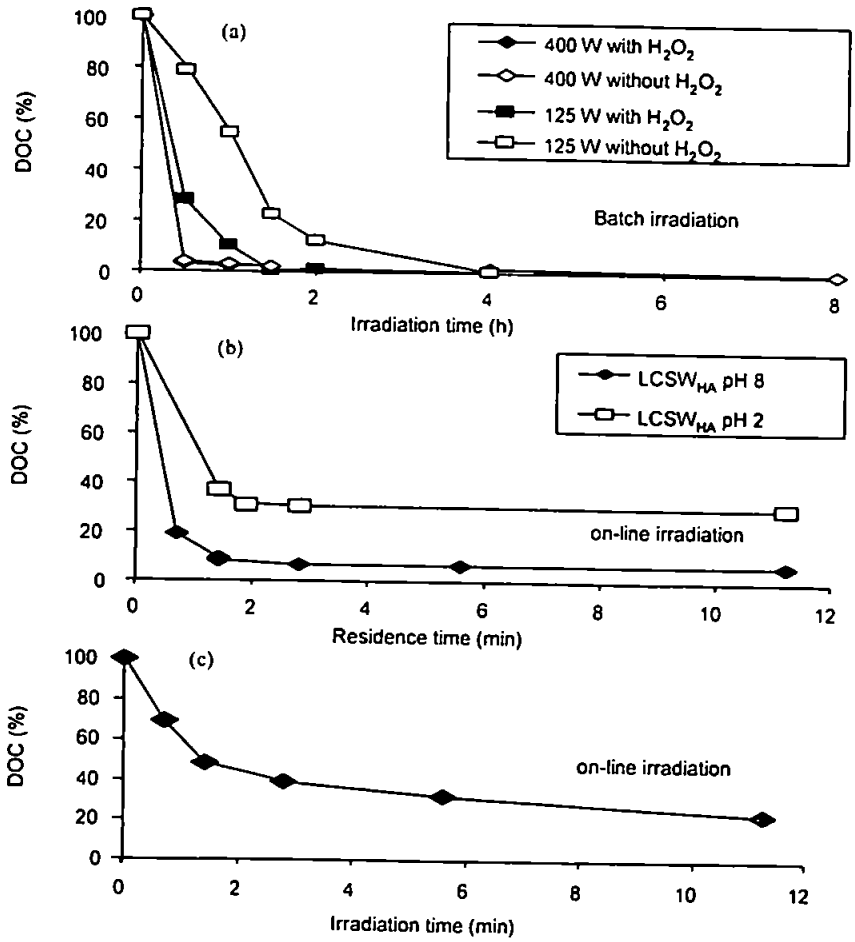

Fig. 2. Fractions of residual organic matter determined using DOC during timed digestion experiments on (a) ultra high purity water–humic acid solutions (20 mg l^{-1} HA), in the presence (15 mM) and absence of H_2O_2, using batch UV digestion with 125 and 400 W Hg lamps; (b) neutral (pH 8) and acidified (pH 2) low carbon seawater–humic acid solutions (6.9 mg l^{-1} HA), in the presence of H_2O_2 (15 mM), using on-line UV digestion with a 400 W Hg lamp; (c) Tamar Estuary water, in the presence of H_2O_2 (15 mM), using on-line UV digestion with a 400 W Hg lamp.

(LOD = 0.08 mg l^{-1} C; 3 s of UHP analysis, $n = 20$). Similar results have been reported by other workers [27] and ascribed to an enhanced formation of hydroxyl radicals (from H_2O_2) which aid the breakdown process.

Breakdown experiments with UHP_{HA} (16.2 mg l^{-1} HA or 6.1 mg l^{-1} C) and $LCSW_{HA}$ (14.4 mg l^{-1} HA or 5.4 mg l^{-1} C) solutions using on-line UV digestion (400 W lamp) in the presence of H_2O_2 (15 mM) showed that breakdown of HA was less efficient in the LCSW matrix. After a sample residence time of 5.6 min in the quartz coil (flow rate 0.5 ml min^{-1}), 20% of the $LCSW_{HA}$ DOC fraction remained, compared with 6.7% of the UHP_{HA} fraction. Fluorescence measurements, however, indicated that the breakdown of both solutions was quantitative, with residual responses of 0.15 and 0.10%, respectively, after a sample residence time of 5.6 min. The conditions used for the on-line UV digestion were, therefore, effective at destroying fluorescent centres in HA molecules, but were not fully effective in completely breaking down organic matter into inorganic constituents (including production of CO_2). A slowing of the photolytic decomposition rate of organic compounds with increasing ionic strength has been observed by other workers [19,20], and linked to the absorption of UV radiation by chloride and other ions and the scavenging of hydroxyl radicals by chloride. In addition, at low pH, coagulation of HA may have occurred, especially at increased ionic strength, and this could be linked to the reduced efficiency of DOC breakdown in $LCSW_{HA}$, compared with UHP_{HA}. These results also show the limitation of using fluorescence spectroscopy for assessing the efficiency of total UV digestion of organic matter. In order to compare the concentration of trace metals released during UV irradiation with the amount of organic matter destroyed, the quantification of residual dissolved organic carbon by HTCO, or similar methods, is required.

Fig. 2b shows the efficiency of on-line UV digestion of acidified (pH 2) and non-acidified (pH 8) $LCSW_{HA}$ (6.95 mg l^{-1} HA or 2.55 mg l^{-1} C) samples, with 8.6 and 32% residual DOC, respectively. Previous investigations ([19] and references therein) indicated that the photolytic decomposition rate of some organic compounds (e.g. phenylalanine and benzene) increases in acidic solutions, while that of others increases with (e.g. trichloroethylene), or remains unaffected by (e.g. 2-propanol) pH. The results of this study show that the influence of pH (enhanced decomposition of HA at higher pH) and ionic strength (lower decomposition efficiency at high ionic strength) on sample decomposition is more pronounced during on-line UV digestion than during batch digestion due to shorter residence times and depletion of dissolved oxygen during on-line UV treatment.

3.2. UV digestion of estuarine and coastal water samples

Fig. 2c shows the results of on-line digestion (400 W lamp) of a sample from the Tamar estuary (DOC 2.27 mg l^{-1} C), which receives treated and untreated sewage discharges and run-off from agricultural fields and moorlands (high in humic and fulvic acids). UV digestion was undertaken in the presence of H_2O_2 (15 mM) at pH 2 and the results show a broad similarity for batch and on-line digestion experiments conducted using $LCSW_{HA}$ solutions, with 23% of DOC still remaining after a residence time in the UV coil of 11.2 min (flow rate 0.25 ml min^{-1}).

3.3. Determination of Cu after UV digestion of estuarine and coastal water samples

UV digestion was undertaken using acidified (pH 2, Q-HCl) samples in the presence of H_2O_2 (15 mM). The Cu available after UV photolysis was determined using FI-CL and AdCSV (as a comparative method). Batch and on-line UV digestion of Tamar water resulted in an increase in the labile Cu concentration with prolonged irradiation times (Fig. 3). A 12 h digestion period was assumed to represent 100% release of organically complexed Cu, and yielded Cu concentrations of 48.6 ± 3.5 nM (FI-CL, $n = 4$) and 48.5 ± 0.6 nM (AdCSV, $n = 3$). For both batch and on-line UV digestion, in the initial stages of irradiation, the labile Cu concentrations determined by AdCSV were slightly higher than those determined by FI-CL after preconcentration on an 8-HQ microcolumn. This difference can be explained by the different analytical conditions of ligand competition during analysis using the two methods. At pH 2, 8-HQ is a stronger ligand for Cu than SA but is also less selective. In its immobilised form on the micro-column, the complexation of Cu by 8-HQ may be hindered

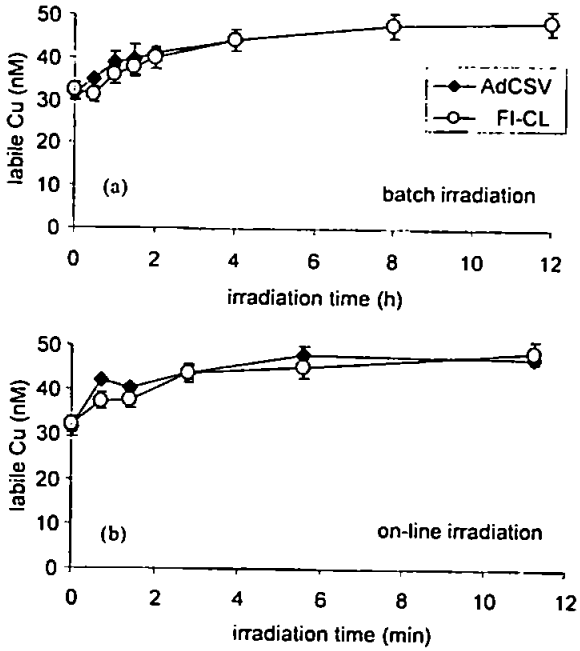

Fig. 3. Labile Cu concentrations (nM) during timed digestion experiments on Tamar Estuary water, in the presence of H_2O_2 (15 mM), using (a) batch and (b) on-line UV digestion with a 400 W Hg lamp. Two methods of Cu determination were used: flow injection with chemiluminescence detection (FI-CL) and adsorptive cathodic stripping voltammetry (AdCSV). Error bars represent +/−35.

by non-selective binding of major seawater cations and also kinetically limited. Therefore, it is important that quoted values for 'dissolved' Cu concentrations in seawater are operationally defined.

Batch digestion for 8 h released 99% of the Cu in the Tamar sample (Fig. 3a, both methods of Cu analysis). On-line UV digestion with a sample residence time of 5.6 min (0.5 ml min^{-1} flow rate) resulted in a 99 and 93% recovery of Cu measured with AdCSV and FI-CL, respectively, while 100% recovery was achieved with a flow rate of 0.25 ml min^{-1} (11.2 min residence time) and FI-CL detection (Fig. 3b). These results indicate that complete release of Cu from complexing organic ligands was achieved using on-line UV digestion, although the measurement of DOC showed that a significant fraction of the organic matter was resistant to UV photolysis using the applied method (see Fig. 2c). This suggests that the functional groups on organic molecules involved in complexing Cu are more susceptible to breakdown than other parts

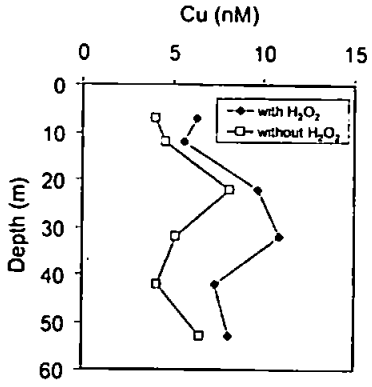

Fig. 4. Depth profiles of dissolved Cu in the Celtic Sea (station 22/06; 51.2°N, 7.2°W). Cu determination using FI-CL detection after batch UV digestion (400 W lamp, 4 h digestion) in the presence (15 mM) and absence of H_2O_2.

of the molecule and/or non-complexing molecules when using on-line UV digestion.

Fig. 4 shows depth profiles for Cu in the Celtic Sea (station 22/06), determined using FI-CL, after batch UV digestion (4 h, 400 W lamp) of filtered and acidified (pH 2, Q-HCl) samples in the absence and presence of H_2O_2 (15 mM). The results show that addition of H_2O_2 to the samples significantly enhanced sample digestion and made 18–52% more Cu available to the 8-HQ preconcentration/matrix removal column. Station 22/06 (51.3°N, 7.3°W) is situated in a coastal region, away from direct land-derived run-off. The DOC concentrations in the samples from this station ranged between 0.88 and 0.96 mg l^{-1} C, which is lower than the DOC concentration in the Tamar. Most of the DOC in the Celtic Sea is biologically produced in situ, and it is likely that this biogenic DOC is more susceptible to UV breakdown than humic acids. DOC analysis in the UV digested samples (4 h, batch UV digestion) resulted in concentrations below the LOD of the TOC analyser (samples with and without added H_2O_2), indicating the ease of breakdown of the organic matter in these coastal water samples. The Cu concentration in the coastal water ranged between ca. 5 and 10.5 nM, which compares well with levels observed in regional coastal seas (7–18 nM, Irish Sea/Liverpool Bay [33]; 3.5–24 nM, Irish Sea/Liverpool Bay [34]; 5–7 nM, western Irish Sea [35]).

Fig. 5 shows depth profiles for Cu from station 18/06 (51.5°N, 6.4°W) determined using FI-CL with

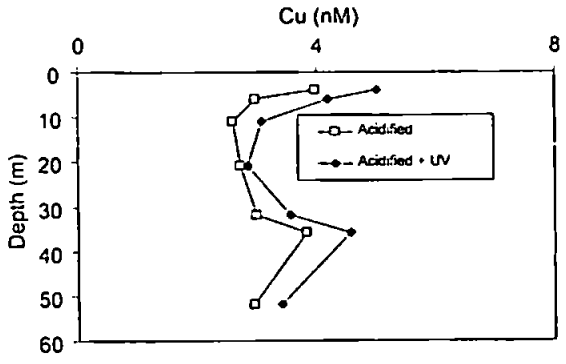

Fig. 5. Depth profiles of dissolved Cu in the Celtic Sea (station 18/06: 51.5°N, 6.4°W). Cu determination using acidified (pH 2) samples and FI-CL detection with and without on-line UV digestion (400 W lamp).

and without addition of H_2O_2 (10 nM) and on-line UV digestion (residence time 10 min). All samples were filtered (0.45 μm) and frozen immediately after collection, stored and thawed and acidified (pH 2, Q-HNO_3) prior to analysis. The results show that between 5 and 29% of the total Cu measured was only liberated after UV digestion, i.e. acidification to pH 2 alone did not release all of the Cu. Clearly further experiments are required in order to establish whether the results can be extrapolated to other seawater matrices (and other trace metals) but it re-emphasises the point that sample treatment protocols have a significant effect on the concentration of Cu measured.

4. Conclusions

Batch and on-line UV digestion using a 400 W medium pressure Hg vapour lamp, in the presence of added H_2O_2, was effective in breaking down Cu complexing organic ligands prior to the determination of Cu using FI-CL. Batch UV experiments, with DOC analyses of treated sample aliquots, indicated that humic acid was broken down in UHP and LCSW within 2 h using a 400 W lamp. On-line UV digestion (400 W lamp) with a sample residence time of 5.6 min was less effective for the breakdown of HA in UHP and LCSW, compared with batch UV digestion (400 W lamp; digestion time of 2–4 h), in terms of residual DOC concentration. Incomplete DOC removal using on-line UV digestion was also observed in Tamar Estuary water, indicating that on-line UV digestion does not fully break down the more residual organic matter fraction. However, fluorescence measurements indicated that both UV digestion approaches were effective at breaking down fluorophores in the sample aliquots. Furthermore, on-line UV digestion (400 W lamp, 5.6–11.2 min residence time) was effective in releasing Cu from complexing organic ligands in an estuarine sample, prior to FI-CL and AdCSV analysis. The results using natural water samples (Tamar Estuary and Celtic Sea) showed that UV digestion prior to 8-HQ micro-column preconcentration is necessary to obtain accurate total dissolved Cu concentrations. The UV digestion of samples, prior to 8-HQ micro-column preconcentration/matrix removal with FI-CL analysis, can also be applied to other metals (e.g. Co, Fe, Mn) and is, therefore, a contamination-free approach to the pretreatment of seawater samples for the determination of total dissolved trace metals. This approach is also compatible with detection by inductively coupled plasma mass spectrometry and inductively coupled plasma atomic emission spectrometry.

Acknowledgements

The authors thank the European Union for funding under the MAST programme (Grant number MAS3-CT97-0143, MEMOSEA), Toby Holland for sample collection in the Celtic Sea during the Propheze cruise, Georgina Spyres for help with the DOC measurements and Andrew Tonkins for the CHN analysis. EPA would like to thank *Analytica Chimica Acta* for the provision of a bursary to attend Euroanalysis XI.

References

[1] H. Zhang, C.M.G. van den Berg, R. Wollast, Mar. Chem. 28 (1990) 285.
[2] K.H. Coale, K.W. Bruland, Limnol. Oceanogr. 33 (1988) 1084.
[3] L.J.A. Gerringa, T.C.W. Poortvliet, H. Hummel, Estuarine Coastal Shelf Sci. 42 (1996) 629.
[4] J.W. Moffett, R.G. Zika, L.E. Brand, Deep-Sea Res. 37 (1990) 27.
[5] M. Gledhill, C.M.G. van den Berg, Mar. Chem. 47 (1994) 41.
[6] E.L. Rue, K.W. Bruland, Limnol. Oceanogr. 42 (1997) 901.
[7] A.E. Witter, G.W. Luther III, Mar. Chem. 62 (1998) 241.

[8] M. Nimmo, C.M.G. van den Berg, J. Brown, Estuarine Coastal Shelf Sci. 29 (1989) 57.
[9] E.P. Achterberg, C.M.G. van den Berg, Deep-Sea Res. II. Top. Stud. Oceanogr. 44 (1997) 693.
[10] K.W. Bruland, Limnol. Oceanogr. 34 (1989) 269.
[11] C.M.G. van den Berg, A.G.A. Merks, E.K. Duursma, Estuarine Coastal Shelf Sci. 24 (1987) 785.
[12] M.J. Ellwood, C.M.G. van den Berg, Mar. Chem. 68 (2000) 295.
[13] C.M.G. van den Berg, M. Nimmo, Sci. Total Environ. 60 (1987) 185.
[14] J. Buffle, Complexation Reactions on Aquatic Systems, Ellis Horwood, Chicester, 1988.
[15] T.T. Gorsuch, The Destruction of Organic Matter, Pergamon Press, Oxford, 1970.
[16] J. Golimowski, K. Golimowska, Anal. Chim. Acta 325 (1996) 111.
[17] M. Kolb, P. Rach, J. Schafer, A. Wild, Fresenius' J. Anal. Chem. 342 (1992) 341.
[18] K. Yokoi, T. Tomisaki, T. Koide, C.M.G. van den Berg, Fresenius' J. Anal. Chem. 325 (1995) 547.
[19] K. Yokoi, M. Yakushiji, M. Hatanaka, K. Kobono, T. Koide, Fresenius' J. Anal. Chem. 365 (1999) 364.
[20] M. Martin-Goldberg, M.S. Shuman, Chem. Speciation Bioavailability 1 (1989) 19.
[21] E.P. Achterberg, C.M.G. van den Berg, Anal. Chim. Acta 291 (1994) 213.
[22] C. Gueguen, C. Belin, B.A. Thomas, F. Monna, P.-Y. Favarger, J. Dominik, Anal. Chim. Acta 386 (1999) 155.
[23] O.C. Zafiriou, Chemistry 5 (1977) 497.
[24] O.C. Zafiriou, J. Joussot-Dubin, R.G. Zepp, R.G. Zika, Environ. Sci. Technol. 18 (1984) 358A.
[25] R.G. Zepp, A.M. Braun, J. Hoigne, J.A. Leenheer, Environ. Sci. Technol. 21 (1987) 485.
[26] W.R. Haag, J. Hoigne, Environ. Sci. Technol. 20 (1986) 341.
[27] D. Saur, in: P.A. Bruttel, J. Schafer (Eds.), Sample Preparation Techniques in Voltammetric Trace Analysis, Metrohm, Herisau, Switzerland, 1992.
[28] K.H. Coale, K.S. Johnson, P.M. Stout, C.M. Sakamoto, Anal. Chim. Acta 266 (1992) 345.
[29] P.J. Worsfold, E.P. Achterberg, A.R. Bowie, R.C. Sandford, R.F.C. Mantoura, in: M.S. Varney (Ed.), Sensors in Oceanography, Gordon and Breach, Amsterdam, 2000.
[30] G. Spyres, M. Nimmo, P.J. Worsfold, E.P. Achterberg, A.E.J. Miller, Trends Anal. Chem. 19 (2000) 498.
[31] W.M. Landing, C. Haraldsonn, N. Pexeus, Anal. Chem. 58 (1986) 3031.
[32] M.L.A.M. Campos, C.M.G. van den Berg, Anal. Chim. Acta 284 (1994) 481.
[33] E.P. Achterberg, C.M.G. van den Berg, Marine Poll. Bull. 32 (1996) 471.
[34] R.E. Laslett, Estuarine Coastal Shelf Sci. 40 (1995) 67.
[35] K. Kremling, D. Hydes, Continental Shelf Res. 8 (1988) 89.